BMI-2104
Volume 1

Radionuclide Release Under Specific LWR Accident Conditions

Volume 1 - PWR-Large, Dry Containment Draft Report

Prepared by:
J. A. Gieseke, P. Cybulskis, R. S. Denning,
M. R. Kuhlman, K. W. Lee

Battelle Columbus Laboratories
Columbus, Ohio 43201

July 1983

DRAFT REPORT

DRAFT REPORT

BMI-2104
Volume 1

Radionuclide Release Under Specific LWR Accident Conditions

Volume 1 - PWR-Large, Dry Containment
Draft Report

Prepared by:
J. A. Gieseke, P. Cybulskis, R. S. Denning,
M. R. Kuhlman, K. W. Lee

Battelle Columbus Laboratories
Columbus, Ohio 43201

July 1983

Prepared for
Office of Nuclear Regulatory Research
U. S. Nuclear Regulatory Commission
Washington, D. C. 20555

DRAFT REPORT

UNITED STATES
NUCLEAR REGULATORY COMMISSION
WASHINGTON, D. C. 20555

JUL 22 1983

Recipients of BMI-2104 Draft Report (Vol. I):

The first published volume of the Battelle Columbus Laboratories draft report, BMI-2104, which contains analysis of the PWR SURRY plant, representing the initial efforts to provide the best estimate of radionuclides release for the postulated and selected severe accident sequences, does not necessarily represent the views, interpretation or acceptance by the United States Nuclear Regulatory Commission, although it was prepared under the auspices of the Agency.

It does, however, represent the available technology and knowledge at the time of the report preparation. The analysis presented in this report was subject to a thorough expert peer review in January 1983.

This version, therefore, contains the incorporation of only some of the comments received during the peer review process; changes were made to the extent that state-of-the-art of knowledge and time permitted.

Since the content of this report was made available to the invited peer review members and observers as well, the decision has been made to publish this volume to introduce the overall approach adopted for this and remaining analyses to a broad distribution.

Because of the already recognized limitations of the PWR SURRY analysis at the time of preparation of this volume (such as the unavailability of the improved MARCH 2.0 code, upper plenum design details, improvements in the other codes employed) and the effect on calculated radionuclide release fractions, the SURRY plant will be the subject of reanalysis according to the overall NRC planned activities. Other volumes of this report may also be revised depending on peer comments.

The remaining sections of the BMI-2104 report containing the following analyses will be published by October-November 1983.

BWR MARK I PEACH BOTTOM	Vol. II
BWR MARK III GRAND GULF	Vol. III
PWR ICE-CONDENSER SEQUOYAH	Vol. IV
PWR SURRY (Recalculated)	Vol. V
PWR ZION	Vol. VI
PEER REVEIW COMMENTS (Summary and evaluation for all plants)	Vol. VII

We invite your comments.

Robert M. Bernero, Director
Accident Source Term Program Office
Office of Nuclear Regulatory Research
U.S. Nuclear Regulatory Commission
Washington, D.C. 20555

TABLE OF CONTENTS

TABLE OF CONTENTS
(Continued)

ACKNOWLEDGMENTS

Battelle's Columbus Laboratories wishes to acknowledge and express appreciation for the computer codes made available for this program by Sandia National Laboratory and the Kernforschungszentrum Karlsruhe, and for the computations and consultation provided by Sandia and the Oak Ridge National Laboratories. Further, members of the Peer Review Group have contributed significantly to this effort by providing comments, suggestions, and information on various reactor systems design.

The support of the U.S. Nuclear Regulatory Commission is gratefully acknowledged, as is the untiring leadership of the NRC staff, particularly Mel Silberberg and Mike Jankowski.

The diligent efforts of many Battelle staff members contributed to the preparation of this report. The following list identifies those staff making major contributions:

RJ Avers
H Chen
R Freeman-Kelly
CS Jarrett
H Jordan
RG Jung
DJ Lehmicke
PM Schumacher
RO Wooton.

1. EXECUTIVE SUMMARY

Physical processes which affect the release of radionuclides from nuclear power plants under accident conditions are becoming more thoroughly understood and can provide a basis for re-evaluating source terms to the environment. Improved characterization of source terms would provide a basis for formulating impacts on and changes to licensing practice, emergency planning, safety goals, and indemnification policy. This study represents the identification and formulation of a systematic, mechanistic approach to estimating source terms and the implementation of this approach through calculations of fission product release to the environment for a large PWR reactor under a selected set of accident conditions. The development and improvement of calculational procedures is an evolutionary process and in the long term must be verified through experimental studies. It is anticipated that as additional information is obtained the accuracy of predictions can be improved and uncertainties reduced.

This study was based on selecting specific plants and accident sequences for consideration and then using consistent and improved analyses of fission product release from fuel, transport, and deposition to predict fission product release to the environment for these specific cases. The approach is comprised of a series of steps performed in sequence such that in the combined analysis, the results are specific to an individual set of accident conditions and each successive transport step is based on results from analyses of the previous step.

The Surry plant was chosen as being representative of a large, dry PWR and accident sequences AB, TMLB', S_2D, and V were considered because they include sequences of high risk, large consequences and, most importantly, considerable range in physical conditions.

After selection of sequences, the stepwise analyses proceeded with the collection of plant design data and the performing of thermal hydraulic analyses for the sequences. Overall thermal hydraulic conditions on a time-dependent basis were estimated with the MARCH code and detailed thermal hydraulic conditions for the primary system estimated with the MERGE code which was developed specifically for use in this program.

The time-dependent core temperatures were used as input to another code developed for this program, CORSOR, which predicts time and temperature dependent mass releases of radionuclides from the fuel within the pressure vessel. Releases during core-concrete interactions of radionuclides remaining with the melt were provided by Sandia National Laboratories using their newly developed model, VANESA.

Using the MARCH/MERGE predicted thermal hydraulic conditions and the CORSOR predicted radionuclide release rates as input, a newly developed version of the TRAP-MELT code was used to predict vapor and particulate transport in the primary coolant circuit. Transport and deposition of radionuclides in the containment were calculated using the NAUA-4 code. Analyses were also performed with CORRAL-2 in order to relate the results to WASH 1400 assumptions.

The calculations performed were of a "best estimate" type using input derived, to the extent possible, from experimental measurements. Types of data employed in the analyses include vapor deposition velocities, aerosol deposition rates, aerosol agglomeration rates, fission product release rates from fuel, particle sizes formed from vaporizing/condensing fuel materials, engineering correlations for heat and mass transfer, and physical properties of various fuel, fission product, and structural materials.

The computation of radionuclide release and transport using mechanistic models is subject to many uncertainties of various magnitudes and importance. It has not been a part of this study to produce quantitative estimates of uncertainties in individual parameters and hence the overall importance of such uncertainties has not been assessed. However, limited evaluations were made of the sensitivity of results to a few specific parameter variations.

The thermal hydraulic calculations for the primary system were carried out with two assumptions of surface area and structural mass for the upper plenum surfaces. In all cases the upper grid plate was calculated to reach or closely approach melting temperatures from the combined radiation and convection heat transfer. Upper plenum surfaces and gas temperatures in the region were sensitive to the mass and surface area assumptions

with the hot cases (preferred estimate at this time -- high area, lower mass) showing average surface temperatures at the time of core slumping as low as about 900 C for the AB case up to about 1400 C for the S_2D sequence. For primary system components in the flow path beyond the upper plenum, the temperatures were estimated to drop off quite rapidly.

Releases of fission products from the fuel both within and external to the pressure vessel were found to be strongly time-dependent for both mass release rates and composition. Temperatures achieved by the molten fuel had a very strong influence on release rates of aerosol-producing materials as illustrated by parametric calculations. The timing of the vaporization release (core-concrete interaction) was not exponential as assumed in WASH 1400 analyses but was essentially in the form of two major peaks resulting from the behavior of the molten core-concrete materials. Total releases as predicted in this study were in fairly close agreement with WASH 1400 for major fission product classes except that the current work predicted more than one order of magnitude less Ru release, about one-third the Sr release, and shifted the Te release toward the melt release period rather than the vaporization release.

Transport and deposition of radionuclides were found to be quite dependent on the accident sequences and the corresponding thermal hydraulic conditions. Reduced temperatures led to increased deposition of vapor species, and reduced flow rates to increased aerosol deposition. Primary system retention of CsOH and CsI for the sequences analyzed ranged from almost 0 to over 85 percent illustrating the sequence dependence.

A sequence dependence of radionuclide attenuation in the containment building was also noted with the most important factors being the time of containment failure, operation of sprays, and steam condensation on particles. In cases where the sprays do not operate and only natural deposition mechanisms are acting, the release to the environment is dependent on the timing of containment failure. When the containment building was assumed to fail early in the accident, additional retention in the containment was only on the order of 50 percent. In contrast, when the containment was assumed to remain intact for approximately 2 days, the retention was on the

order of 99.9 percent. For cases where containment sprays operate, washout of aerosols is rapid and very effective.

Overall release fractions from the containment reflect new predictions of release from the fuel, attenuation in the primary system, and attenuation in the containment. The total release fractions vary in general from slightly less than the WASH 1400 estimates to more than an order of magnitude less depending on the sequence.

It is to be recognized that the estimates of release fractions are subject to uncertainties in the data and computer models employed in the calculations and are expected to have been influenced by assumptions regarding plant geometry, thermal hydraulics, deposition mechanisms, and sequence events. The effects of these assumptions will be investigated as this study continues.

2. INTRODUCTION

The radiological effects associated with fission product release from commercial light water reactors during severe accident conditions have been the subject of considerable concern and the impetus for much research. As research has progressed, the physical processes controlling the magnitude of fission product releases have become more thoroughly understood and the ability to estimate fission product releases has been improved.

The design bases and siting criteria for most of the existing population of U.S. reactors were based on the use of the TID-14844[2.1] assumptions regarding the release of fission products to the containment in a severe accident. Although representative of the state of knowledge at the time, a better understanding of the behavior of fission products in severe accidents has developed over the intervening years and many of the TID-14844 assumptions are now recognized as requiring re-evaluation. A more mechanistic treatment of fission product release was developed for the Reactor Safety Study (WASH 1400)[2.2] and since that time the WASH 1400 source term to the environment for accident sequences has been used extensively. Obtaining an improved characterization of the source of fission products to the environment in accidents is therefore an essential step in the comprehensive evaluation of current source term assumptions and would serve as a basis for formulating impacts on and changes to licensing practice, emergency planning, safety goals and indemnification policy. For this reason the NRC undertook a review of the state of knowledge regarding procedures available for predicting fission product release and transport and in June of 1981 issued the report "Technical Bases for Estimating Fission Product Behavior During LWR Accidents".[2.3]

As part of the "Technical Bases Report", the assumptions, procedures, and available data needed for predicting fission product behavior were evaluated and calculations were made of fission product attenuation along the various flow paths from the fuel to the environment. Because of the limitations of available computational tools at that time, release from the fuel and transport through various compartments along the flow path were treated separately and therefore possible interactions were not

considered. This procedure is the subject of the first major comment on the "Technical Bases Report" (NUREG 0772, Appendix F) and was recognized as a shortcoming of that report. The calculations and evaluations being presented here are intended to overcome this shortcoming as well as to provide analyses performed with improved computational procedures.

This report builds on previous computer modeling work performed at Battelle-Columbus, at Sandia and in the Federal Republic of Germany, and on experimental and model evaluation work performed at Oak Ridge, EG&G Idaho, Sandia, and Pacific Northwest Laboratories. It is to be noted that in addition to the calculations performed at Battelle-Columbus, calculations concerned with the thermal as well as the fission product release aspects of molten core-concrete interactions were performed by Sandia. Research efforts specifically directed toward increasing our understanding of fission product release and transport under severe accident conditions are currently under way at the laboratories listed above as well as at other research installations around the world. It is anticipated that over the next few years considerable progress will be made in this area. Therefore this report must be considered as an expression of current knowledge with the expectation that validation or modification of the calculated fission product releases will be forthcoming.

It is to be recognized that this report describes an analytical approach for estimating radionuclide transport and deposition which incorporates physical and chemical processes on a mechanistic basis. This approach is being evaluated for use in predicting fission product source terms for release to the environment on a specific case-by-case basis (reactor, accident sequence) and when verified would be expected to replace the generic tabular release fractions such as those in Table 6, Appendix V, WASH 1400 where release fractions are given for broad classes of accidents.

The purpose of this report is then to:

(1) Develop updated release-from-plant fission product source terms for four types of nuclear power plants and for accident sequences giving a range of conditions. The estimated source terms are to be based

on consistent step-by-step analyses using improved computational tools for predicting radionuclide release from the fuel, and transport and deposition.

(2) Determine the effects on fission product releases associated with major differences in input parameters associated with plant design and accident sequences.

(3) Provide in-plant time and location dependent distributions of fission product mass for use in equipment qualification considerations.

It is not necessarily the intent of this work to produce an all encompassing definition of source terms but rather to make best estimates of source terms for a range of typical plants and several risk-significant sequences covering a wide range of conditions. These analyses were to be made with the best available techniques, in a consistent manner following along with release pathways for fission products, and at a level of detail consistent with current knowledge of pertinent physical processes. Based on state-of-the-art techniques, these best-estimate analyses should provide an indication of the conservatisms inherent in current source term assumptions and guidance for the development of new source terms. It is important to note that the analytical methods and corresponding predictions are based on currently available information and are subject to revision and improvement as better analytical procedures are developed and as a more extensive experimental base evolves. The preparation of this report, therefore, is an evolutionary process which will be carried out over a period of time with verification and possibly revision of the procedures continuing over several years beyond that date.

As a part of that evolutionary process, it is to be noted that this Volume I report is to be revised using improved analytical procedures and incorporating comments and suggestions from participants at a series of NRC sponsored "Peer Review Meetings". This volume is being published as a means for describing overall procedures, analytical methods to be used throughout this study. Subsequent volumes of this report will cover other plant designs (both PWR and BWR) and describe additional or revised analytical procedures used in the accompanying calculations.

References

(2.1) DiNunno, J. J., et al, "Calculation of Distance Factors for Power and Test Reactors Sites", TID-14844 (March 23, 1962).

(2.2) "Reactor Safety Study -- An Assessment of Accident Risks in U.S. Commercial Nuclear Power Plants", WASH-1400, NUREG-75/014 (October, 1975).

(2.3) "Technical Bases for Estimating Fission Product Behavior During LWR Accidents", NUREG-0772 (June, 1981).

3. GENERAL APPROACH

The general philosophy behind this study is that mechanistic predictions of radionuclide release and transport are possible if proper modeling is performed to represent the physical and chemical processes occurring during LWR accidents. The study, then, represents an attempt at describing in a reasonably complete but tractable fashion the processes influencing the radionuclide release to the environment for selected plants and accident conditions. The general approach taken in this study was specified by the objectives which called for a consistent analysis of radionuclide behavior by following their transport along flow paths from their release into the core region up to their final release to the environment. Nevertheless, numerous decisions and assumptions were required for the analyses. These decisions included selections of plants and sequences for consideration, choices of analytical tools to be used as available or upgraded, evaluations and incorporation of experimental data, and determinations of major physical effects which would be considered on a parametric variation basis to illustrate the sensitivity of calculations to such variations. Such decisions and assumptions are discussed throughout this report as they arise in their technical context. However, some of the major considerations will be reviewed and the steps comprising the overall approach will be discussed in this section.

This study was based on selecting specific plants and accident sequences for consideration and then using consistent and improved analyses of fission product release from fuel, transport, and deposition to predict fission product release to the environment for these specific cases. The approach consists of a series of steps performed in sequence such that in the combined analysis, the results are specific to an individual set of accident conditions and each successive transport step is based on results from analyses of the previous step.

The first major step in the process was the selection of types of nuclear power plant designs to be considered and a specific plant to represent each type. The types to be considered were: large, dry PWRs; Mark I BWRs; Mark III BWRs; and ice condenser type PWR designs. The specific plants chosen to represent each type are the Surry and Zion, Peach Bottom, Grand

Gulf, and Sequoyah plants. These selections were made on a combined basis of typicality of design and availability of design details needed for analyses.

Accident sequences were chosen for each plant design based on contribution to risk and on a desire to have a range of physical conditions represented by the analyses. The plants and selected accident sequences are listed below:

PWR Large Dry Containment (Surry)	BWR Mark I (Peach Bottom)
AB	TC
S_2D	AE
V	TW
TMLB'	

BWR Mark III (Grand Gulf)	PWR Ice Condenser Containment (Sequoyah)
TPI	S_2HF
TQUV	TMLB'
TC	TML

Following the selection of plants and sequences the required plant design data were collected and thermal hydraulic analyses performed for the accident sequences. Overall thermal hydraulic conditions on a time-dependent basis were estimated with the MARCH code,[3.1] and detailed thermal hydraulic conditions for the primary system estimated with the MERGE code which was developed specifically for use in this program.

The time-dependent core temperatures were used as input to another code developed for this program, CORSOR, which predicts time and temperature dependent mass releases of radionuclides from the fuel within the pressure vessel. Releases during core-concrete interactions of radionuclides remaining with the melt were provided by Sandia National Laboratories using their newly developed model, VANESA.

Using the MARCH/MERGE predicted thermal hydraulic conditions and the CORSOR predicted radionuclide release rates as input, a newly developed

version of the TRAP-MELT code, was used to predict vapor and particulate transport in the primary coolant circuit.

Transport and deposition and radionuclides in the containment were calculated using the CORRAL-2[3.2] and NAUA-4[3.3] codes.

The basic stepwise procedure described above is illustrated in Figure 3.1 which shows the relationships among the computational models. The calculations were of a "best estimate" type using input derived, to the extent possible, from experimental measurements. Types of data employed in the analyses include vapor deposition velocities, aerosol deposition rates, aerosol agglomeration rates, fission product release rates from fuel, particle sizes formed from vaporizing/condensing fuel materials, engineering correlations for heat and mass transfer, and physical properties of various fuel, fission product and structural materials.

In preparation for performing calculations of thermal hydraulic conditions and radionuclide transport and deposition, it was necessary to make a number of assumptions or select conditions from among several options. Assumptions of a detailed nature are identified throughout the report; however, major assumptions are listed in the analyses. The assumptions are listed in the categories of geometry, thermal hydraulics, mechanisms, and sequences.

Geometry

(1) Surfaces within the containment building available for radionuclide deposition include only the major geometrical features of the building.

(2) The reactor containment is a single compartment and there is no radionuclide attenuation along any pathway to this well-mixed compartment except for the primary coolant system.

(3) There is no attenuation of radionuclides as they pass through leak paths in the containment shell.

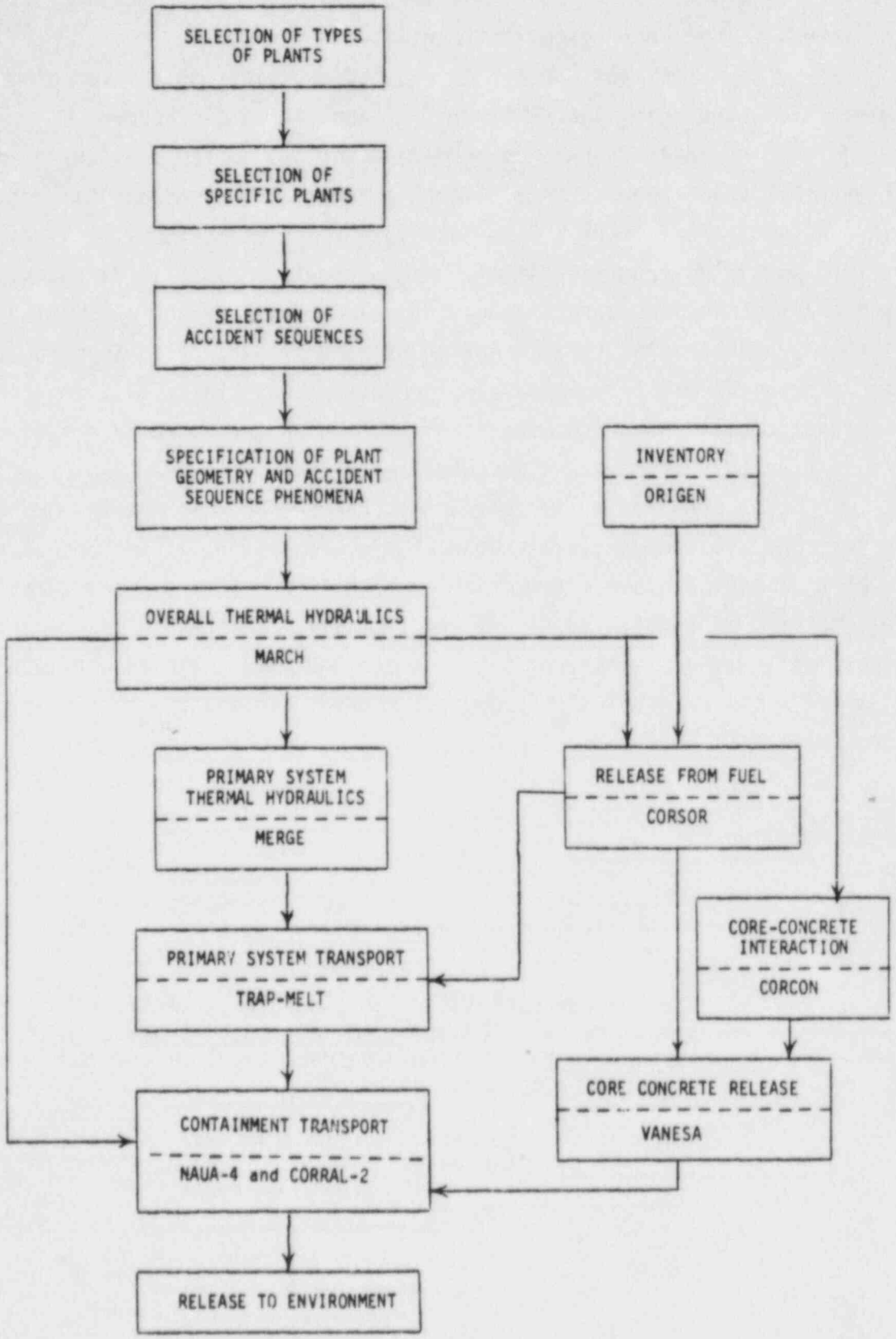

FIGURE 3.1. INFORMATION FLOW FOR RELEASE, TRANSPORT, AND DEPOSITION CALCULATION

Thermal Hydraulics

(4) Flow in the primary coolant system is restricted to direct leak paths.

(5) The upper plenum geometry is modeled in terms of surface areas, steel thicknesses, and compartment heights rather than with exact geometries.

(6) Decay heating of surfaces by deposited fission products is neglected.

(7) No operator intervention occurs that would lead to cooling of the steam generators.

Mechanisms

(8) Neither deposition nor resuspension of radionuclides occurs during reactor coolant system depressurization at the time of pressure vessel melt-through.

(9) In the long term (after pressure vessel failure), deposited radionuclides remain in the primary system indefinitely.

(10) No change in fission product physical or chemical properties results from radioactive decay.

Sequences

(11) In the V sequence, all fission product flow passes back through the primary system after melt-through (no mixing into containment) and does not deposit during transit.

(12) There is no scrubbing of the vaporization release by an overlying layer of water in the S_2D sequence.

(13) Core drop in the pressure vessel does not cause a flow pulse to force fission products away from the core region.

Many of the above assumptions will be relaxed or changed to accommodate best estimates of conditions and occurrences as this study progresses in the future.

The computation of radionuclide release and transport using mechanistic models is subject to many uncertainties of various magnitudes and importance. It has not been a part of this study to produce quantitative estimates of uncertainties in individual parameters and hence the overall importance of such uncertainties has not been assessed. Where practical, qualitative (and in some cases quantitative) estimates of uncertainties have been noted.

In several cases, calculations have been made with several values for particular parameters to illustrate the impact of uncertainties in the parameters on final or intermediate results. Assumptions regarding average and peak fuel temperatures and fission product release rate coefficients were varied around best estimate values to illustrate their importance to overall release rates from the fuel for fission products. A variety of containment failure modes were considered to evaluate the effects of failure time on releases to the environment. Two sets of assumptions leading to "cold" and "hot" temperatures in the upper plenum were used to illustrate the importance of primary system thermal conditions. Finally, for one accident sequence it was assumed that Te would remain with molten fuel materials until released during the core-concrete interaction to illustrate the importance of this possibility.

Some of the uncertainties in the analyses and procedures presented in this report that are currently considered to be of significance can be identified. The following list is presented as examples of those uncertainties that are believed significant and warrant further evaluation through more detailed analyses than those performed in this study.

(1) The simplified fuel melting model in MARCH 1.1 (i.e., a single melting temperature) could bias the predicted release of material from overheated fuel, particularly regarding the source of inert and low volatility fission product aerosols.

(2) The rate coefficients for the release of fission products from overheated fuel are empirical, rather than mechanistically based, and rely largely on scaled, simulant experiments.

(3) The model for the release of fission products and inert materials during the attack of concrete has a very limited experimental basis.

(4) The flow patterns in the reactor coolant system, in particular in the upper plenum region of the PWR, are uncertain. The adequacy of the simple thermal hydraulic models used in this study will require experimental verification.

(5) Primary system transport models used in these analyses have not been validated against integral experiments.

(6) The mode and timing of the containment failure in severe accident sequences can have a major influence on fission product behavior but are subject to large uncertainty.

(7) The calculation methods for water condensation in the containment are based on limited, small-scale experiments and require verification at larger scales.

(8) Deposition velocities for vapor species used in the TRAP-MELT calculations were taken as mid-points in order of magnitude ranges of experimental data. More accurate data would reduce the uncertainty in these parameters and in the resulting rates for deposition by sorption.

References

(3.1) Wooton, R. O. and Avci, H. I., "MARCH (Meltdown Accident Response Characteristics) Code Description and Users' Manual", NUREG/CR-1711, BMI-2064 (October, 1980).

(3.2) Reactor Safety Study, WASH 1400, Appendix VII (1975).

(3.3) Bunz, H., Koyro, M., and Schock, W., "A Code for Calculating Aerosol Behavior in LWR Core Melt Accidents Code Description and Users' Manual".

4. PLANT SELECTION AND ACCIDENT SEQUENCES

4.1 General Plant Description

A pressurized water reactor with a large high pressure containment design is the first reactor type to be considered in this study. In actuality, there are large variations in the design of large high-pressure containments in terms of the volume of the containment building and the design pressure of the containment. To some extent, generic accident sequences can be defined which are independent of the variations that exist in the nuclear steam supply system and balance of plant designs. For example, the sequence AB6 (large LOCA, loss of all AC power and failure of containment by overpressurization) could occur in any PWR design. This is because the general safety philosophy and safety functions provided to protect the plant are the same. Because the different vendors and architect-engineers have chosen different approaches to satisfy these safety functions, the likelihood of each sequence may vary greatly between plant design; similarly, the accident timing and sequence of events in a sequence may also vary depending on the design.

The specific plant design selected to characterize large high-pressure designs is the Surry Unit 1 plant. In some respects, the selection is not ideal. The Surry plant is an older design. In comparison with average parameters for U.S. designs, the power output is low, the containment volume is small, and the containment design pressure is low. By the use of parametric variations, it has been possible to examine some of the important differences in containment design, however. An important reason for selecting the Surry plant was that this was the design analyzed in the Reactor Safety Study. Thus, a direct comparison can be made between the magnitudes of the predicted source terms.

The Surry unit is a pressurized water reactor (157-inch diameter vessel with 157 fuel assemblies) designed by Westinghouse. A detailed description of plant data is provided in Table 4.1. The reactor is designed to operate at a nominal power of 2441 MW(t) and a reactor coolant system pressure of 2250 psia. The containment is a steel-lined reinforced

TABLE 4.1. PWR DATA

Nominal power	2,441 Mwt	
	8,331 x 10^6 Btu/hr	
Internal energy of water	246.9 x 10^6 Btu	(2.66 x 10^{10} kg-m)
Sensible heat in the core	16.35 x 10^6 Btu	(1.76 x 10^9 kg-m)
Total water in the system	423,200 lb	(192,000 kg)
Aug. temperature (Excl. pres.)	571.8 F	(300 C)
Pressure	2280 psig	(15.7 MPa)
Reactor coolant system volume	8387 ft^3	(237.5 m^3)
Pressurizer volume, total	1,336 ft^3	(37.83 m^3)
water	816 ft^3	(23.1 m^3)
steam	520 ft^3	(14.7 m^3
Three accumulators, total volume	4,350 ft^3	(123.2 m^3)
water volume	2,775 ft^3	(78.58 m^3)
pressure	665 psig	(4.585 MPa)
temperature	120 F	(48.9 C)
Containment recirculation spray		
2 systems, flow each	3,500 gpm	(220.8 l/s)
Containment free volume	1.8 x 10^6 ft^3	(5.1 x 10^4 m)
Initial temperature	100 F	(3.778 C)
Initial pressure	10 psia	(6.89 x 10^4 Pa)
Dewpoint	80 F	(26.7 C)
Primary system hot metal	1,686,285 lb	(766,000 kg)
Temperature	572 F	(300 C)

Containment Heat Sinks

	Thickness	Area
Walls inside containment	1.0 ft (0.3048 m)	3,320 ft^2 (308.4 m^2)
Walls inside containment	2.0 (0.6096	27,600 (2564)
Walls inside containment	3.0 (0.9144	19,400 (1802)
Walls inside containment	4.0 (1.219)	5,000 (464.5)
Walls inside containment	6.5 (1.981)	2,100 (195.1)
Containment wall	4.5 (1.372)	46,747 (4343)
Dome	2.5 (0.762)	25,000 (2323)
Floor above foundation mat	2.0 (0.6096)	11,250 (1045)
Foundation mat	10.0 (3.048)	11,250 (1045)
Containment liner		
Walls	0.38 in. (0.9652 cm)	46,747 (4343)
Dome	0.50 in. (1.27 cm)	25,000 (2323)
Floor	0.25 (0.635 cm)	11,250 (1045)
Miscellaneous metal - 1,200,000 lb (544,308 kg)		
Core		
Equivalent diameter	119.7 in. (3.04 m)	
Active height	144.0 in. (3.658 m)	
L/D	1.202	
Total cross sectional area	78.3 ft^2 (7.27 m^2)	

TABLE 4.1. PWR DATA (CONTINUED)

Core (Continued)		
No. of fuel assemblies		157
Rods per assembly		204
Pitch		0.563 in. (1.430 cm)
Assembly dimensions		8.426 in. square
Fuel rod diameter		0.422 in. (1.072 cm)
Clad (Zr-4) thickness		0.0243 in. (0.0617 cm)
Total number of fuel rods		32,028
Core weight		226,200 lb (102,700 kg)
UO_2		175,600 lb (79,820 kg)
Zircaloy		36,300 lb (16,500 kg)
Misc.		14,300 lb (6,500 kg)
Fuel pellet diameter,	Region 1	0.3669 in. (0.9319 cm)
	2 and 3	0.3659 in. (0.9294 cm)
Fuel pellet length		0.6 in. (1.524 cm)
Diametral gap,	Region 1	0.0065 in. (0.01651 cm)
	2 and 3	0.0075 in. (0.01905 cm)
Fuel density,	Region 1	94%
	2	92
	3	91
Fuel enrichment,	Region 1	1.85 w/o
	2	2.55
	3	3.10
No. of grid spacers		7
Neutron adsorber		Ag-In-Cd
Clad		304 ss
Clad thickness		0.024 in. (0.06096 cm)
No. of control assemblies		53
Full length		48
Part length		5
Rods per assembly		20
Burnable poison rods		816
No. per assembly		12
No. of assemblies		68
Material		Borosilicate glass
O.D.		0.4395 in. (1.116 cm)
I.D.		0.2365 in. (0.6007 cm)
Clad		304 ss
Boron (natural) loading		0.0429 g/cm
Reactor vessel		
I.D. of shell		157 in. (3.99 m)
Belt line thickness (w/o clad)		7.875 in. (0.2000 m)
Head thickness		5.0 in. (0.127 m)
Clad thickness		0.125 in. (0.3175 m)
Overall height		40 ft-5 in. (12.32 m)

TABLE 4.1. PWR DATA (CONTINUED)

Reactor vessel (continued)	
Inlet nozzles	27.5 in. (0.699 m) tapered to 35.4 in. (0.899 m)
Outlet nozzles	29 in. (0.737 m)
Water volume with core and internals in place	3,718 ft^3 (1.053 x 10^2 m^3)
Core barrel I.D.	133.9 in. (3.401 m)
O.D.	137.9 in. (3.503 m)
Thermal shield I.D.	142.6 in. (3.622 m)
O.D.	148.0 in. (3.759 m)
Safety Injection Charging Pumps	
Number	3
Design pressure, discharge	2750 psig (18.96 MPa)
Design pressure, suction	250 psig (1.724 MPa)
Design temperature	250 F (121 C)
Design flow	150 gpm (9.46 l/s)
Maximum flow	600 gpm (37.8 l/s)
Design head	5800 ft (1768 m)
Low Head Safety Injection Pumps	
Number	2
Design pressure, discharge	300 psig (2.07 MPa)
Design temperature	300 F (148.9 C)
Design flow	3000 gpm (189.2 l/s)
Design head	225 ft (68.58 m)
Maximum flow	4000 gpm (252.3 l/s)
Containment Spray Pumps	
Number	2
Design flow	3,200 gpm (201.9 l/s)
Design head	225 ft (68.58 m)
Design pressure	250 psig (1.724 MPa)
Recirculation Spray Pumps Inside Containment	
Number	2
Design flow	3500 gpm (220.8 l/s)
Design head	230 gpm (14.5 l/s)
Recirculation Spray Pumps Outside Containment	
Number	2
Design flow	3,500 gpm (220.8 l/s)
Design head	249 ft (75.89 m)
Recirculation Spray Coolers	
Number	4
Design duty, each	55,534,520 Btu/Hr (16.3 MW)
Refueling Water Storage Tank	
Volume	350,000 gal (1.32 x 10^6 l)
Boron concentration	2,500 ppm
Design pressure	Hydraulic head
Design temperature	150 F (65.6 C)
Water temperature	45 F (7.22 C)

concrete structure with a free volume of 1.8×10^6 ft^3; it is operated subatmospheric with initial pressure and temperature of 10 psia and 100 F, respectively. Figure 4.1 illustrates the layout of the containment design. The plant systems that perform critical safety functions are depicted conceptually in Figure 4.2.

4.2 Selection Basis and General Description of Accident Sequenes

The four accident sequences selected for the large dry PWR plant design analysis were AB, TMLB', S_2D, and V. Table 4.2 relates the letter used in the accident identifier to the type of event and to the failure of the engineered safety systems. Two criteria were used in selecting sequences. First, it was desired to examine sequences that would be expected to be risk dominant for a number of design variations within the large high-pressure containment category of PWRs. Secondly, it was considered important to cover a range of accident conditions and engineered safety system performance within the reactor coolant system and containment building.

Although the large, high pressure PWR containment design is often referred to as "dry", a great quantity of steam would be released to the containment building in each of the sequences analyzed other than the V sequence in which the release is to the safeguards building. In these cases steam condensation on the walls and on aerosols can have a significant influence in enhancing the natural removal of radionuclides from the volume atmosphere. Even more effective are the containment spray systems in those sequences in which they are expected to operate. Sequences were selected to illustrate the performance of the containment system with and without spray operation.

An aspect of the Three Mile Island 2 accident that played an important role in limiting the release of radionuclides to the containment atmosphere was the presence of a large quantity of water in the pathway of release to the environment. This is not characteristic of the accident sequences selected for analysis. In these sequences fuel heatup would not begin until the water level had dropped below the top of the core. Very

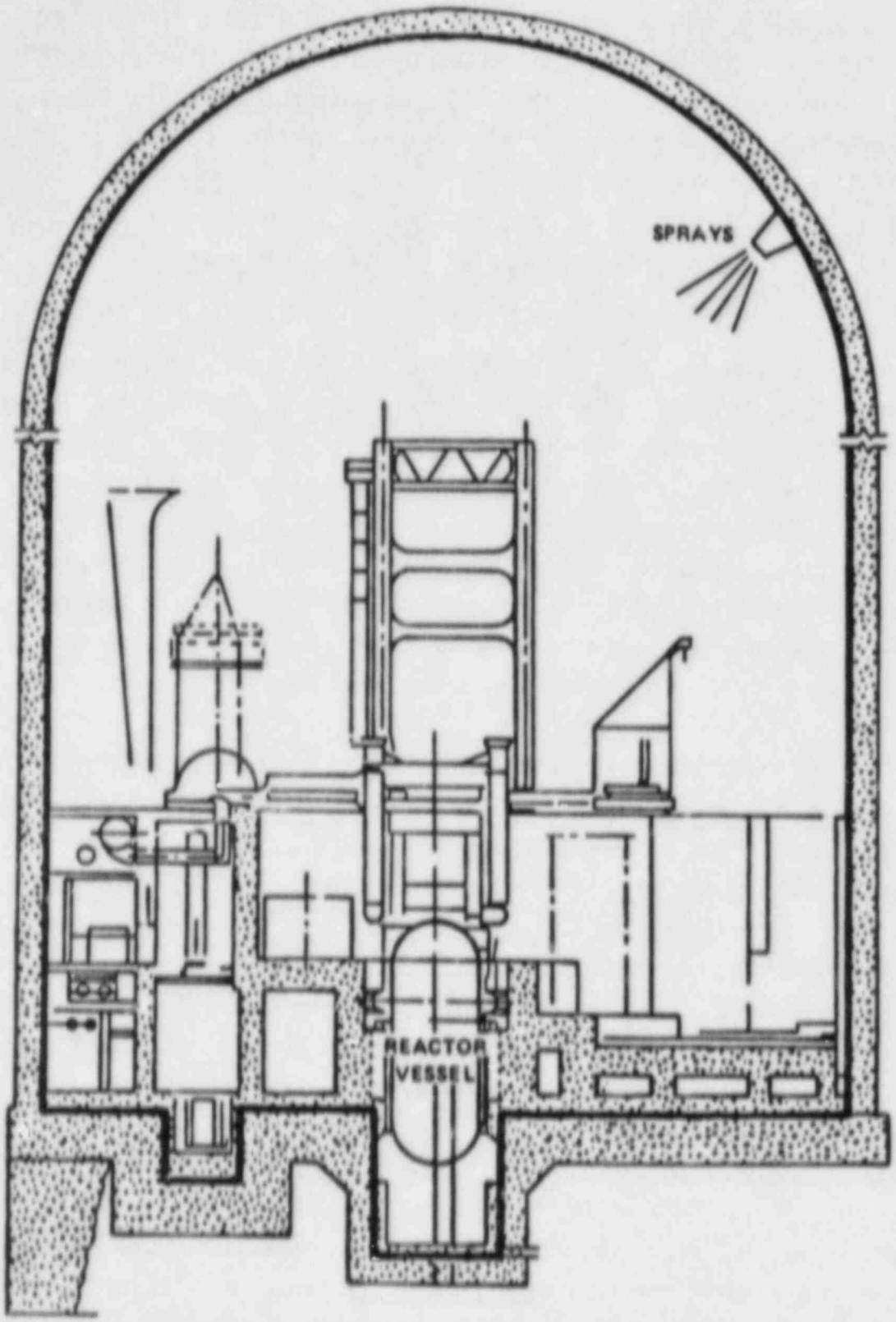

FIGURE 4.1. LARGE, HIGH PRESSURE CONTAINMENT

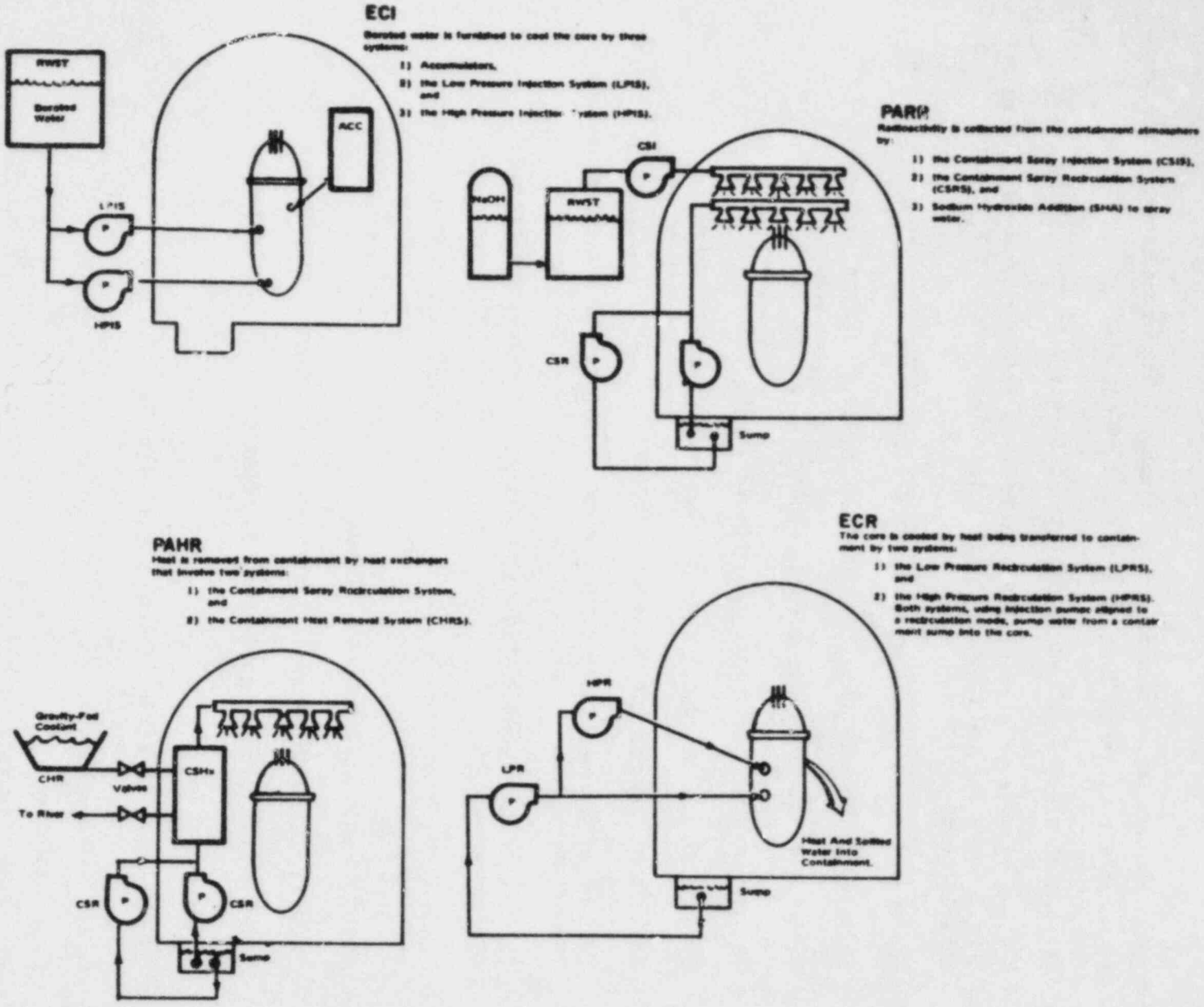

FIGURE 4.2. ILLUSTRATIONS OF PWR SYSTEMS USED TO PERFORM ESF FUNCTIONS

TABLE 4.2. KEY TO PWR ACCIDENT SEQUENCE SYMBOLS

A - Intermediate to large loss of coolant accident (LOCA).

B - Failure of electric power to engineered safety features (ESF).

B' - Failure to recover either onsite or offsite electric power within about 1 to 3 hours following an initiating transient which is a loss of offsite AC power.

C - Failure of the containment spray injection system.

D - Failure of the emergency core cooling injection system.

F - Failure of the containment spray recirculation system.

G - Failure of the containment heat removal system.

H - Failure of the emergency core cooling recirculation system.

K - Failure of the reactor protection system.

L - Failure of the secondary system steam relief valves and the auxiliary feedwater system.

M - Failure of the secondary system steam relief valves and the power conversion system.

Q - Failure of the primary system safety relief valves to reclose after opening.

R - Massive rupture of the reactor vessel.

S_1 - A small LOCA with an equivalent diameter of about 2 to 6 inches.

S_2 - A small LOCA with an equivalent diameter of about 1/2 to 2 inches.

T - Transient event.

V - Low pressure injection system check value failure.

Containment Failure Modes:

α = steam explosion

β = containment isolation failure

γ = overpressurization due to hydrogen combustion

δ_e = early overpressure failure due to steam and noncondensible gases

δ_l = delayed overpressure failure due to steam and noncondensible gases

ε = basemat melt-through

hot steam and hydrogen leaving the melting core would be expected to superheat the structures in the pathway to the containment. Other sequences in which the exiting gases would contact water as in the TMI 2 accident are possible, particularly those involving the partial performance of emergency core cooling systems. Depending on the subsequent fate of the water, contact with water would be expected to be effective in retaining fission products within the liquid phase.

4.2.1 Sequence AB (Loss of Coolant Accident, Loss of AC Power)

A large pipe break accident was selected for analysis because it represents one end of the spectrum of reactor coolant system conditions during core meltdown. Depressurization of the reactor coolant system would be expected to occur rapidly following the break. In the case of loss of all AC power, the accumulators would discharge into the vessel to supply some emergency coolant but the pumped ECC injection system would not operate. As the water level would decrease in the core, heatup of the fuel and fission product release would occur at the same pressure as the containment building atmosphere. A break location in the hot leg rather than the cold leg was selected in order to examine a case involving a minimum pathway and presumably minimum fission product retention within the reactor coolant system. The flow path for fission products from the core, to the upper plenum, and to the hot leg break location is illustrated in Figure 4.3. Flow through the other loops is assumed to be blocked in this sequence by hydrogen and possibly by water seals in the low points of the system. The flow path during the vaporization release period is shown in Figure 4.4.

In terms of reactor coolant system response, there would be little difference between the cases AB and AD (involving failure of pumped ECC injection rather than loss of all AC power). The containment conditions for AD would be very similar to those of another case analyzed S_2D. It was felt that the AB case provided an opportunity to examine a number of interesting containment failure modes in which natural deposition was the retention mode.

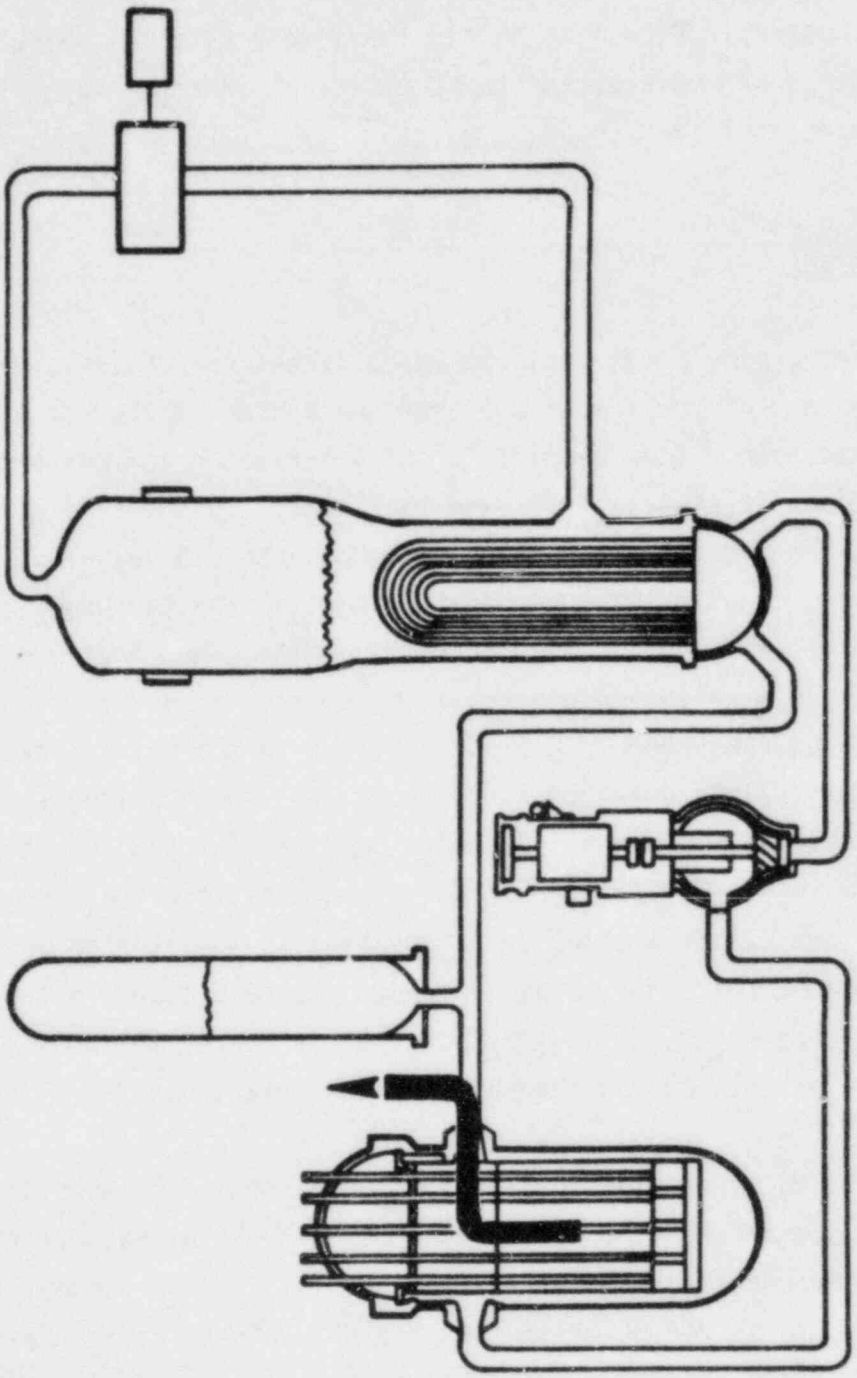

FIGURE 4.3. FLOW PATH FOR FISSION PRODUCT TRANSPORT IN SEQUENCE AB

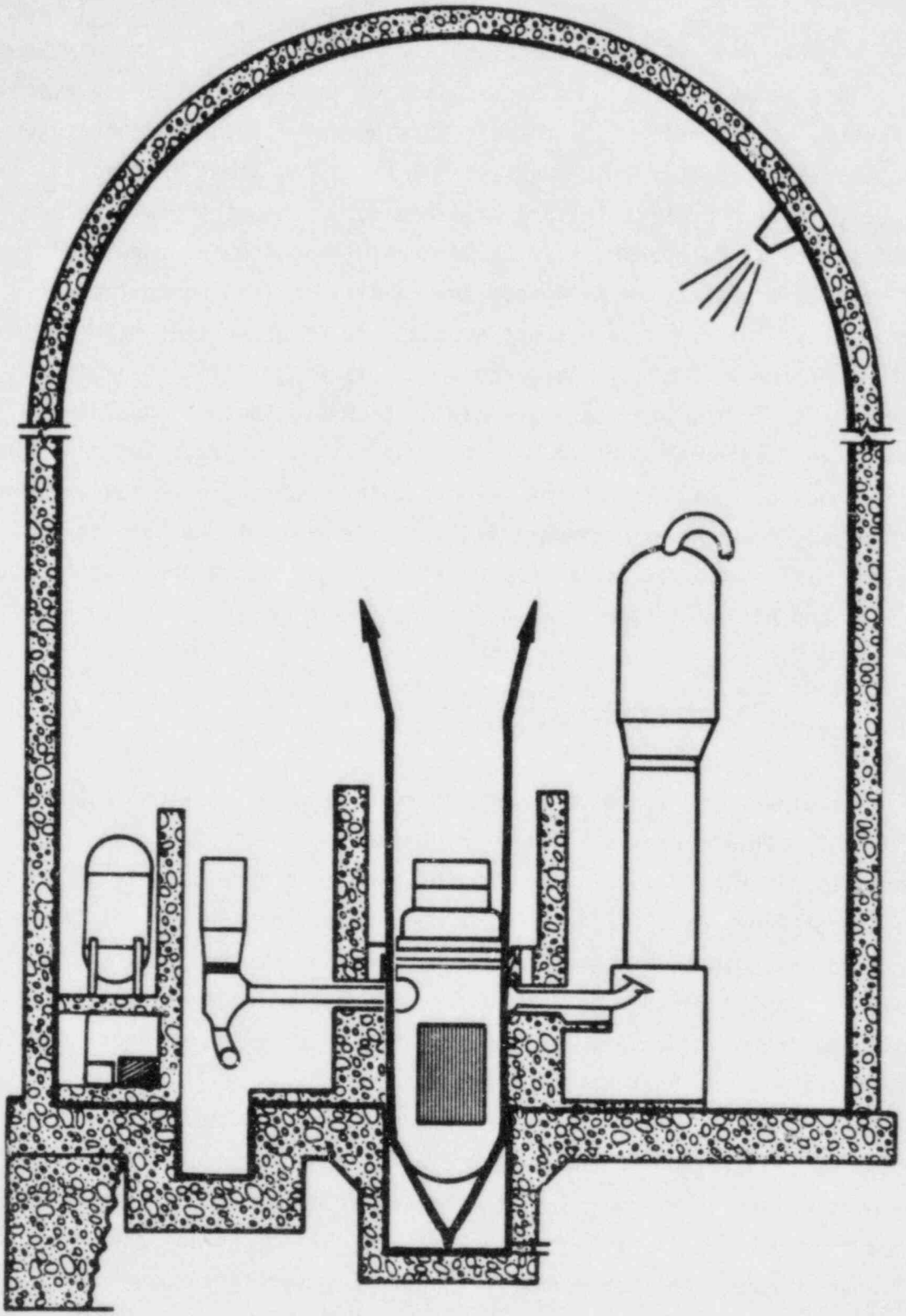

FIGURE 4.4. FLOW PATH FOR VAPORIZATION RELEASE

The case of containment isolation failure (β) is one of the modes of failure examined. For the Surry plant the probability of isolation failure is quite small since the plant is operated with the containment pressure significantly less than atmospheric. For other PWR designs this may be a major potential failure mode however. The other two failure modes examined are early overpressure failure resulting from hydrogen combustion and delayed overpressure failure. The conditions leading to the early overpressure failure mode are not expected to occur in this sequence. Because of the potentially large consequences of this failure mode and the uncertainity in the processes associated with the failure mode, the associated fission product release was evaluated. Delayed overpressure failure and melt-through of the basemat without aboveground failure are the most likely modes of containment failure. Because of the long delay to failure, the consequences of these two modes of failure are expected to be similar and differ primarily in the magnitude of noble gas release.

4.2.2 Sequence TMLB' (Transient, Loss of Primary System Heat Removal)

The TMLB' sequence was found to be a major risk contributor in WASH 1400. The predicted release fractions for the containment overpressurization failure mode for this sequence were used to characterize release category PWR 2. The reactor coolant system behavior of TMLB' is in sharp contract to AB because the reactor coolant system pressure remains elevated (~2500) during core heatup and fission product release. The beginning of core uncovery is also delayed for a few hours providing some time for the decay heat power to be reduced.

The flow path for fission products through the reactor coolant system is illustrated in Figure 4.5. Prior to core uncovery the water in the pressurizer is predicted to be carried from the pressurizer with the steam flow or to fall back into the hot leg during periods when the relief valve is closed. Another scenario is possible for this sequence which involves failure of the reactor pump seals and in this case behavior is expected to be similar to a cold leg break.

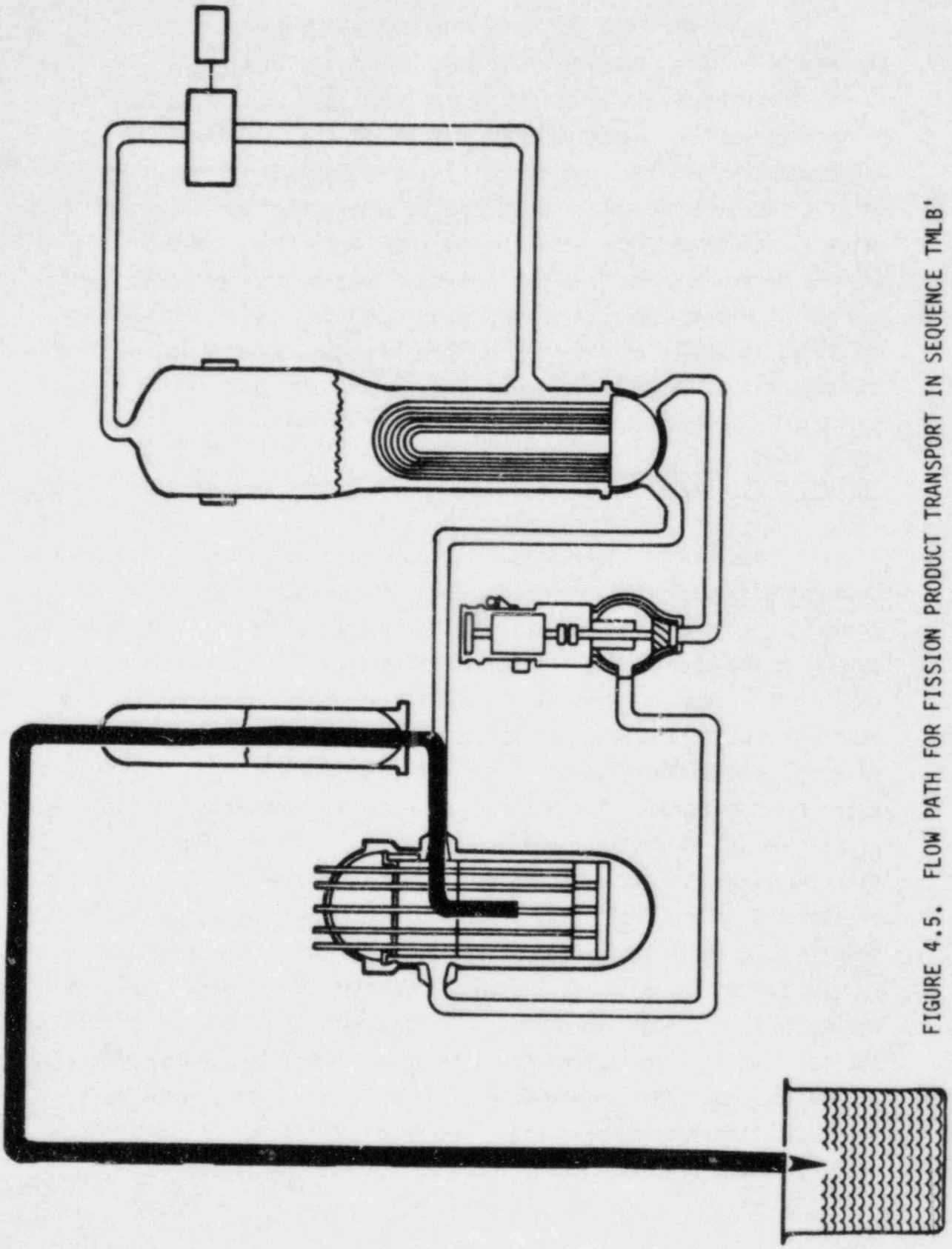

FIGURE 4.5. FLOW PATH FOR FISSION PRODUCT TRANSPORT IN SEQUENCE TMLB'

As in the AB case, containment sprays are assumed to be inoperable in this sequence. One objective for selecting the TMLB' case was to investigate the effect of containment failure time on fission product retention. Early and late failure of the containment by overpressurization are considered. The conditions which could lead to early failure of the containment involve interaction between molten core material and accumulator water in the reactor cavity. The magnitude of the ensuing pressure spike of steam depends on mixing and heat transfer processes that are uncertain. Although early failure is considered unlikely, it was felt that this failure mode should be evaluated because of the potentially large consequences associated with it.

4.2.3 Sequence S_2 D (Small Pipe, Failure of ECC System)

Because of the availability of containment cooling and the containment spray systems in this sequence, the expected release of fission products to the environment would be quite small. As a result, the contribution to the predicted public health risk would also be expected to be small. This type of event is comparatively likely, however, relative to other core melt sequences and is of interest for this reason. This is the only sequence analyzed in which the effectiveness of the containment safety features is examined. The behavior of hydrogen combustion in this case is of particular interest because steam inerting will not be present as in other sequences. Core meltdown occurs with elevated reactor coolant system pressure as in the TMLB' case but at slightly lower pressures and with leakage from the reactor coolant system augmented by the depressurization.

The flow path of fission products in the primary system is illustrated in Figure 4.6. Other possible flow paths to the break through the intact loops were considered to be sealed by water in the low points of the primary system. If the flow path through the two intact loops is also available, the residence time and retention of fission products in the primary system would be greater than for the case analyzed.

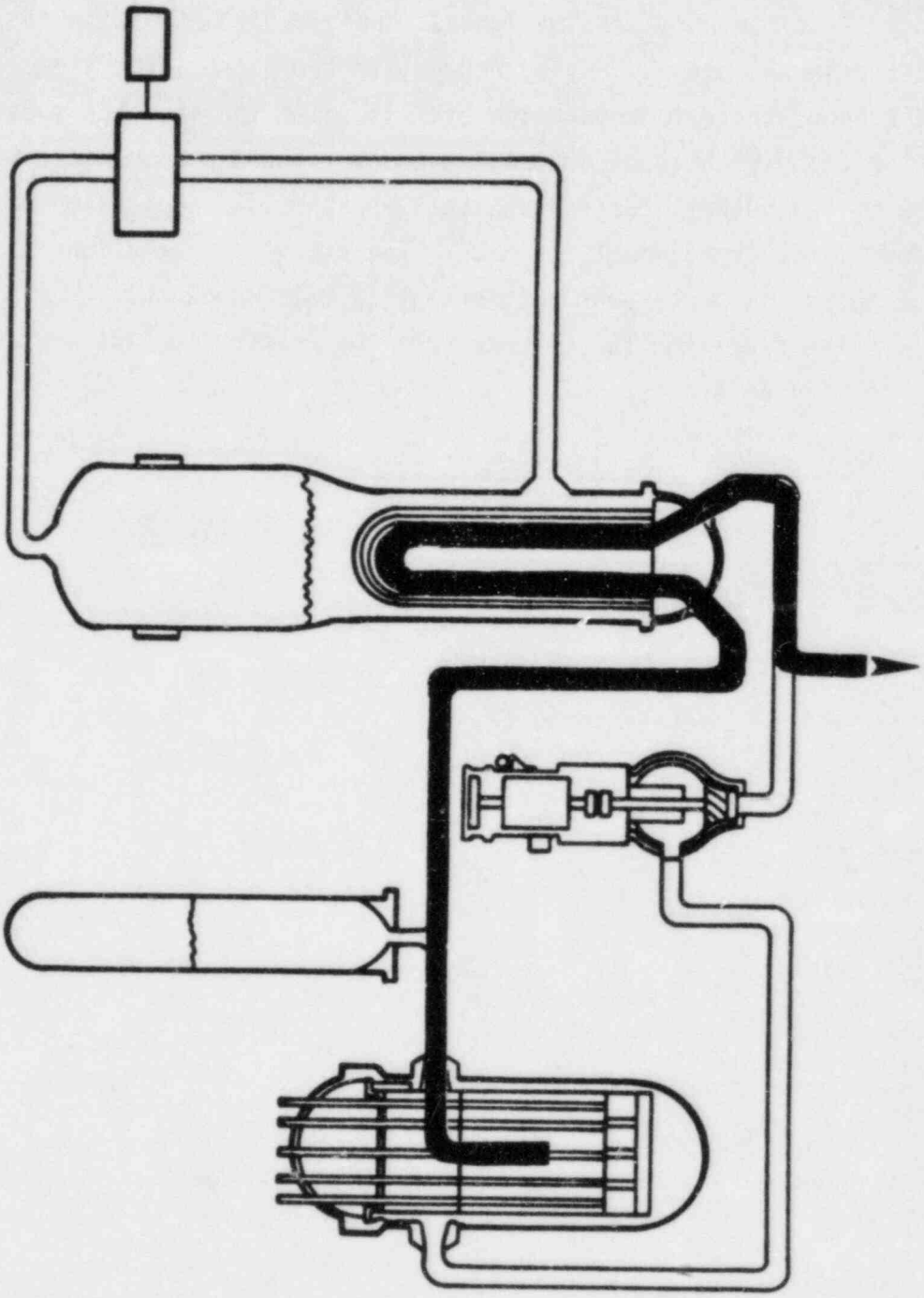

FIGURE 4.6. FLOW PATH FOR FISSION PRODUCTS IN SEQUENCES S_2D AND V

4.2.4 Sequence V (Interfacing Systems Loss of Coolant Accident)

This sequence was the largest individual contributor to risk identified in WASH 1400. Having recognized the potential system weakness, it has been possible to reduce the likelihood of the sequence substantially. The interfacing LOCA is of interest even at reduced probability, however, because of the pathway for release that bypasses the protection normally provided by the containment building. The amount of retention in the reactor coolant system is particularly important in this sequence.

The flow path for release from the reactor coolant system is illustrated in Figures 4.6 and 4.7.

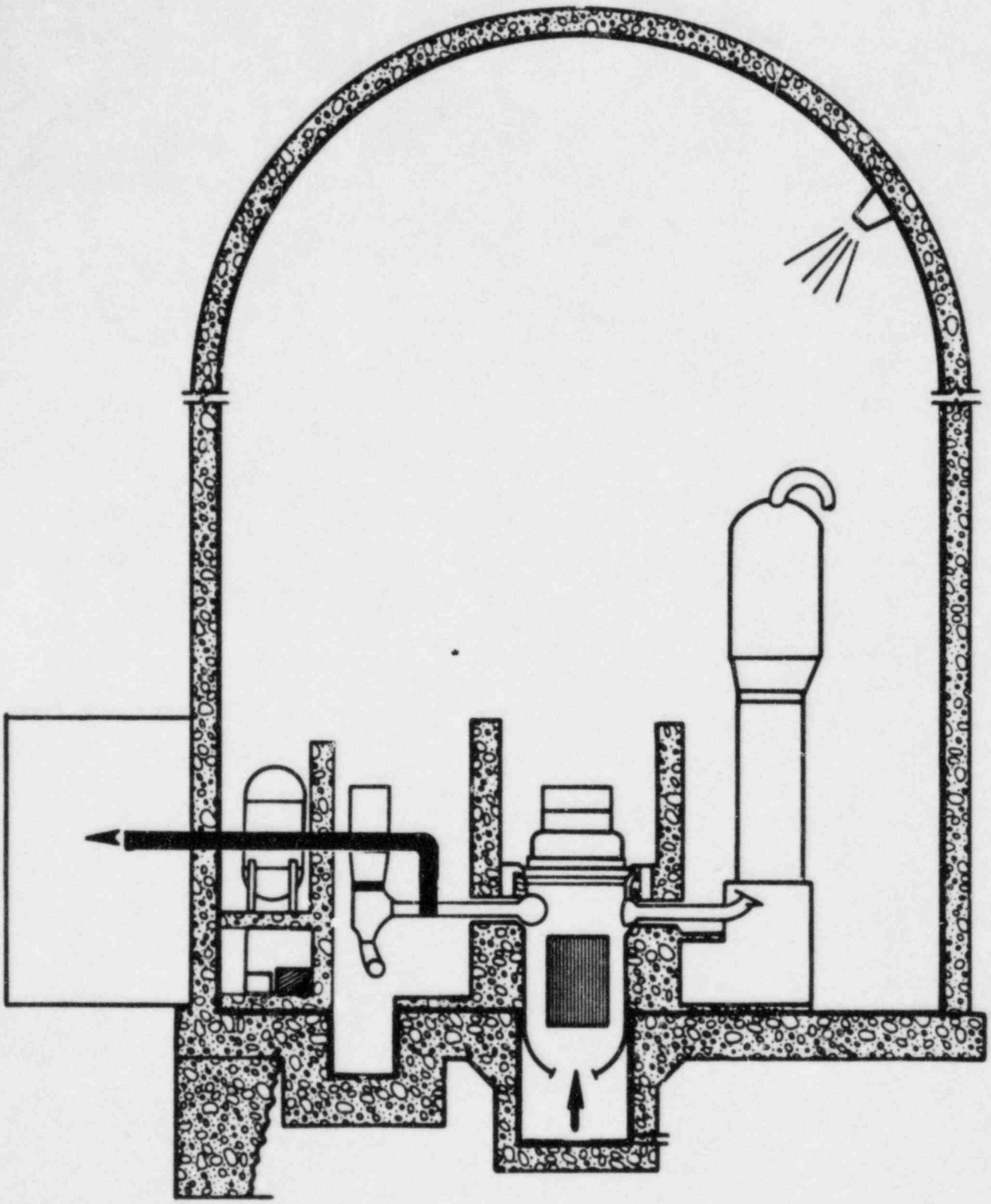

FIGURE 4.7. RELEASE PATHWAY TO SAFEGUARDS BUILDING IN SEQUENCE V

5. ANALYTICAL METHODS

5.1 Thermal-Hydraulic Behavior

This section provides descriptions of the computer codes MARCH 1.1[5.1] and MERGE[5.2] employed to analyze the thermal-hydraulic response of the reactor core, the primary coolant system and the containment system in light water reactors to the accident sequences previously described. An improved version of the MARCH code, MARCH 2, is currently under development and will be employed in the analyses of the containment designs examined later in this program. The principal differences that would be expected between results obtained if MARCH 2 had been used rather than MARCH 1.1 are a more rapid heatup (due to higher predicted decay heat levels), smoother flows in the reactor coolant system, and possibly greater production of hydrogen. All of the differences observed between MARCH 2 and MARCH 1.1 results to date have been within the uncertainties associated with the thermal-hydraulic analysis of core meltdown accidents. Brief descriptions of the MARCH 1.1 and MERGE computer codes follow. A more detailed description of the MERGE code is presented in Appendix A because of its development during the course of this program.

5.1.1 MARCH 1.1

The MARCH (Meltdown Accident Response CHaracteristics) code provides the analysis of the various thermal-hydraulic processes during reactor meltdown accidents. MARCH contains a number of interrelated and coupled subroutines each of which treats a particular process or phase of the accident. The principal subroutines are noted below. PRIMP evaluates the primary coolant system response including the pressure history and the coolant leakage. Models for secondary system heat transfer for PWRs and emergency core cooling system operation are incorporated in BOIL. These features are essential for the analysis of small break and transient accident sequences. BOIL is the only element of MARCH that was available at the time of the Reactor Safety Study.[5.3] The initial version of BOIL described the boiloff of water from the reactor vessel and the meltdown of

the core up to the point of core support failure; it assumed a large LOCA as the initiating event. The current version of BOIL provides continuous transitions for core collapse, grid plate failure, and the dropping of the core debris into the lower head of the reactor vessel; a number of user selected options are provided for these transitions. It should be noted that the BOIL subroutine in MARCH provides the essential reactor coolant system thermal-hydraulic input required in MERGE. HEAD evaluates failure of the reactor vessel head under the combined loads of the pressure in the vessel and the hydrostatic head of the core debris. Reduction in the strength of the head results from heating of the wall as well as penetration of the melt front. The HOTDROP subroutine describes the interaction of the core debris with water in the reactor cavity following vessel melt-through, including such effects as debris fragmentation, heat transfer, and chemical reactions. The interaction of the core debris with concrete is described by the INTER[5.4] code; the latter was written at Sandia National Laboratories and has been adapted and integrated by BCL into MARCH. The FPLOSS routine describes the release of the radionuclides from the fuel and partitions the heat source between the groups of fission products. The release assumptions made in FPLOSS are not consistent with the more recent data in the CORSOR code. FPLOSS is only used to follow the movement of sources of decay heat within the containment, however. The principal effect on the predicted environmental source term of radionuclides would result from slight differences in the heating rate of fuel near melting and following melting. Other uncertainties in the behavior of the fuel following melting and the approximate treatment of molten fuel behavior in MARCH have much greater significance. The MACE routine describes the containment temperature and pressure history taking into account nuclear heat generation, hydrogen burning, heat losses to structures, effects of containment safeguards, intecompartment flows, leakage to the outside, etc. MACE is continuously coupled to the other subroutines in MARCH. It may be noted that the MACE subroutine in MARCH provides the essential containment thermal-hydraulic input required in the fission product transport codes to be discussed later.

5.1.2 MERGE

At the time of the writing of the MERGE code, the existing computer codes which describe the thermal-hydraulic behavior of a core meltdown accident were not capable of analyzing the flow and temperatures in the volumes of the reactor coolant system downstream of the core in the pathway for release to the containment. In the "Technical Bases Report" on Fission Product Behavior,[5.5] which was undertaken by the NRC in 1981, analyses indicated that in at least some accident sequences, the retention of fission products in the reactor coolant system could be significant. In order to support the performance of more realistic analyses of fission product retention with the TRAP-MELT code, an effort was undertaken to write a simple stand-alone code, MERGE, which could be used to predict gas temperature, surface temperature, and flow within the RCS based upon the conditions of gases leaving the core as predicted by the MARCH code.

Before running MERGE, it is first necessary to perform a MARCH calculation. The output of MERGE is then used as input to the TRAP-MELT code. The MARCH output results used by MERGE are: the primary system pressure, the flow rate of hydrogen leaving the core, the flow rate of steam leaving the core and the average temperature of gases leaving the core. The MERGE analysis accounts for the conservation of mass by species and conservation of energy. It is assumed that the gases within a volume are well mixed and have the same temperature and that the pressure differential between volumes is negligible. The equations are solved with an explicit time difference scheme. At a particular time step, conditions within the first volume downstream of the core are calculated first and the solution proceeds from each volume to the next downstream volume. Knowing the initial conditions and inlet flow conditions for each volume, it is necessary to solve for the value of the outlet flow from the volume that yields the known pressure. Heat transfer between the flowing gas and structures is accounted for. Forced laminar, forced turbulent, and natural convection heat transfer coefficients are available depending on the appropriate regime. A radiative term is added to the coefficient. In addition radiative heat transfer from the core to the first structure is calculated based on a MARCH calculated radiative flux.

The user of MERGE should be aware of some of the approximations and limitations of the code. In the MERGE analysis, it is assumed that the flow of gases in the upper plenum is one-dimensional. In reality, it would be expected that circulation patterns would be established in this region due to the strong temperature gradients. Whether a more detailed analysis is required for this region must be determined based on the results of sensitivity studies with the TRAP-MELT code. The need for validation experiments must also be evaluated.

5.2 Radionuclide Release From Fuel

5.2.1 Source Within Pressure Vessel

CORSOR

CORSOR is a simple correlative code which provides estimates of aerosol and fission product release rates from the core during the period of core melting in a light water reactor. Quantifying the aerosol and fission product release from the core region is an important first step in the determination of the radionuclide source term for the containment during a hypothetical severe core damage accident. The timing of the release of various materials is an important influence on their retention in the reactor coolant system. This is because the timing of release determines which species emanating from the core will be available for interaction. The timing also determines the residence time of the released materials and the temperatures which they encounter in the RCS, since these are both dynamic parameters. Simplistic source terms, such as constant or linearly increasing release rates with concurrent releases for all radionuclides, may therefore lead to unrealistic estimates of radionuclide transport behavior.

The CORSOR program computes fission product and structural material release from the core as a function of time and temperature. The code is capable of considering up to 10 radial and 24 axial divisons of the core for a total of 240 nodes and 16 separate species. The basic flow chart for the CORSOR code is depicted in Figure 5.1. The initial inventories of various fission products are obtained from the program ORIGEN[5,6] and, in

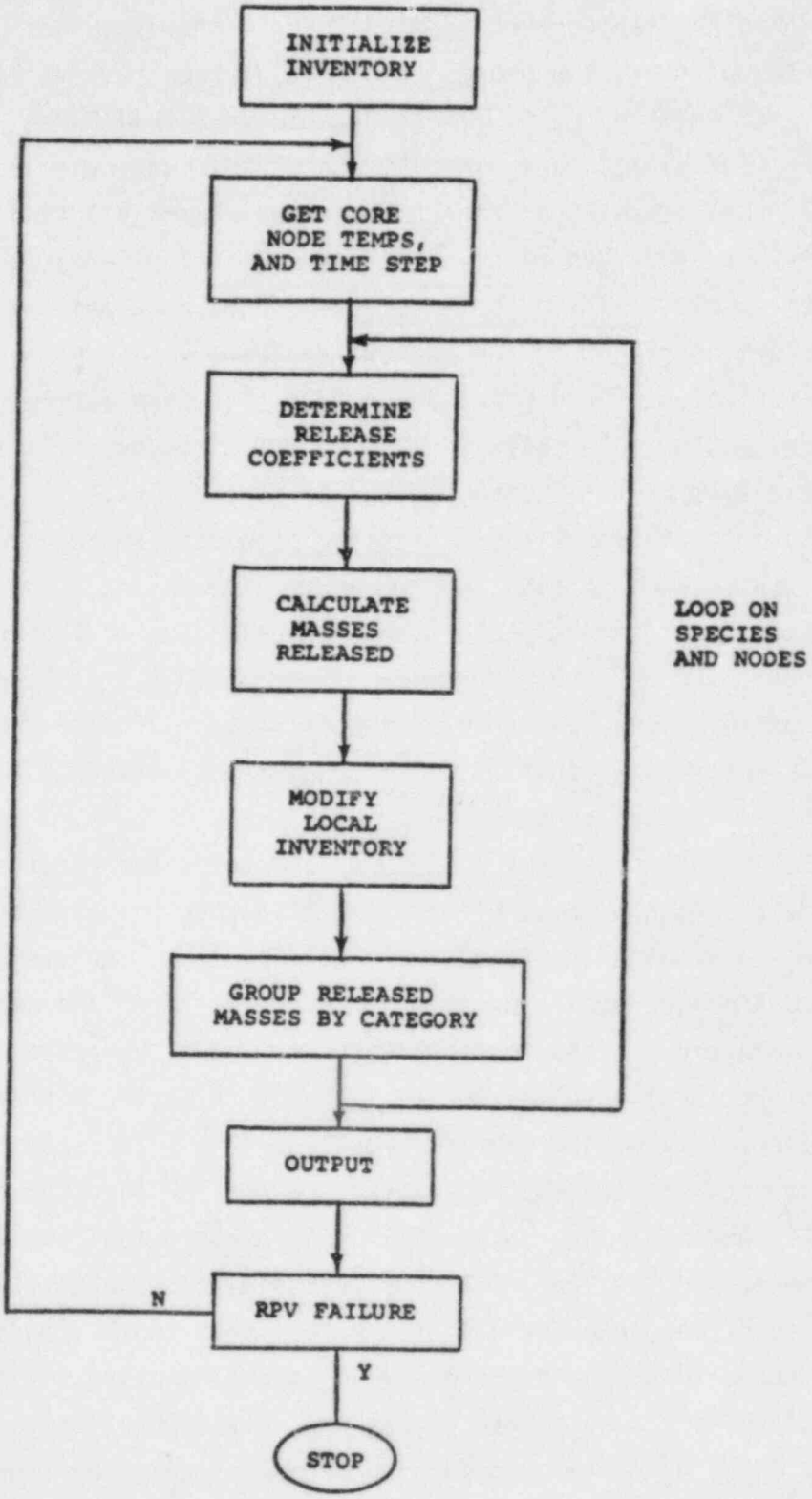

FIGURE 5.1. FLOW CHART OF THE CORSOR PROGRAM

this study, are apportioned among 120 core regions specified by axial height and radial displacement from the core centerline. In this study the inventories of fission products have been divided equally by fuel volume irrespective of position within the core. In an actual PWR the distribution would vary both axially and radially and would change with time. Typically in a PWR, fuel is shifted between three radial zones during its irradiation history. In order to flatten the power distribution across the core the freshest fuel is placed in the outside zone of the core and the most highly burned up fuel is placed in the central region. An abrupt change in the spatial distribution of radionuclides occurs therefore at the time of refueling but then continues to shift during the cycle as the fissile inventory is preferentially depleted in the regions of higher flux.

Alternate distributions of fission products can be used in the CORSOR program and the effect on fission product release rates of the "flat-flux" assumption can be quantitatively assessed by examination of the results of parametric studies such as those described in Appendix B. It is expected that uncertainties in the release rate coefficients will have a more significant effect on release rates than will the assumptions regarding fission product distribution among core regions.

Temperatures at each of the nodes are obtained from the MARCH code for each of a number of time steps beginning at the start of the accident and continuing to a user specified time. An average temperature is computed over each time span during core heatup and melting, and if the temperature is less than 900 C for any node, no release will occur from that node. The value, 900 C, is taken to be the average tempeature for failure of the cladding of a fuel rod.[5.5] The sensitivity of CORSOR release estimates to the temperature set for cladding failure is discussed in Appendix B. When any axial position in a fuel bundle achieves a temperature of 900 C, a gap release of certain volatile fission products is calculated by the code for all of the fuel rods in that radial zone. This is intended to simulate the gap release accompanying the bursting of individual fuel rods. This release occurs due to accumulation in the gap between fuel and cladding of certain fission products caused by migration within the fuel. The amount of the gap release is taken to be 5 percent of the initial amount present for cesium, 1.7 percent for iodine, 3 percent for the noble

fission gases, .01 percent for tellurium and antimony, and .0001 percent for barium and strontium. Since this emission is very small in comparison with the melt release, and is concurrent with the melt release, it is not treated separately in any of the transport analyses. Clearly, the gap release would require more careful analysis if less severe hypothetical accident conditions were considered.

Subsequent mass release as the nodes progress towards melting is calculated on a nodal basis as the product of the amount of each species remaining, the release rate coefficient, and the time interval of integration. The mass released is then summed over all the nodes in the core for each species to give a total mass released during the time step. It should be noted that the MARCH code predictions for core temperatures do not take into account the heat of vaporization of materials released from the core.

The computation of the fractional release rate coefficients for fission products is based on empirical correlations derived from experiments performed by Lorenz, Parker, Albrecht, and others.[5.7-5.13] The data from these experiments were graphed and curves developed as depicted in Figure 5.2. A fractional release rate coefficient, K(T), is derived for each species by fitting an equation of the form:

$$K(T) = Ae^{BT},$$

to correspond to each of these curves. The resulting values of A and B for three different temperature regions of the graph are given in Table 5.1 and are basically the same as those defined in Appendix B of the "Technical Bases Report" but have, in some cases, been adjusted to account for updated evaluations.[5.14] It should be noted that the fractional release rate is a function of temperature and elemental species only, and any effects of pressure and specific surface area of the melt on the release rate are not considered. Additionally, details of complex phase interactions of various components within the melting core are, for the most part, not known quantitatively and hence the release rates are valid only to the extent that the experiments upon which the release rates are based adequately modeled a core meltdown situation.

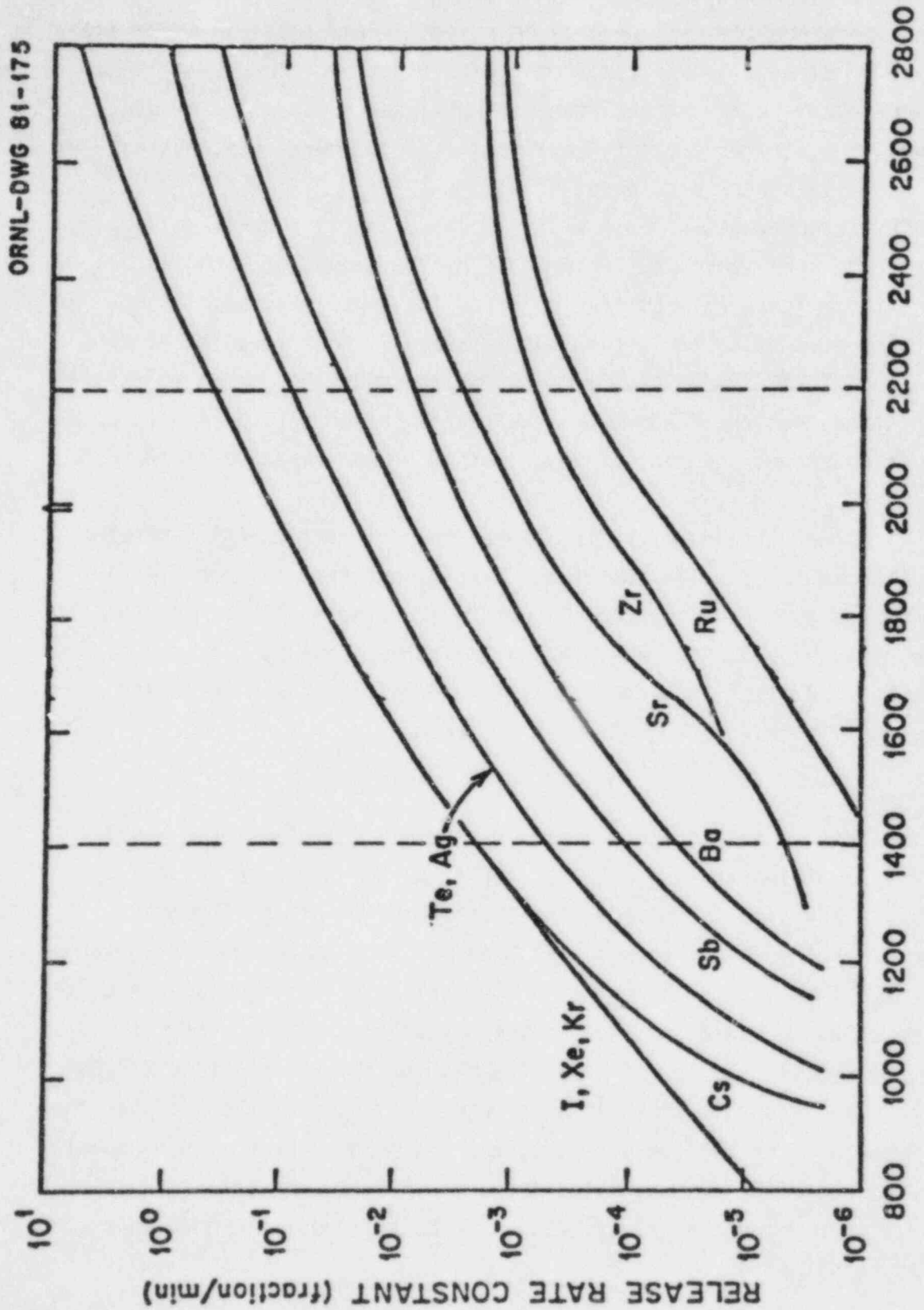

FIGURE 5.2. FISSION PRODUCT RELEASE RATE CONSTANTS FROM FUEL-SMOOTHED CURVES (Courtesy of R. Wichner, Oak Ridge National Laboratory)

TABLE 5.1. VALUES USED FOR THE CONSTANTS A AND B IN THE APPROXIMATION OF THE RELEASE RATE COEFFICIENTS, $K(T) = Ae^{BT}$

Fission product group	800°C < T ≤ 1400°C A	B	1400°C < T ≤ 2200°C A	B	T > 2200°C A	B
I, Xe, Kr	7.02E-09[a]	0.00886	2.02E-07	0.00667	1.74E-05	0.00460
Cs	7.53E-12	0.0142	2.02E-07	0.00667	1.74E-05	0.00460
Te, Ag	3.88E-12	0.0135	9.39E-08	0.00630	1.18E-05	0.00411
Sb	1.90E-12	0.0128	5.88E-09	0.00708	2.56E-06	0.00426
Ba	7.50E-14	0.0144	8.26E-09	0.00631	1.38E-05	0.00290
Mo	5.01E-12	0.0115	5.93E-08	0.00523	3.70E-05	0.00200
Sr	2.74E-08	0.00360	2.78E-11	0.00853	9.00E-07	0.00370
Zr[b]	6.64E-12	0.00631	6.64E-12	0.00631	1.48E-07	0.00177
Ru	1.36E-11	0.00768	1.36E-11	0.00768	1.40E-06	0.00248
Fuel[b]	5.00E-13	0.00768	5.00E-13	0.00768	5.00E-13	0.00768
Cladding[b] (Zr)	6.64E-12	0.00631	6.64E-12	0.00631	1.48E-07	0.00177
(Sn)	1.90E-12	0.0128	5.88E-09	0.00708	2.56E-06	0.00426
Structure[b]	6.64E-10	0.00631	6.64E-10	0.00631	1.48E-05	0.00177

[a] 7.02E-09 denoted 7.02×10^{-9}.

[b] The values for A and B for these elements were altered from the Technical Bases Report. See discussion in text.

There are several uncertainties associated with the CORSOR predictions which are not immediately apparent. These uncertainties most strongly impact the predicted aerosol release rates, rather than the more volatile materials whose releases are less sensitive. One difficulty in predicting aerosol release is due to the fact that as the core melting progresses, the temperatures increase throughout the core until, eventually, a loss of geometry would be expected to occur. There is no means currently available of predicting the manner in which this will occur. The assumption used in the MARCH code is that the entire core will slump at the time 75 percent of the nodes in the core are molten. The core is presumed to be quenched by the water remaining in the lower plenum at this time, resulting in a very much reduced rate of aerosol generation. In CORSOR this phenomenon is simply simulated by halting the release of all materials at the time of core slumping. No subsequent release is considered in these analyses until the core-concrete interactions begin.

The behavior of the control rods during core melting is also a source of uncertainty with respect to aerosol generation. In the sequences modeled here the rods are fully inserted into the core, and it is assumed that these rods are at the same temperatures as the core node in which they reside. Thus the release of control rod materials is simulated in CORSOR by the addition of the tin and steel to the inventory of materials available for release. The burnable poison rods are not considered as a source of aerosol material though it is understood that the boron present in these may play a role in aerosol formation. No release rate information is available for the cadmium in the control rods, and this material may be a significant contributor to the total aerosol mass. In the analyses presented in this document, the silver contained in the control rods has been treated as not being available for aerosol generation. This is an important consideration since release of this silver, at the rates specified for the fission product (fuel rod) silver, would enhance the aerosol production greatly. In the case of the TMLB' sequence considered here, for example, the increase in aerosol mass generation which would be caused by this silver is by a factor of approximately three. Preliminary experimental evidence suggests that when the control rods burst, the liquefied silver will be expelled from the rods and will form a solution with the zirconium cladding which

has a lower vapor pressure and thereby greatly reduces the participation of silver in the aerosol formation. The potential importance of the control rods as a source of aerosol early in the melt period, and the considerable uncertainties which exist regarding their failure mode and subsequent behavior make them worthy candidates for continued experimental investigation.

One further point regarding the calculation of release rate coefficients should be noted here. During core melting, the MARCH code predicts instances of core nodal temperatures above the UO_2 melting point which are not regarded as being realistic. The use of these high values in the expression for the release rate coefficients would lead to excessively high estimates of release rates for the lower volatility materials. The release rates calculated in this work therefore are calculated using a temperature value of 2760 C in place of any values predicted by MARCH in excess of this value. This selection of a maximum temperature was based upon the approximate UO_2 melting temperature of 2880 C.[5.15] The "Technical Bases Report" states that the melting point of UO_2 may be lowered by up to 300 C with the addition of ZrO_2, and even lower with other compounds, such as control rod material. Thus, it is not clear at present what this maximum achievable temperature should be. Appendix B considers the sensitivity of the CORSOR predictions to uncertainties in the maximum temperature, as well as core temperature values and release rate coefficients employed in the calculations.

5.2.2 Source from Melt-Concrete Interactions

The release of fission products and nonradioactive aerosols during the interactions of molten core materials with concrete plays an important role in determining the risk of severe reactor accidents. Aerosol production and fission product release from core debris outside the reactor vessel can persist for many hours. The aerosols produced in this way do not usually have to traverse a convoluted pathway before they enter the reactor containment as do aerosols produced in the reactor vessel. The accentuated inventory of aerosols in the reactor containment brought on by ex-vessel core debris interactions could lead to rapid agglomeration and settling of the condensed

fission products released during the in-vessel phases of an accident. If containment failure is delayed, the primary source of radioactivity released to the environment would come from the ex-vessel sources.

Release of fission products from core debris interacting with concrete can compensate for any inhibition in the release of volatile species during the in-vessel phase of an accident. This compensation arises because gases from the thermal decomposition of concrete that sparge through the melt drive the release processes. Ex-vessel processes can also lead to the release of fission product elements that are ordinarily quite refractory. This, again, is because of the strong driving force produced by gas sparging and the unusual melt chemistry that arises during ex-vessel interactions of core debris with concrete.

Also of importance is the generation of aerosols from nonradioactive materials such as concrete and steel during ex-vessel interactions. The additional concentrations of suspended particulate in the containment brought on by these aerosols act to mitigate naturally the inventory of radioactivity released from the fuel that would then be available for release to the environment. This additional material, on the other hand, poses yet another threat to equipment in containment whose performance is degraded by the presence of aerosols.

A mechanistic model of fission product release and aerosol generation during core debris interactions with concrete was used in this work. This model was based on observation from experiments involving high temperature melts on concrete and information from analogous industrial processes. Two broad mechanisms of aerosol formation are considered in the model-vaporization of melt species accentuated by gas sparging and mechanical formation of aerosols by violent agitation of the molten debris sparged with concrete decomposition gases. Vaporization processes are responsible for the most intense aerosol generation during ex-vessel core debris interactions. Mechanical processes provide a mechanism for aerosol formation that persists even when debris temperatures are so low little vaporization of species in the debris can occur.

The model used as input predictions of melt temperature, concrete erosion rate, and gas generation rate from the CORCON model of melt-concrete interactions. It computes the thermochemical limits of vaporization from

the melt. Then, it compares the extent of vaporization recognizing kinetic barriers, such as mass transport, to the approach to the thermochemical limits. Mechanical aerosol generation is estimated by analogy to experimental data with simulant systems.

More complete descriptions of the model are to be found in Appendix C. Results of accident calculations for the AB, AB-tellurium, V, S_2D, and TMLB' sequences are also collected in this appendix. These results include aerosol mass generation rates, material density, aerosol composition, and mean aerosol particle size. Some of the more important uncertainties in these predictions are also described in the appendix.

5.3 Radionuclide Transport and Deposition

5.3 1 Transport in Reactor Coolant System

TRAP-MELT

The TRAP-MELT code that was used for the primary system radionuclide transport analyses of this study is an extensively developed version of the published[5.16] TRAP-MELT code used for NUREG-0772.[5.5] Major changes were made in the treatment of aerosol particle transport and behavior and in radionuclide condensation on and evaporation from particles. In addition, the internal data base of the code was increased to include physical properties data for tellurium and cesium hydroxide. An outline of the code, highlighting these changes, is given below. A more detailed description is given in Appendix D.

The TRAP-MELT model is designed to treat radionuclide transport in an arbitrary flow system whose thermal hydraulic conditions as functions of time are given. For the analyses of this study, for example, such data as are needed by TRAP-MELT to sufficiently define the thermal hydraulic conditions of the primary system investigated, were generated by the MERGE code which is described elsewhere in this report. In addition, TRAP-MELT requires the definition of source terms for each radionuclide to be considered. These terms were developed by the CORSOR code for the present study and this code is also described elsewhere in this report.

Once the flow system to be investigated is defined, it is subdivided into a series of control volumes that can, in principle, be arbitrary in number and flow connections and that are chosen on the basis of characteristic geometry, thermal hydraulic conditions and suspected significant radionuclide behavior -- such as change of phase, agglomeration, or deposition. Radionuclides in each control volume are assigned, with uniform distribution, to one of two carriers: the wall surfaces and the gas phase. Each radionuclide is allowed to reside on these carriers in either particulate (liquid or solid) or vapor form so that by combining carrier with form in the concept of "state", the condition of a radionuclide in a given control volume is completely determined by its state. TRAP-MELT thus considers the five states:

- Carrier gas, vapor
- Carrier gas, particle
- Wall surface, vapor
- Wall surface, particle
- Wall surface, chemisorbed vapor.

This list of states is not necessarily exhaustive (for instance, for two-phase flow, the carrier water must be considered) and the logic of the code has been chosen to readily accept an arbitrary number of states.

Radionuclide transport can occur among the five states of an individual control volume or between certain states of different control volumes if these are connected by fluid flow. The former types of transport are modeled or correlated in the code itself. The latter are assumed to occur in phase with the fluid flow as developed by codes such as MERGE and imposed on the system. Sources of radionuclides to the system may occur in any volume and any state and must be read into the code as mass rate functions of time.

At present, the intravolume transport mechanisms contained in TRAP-MELT are:

- Competitive condensation on, or evaporation from wall surfaces and particles of the species cesium iodide, cesium hydroxide, and tellurium
- Irreversible sorption of molecular iodine, cesium hydroxide, and tellurium on stainless steel surfaces
- Particle deposition on surfaces due to
  - Settling
  - Diffusion from laminar and turbulent flow
  - Inertial impaction from turbulent flow
  - Thermophoresis.

Particle transport (and evaporation/condensation from/on particles) depends on particle size. This is taken into account in TRAP-MELT by considering a discretized particle size distribution that is subject to change, in each volume, by the deposition processes themselves, by possible particle sources, by flow of particles from other volumes, by flow of particles out of the volume in question and by agglomeration. The last can be due to many mechanisms. TRAP-MELT considers the following agglomeration mechanisms:

- Brownian
- Gravitational
- Turbulent (shear and inertial).

The system of first order differential equations that results from consideration of the above listed transport mechanisms is conveniently split into three classes from considerations of stiffness as well as linearity. Most of the deposition mechanisms (transfer from gas to wall surface carrier) are first order in the concentration of radionuclide species on the carrier from which the transfer occurs. They constitute the first class, whose transport scheme can be written in the form:

$$\frac{dC}{dt} = S + MC, \qquad (5.1)$$

where C is the concentration vector of the species in question for each state and volume, S is the source rate vector for each state and volume and M is the transport matrix between all states and volumes. Because the

deposition terms are taken as first order, M is independent of C and depends, with S, on time only. It is thus possible to solve Equation (5.1) as a set of first order differential equations with constant coefficients by standard techniques. This is done in TRAP-MELT for the class of linear mechanisms. Condensation and evaporation, which have a much shorter time constant than the linear processes, constitute the second class and are treated outside this framework but in parallel to it, as is particle agglomeration, which constitutes the third class of mechanisms in the TRAP-MELT code.

The philosophy of this parallel treatment is as follows: Equation set (5.1) is taken as the master time translation operation of the radionuclide system. Time stepping is adjusted so that S and M change little over a time step and that the time step does not exceed one-third the smallest flow residence time for any control volume. The latter assures that the system does not translate excessively between couplings to the other two classes of mechanisms. In addition, the characteristic coagulation time for the aerosol in each volume is evaluated and compared to the master time step. If the former is short compared to the latter, the master time step is appropriately reduced.

At the beginning of each time step, phase transitions of radionuclides are effected by examining each control volume in turn and solving the molecular mass transport equations for vapor transport among the gas phase, particles, and wall surfaces. Because of the low heats of vaporization of the radionuclides in question, this is done isothermally. Transfer to the walls assumes the Dittus-Boelter[5.17] correlation for pipe flow; transfer to the particles is by diffusion based on the size distribution present at the beginning of the time step. Redistribution of the vapor phase occurs in a time small compared to the master time step and therefore essentially decouples from the other processes considered. This justifies the time parallel solution treatment.

Once redistribution of the vapor phase has been effected, its effect on the existing particle size distribution (in the volume in question) is calculated by assuming each size class to gain (or lose) mass in proportion to the rate of vapor transfer to (from) that size class. Conservation of number for each size class then dictates redistribution among,

in general, two new contiguous size classes with distribution among these determined by mass conservation.

At the end of a time step, the particle size distribution in each volume is re-evaluated over that time step as a consequence of possible particle agglomeration, sources, and flow terms. The agglomeration algorithm has been excerpted from the QUICK[5.18] aerosol behavior code which is based on a size discretization scheme.

The approximations inherent in this parallel treatment are minimized by relegating mass redistribution and conservation to the master Equation (5.1) (except for redistribution due to radionuclide phase change). Agglomeration and particle evaporation/condensation serve only to modify the particle size distribution and therefore affect particle deposition indirectly through mass distribution averaged deposition velocities. Thus the aerosol aspect is solved (over a master time step) completely in parallel to Equation (5.1), using all sources flow terms and particle removal terms evaluated for each size class considered. The resultant distribution is used to evaluate average particle deposition terms for use in the master equation only. Similarly, re-evaluation of the particle size distribution due to radionuclide phase change affects these average deposition terms only.

In addition to the time-dependent thermal hydraulic conditions and mass input rates (source) by species, the TRAP-MELT code requires input information on initial particle size distribution of the source, control volume geometry, and physical properties of species (including deposition velocities on surface materials). Output provided by the code is in terms of time and location dependent mass by species and state as well as size distribution of suspended particulate material.

There are a number of uncertainties which affect the TRAP-MELT code predictions of primary system retention of mateials. It is obvious that any errors or imprecisions in the input to the code will affect the quality of the results. This applies to the primary system thermal hydraulics as provided by the MERGE code and the core release rates determined by the CORSOR code. The extent of interaction among the materials released from the melting core is determined largely by the timing of their releases,

and this represents a less straightforward, but no less important potential effect on the code's results due to input inaccuracies.

The experimentally determined vapor deposition velocities for Te, CsOH, and I_2 on hot surfaces may not represent an accurate description of the process as it occurs in the RCS because of the imprecision in the available data and because the experimental systems employed may differ from the RCS conditions they were intended to simulate. Nevertheless, what data are available have been incorporated since these analyses are intended to reflect the state of the art. Additional uncertainties which affect the vapor deposition, as well as aerosol deposition, arise from potentially inadequate specifications of primary system geometry and flow patterns. These items are of particular concern in the upper plenum region of the PWR considered in these analyses. It will be clear in the analysis presented in this document that the upper plenum is a very important potential contributor to fission product retention in the primary system.

The disposition of materials suspended in the RCS at the time of core slumping or at RPV depressurization can have significant inpact on retention calculated for some of the sequences analyzed. This is because a portion of the fission products and aerosol emitted from the core have not escaped the RCS at the time of core slumping, and are still available for injection into the containment. The large burst of steam which accompanies core slumping or depressurization on RPV failure will rapidly sweep out the RCS, and the very short transit time to the containment is expected to lead to minimal retention of these materials. Thus, in the analyses in this document, the material which is suspended in the RCS at the time of core slump or RPV failure is assumed to be injected into the containment as a "puff" release, with no further retention in the primary system.

The analyses in this document are subject to some uncertainties which may result in overprediction of the amount of retention which occurs in the primary system. A mechanism not included in the current analyses is the structure heatup due to decay heat from the deposited fission products. Such heatup of surfaces upon which are deposited species of intermediate volatility, e.g., CsI and CsOH, would lead to their re-evolution and transport through the RCS to regions of lower surface temperature or to the containment. Thus, the deposition of these species may be self limiting to

some extent. The analyses presented here also do not account for any resuspension of deposited materials during the vigorous flows through the RCS following core slumping in the lower plenum or during the depressurization which occurs at RPV failure during the S_2D and, particularly, the TMLB' sequences.

5.3.2 Transport in Containment

CORRAL 2

The CORRAL (Containment of Radionuclides Released After Loca) code describes fission product transport and deposition in containment systems of water-cooled reactors. CORRAL 2[5.19], the version used here, has been revised and generalized from the program written for the Reactor Safety Study[5.3] but retains the identical fission product removal mechanism descriptions and solution techniques. The containment is represented by up to 15 individual compartments connected in any combination of series or parallel arrangements. Radionuclide release into the containment by any of four release mechanisms for each of eight groups of fission products can be specified. The four release mechanisms are: gap (cladding rupture) release, fuel melting, fission product vaporization, and steam explosion (oxidation) release. The eight groups of radionuclides considered are: noble gases, molecular iodine, organic iodine, cesium-rubidium, tellurium, barium-strontium, ruthenium, and lathanum. Radionuclides can be removed from the atmosphere by particle settling, deposition, spray removal, pool scrubbing, filters, etc. Input requirements for CORRAL include: description of the containment system, engineered safeguards parameters, timing of accident events, thermodynamic conditions as a function of time, intercompartment flows, leakage rates, and fission product release component fractions. The code uses this input to continuously compute changing properties and fission product removal rates as a function of time. These values are used in incremental solutions to the coupled set of differential equations to obtain the time dependent fission product concentrations and accumulations in each compartment of the containment. The principal output consists of cumulative fractional releases

from containment with time for each of the fission product groups. The basic flow chart for CORRAL is shown in Figure 5.3.

NAUA-Mod 4

The NAUA code was developed at the Kernforshungszentrum Karlsruhe, West Germany, for calculating aerosol behavior in LWR core melt accidents.(5.20) It is based on mechanistic modeling of aerosol agglomeration and deposition within a containment vessel where thee may exist a condensing steam atmosphere. The model employed for steam condensation on particles was validated by small-scale experimental measurements(5.21) and larger scale validation is being planned.

The NAUA code calculates physical processes, excluding chemical changes and radioactive decay. The removal processes considered include gravitational settling and diffusional plateout. Interactive processes include Brownian and gravitational agglomeration and steam condensation. Aerosol sources and leakage are also included. Compositional changes which would result from time-dependent compositions for the input aerosol are tracked by the code.

The particle size distribution is defined by a number of monodisperse fractions. With this the governing integro-differential equation is transformed into a system of coupled first order differential equations. In effect, the particle size fractions interact and deposit according to the included mechanisms generating a time-dependent distribution of mass among the various size fractions. Steam condensation is handled in a separate integration. Output from the code includes mass concentrations of condensed water and dry aerosol materials airborne and on surfaces as well as particle size distributions at various times throughout the calculation.

Since the original version of the NAUA codes does not have any provision for engineered safeguard, calculations were made by adding the removal mechanism for aerosol particles due to spraying as follows:

$$\frac{dn}{dt} = -\varepsilon\pi R^2 N \, (V_g - v_g) n \qquad (5.2)$$

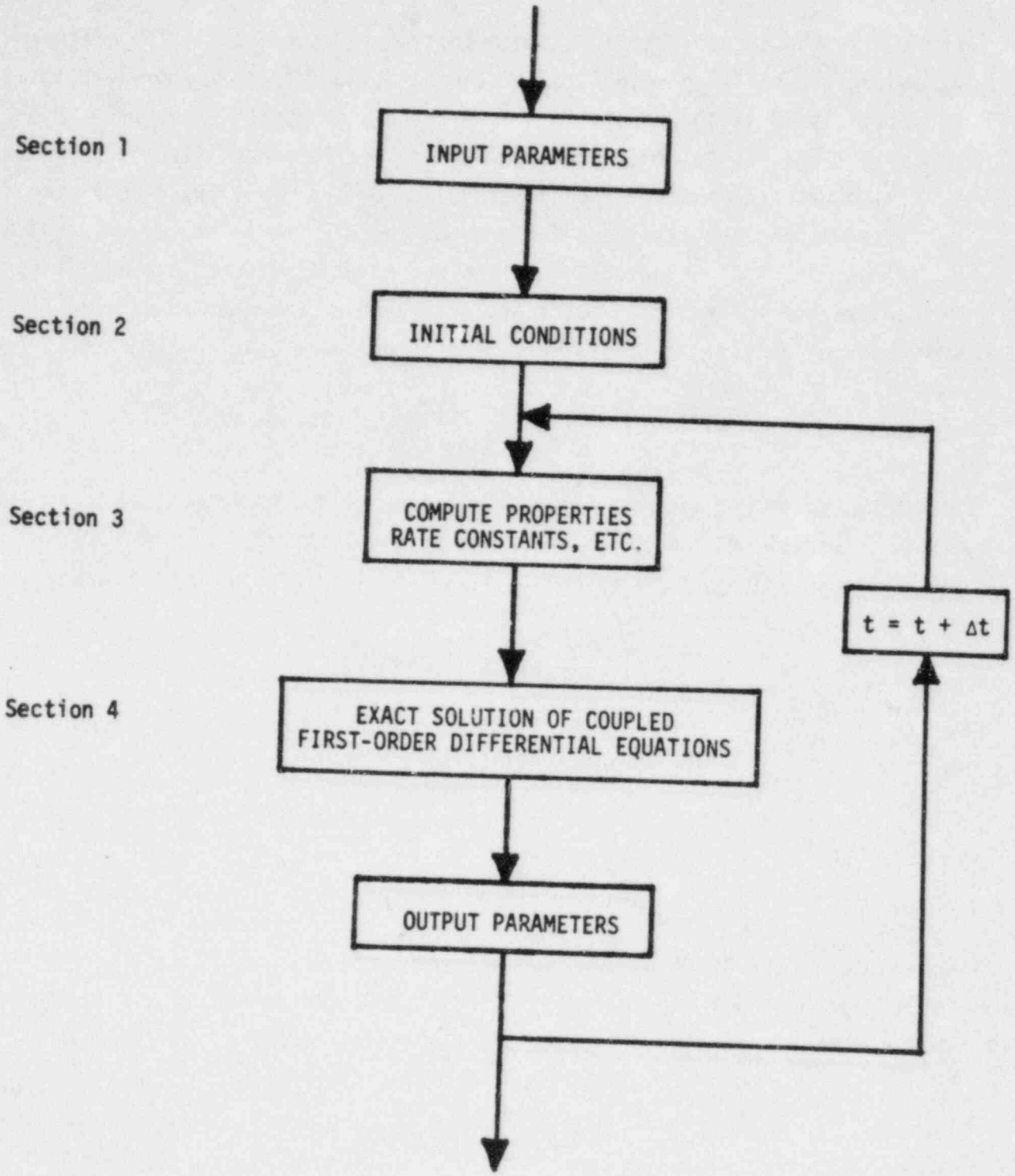

FIGURE 5.3. CORRAL CODE FLOW DIAGRAM

where n is the aerosol particle concentration, ε is the collision efficiency, V_g and v_g are settling velocities of the spraying drop and aerosol particles, respectively, R is the radius of the spraying drop and N is the water drop concentration. It is well known that due to hydrodynamic interaction between a falling water drop and airborne particles, only a small fraction of the particles within the cross section area of the water drop are removed by spraying. In order to account for this hydrodynamic effect, the collision mechanisms due to inertial impaction, interception, and due to Brownian diffusion of aerosol particles were used by defining ε in Equation (5.2) as:

$$\varepsilon = \varepsilon_I + \varepsilon_R + \varepsilon_D \tag{5.3}$$

where ε_I, ε_R and ε_D are the collision efficiency due to intertial impaction, interception, and Brownian diffusion, respectively. The following collision efficiency models were utilized for the three mechanisms.

$$\varepsilon_I = \frac{Stk^2}{(Stk + 0.35)^2} \tag{5.4}$$

$$\varepsilon_R = \frac{1.5(r/R)^2}{(1+r/R)^{1/3}} \tag{5.5}$$

$$\varepsilon_D = 3.5\ Pe^{-2/3} \tag{5.6}$$

where Stk is the Stokes number for aerosol particles based on a characteristic length of water drop radius R, r is the particle radius, Pe is the Peclet number. The Stokes number and the Peclet number are defined as

$$Stk = \frac{2\ r^2 \rho_p V_g C}{9\mu R}$$

$$Pe = \frac{2V_g R}{\bar{D}}$$

where $\bar{D}$ is the diffusion coefficient of aerosol particle

v_g is the settling velocity of water drop

C is the Cunningham slip correction factor

ρ_p is the particle density

μ is the gas viscosity.

In general, for relatively large particles, the inertial effects on the overall collision efficiency are larger than the interception term because the water drops are much larger than the aerosol particles. As particle size becomes smaller, the Brownian diffusion term will become increasingly important. It shcuild also be mentioned that Equation (5.4) is given by Hetsroni[5.22] and Equations (5.5) and (5.6) are based on the work of Lee and Gieseke[5.23, 5.24].

Another particle deposition mechanism called diffusiophoresis that results from steam condensation onto containment walls was added to the NAUA code. Diffusiophoresis involves two mechanisms -- a net flow of gas toward the wall surface known as Stephan flow and a molecular weight gradient caused by the steam concentration gradient. In general, the Stephan flow effects are much larger than those from the molecular weight gradient and result in deposition of particles on the wall surface. The condensation rate toward wall surfaces calculated by the MARCH code has been utilized to calculate deposition due to the diffusiophoresis mechanism. The result of a sample calculation activating this mechanism can be found in Section 7.3.1.

References

(5.1) Wooton, R. O. and Avci, H. I., "MARCH (Meltdown Accident Response Characteristics) Code Description and Users' Manual", NUREG/CR-1711, BMI-2064 (October, 1980).

(5.2) Freeman-Kelly, R., "A Users' Guide for MERGE", Battelle's Columbus Laboratories, October, 1982.

(5.3) U.S. Nuclear Regulatory Commission, "Reactor Safety Study -- An Assessment of Accident Risks in U.S. Commercial Nuclear Power Plants", WASH 1400 (NUREG-75/014), October, 1975.

(5.4) Murfin, W. B., "A Preliminary Model for Core-Concrete Interactions", SAND77-0370, Sandia National Laboratory, August, 1977.

(5.5) "Technical Basis for Estimating Fission Product Behavior During LWR Accidents", NUREG-0772 (June, 1981).

(5.6) Bell, M. J., "ORIGEN, The ORNL Isotope Generation and Depletion Code", ORNL-4628 (1973).

(5.7) Lorenz, R. A., et al, "Fission Product Release from Highly Irradiated LWR Fuel", NUREG/CR-0722 (1980).

(5.8) Lorenz, R. A., Collins, J. L., and Malinauskas, A. P., "Fission Product Source Terms for the LWR Loss-of-Coolant Accident", NUREG/CR-1288 (1980).

(5.9) Lorenz, R. A., et al, "Fission Product Release from Highly Irradiated LWR Fuel Heated to 1300-1600 C in Steam", NUREG/CR-1386 (1980).

(5.10) Lorenz, R. A., "Fission Product Release from BWR Fuel Under LOCA Conditions", NUREG/CR-1773 (1981).

(5.11) Parker, G. W., Martin, W. J., and Creek, G. E., "Effect of Time and Gas Velocity of Distribution of Fission Products from UO_2 Melted in a Tungsten Crucible in Helium", Nuclear Safety Program Semi-Annual Report for period ending June 30, 1963, ORNL-3483, 19-20 (1967).

(5.12) Albrecht, H., Matschoss, V., and Wild, H., "Experimental Investigation of Fission and Activation Product Release from LWR Fuel Rods at Temperatures Ranging from 1500-2800 C", proceedings of the Specialists' Meeting on the Behavior of Defected Zirconium Alloy Clad Ceramic Fuel in Water Cooled Reactors, 141-146 (September, 1979).

(5.13) Albrecht, H., Matschoss, V., and Wild, H., "Release of Fission and Activation Products During Light Water Reactor Core Meltdown", Nuclear Technology, 46, 559-565 (1979).

(5.14) Niemczyk, S. J. and McDowell-Boyer, L. M., "Technical Considerations Related to Interim Source Term Assumptions for Emergency Planning and Equipment Qualification", ORNL/TM-8275 (1982).

(5.15) Weast, Robert C., Ed., CRC Handbook of Chemistry and Physics, 59th Edition, (1978).

(5.16) Jordan, H., Gieseke, J. A., and Baybutt, P., "TRAP-MELT Users' Manual", NUREG/CR-0632, BMI-2017 (February, 1979).

(5.17) Geankoplis, C. J., "Mass Transport Phenomena", Holt, Rinehart, and Winston (1972).

(5.18) Jordan, H., Schumacher, P. M., and Gieseke, J. A., "QUICK Users' Manual", NUREG/CR-2105, BMI-2082 (April, 1981).

(5.19) Burian, R. J. and Wooton, R. O., "CORRAL-2 Users' Manual", Battelle's Columbus Laboratories (January, 1977).

(5.20) Bunz, H., Koyro, M., and Schock, W., "A Code for Calculating Aerosol Behavior in LWR Core Melt Accidents Code Description and Users' Manual".

(5.21) Schock, W., Bunz, H., and Koyro, M., "Messungen der Wasserdampfkondensation an Aerosolen unter LWR-un-falltypischen Bedingungen", KfK 3153 (August, 1981).

(5.22) Hetsroni, G., "Handbook of Multiphase Systems", McGraw Hill Book Company and Hemisphere Pub. Co. (1982).

(5.23) Lee, K. W. and Gieseke, J. A., J. Aerosol Science, 11, 335 (1980).

(5.24) Lee, K. W. and Gieseke, J. A., Environ. Sci. & Technol., 13, 446 (1979).

6. BASES FOR TRANSPORT CALCULATIONS

6.1 Plant Geometry and Thermal Hydraulic Conditions

The MARCH Code (Version 1.1) was operated for each of the four accident sequence analyzed. The results of the MARCH analyses are used as input for three aspects of the fission product release and transport calculations:

(1) The predicted time-dependent temperatures of the fuel are used by CORSOR to calculate fission product release.

(2) The primary system pressure and flow of steam and hydrogen from the core are input to MERGE to calculate primary system thermal-hydraulics.

(3) The thermal-hydraulic conditions in the containment building are input to the containment tansport codes.

A summary of important reactor characteristics, containment parameters, and MARCH options is presented in Table 6.1*.

One of the most significant areas of modeling uncertainty for thermal-hydraulic analysis for this study has been the behavior of the flow in the reactor coolant system in the pathway of release to the containment. In particular the conditions in the upper plenum and upper dome region are quite uncertain and could be expected to have a significant effect on the transport of radionuclides. The first problem in describing flow behavior in this region is in obtaining an adequate characterization of the structures. These structures are not described in detail in publicly available reports because of proprietary design features. It was therefore necessary to make some estimates of the total masses and surface areas of structures in this region. In addition, even if the geometries of these structures had been well known, there is significant uncertainty in what the flow patterns are in the upper plenum and dome and as a result how effectively

---

*All tables in this section of the report have been placed at the end of the section.

the flow reaches the available surfaces. In order to encompass possible thermal-hydraulic conditions, two representations of the effective structures were made. In the first case the upper plenum was represented as two serially connected volumes containing 45,360 kg (100,000 lb) of steel with an effective surface area of approximately 929 m^2 (10,000 ft^2). The current version of TRAP only considers one structure with a given surface to mass ratio within a volume. The sensitivity of results to this approximation will be investigated later in the program. Since some of the structures in the upper plenum are significantly more massive than others, the representation in the first case probably overestimates the effective heat capacity of the upper plenum mass. As a result, the temperature of the gases entering the hot leg is probably calculated to be cooler than would actually be expected. In the second case, the total mass of the upper plenum structures was taken to be 11,325 kg (25,000 lb) and the surface area 454.5 m^2 (5,000 ft^2). Table 6.2 provides the geometric representation of the reactor coolant system for each of the sequences analyzed. These values were estimated without the benefit of design drawings and should be considered representative rather than exact. Westinghouse Electric Corporation has subsequently provided details on the upper plenum geometry which will be used in later analyses.

In the following sections of the report, the results obtained with the MARCH and MERGE codes are described for each of the accident sequences. In Section 6.1.5, some of the uncertainties in the analyses and sensitivities to assumptions are discussed.

6.1.1 Sequence AB (Hot Leg)

A large pipe-break accident with failure of the active emergency core coolant injection system, as would result from total loss of AC power, would be expected to result in comparatively rapid core meltdown. This is because core uncovery would occur very early in the accident while the decay heat level is high. The total loss of electric power will also preclude the operation of containment safety features. Table 6.3 indicates the times of key events as predicted by the MARCH code for the input and modeling

assumptions utilized. Table 6.4 provides details of the core and primary system conditions for this sequence. Core uncovery, heatup, and melting would occur at low primary system pressure corresponding to the pressure of the containment. The temperature of selected fuel regions is illustrated as a function of time in Figure 6.1.

Prior to the accident, the piping and structures in the reactor coolant system would be in the temperature range of 290-315 C. Because heatup of the fuel and the release of fission products would occur at about 172 kPa (25 psia), these surfaces would be expected to be considerably superheated. In addition, because of the high boiloff rate (high decay heat level) and low density of gases in the primary system (low primary system pressure), the velocity of gases passing through the reactor coolant system would be high in comparison to other accident sequences. At the time of core uncovery, the velocity of steam in the upper plenum is estimated to be approximately 1/2 meter/sec (2 feet/sec). The total residence time in the system from leaving the core to exiting the break in the hot leg would be approximately 10 seconds. As the water level in the core drops, the production of steam decreases accordingly. Just prior to slumping into the lower plenum, most of the steam that is being generated is predicted to be reduced to hydrogen.

Temperatures in several volumes of the reactor coolant system are illustrated in Figures 6.2 and 6.3. The upper grid plate is predicted to melt under the combined heat load of the exiting gases and radiation from the top of the core. Based on a plug flow velocity, the Reynolds Number in the upper plenum is predicted to be in the range of 100-1000 indicating laminar flow. The Rayleigh Number is within the range of 10^7-10^9. Natural convection provides the principal mechanism for transferring heat from the hot gas to structures in the upper plenum. The maximum temperature of gases leaving the hot leg is estimated to be in the range of 500-1100 C depending on the representation of the upper plenum structures. A significant temperature difference, on the order of 250 C is predicted between the gas and structure temperatures in the upper plenum. A schematic of the gas flow path for AB (Case 1) is illustrated in Figure 6.4. A schematic of the gas

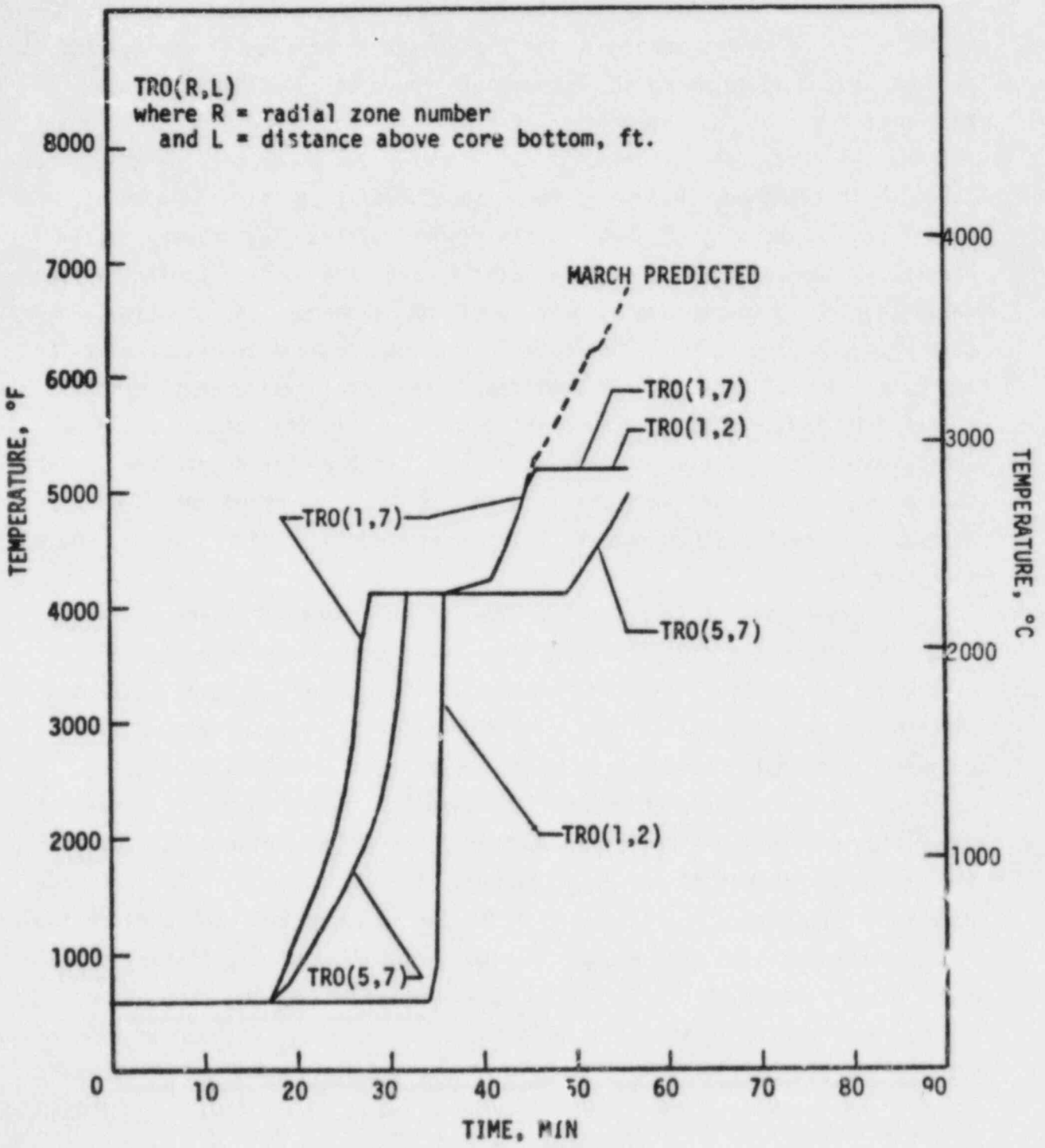

FIGURE 6.1. TEMPERATURES OF SELECTED FUEL REGIONS AS A FUNCTION OF TIME--SURRY ABHL SEQUENCE

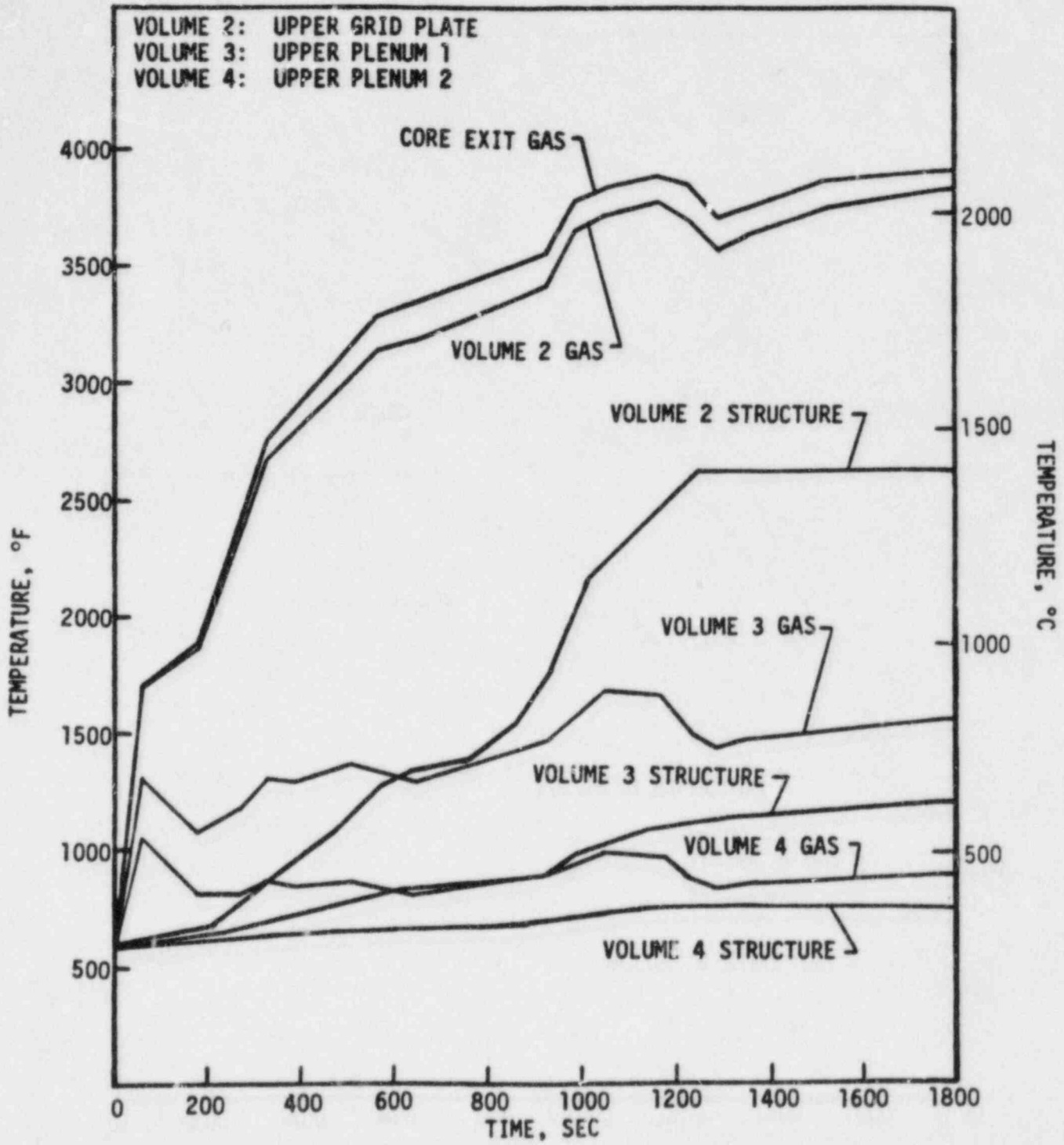

FIGURE 6.2. TEMPERATURES OF VOLUMES OF THE PRIMARY SYSTEM VERSUS TIME AFTER THE ONSET OF CORE MELTING--SURRY ABHL SEQUENCE (CASE 1)

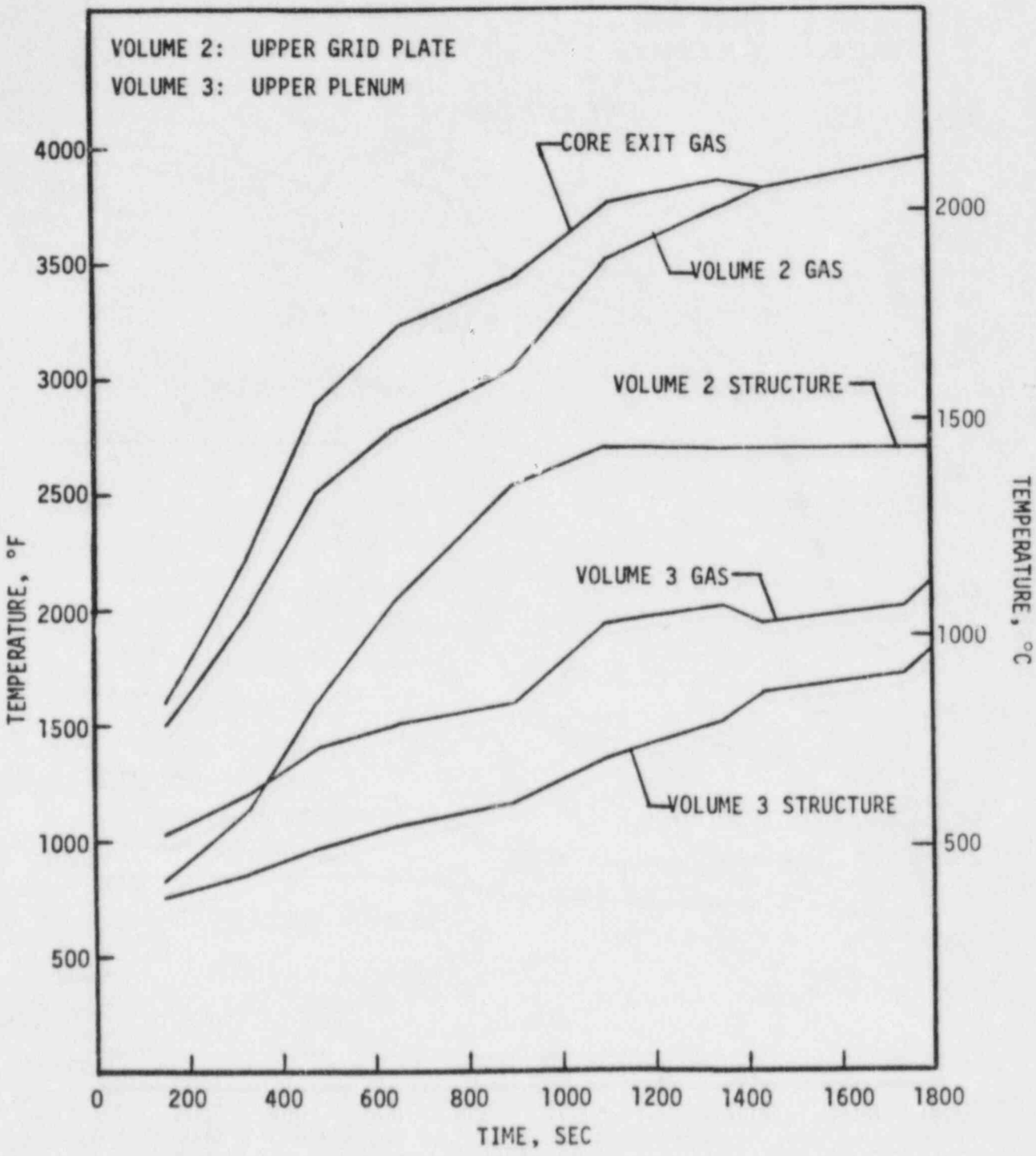

FIGURE 6.3. TEMPERATURES OF VOLUMES OF THE PRIMARY SYSTEM VERSUS TIME AFTER THE ONSET OF CORE MELTING--SURRY ABHL SEQUENCE (CASE 2)

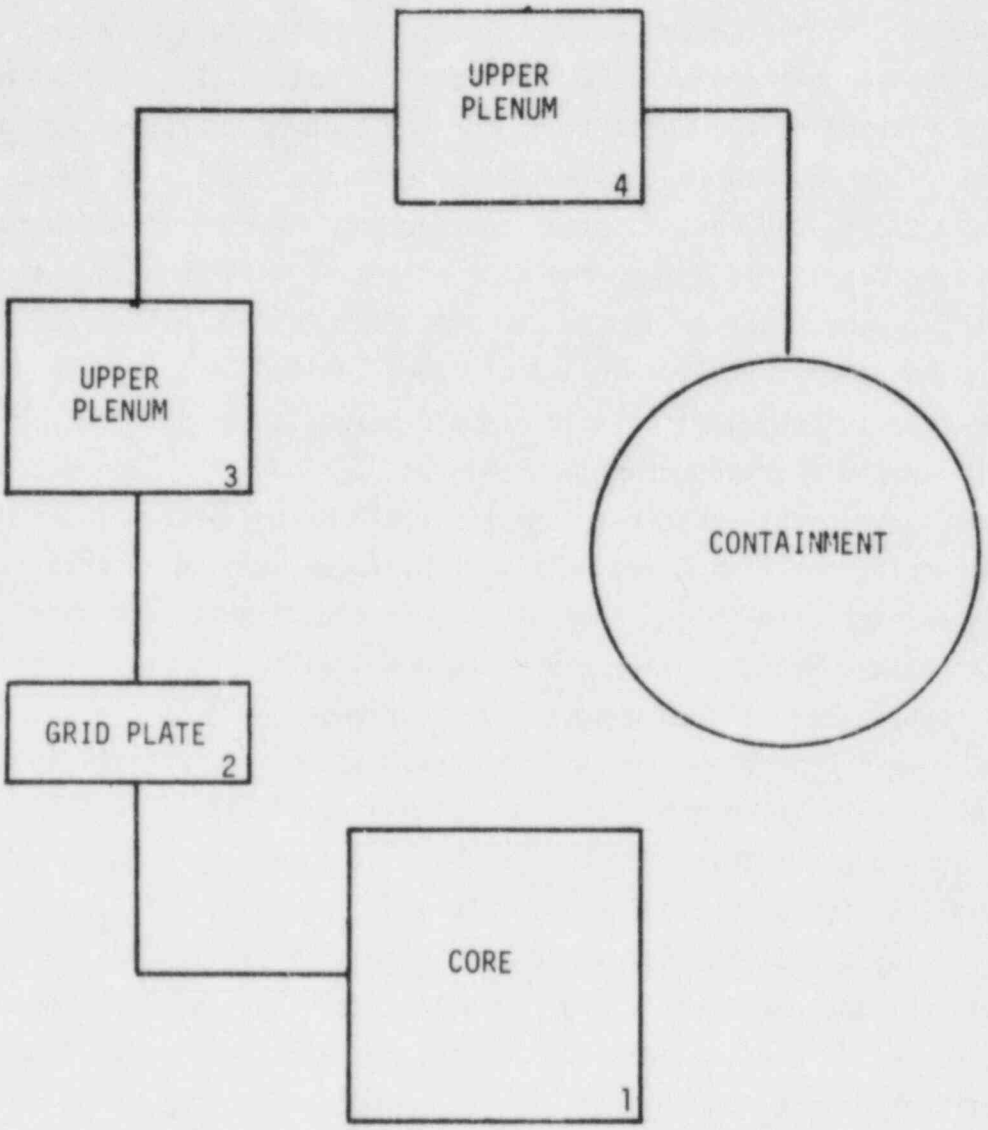

FIGURE 6.4. SCHEMATIC OF CONTROL VOLUMES FOR THE SURRY AB SEQUENCE (CASE 1)

flow path for AB (Case 2) would combine the two upper plenum volumes into one volume.

Four possible times and modes of containment failure have been investigated for this sequence: failure to isolate, early overpressure failure, delayed overpressure failure, and basemat melt-through. The pressure time history of the containment for the delayed overpressure case is illustrated in Figure 6.5. Table 6.5 presents the details of the containment response for the various cases considered. The earliest overpressure failure time considered was at the time of vessel melt-through. If the hydrogen from the reaction of the Zircaloy cladding with steam accumulated without burning up to this time and was then ignited, pressure levels sufficient to lead to containment failure could result. Such a large burn is reflected in the sharp pressure increase at 81 minutes in Figure 6.5. Different containment pressure responses would be predicted if the assumptions regarding the timing and extent of hydrogen burning were varied. It may be noted that the interaction of the hot core debris with water following head failure would provide a very strong ignition source. The likelihood of containment failure due to such a hydrogen burn (or any other event) would of course depend on the failure pressure utilized as well as magnitude of the pressure. The quantification of the probability of containment failure is not a part of this effort. If the containment were to survive such early challenges, failure due to long-term overpressurization would be significantly delayed. In the Surry design the reactor cavity and the containment sump are not connected. After reactor vessel penetration the principal driving force for pressurization would be the release of gases from the decomposition of the concrete. This is the mechanism that leads to the long-term pressurization and failure illustrated in Figure 6.5. Considering the length of time required to reach the assumed failure level of 0.69 MPa (100 psia), it is possible that overpressure failure could be preceded and precluded by basemat penetration.

Table 6.6 summarizes the containment leakages for the various cases considered derived from the MARCH results and used in the evaluation of the fission product release from containment.

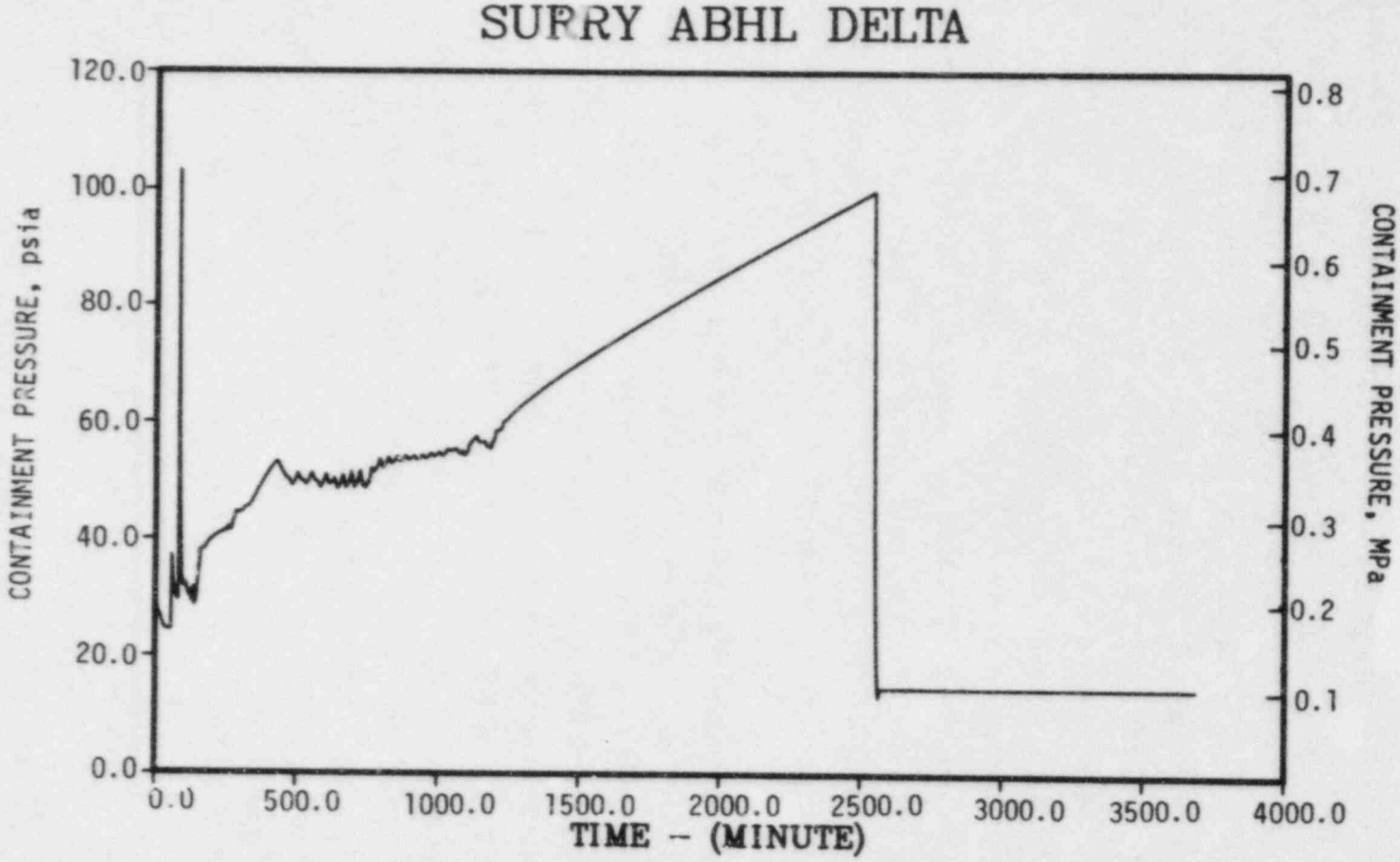

FIGURE 6.5. CONTAINMENT PRESSURE VERSUS TIME--AB SEQUENCE

6.1.2 Sequence TMLB'

In the transient sequence TMLB', ability to remove heat from the reactor coolant system is lost and containment safety features are not available due to loss of all electric power. Decay heating following reactor shutdown boils off the water in the secondary side of the steam generators. After steam generator dryout, the primary system pressure rises to the relief valve setpoint and reactor coolant is discharged through the relief line to the discharge tank and ultimately to the containment building. Table 6.3 indicates the times of key events as predicted by the MARCH code. Core and primary system conditions are given in Table 6.4. The temperature transient of selected fuel regions is illustrated in Figure 6.6. Core uncovery, heatup, and melting occur with the primary system pressure at approximately 17.24 MPa (2500 psia). Because of the high density of steam at this pressure, the flow velocity in the primary system would be quite small, approximately 1/2 cm/sec (1 foot/min).

The Reynolds Number in the upper plenum is predicted to be in the laminar regime as for the AB case assuming the plug flow velocity. The Rayleigh Number, however, is substantially larger in the range of 10^{11}-10^{14}. Thus, significant mixing could occur in the upper plenum driven by temperature gradients and the buoyancy of hydrogen. The temperatures of the gas and structures in the volumes of the primary system are illustrated in Figures 6.7 and 6.8. A schematic of the gas flow path for TMLB' (Case 1) is illustrated in Figure 6.9. A schematic of the gas flow path for TMLB' (Case 2) would combine the two upper plenum volumes into one volume.

The containment pressure time history for the TMLB' sequence is illustrated in Figure 6.10; additional details on containment conditions are given in Table 6.5. Two specific containment failure times were evaluated, an early and a late failure. The early failure was assumed to be the result of the rapid steam generation from the interaction of the core debris with accumulator water in the reactor cavity. Such an interaction is the cause of the rapid pressure rise at 276 minutes in Figure 6.10. The failure of the vessel bottom head releases the high pressure steam from the primary system to the containment as well as discharging the core debris into the

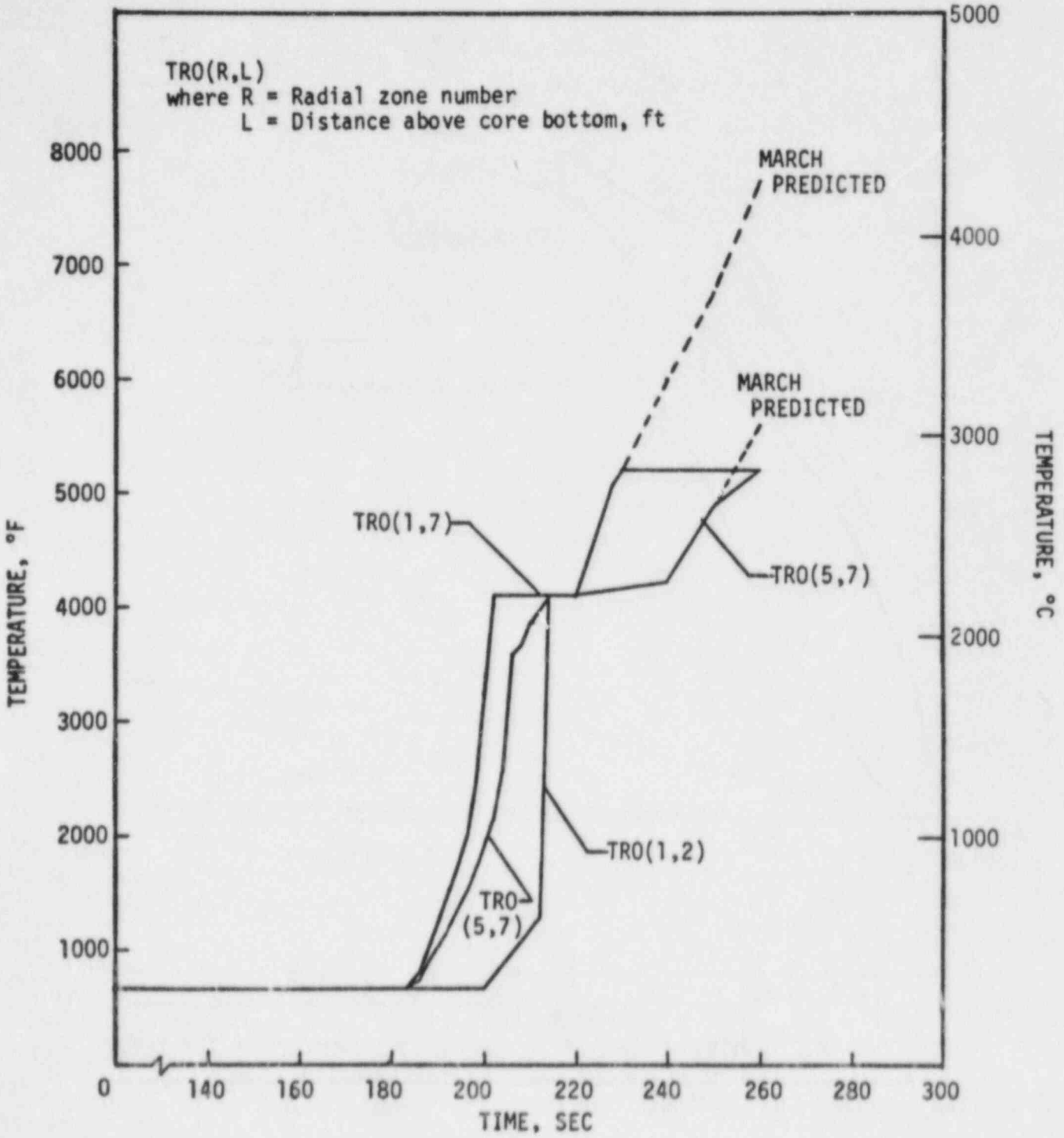

FIGURE 6.6. TEMPERATURES OF SELECTED FUEL REGIONS AS A FUNCTION OF TIME--SURRY TMLB' SEQUENCE

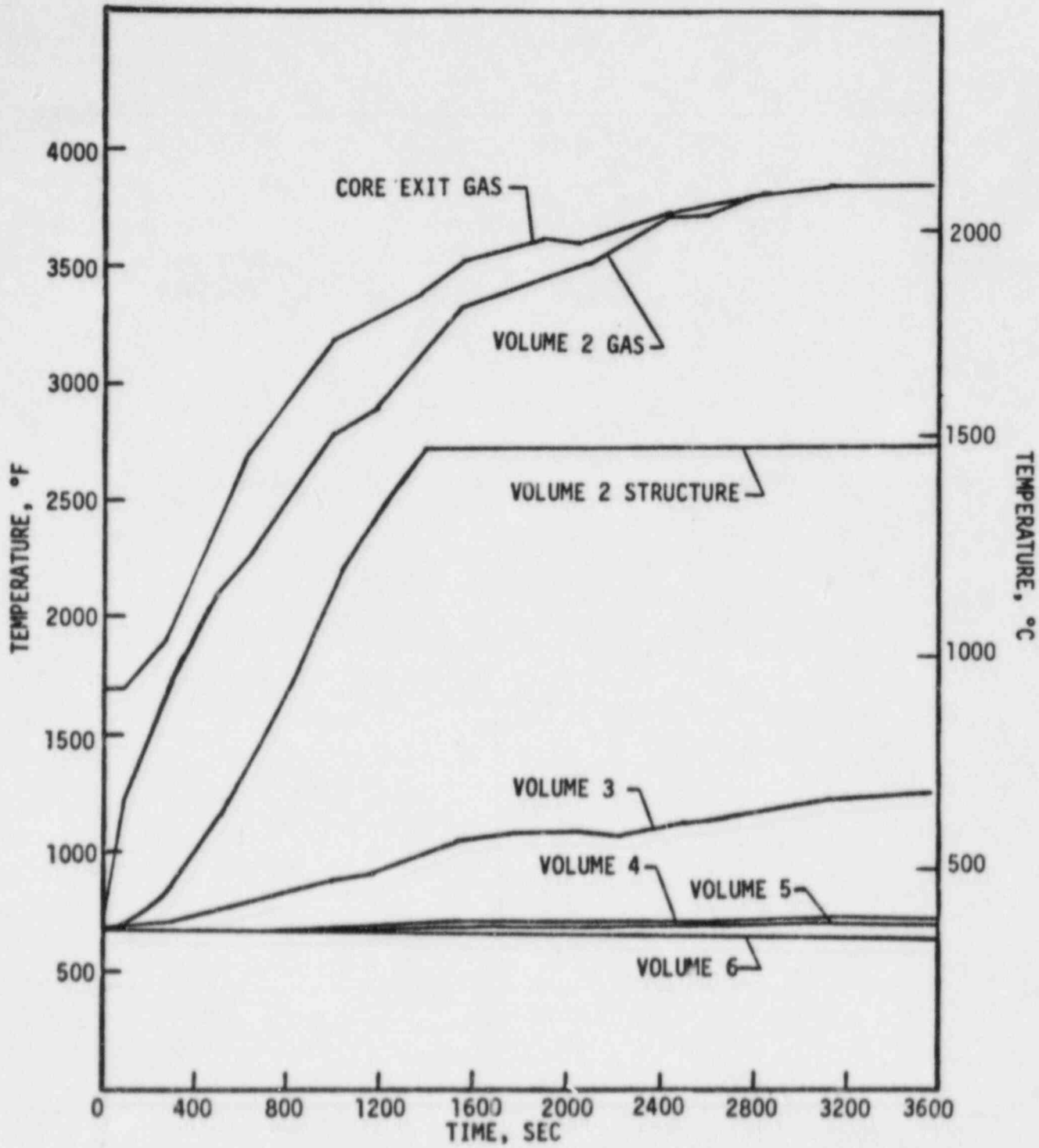

FIGURE 6.7. TEMPERATURES OF VOLUMES OF THE PRIMARY SYSTEM VERSUS TIME AFTER THE ONSET OF CORE MELTING--SURRY TMLB' SEQUENCE (CASE 1)

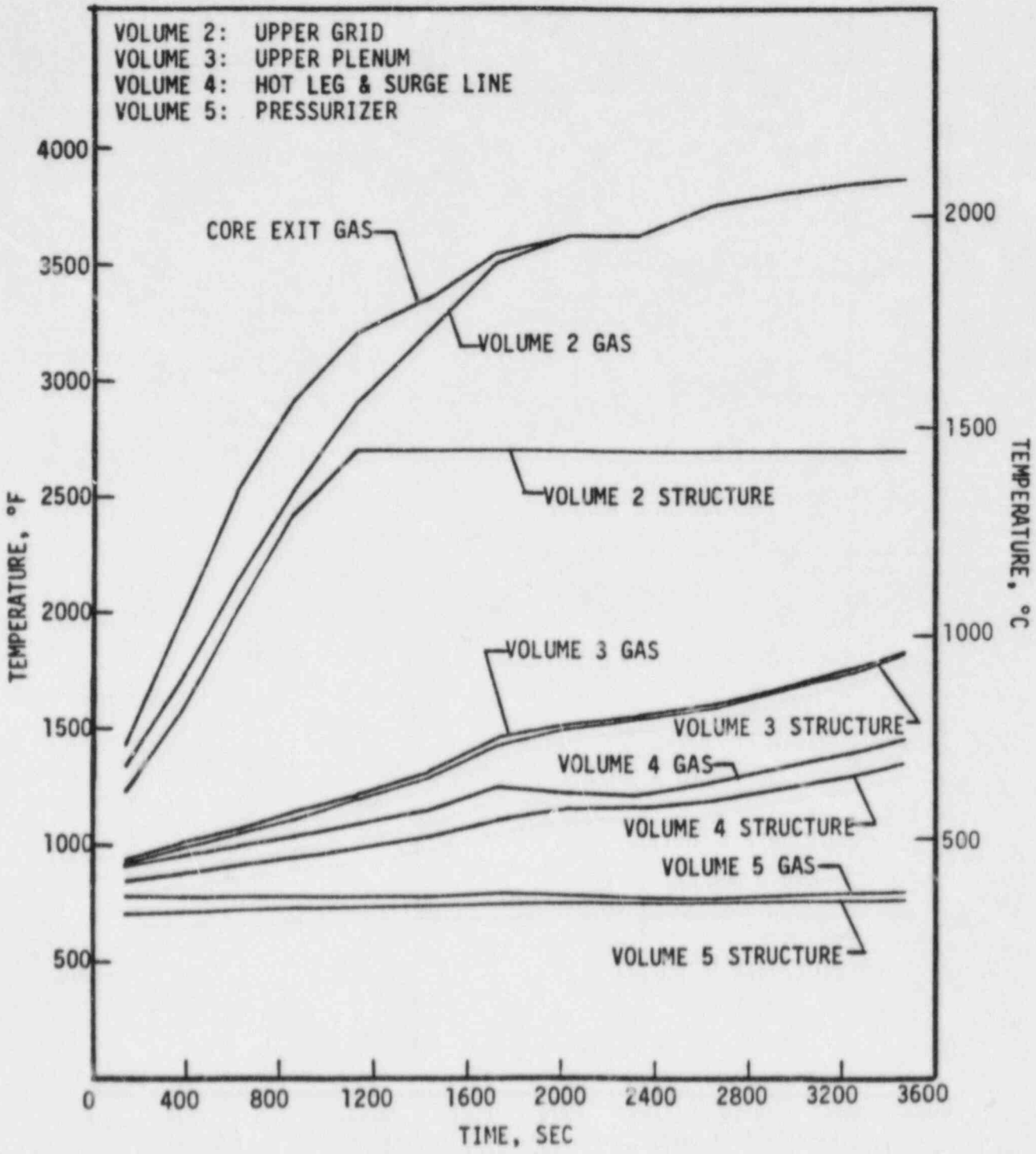

FIGURE 6.8. TEMPERATURES OF VOLUMES OF THE PRIMARY SYSTEM VERSUS TIME AFTER THE ONSET OF CORE MELTING--SURRY TMLB' SEQUENCE (CASE 2)

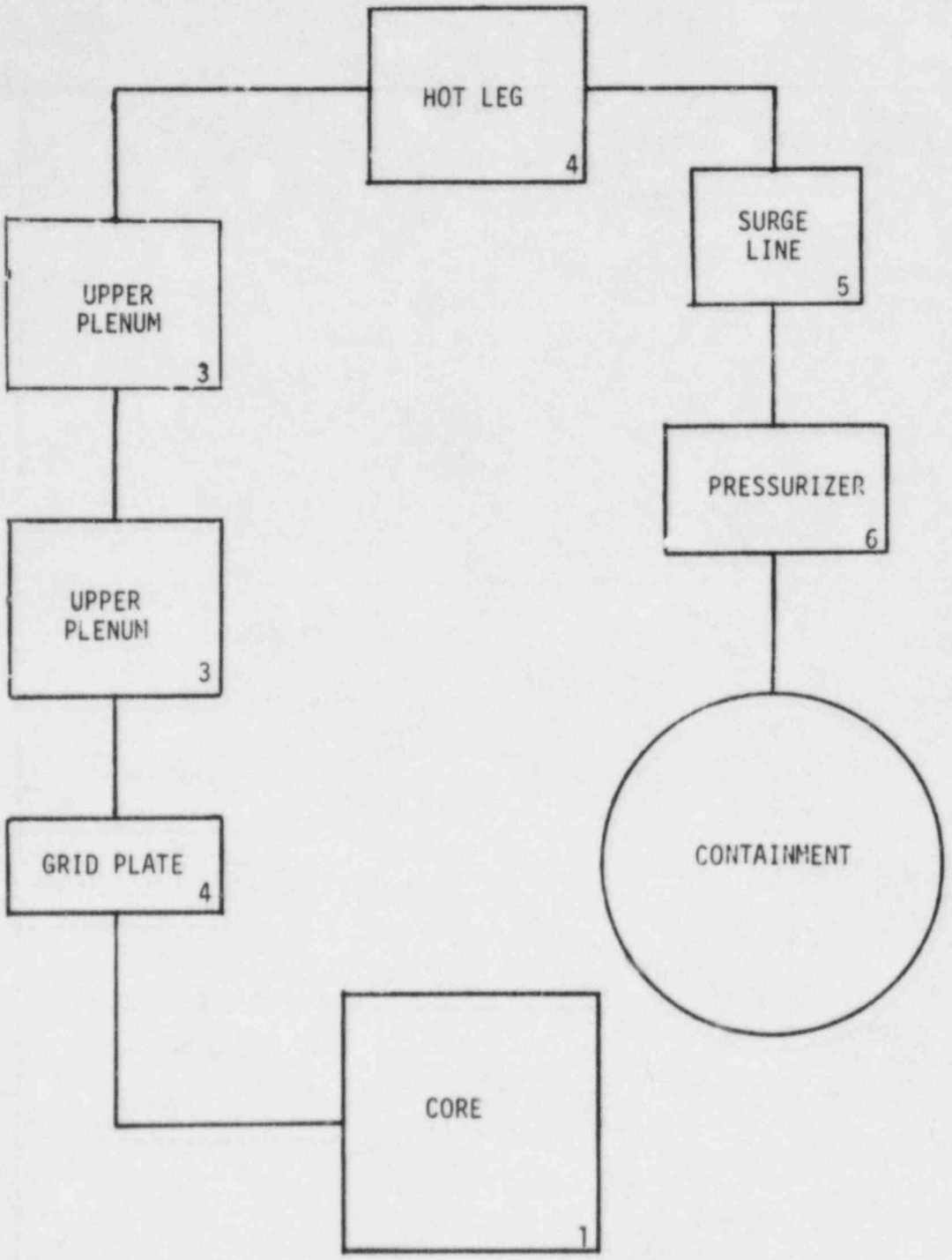

FIGURE 6.9. SCHEMATIC OF CONTROL VOLUMES FOR THE SURRY TMLB' SEQUENCE (CASE 2)

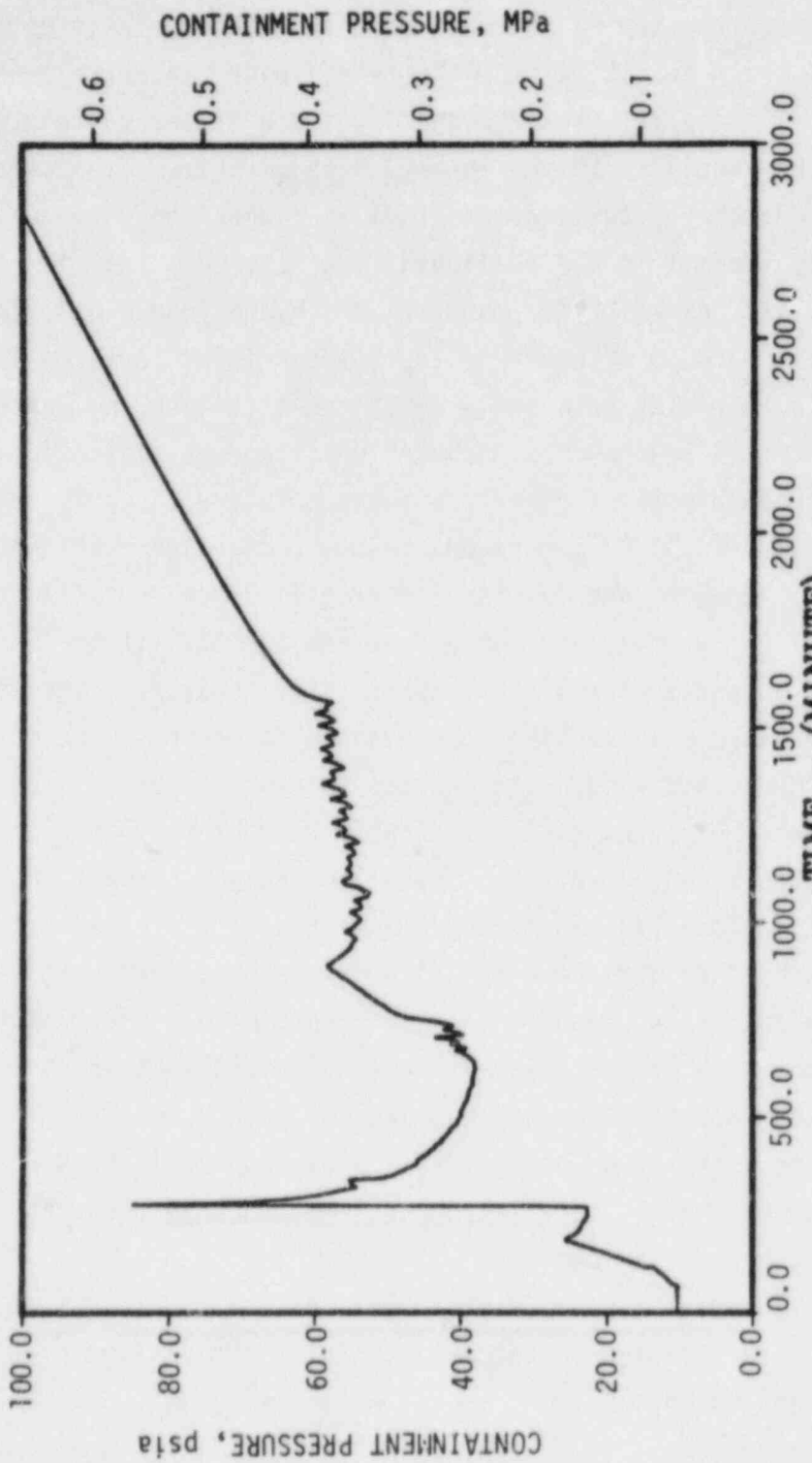

FIGURE 6.10. CONTAINMENT PRESSURE VERSUS TIME--TMLB' SEQUENCE

reactor cavity; the drop in the primary system pressure allows the accumulators to discharge onto the top of the core debris. MARCH calculates the rate of steam production resulting from the debris-water interaction using an input debris particle size; the rate and magnitude of the calculated pressure rise can be sensitive to the assumed particle size. The steam generation as calculated for the present study is limited only by heat transfer considerations, subject to the availability of stored energy in the debris and availability of water for evaporation; hydrodynamic effects that may tend to limit the access of water to the hot debris are not considered. In assuming the occurrence of this early containment failure, no representation is made as to the likelihood of such failure; the quantification of the probability of containment failure due to such interactions is beyond the scope of this study. It is suggested, however, that the magnitude of the pressures resulting from debris-water interactions may be sufficiently high that the possibility of failure should be considered. If the containment maintains its integrity through the above early pressure transient, the containment pressure will decline somewhat due to condensation of steam on internal structures, but will later increase again due to the attack of the concrete basemat by the hot core and structural debris. Since the gas and vapor input rates from concrete decomposition are low, except when the debris is very hot, a long time would be required for the pressures to build up to levels at which the likelihood of failure is significant. This is illustrated by the long term pressure rise in Figure 6.10. Since it may take a long time to reach pressure levels leading to failure, it is possible that basemat melt-through may precede and preclude such a long-term overpressure failure. It may be noted that the high partial pressures of steam in the containment atmosphere throughout most of this sequence are predicted to preclude hydrogen burning.

Figure 6.6 summarizes the containment leak rate information derived from the MARCH results and used in the evaluation of the fission product release from the containment.

6.1.3 Sequence V

The V sequence or interfacing systems LOCA is initiated by the failure of the check valves separating the low pressure emergency core cooling system from the primary coolant system. The release of the high pressure primary coolant inventory to the low pressure piping would not only lead to the failure of the emergency core cooling system but also provide a path for the release of radioactivity that bypasses the primary containment. It is also possible that the primary system blowdown would result in the failure of the safeguards or the auxiliary building.

The interfacing systems LOCA sequence is of particular interest because the containment building is bypassed for much of the sequence and the primary system could represent the principal location for the retention of fission products released from the core. The possibility of retention in the safeguards (or auxiliary) building also exists if it does not also fail, but would be quite design dependent. The thermal-hydraulic behavior of the system during the period of fuel melting is similar to that of the Sequence AB. Following a period of 1/2 hour in which blowdown and loss of reactor coolant inventory lead to the point of core uncovery, melting of fuel would occur over an interval of another 1/2 hour. The timing of key events is presented in Table 6.3. The core and primary system characteristics at key times during the sequence are given in Table 6.4. In this case, the primary system pressure would be slightly more elevated (0.68 MPa) and the velocity in the upper plenum would be reduced to approximately 10 cm per second. The velocity of the steam and hydrogen flowing back through the ECC injection line to the auxiliary building would be 5.5 m per second. The residence time in the reactor coolant system from core exit to the atmosphere of the auxiliary building would be on the order of 1 minute with the majority of the time spent in the upper plenum. The predicted temperatures of gases and structures in the flow path to the auxiliary building are illustrated in Figures 6.11 and 6.12. The results are similar to those obtained for the AB sequence. A schematic of the gas flow path for V (Case 1) is illustrated in Figure 6.13. A schematic of the gas flow path for V (Case 2) would combine the two upper plenum volumes into one volume. The

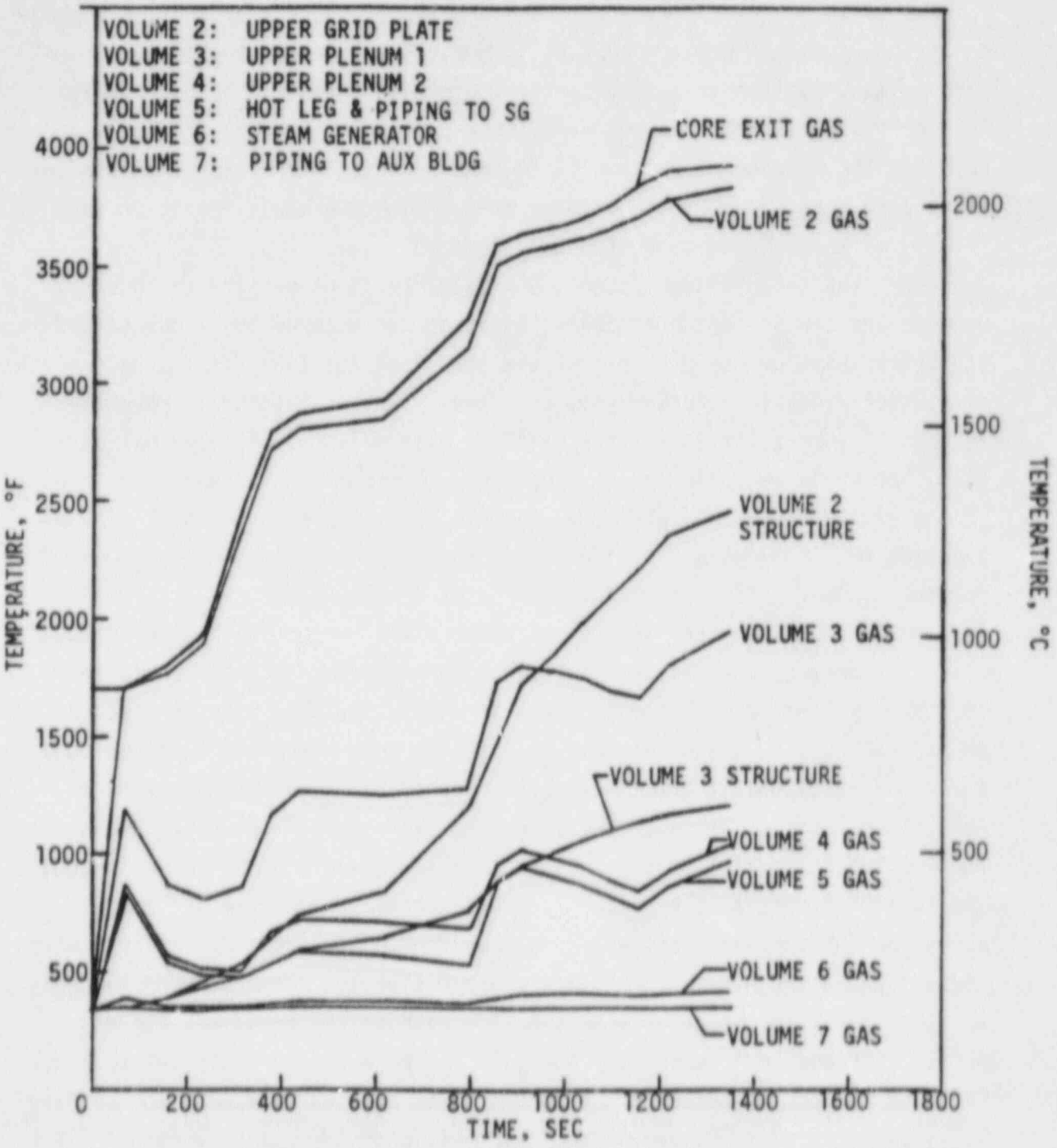

Figure 6.11. TEMPERATURES OF VOLUMES OF THE PRIMARY SYSTEM VERSUS TIME AFTER THE ONSET OF CORE MELTING--SURRY V SEQUENCE (CASE 1)

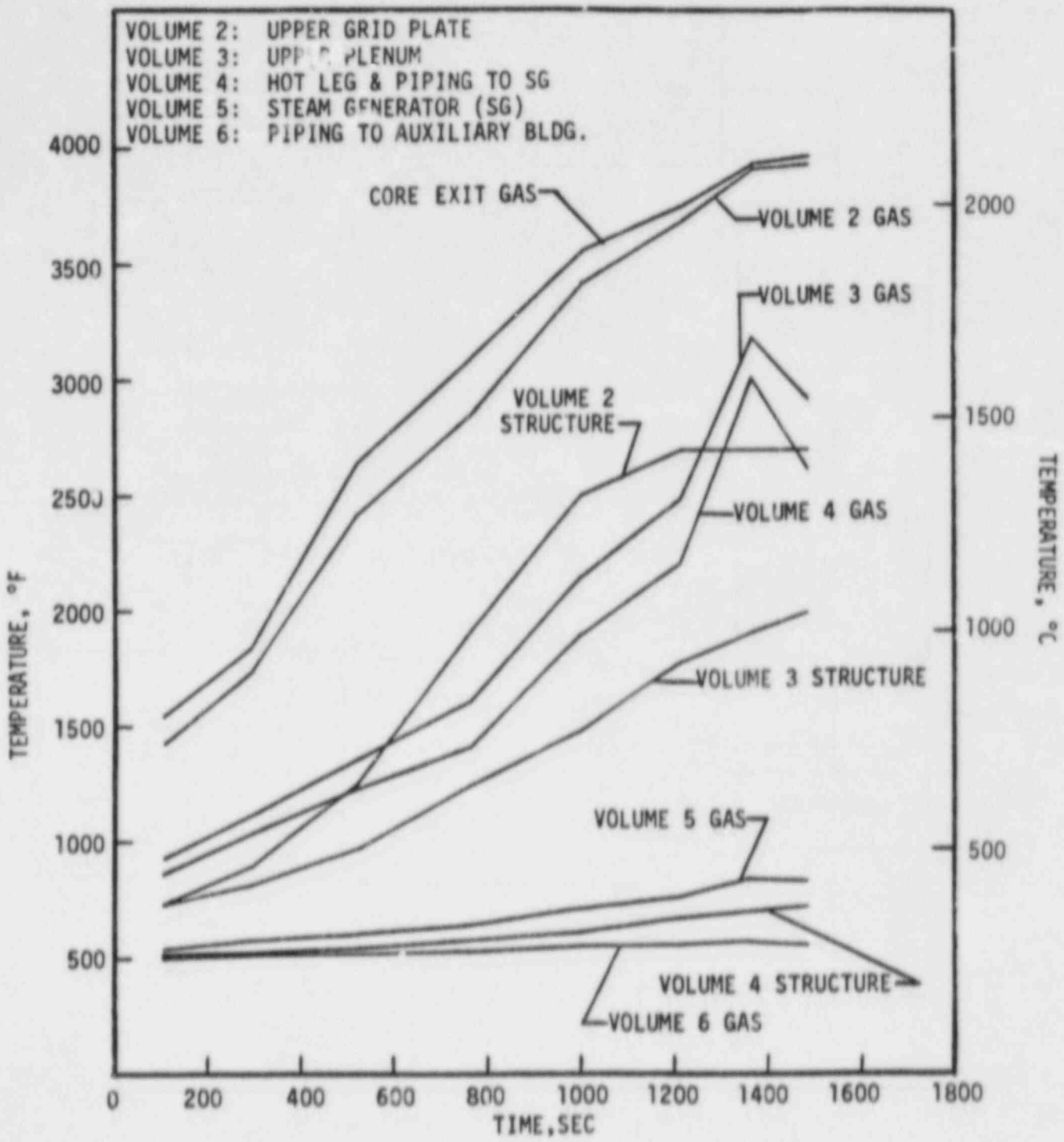

FIGURE 6.12. TEMPERATURE OF VOLUMES OF THE PRIMARY SYSTEM VERSUS TIME AFTER THE ONSET OF CORE MELTING -SURRY V SEQUENCE (CASE 2)

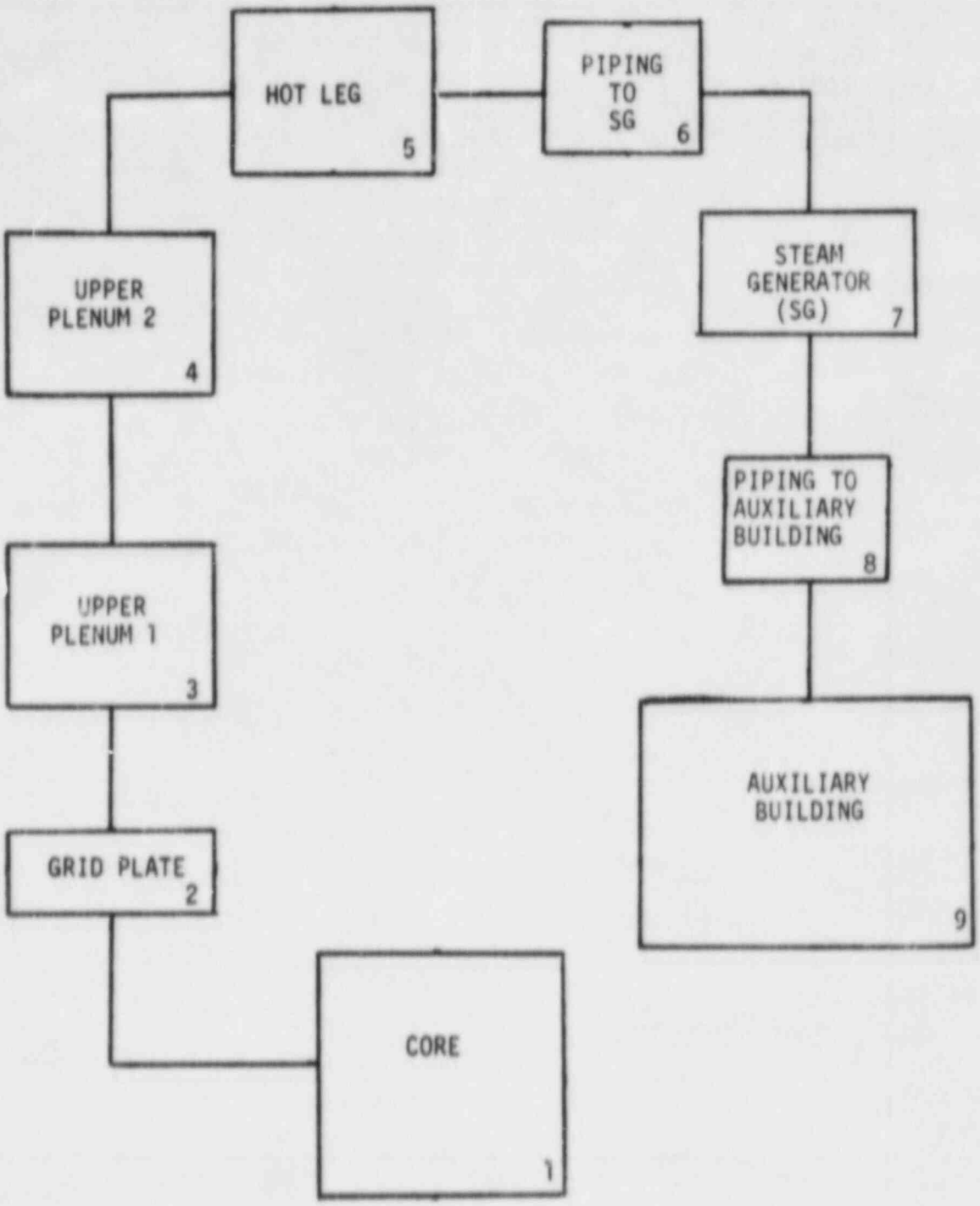

FIGURE 6.13. SCHEMATIC OF CONTROL VOLUMES FOR THE SURRY V SEQUENCE (CASE 1)

auxiliary building and containment characteristics at various times during the sequence are given in Table 6.5. Table 6.6 summarizes the containment leakage flows derived from the MARCH analyses and used to evaluate fission product release to the environment.

6.1.4 Sequence S_2D

The small pipe break accident sequence with failure of ECC injection involves conditions intermediate to the high pressure meltdown sequence TMLB' and the low pressure sequences AB and V. Two containment failure modes are considered: an early overpressure failure resulting from hydrogen combustion at the time of vessel penetration and basemat melt-through failure with no direct atmospheric failure of the containment. The timing of significant events is given in Table 6.3. Core and primary system parameters are summarized in Table 6.4. The predicted temperatures of gases and structures in the primary system are illustrated in Figures 6.14 and 6.15. Except for the upper grid plate, the gas temperature in the upper plenum is predicted to be within about 40-90 C of the structure temperature. A schematic of the gas flow path for S_2D (Case 1) is illustrated in Figure 6.16. A schematic of the gas flow path for S_2D (Case 2) would combine the two upper plenum volumes into one volume.

Table 6.5 summarizes the containment response at key times during the accident sequence. Since the containment sprays are operational, pressure in the containment would remain relatively low during the accident unless large quantities of hydrogen accumulate and burn rapidly. This is illustrated by the pressure history for the melt-through case in Figure 6.17. For the case of failure due to a hydrogen burn, the latter was assumed to take place following vessel failure when the hot core debris entered the reactor cavity. This burn produced a peak pressure of about 0.62 MPa (90 psia); the calculated peak pressure can be sensitive to the timing of the assumed burn. In assuming containment failure due to such a burn, no representation is made as to the likelihood of failure. If the containment maintains its integrity through challenges such as hydrogen burning, it is

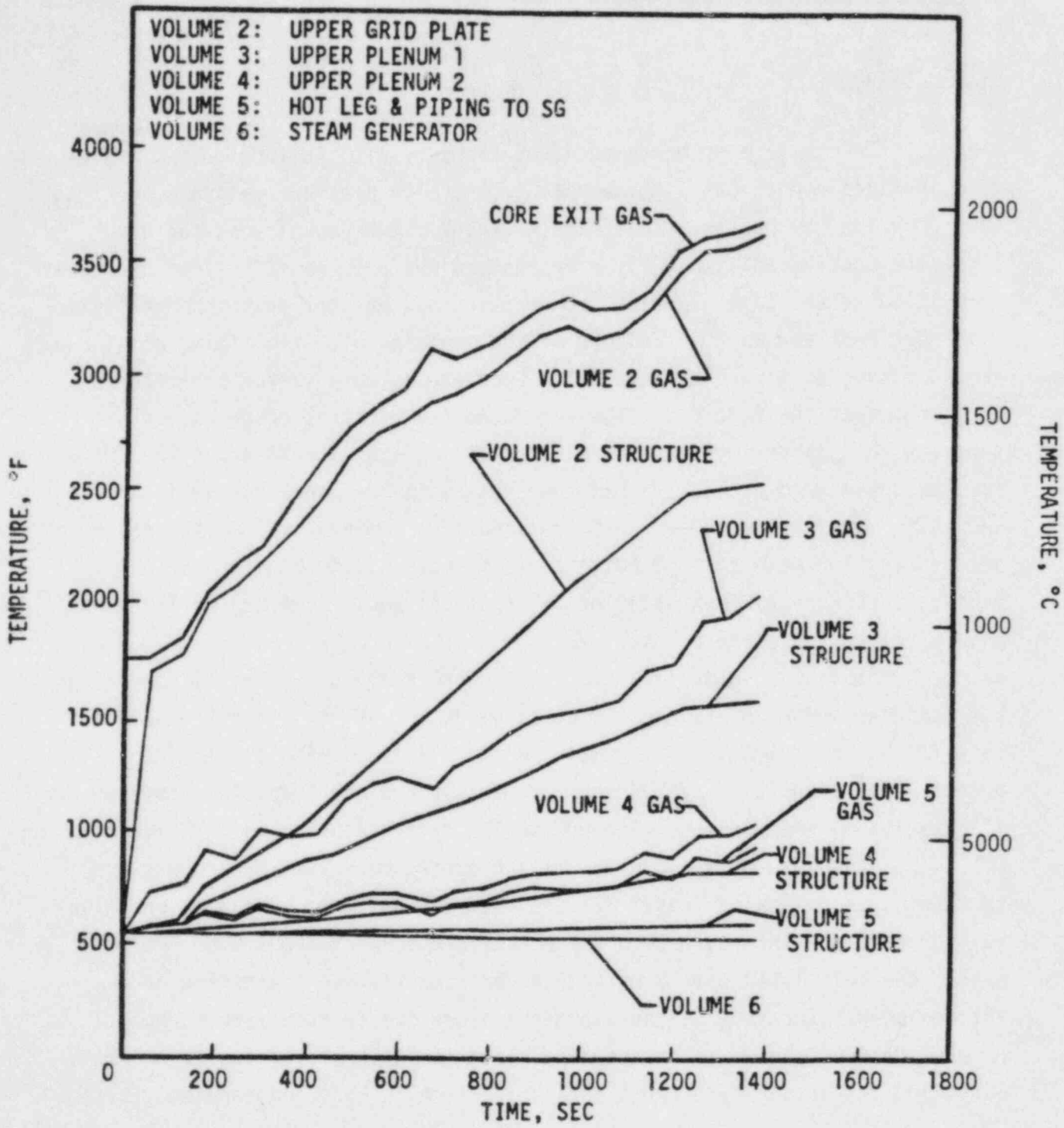

FIGURE 6.14. TEMPERATURES OF VOLUMES OF THE PRIMARY SYSTEM VERSUS TIME AFTER THE ONSET OF CORE MELTING--SURRY S_2D SEQUENCE (CASE 1)

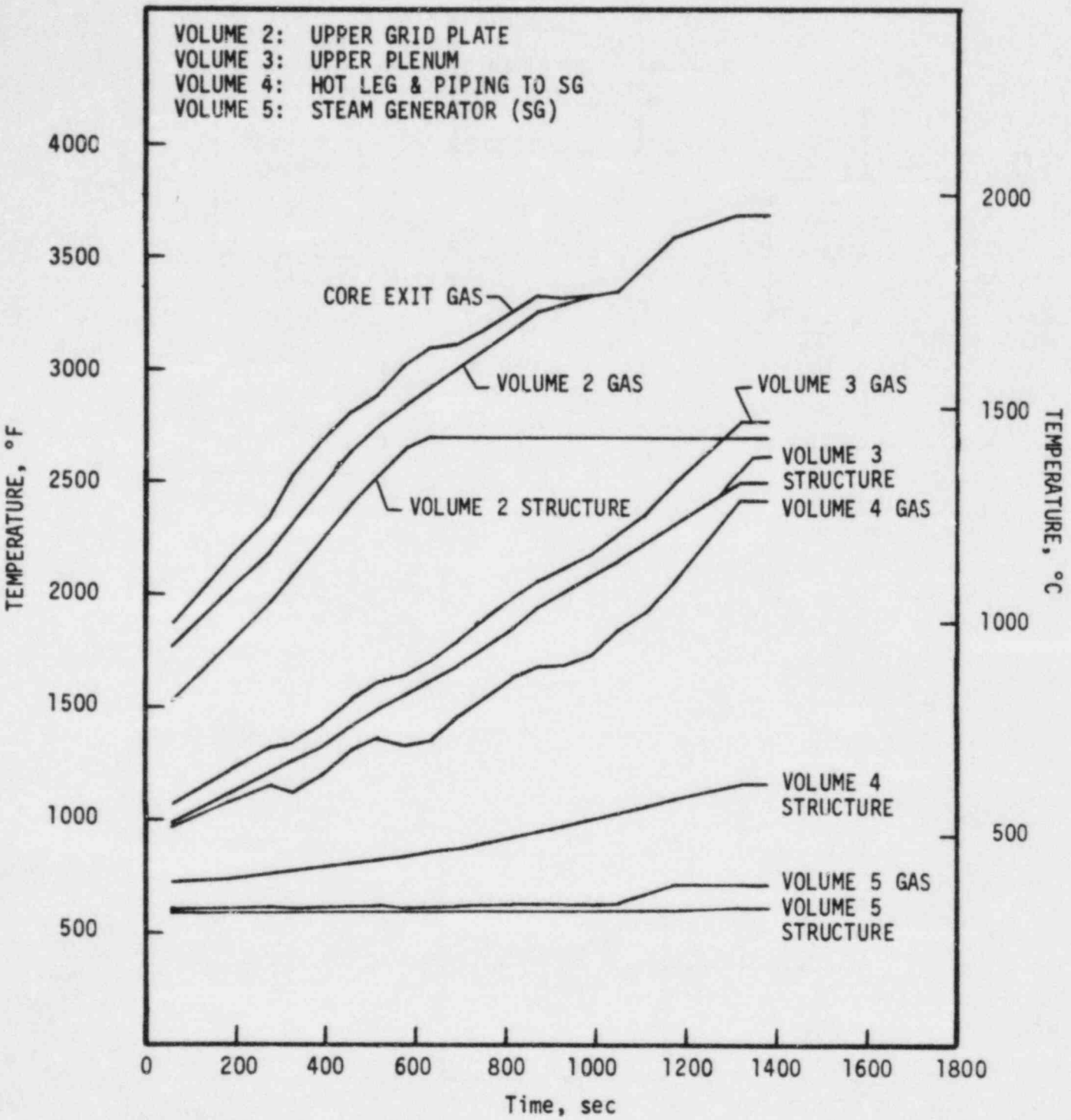

FIGURE 6.15. TEMPERATURES OF VOLUMES OF THE PRIMARY SYSTEM VERSUS TIME AFTER THE ONSET OF CORE MELTING--SURRY S_2D SEQUENCE (CASE 2)

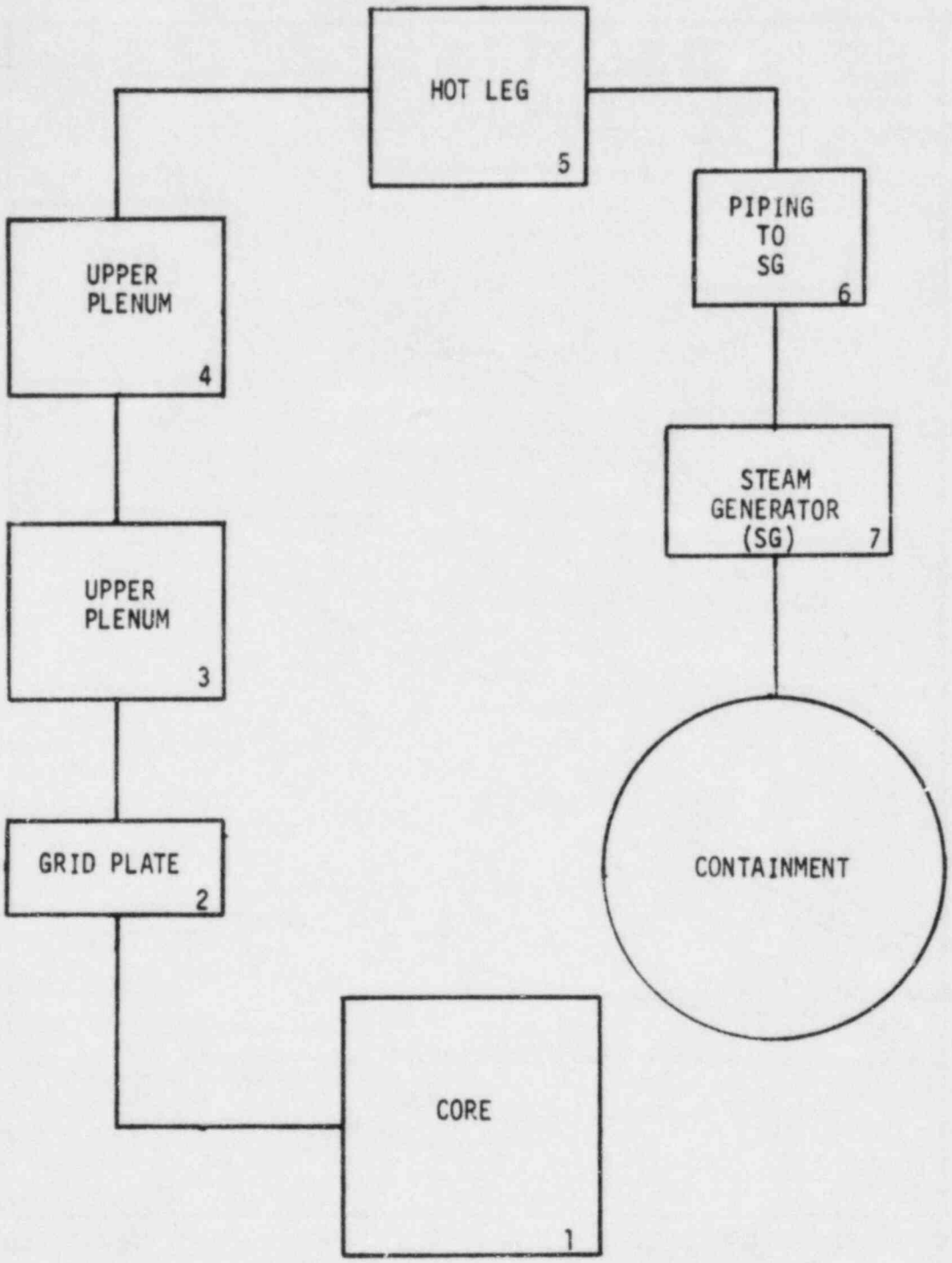

FIGURE 6.16. SCHEMATIC OF CONTROL VOLUMES FOR THE SURRY S_2D SEQUENCE (CASE 1)

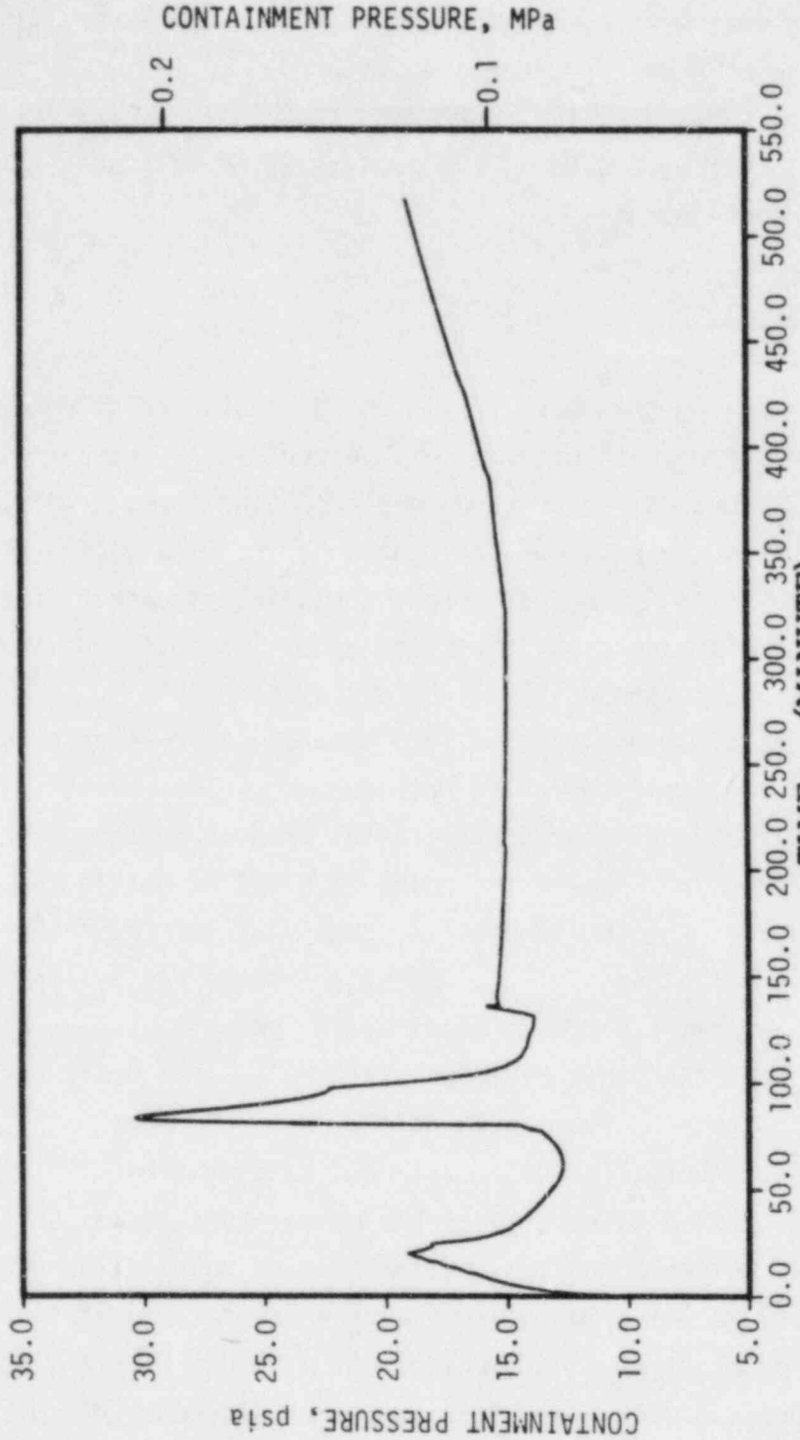

FIGURE 6.17. CONTAINMENT PRESSURE VERSUS TIME--S_2D SEQUENCE

likely that the basemat will eventually be penetrated due to the attack of the concrete by the core and structural debris.

Table 6.6 summarizes the containment leakages derived from the MARCH calculations that were used in the evaluation of fission product releases from the containment.

6.1.5 General Discussion

The release and transport of fission products are strongly influenced by the thermal-hydraulic behavior of the accident. The computer codes MARCH 1.1 and MERGE that have been used to predict the thermal-hydraulic conditions treat various aspects of accident behavior with different degrees of confidence. In the following paragraphs the principal areas of uncertainty in the analyses, simplifying assumptions and approximations, and the implications to fission product transport will be discussed.

In the MARCH 1.1 analyses of fuel heatup, the reactor core was subdivided into 24 axial and 10 radial mesh regions. The variation that would occur in the timing of heatup and fission product release across the core is well characterized. Up to the point of cladding melting and fuel/cladding liquefaction, the theoretical treatments of the thermal behavior of the fuel and oxidation of the cladding are supported by experimental data. Reasonable agreement has been obtained in the past between different computer codes in analyzing this behavior. The MARCH code makes the simplifying approximation that the fuel would melt at a single characteristic temperature which is input. The selected input melting temperature of 2550 K (4130 F) has been chosen to be between the temperature at which the fuel would dissolve into molten zirconium and the melting point of uranium dioxide. In the actual system, melting would occur over a broad range of temperatures up to the melting point of uranium dioxide. As a result of the single melting point approximation, the peak fuel temperatures predicted by MARCH may be underestimated for some quantity of fuel. The time for which fuel stays at elevated temperature is also very dependent on modeling uncertainties. These uncertainties will have little effect on the predicted release of volatile

fission products but could affect the vaporization of involatile materials, most likely by underprediction.

The MARCH analyses for the present study utilized meltdown model "A" with no movement of fuel out of the core until 75 percent of the core was molten; at that point the entire core was assumed to slump into the lower head of the reactor vessel. Because of the simplistic treatment of fuel slumping, it is possible for predicted core temperature prior to core collapse to significantly exceed the melting point of uranium dioxide. Recognizing that the extreme core temperature predictions are likely not real, the maximum temperatures supplied to CORSOR were limited to the melting point of uranium dioxide. The assumption of a coherent collapse of the entire core into the vessel bottom head also affects the timing of reactor vessel dryout and subsequent analyses of head heatup and failure.

The MERGE code was developed specifically for the analysis of reactor coolant system temperatures in this study. There is very little past experience in performing this type of analysis. The flow patterns in the system could be quite complex, particularly in the upper plenum region, and are treated approximately. Furthermore, detailed design data were not available to the analysts and estimates had to be made based upon descriptions provided within Safety Analysis Reports.

The flow within the reactor coolant system is treated as one-dimensional with well-mixed volumes. Natural convection within the upper plenum is considered in predicting the heat transfer to structures. Although convection patterns are not examined explicitly, the mixing which is expected to result would be consistent with the well-mixed approximation. The extent to which the flow reaches and mixes with the uppermost regions of the upper plenum (referred to as the upper dome or upper head) is not clear at this time, however, and has been treated parametrically. The one-dimensional treatment of the upper plenum does not take into account the radial temperature profile of gases leaving the core and transporting through the upper plenum. The calculated temperatures are averages across the flow cross section and would be expected to be higher near the center and cooler near the periphery.

In a number of sequences, the upper grid plate is predicted to melt under the combined heat loads of radiation from the top of the core and convection from hot gases. Cooling on the upper plenum side of these structures is not included in the analyses. Conversely, the radial temperature gradient above the core is also not treated which would tend to make the central regions hotter than predicted. The question of whether or not this structure would actually melt was not considered to be of great significance to the study and has not been pursued further.

As demonstrated later in this report, the timing of containment failure has a major impact on the predicted release of fission products to the environment. The pressure level at which the containment would be expected to fail is input into MARCH. To the extent that this failure pressure is uncertain (typically it is quite uncertain), it would tend to compound any uncertainties associated with MARCH code calculations. The thermal hydraulic conditions within the containment can be predicted with relative confidence if the driving forces are well defined. The principal early challenges to containment integrity are due to rapid steam generation from core debris interaction with water and from the burning of hydrogen. The analysis of steam generation from debris quenching is particularly uncertain and sensitive to the input and modeling assumptions utilized. This phenomenology is inherently uncertain and one in which unique answers, except in a bounding sense, cannot be expected.

The prediction of the pressures due to hydrogen burning is fairly straightforward if the initial conditions and the timing of the burn are known; however, this is generally not the case and key assumptions must be made. The amount of hydrogen present in the containment at any point in time is subject to the uncertainties in the prediction of core slumping, vessel failure, debris interactions in the cavity, etc. For any set of conditions the composition of the atmosphere and its potential flammability can be tracked as a function of time. Except in the presence of igniters, however, the occurrence of ignition cannot be predicted and must be assumed. Typically containment integrity would be challenged by large coherent burns, but would not be challenged by extended combustion; the timing of the ignition is the key difference between the two predictions.

Tables 6.7 and 6.8 provide information on which the calculations of radionuclide transport and deposition in the containment were based. Table 6.7 gives containment geometrical data and Table 6.8 provides containment spray parameters.

6.2 Radionuclide Sources

6.2.1 Source Within Pressure Vessel

Inventory

The reactor fission product inventory which was used in all four sequences considered in this report is based upon ORIGEN calculations for the Surry plant with a three region model with the maximum burnup corresponding to 33,000 MW days/ton. Table 6.9 contains the inventory of certain significant species and of the fission product groups considered in the Reactor Safety Study. Since release rate information is not available for all of these species, rates for members of the various groups were taken to be equal when no other information was available.

The nonfission product materials, which constitute the bulk of the aerosol particles released during core melting are tabulated in Table 6.10. The value for Ag in this table is based on a total of 1060 control rods composed of 80 percent Ag, 15 percent In, and 5 percent Cd. For the CORSOR predictions used, however, the control rod silver was not released according to the release specified in the "Technical Bases Report". After publication of that report, experimental evidence has become available which indicates that this silver is not a likely source of aerosol. (For one CORSOR run, this silver mass was assumed to be released during core melting, resulting in a predicted threefold increase in the mass of nonfission product aerosol generated during the melting.)

Release From Fuel

The rates for radionuclide release from the fuel were computed using the CORSOR code for the core temperature profiles specific to each accident sequence. The percent of inventory released for each species is given in Table 6.11 and the mass release rates for cesium, iodine, tellurium, and aerosol material are given in Tables 6.12 through 6.15 for the AB, TMLB', S_2D, and V sequences. Aerosol materials were considered to be the sum of fission products Sb, Sr, Ba, Ru, Mo, Zr, Ag along with nonfission products, Fe, UO_2, Zr (cladding, and Sn). No release was assumed after core slumping until melt-through. After melt-through release during the core-concrete interaction was taken as a release to the containment.

The nonvolatile materials emitted from the melting core will coagglomerate rapidly to form particles which can be characterized by a fixed composition at any given time. Since the release rates for the various species change with time in a variety of ways, however, the composition of the emitted particles is expected to change as a function of time. Figures 6.18 through 6.21 display the predicted aerosol mass composition near the beginning of significant aerosol release, and near the assumed end of in-vessel areosol release. There are no striking differences among the sequences. For each of them, the areosol mass composition is clearly dominated by the nonfission product materials, due to the much larger inventory of these species. Each sequence also displays the depletion of the aerosol fraction composed of the fission products Mo, Ba, Ag, and of Sn as the melt release continues, and the enhancement of the UO_2 fraction of the particles. The aerosol composition is not modeled within the primary system transport calculations, but the use of CORSOR predicted release rates and consideration of the residence time of the areosol in the primary system permit one to estimate the composition of the aerosol which enters the containment.

It is to be noted that the areosol mass release rates from the total core predicted with the CORSOR code are quite sensitive to release rate coefficient and fuel melting temperature (maximum temperature reached), while cladding burst temperature is less of a controlling factor. Conversely, cesium and iodine release rates are nearly unaffected by these factors.

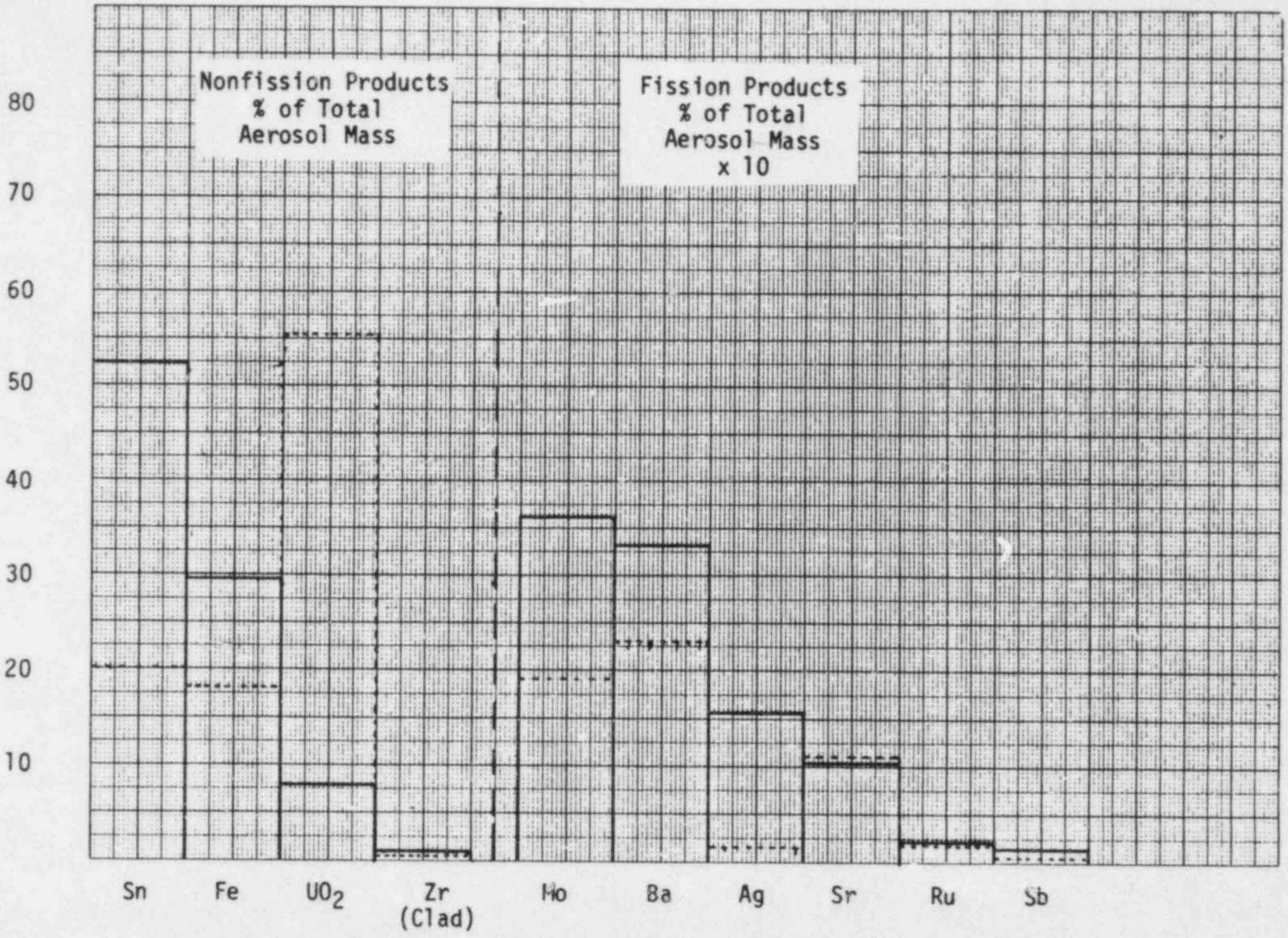

FIGURE 6.18. COMPOSITION OF AEROSOL EMITTED BY CORE AT FRACTION OF CORE MELTED = 10% (——) AND JUST PRIOR TO CORE SLUMP (---). PREDICTIONS FROM CORSOR FOR AB SEQUENCE.

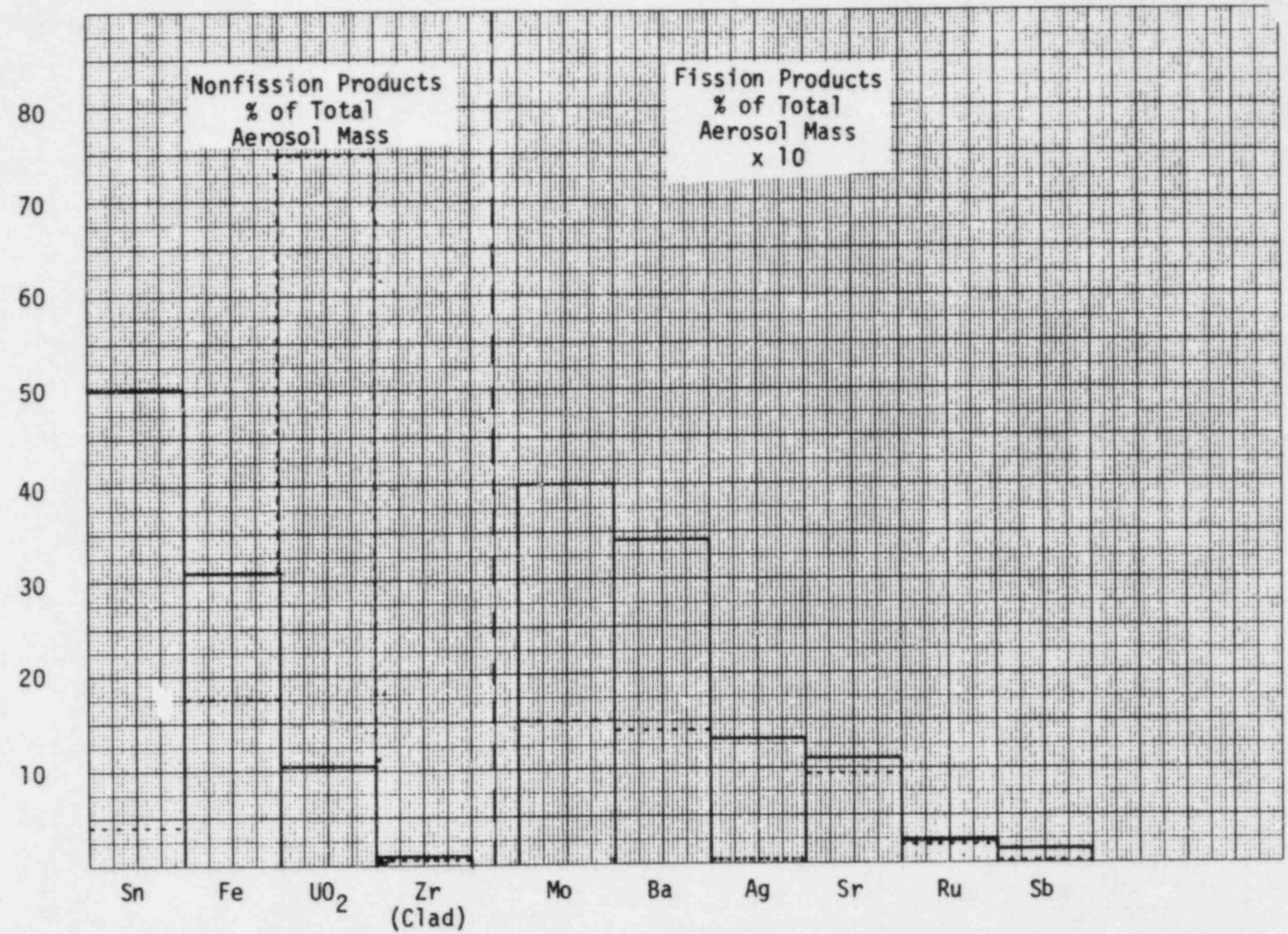

FIGURE 6.19. COMPOSITION OF AEROSOL EMITTED BY CORE AT FRACTION OF CORE MELTED = 10% (——) AND JUST PRIOR TO CORE SLUMP (---). PREDICTIONS FROM CORSOR FOR TMLB SEQUENCE.

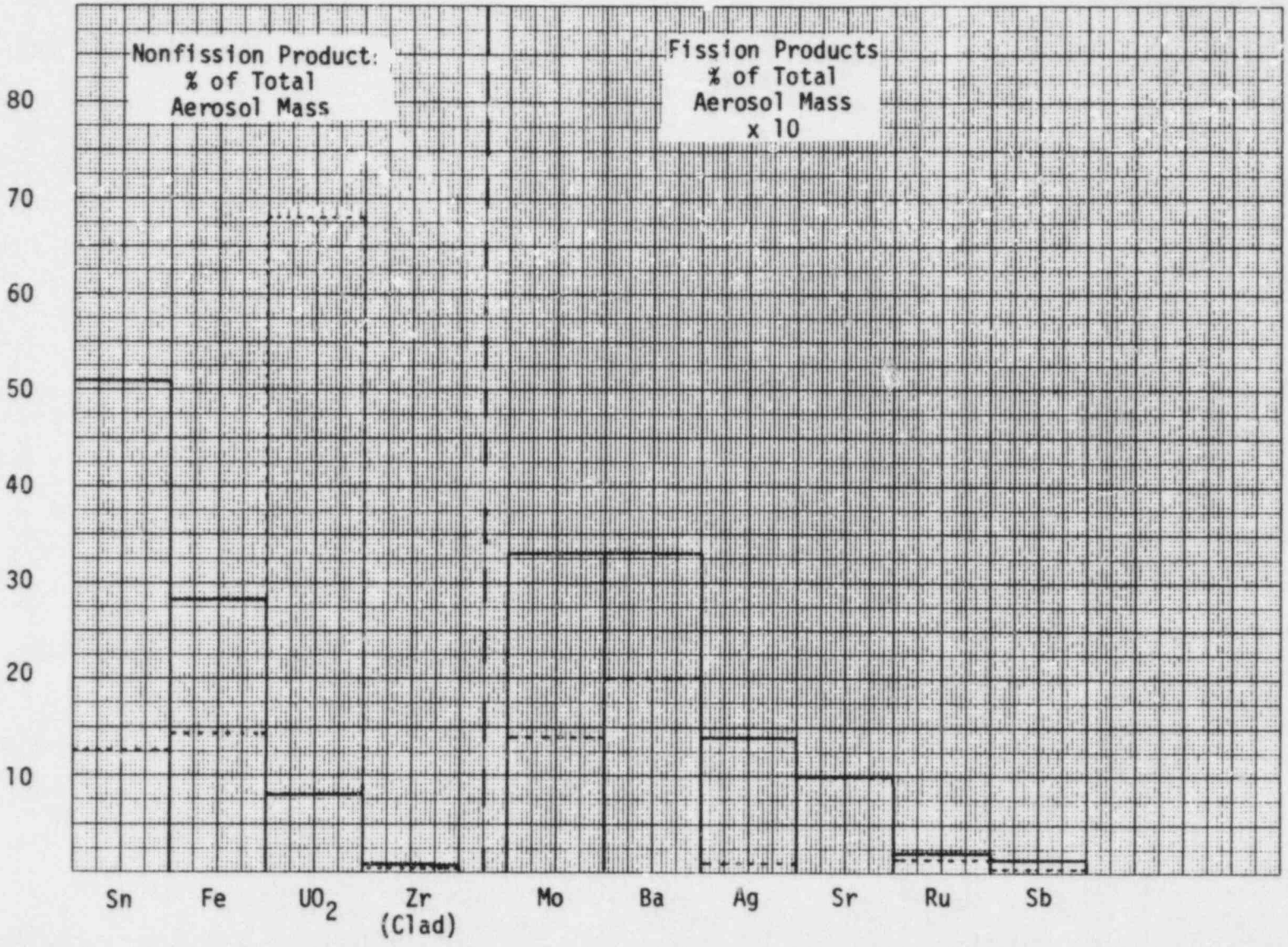

FIGURE 6.20. COMPOSITION OF AEROSOL EMITTED BY CORE AT FRACTION OF CORE MELTED = 10% (——) AND JUST PRIOR TO CORE SLUMP (---). PREDICTIONS FROM CORSOR FOR S_2D SEQUENCE.

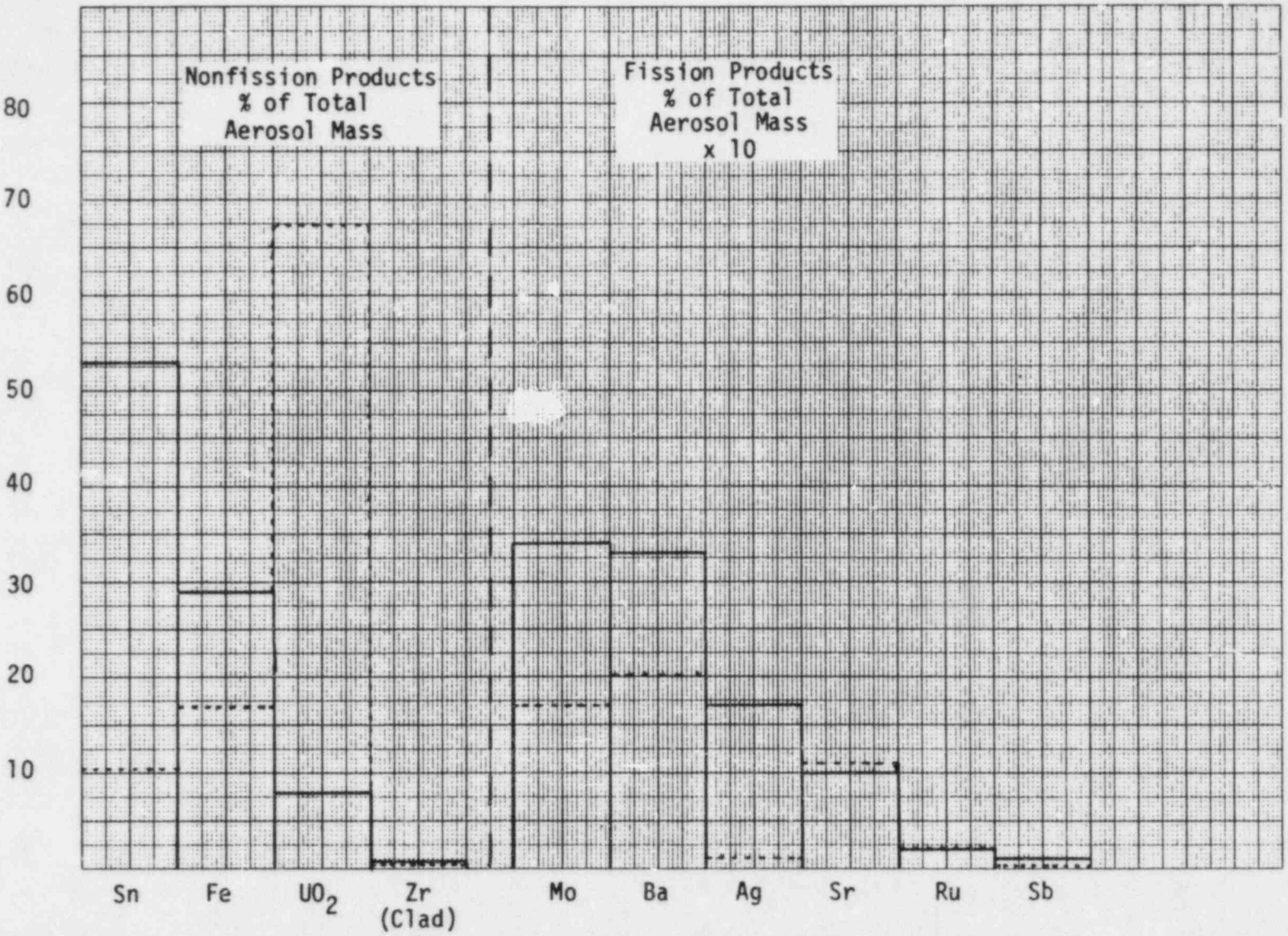

FIGURE 6.21. COMPOSITION OF AEROSOL EMITTED BY CORE AT FRACTION OF CORE MELTED = 10% (——) AND JUST PRIOR TO CORE SLUMP (---). PREDICTIONS FROM CORSOR FOR V SEQUENCE.

Analyses to illustrate this sensitivity are presented and discussed in Appendix B. The importance of uncertainties in such factors on estimates of material eventually released from the containment has not been evaluated.

The species of interest in transport were taken to be cesium iodide, cesium hydroxide, tellurium, and aerosol. Iodine in the primary system was estimated to be completely reacted with cesium. This estimation is based on consideration of the chemical thermodynamic equilibrium state as predicted in the "Technical Bases Report"[6.1]. Tables 6.13 through 6.16 present the mole ratios for H/I, Cs/I, and H/O as well as MERGE predicted gas temperatures in primary system control volumes at various times. Using these tables and Figures C.1 through C.4 in the "Technical Bases Report" it is evident that except for time 1608 seconds after start of melt in sequence V there is no I_2 expected while CsI is always the overwhelmingly preferred iodine form. This conclusion is supported further by predictions of Torgerson[6.2].

It is necessary to select an initial particle size for those materials forming the aerosol species. It has been shown[6.3] that when significant agglomeration occurs, the initial aerosol size has a negligible effect on subsequent aerosol behavior after agglomeration has proceeded for a very short time. Nevertheless, initial particle sizes were chosen to correspond to the best available information. Numerous reviews of experimental mean aerosol sizes from vaporizing and condensing fuel will be from slightly below 0.01 μm to about 0.1 μm with the most likely size being about 0.05 μm. A number median radius of 0.05 μm and a geometric standard deviation of 1.7 were assumed in the current analyses.

After the molten core is predicted to slump into the lower plenum of the reactor vessel in the MARCH analysis, the in-vessel release of fission products is assumed to be terminated. The extent to which the molten fuel would be expected to be fragmented and cooled in the lower plenum is uncertain. If the molten fuel were not rapidly cooled, however, it would fall to the bottom, attack the vessel head and penetrations, and lead to rapid failure. On the other hand, if the molten fuel were dispersed and quenched, the resulting core debris would heat up and remelt following boil-off of the residual water. Vessel failure would be expected, however, when

the debris reached temperatures that are well below the temperatures attained earlier in the melt period.

6.2.2 Sources Within the Containment

Radionuclides enter the containment as they are transported through the primary system and on melt-through of the reactor pressure vessel, that material still suspended in the RCS is transported into the containment as the RPV and containment pressures are equalized. The final source considered is that material released during the core-concrete interaction. Because of a lack of release information or even more generally a lack of evidence that they are of potential importance, sources sometimes postulated as arising from steam explosions (oxidation release) or from jet emission of hot, molten corium on RPV failure were not included in these analyses.

Release from Primary System

The source to the containment of material penetrating the primary system is defined in mass input rate by species of interest and on a time-dependent basis by the output from the TRAP-MELT calculations. Also provided in the TRAP-MELT output is the size distribution of the particulate material. This calculated information is included in the subsequent report section on results.

Release from Core-Concrete Interaction

The Sandia model described previously was applied to the melt composition resulting from the molten core materials as depleted in various species as computed with the CORSOR code. Added to this mix of core materials was 1.02×10^5 kg of iron, 1.60×10^4 kg of chromium, and 8.91×10^3 kg of nickel. These represent the mass of the lower RPV plenum estimated to be melted during passage of the molten core materials. The concrete was assumed to be basically a basaltic concrete. Table 6.20 provides the

composition of the melt reaching the concrete. Figure 6.22 shows the total mass releases from the core-concrete interaction with time. The composition of this release is given for each sequence in Appendix C. Note that in the tables a special case called AB-tellurium has been included where the assumption has been made that the entire tellurium inventory is retained with the molten core materials until it reaches the concrete. This parametric variation from the previous AB-hot leg case has been considered because of the known affinity of Te for molten metals.

One of the release mechanisms considered in WASH-1400 was referred to as the oxidation (steam explosion) release. This mechanism was assumed to lead to an enhanced release of some radionuclides in the event of the dispersal of finely fragmented fuel in the containment building atmosphere in a steam explosion. The primary effect was a greatly increased release of ruthenium to the containment and to the environment in accidents in which a steam explosion was predicted to result in containment failure. Current understanding of steam explosion phenomena indicates that the likelihood of a steam explosion in the reator coolant system leading to containment failure was overestimated in WASH 1400. In contrast, the probability of a steam explosion occurring in the reactor cavity following melt-through of the bottom of the reactor vessel may be quite high. The possibility of some dispersal of fuel particles within the containment building must therefore be considered. Attempts to measure the atmospheric dispersal of steam explosion debris in experiments at Sandia have been unsuccessful because of carryback with splashed water. Anticipating similar behavior for a steam explosion in the reactor cavity, an oxidation source term was not included in the analyses in this report.

Source Term for Volatile Iodides

In a previous section it has been shown that the thermodynamics of the cesium-iodine-hydrogen-oxygen system indicate that iodine will be present primarily as a nonvolatile iodide in the primary coolant system. After release from the primary system, a small fraction of the iodine inventory in the containment is believed to be present as volatile iodides.[6.1]

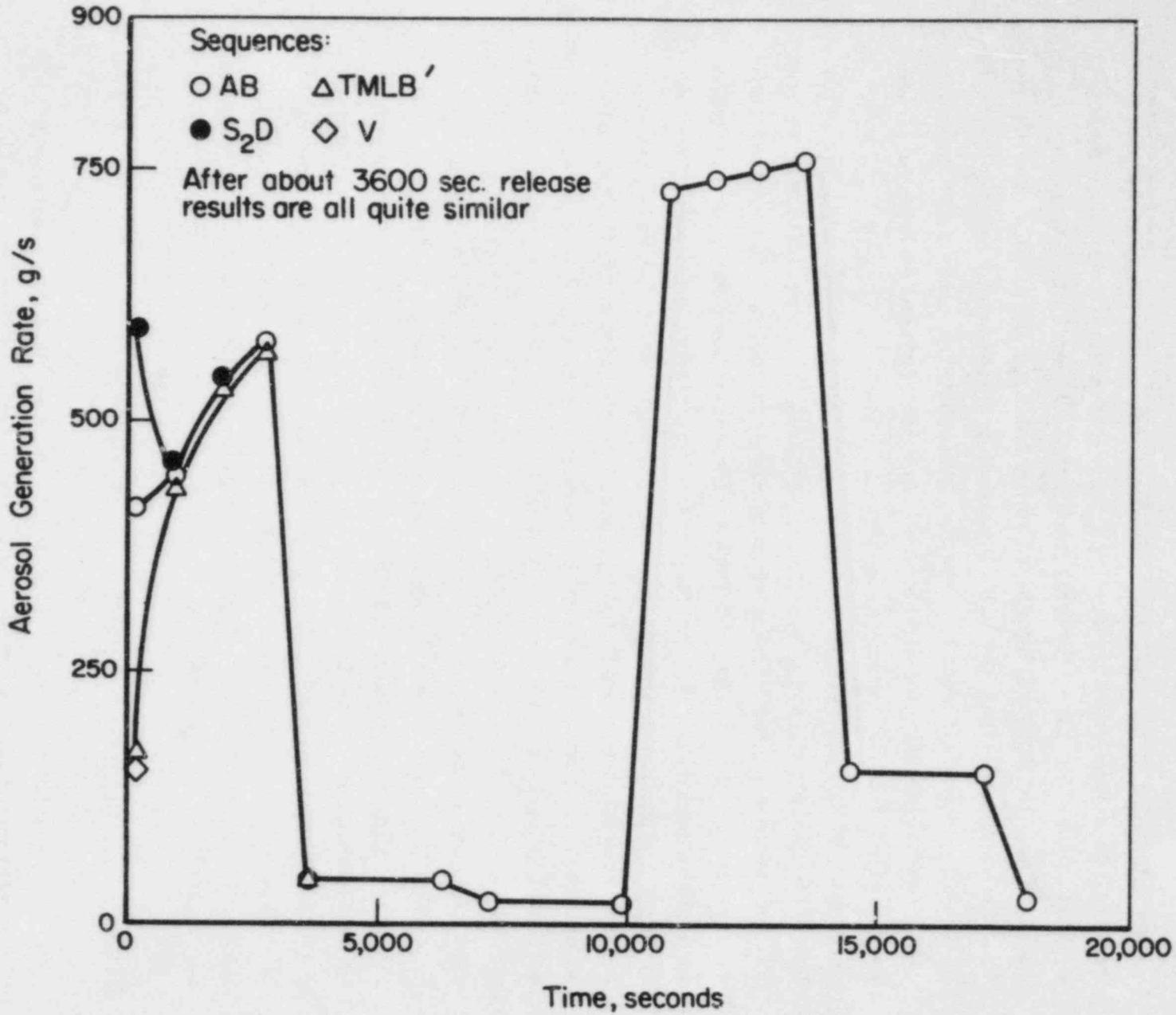

FIGURE 6.22. AEROSOL GENERATION VERSUS TIME

The presence of volatile iodide species in containment-type systems has been observed in experiments[6.6] and in the TMI-2 post-accident containment atmosphere.[6.7] At present, the mechanisms responsible for the generation of these volatile iodides are not well understood. Since a theoretical model is not available, an empirical approach has been selected for the formulation of a source term for volatile iodides. This source term consists of two components. One component represents the fraction of the containment iodine inventory which is present as volatile iodides before containment failure. The second component represents a generation rate for volatile iodides after containment failure. The containment inventory of volatile iodides present prior to containment failure was estimated from levels observed in TMI-2[6.7] and from estimates of the probable detection limits in relevant experiments.[6.8] The volatile iodide generation rate was estimated from a conservative evaluation of the measurements of the airborne iodine levels in the TMI-2 containment over the time period from 100-2000 hours after reactor trip. Based on these estimates it has been assumed for this study that 0.05 percent of the containment iodine inventory will be present as volatile iodides prior to containment failure and after containment failure, additional volatile iodides will be generated at a rate of 2×10^{-7} fraction/hour of the containment iodine inventory.

Of this volatile iodine source, it is believed that a fraction of the iodine inventory in a reactor containment will be present as volatile organic iodides (predominantly CH_3I).[6.1] (Other volatile species may also be present.) Therefore, in the analysis of reactor accidents involving a radionuclide release from the reactor system and containment failure, formation in the containment and subsequent release of organic iodides should be considered. Unfortunately, the mechanism responsible for the generation of organic iodides has not yet been elucidated. As a result, it is not yet possible to establish a definitive source of organic iodides. Early estimates of the organic iodine source terms were based on a conservative interpretation of experimental systems studies.[6.6,6.9] Early thermodynamic studies predicted that organic iodides should be present in much smaller concentrations than observed in experiments.[6.10] These calculations predicted that CH_3I would comprise only $\sim 10^{-4}$ percent of the

total gaseous iodine inventory modeled. Experimental data[6.6] and "chemical species specific" measurements of the TMI-2 airborne iodine inventory[6.7] imply that the concentration of organic iodides present in a reactor containment during and following an accident may be higher than the concentrations predicted by thermodynamic calculations for an equilibrium system. Additionally, observations of the airborne iodine behavior at TMI-2[6.7] imply the presence of competing sources and sinks for volatile iodine species. In light of these data, a kinetic description may be required to adequately quantify the time dependence of the organic iodide concentration in reactor containments during and following reactor accidents. Pending results of studies, such as those which are currently under way,[6.2] use of a general source term for volatile iodides rather than separate source terms for CH_3I, I_2, etc., has been assumed as noted above.

TABLE 6.1. REACTOR CHARACTERISTICS, CONTAINMENT PARAMETERS, AND MARCH OPTIONS FOR LARGE DRY PWR CONTAINMENT (CONTINUED)

ECC storage and injection tanks

	Accumulator		RWST	
Weight of water	171,300 lb	77,700 kg	2.92×10^6 lb	1.3245×10^6 kg
Initial pressure	665 psia	45.9 MPa	14.7 psia	0.1 MPa
Temperature	120 F	48.89 C	45 F	7.22 C

Fractional value of RWST to start ECC recirculation: 0.01

Fractional value of RWST to start spray recirculation: 0.143

Large LOCA blowdown

Time, min	Enthalpy		Blowdown Rate	
	Btu/lb	J/kg	lb/min	kg/s
0	602.7	288,400	2.115×10^6	1.599×10^4
.20	602.7	288,400	2.115×10^6	1.599×10^4
.201	89.73	42,930	2.770×10^5	2.094×10^3
.401	89.73	42,930	2.770×10^5	2.094×10^3

Calculated model input

Core heatup section:

Number of radial zones: 10

Number of axial zones: 24

Meltdown model: BOIL model A

Core melting temperature: 4130 F (2277 C)

Core collapse: Occurs when 75 percent of core has melted

Zircalloy - water reaction: ORNL-TM-41 data, steam limited, continues for melted nodes, complete reaction of molten Zircaloy in the bottom head.

TABLE 6.1. REACTOR CHARACTERISTICS, CONTAINMENT PARAMETERS, AND MARCH OPTIONS FOR LARGE DRY PWR CONTAINMENT (CONTINUED)

End of blowdown conditions for large LOCA:

Water in vessel: core covered

Peak core temperature: 1700 F (927 C)

Accumulators: empty

Bottom head failure section:

Head melting temperature: 2800 F (1538 C)

Debris melting temperature: 4130 F (2277 C)

Heat loss from top of debris: none

Debris thermal conductivity: 8 Btu/hr ft F (0.1384 w/cm/C)

Tensile strength of vessel: σ = min (500,000, 1.49×10^{16} TEMP$^{-3.9105}$), lb/in^2

Reactor cavity processes, debris fragmentation:

Particle diameter: 0.5 inch (1.27 cm)

Particle thermal conductivity: 2.0 Btu/hr ft F (0.0346 w/cm/C)

Reactor cavity processes, concrete decomposition:

Metal-concrete interface heat transfer coefficient: HIM = 0.01 w/cm^2 K

Oxide-concrete interface heat transfer coefficient: HIO = 0.01 w/cm^2 K

Top surface emissivity: E = 0.5

Heat to cover water: surface boiling plus 50 percent of area radiating at internal temperature of top layer.

Containment Section:

Atmosphere-wall heat transfer coefficient:

$h = h_c$ (TSAT-TWALL) + 0.19 (T-TWALL)$^{4/3}$ /(T-TWALL)

h_c = 0 if TSAT < TWALL

2.0 < h_c = Uchida data < 280 Btu/hr ft^2 F

Containment break area: 7.0 ft^2 overpressure failure (0.65 m^2)

0.349 ft^2 isolation failure (0.0324 m^2)

TABLE 6.1. REACTOR CHARACTERISTICS, CONTAINMENT PARAMETERS, AND MARCH OPTIONS FOR LARGE DRY PWR CONTAINMENT (CONTINUED)

Failure of safety systems: (1) All ECC flow is stopped when core melt starts. (2) Containment failure fails the containment sprays (3) Containment failure fails ECR if sump is saturated.

TABLE 6.2. GEOMETRY OF CONTROL VOLUMES OF THE REACTOR COOLANT SYSTEM FOR EACH ACCIDENT

Accident Sequence	Control Volume	Diameter, ft	Length, ft	Thickness, ft	Flow Area, ft^2	Heat Transfer Area, ft^3	Gas Volume, ft^3
AB (Case 1)	Upper Grid	0.4592 (.14 m)	0.0883 (.0269 m)	--	26.0 (2.415 m^2)	20.0 (1.858 m^2)	53.0[a] (1.5 m^3)
	Upper Plenum 1	0.4027 (.1227 m)	5.195 (1.583 m)	--	50.0 (4.645 m^2)	5051.0 (469.3 m^2)	460.0 (13.0 m^3)
	Upper Plenum 2	0.4027 (.1227 m)	5.195 (1.583 m)	--	50.0 (4.645 m^2)	5051.0 (469.3 m^2)	510.0 (14.4 m^3)
AB (Case 2)	Upper Grid	0.4592 (.14 m)	0.0883 (.0269 m)	0.0365 (.0111 m)	26.0 (2.415 m^2)	161.5 (15.00 m^2)	53.0[a] (1.5 m^3)
	Upper Plenum	0.4027 (.1227 m)	10.39 (3.1669 m)	0.0051 (.00155 m)	100.0 (9.29 m^2)	5000.0 (464.5 m^2)	1017.0 (28.8 m^3)
TMLB' (Case 1)	Upper Grid	0.4592 (.14 m)	0.0883 (.0269 m)	--	26.0 (2.415 m^2)	20.0 (1.858 m^2)	53.0[a] (1.5 m^3)
	Upper Plenum 1	0.4027 (.1227 m)	5.195 (1.583 m)	--	50.0 (4.645 m^2)	5051.0 (469.3 m^2)	460.0 (13. m^3)
	Upper Plenum 2	0.4027 (.1227 m)	5.195 (1.583 m)	--	50.0 (4.645 m^2)	5051.0 (469.3 m^2)	510.0 (14.4 m^3)
	Hot Leg	2.42 (.7376 m)	6.40 (1.95 m)	--	4.6 (.427 m^2)	53.0 (4.92 m^2)	30.0 (.85 m^3)
	Surge Line	1.0 (.3048 m)	33.0 (10.06 m)	--	0.785 (.0729 m^2)	113.0 (10.5 m^2)	26.0 (.736 m^3)
	Pressurizer	7.0 (2.1336 m)	33.78 (10.296 m)	--	40.0 (3.716 m^2)	750.0 (69.68 m^2)	1300.0 (36.81 m^3)
TMLB' (Case 2)	Upper Grid	0.4592 (.14 m)	0.0883 (.0269 m)	0.0365 (.0111 m)	26.0 (2.415 m^2)	161.5 (15. m^2)	53.0 (1.5 m^3)
	Upper Plenum	0.4027 (.1227 m)	10.39 (3.1669 m)	0.0051 (.00155 m)	100.0 (9.29 m^2)	5000.0 (464.5 m^2)	1017.0 (28.8 m^3)
	Hot Leg	2.42 (.7376 m)	6.40 (1.95 m)	0.2083 (.06349 m)	4.6 (.427 m^2)	53.0 (4.92 m^2)	30.0 (.85 m^3)
	Surge Line	1.0 (.3048 m)	33.0 (10.06 m)	0.06 (.01829 m)	0.785 (.0729 m^2)	113.0 (10.5 m^2)	26.0 (.736 m^3)
	Pressurizer	7.0 (2.1336 m)	33.78 (10.296 m)	0.3548 (.1081 m)	40.0 (3.716 m^2)	750.0 (69.68 m^2)	1300.0 (36.81 m^3)
V (Case 1)	Upper Grid	0.4592 (.14 m)	0.0883 (.0269 m)	--	26.0 (2.415 m^2)	20.0 (1.858 m^2)	53.0[a] (1.5 m^3)
	Upper Plenum 1	0.4027 (.1227 m)	5.195 (1.583 m)	--	50.0 (4.645 m^2)	5051.0 (469.3 m^2)	460.0 (13. m^3)
	Upper Plenum 2	0.4027 (.1227 m)	5.195 (1.583 m)	--	50.0 (4.645 m^2)	5051.0 (469.3 m^2)	510.0 (14.4 m^3)
	Hot Leg[b]	2.42 (.7376 m)	31.40 (9.57 m)	--	9.2 (.855 m^2)	244.5 (22.71 m^2)	144.2 (4.08 m^3)
	Steam Generator	0.0646 (.01969 m)	76.0 (23.16 m)	--	16.2 (1.505 m^2)	51,500.0 (4784.5 m^2)	845.0 (23.93 m^3)
	Piping to Aux Bldg	0.5 (.1524 m)	202.5 (61.72 m)	--	0.1963 (.0182 m)	320.0 (29.73 m^2)	40.0 (1.13 m^3)
V (Case 2)	Upper Grid	0.4592 (.14 m)	0.0883 (.0269 m)	0.0365 (.0111 m)	26.0 (2.415 m^2)	161.5 (15. m^2)	53.0[a] (1.5 m^3)
	Upper Plenum	0.4027 (.1227 m)	10.39 (3.1669 m)	0.0051 (.00155 m)	100.0 (9.29 m^2)	5000.4 (464.5 m^2)	1017.0 (28.8 m^3)
	Hot Leg[b]	2.42 (.7376 m)	31.40 (9.57 m)	0.2083 (.06349 m)	9.2 (.855 m^2)	244.5 (22.71 m^2)	144.2 (4.08 m^3)
	Steam Generator	0.0646 (.0197 m)	76.0 (23.16 m)	0.0045 (.00137 m)	16.0 (1.486 m^2)	51,500.0 (4784.5 m^2)	845.0 (23.93 m^3)
	Piping to Aux Bldg	0.5 (.1524 m)	202.5 (61.72 m)	0.0265 (.00808 m)	0.1963 (.0182 m^2)	320.0 (29.73 m^2)	40.0 (1.13 m^3)
S_2D (Case 1)	Upper Grid	0.4592 (.14 m)	0.0883 (.0269 m)	--	26.0 (2.415 m^2)	20.0 (1.858 m^2)	53.0[a] (1.5 m^3)
	Upper Plenum 1	0.4027 (.1227 m)	5.195 (1.583 m)	--	50.0 (4.645 m^2)	5051.0 (469.3 m^2)	460.0 (13. m^3)
	Upper Plenum 2	0.4027 (.1227 m)	5.195 (1.583 m)	--	50.0 (4.645 m^2)	5051.0 (469.3 m^2)	510.0 (14.4 m^3)
	Hot Leg[b]	2.42 (.7376 m)	31.40 (9.57 m)	--	9.2 (.855 m^2)	244.5 (22.71 m^2)	144.2 (4.08 m^3)
	Steam Generator	0.0646 (.0197 m)	76.0 (23.16 m)	--	16.0 (1.486 m^2)	51,500.0 (4784.5 m^2)	845.0 (23.93 m^3)
S_2D (Case 2)	Upper Grid	0.4592 (.14 m)	0.0883 (.0269 m)	0.0365 (.0111 m)	26.0 (2.415 m^2)	161.5 (15. m^2)	53.0[a] (1.5 m^3)
	Upper Plenum	0.4027 (.1227 m)	10.39 (3.1669 m)	0.0051 (.00155 m)	100.0 (9.29 m^2)	5000.0 (464.5 m^2)	1017.0 (28.8 m^3)
	Hot Leg[b]	2.42 (.7376 m)	31.40 (9.57 m)	0.2083 (.06349 m)	9.2 (.855 m^2)	244.5 (22.71 m^2)	144.2 (4.08 m^3)
	Steam Generator	0.0646 (.0197 m)	76.0 (23.16 m)	0.0045 (.00137 m)	16.0 (1.486 m^2)	51,500.0 (4784.5 m^2)	845.0 (23.93 m^3)

(a) Includes 50 ft^3 of gas volume from the upper plenum.
(b) Includes piping from hot leg to steam generator.

TABLE 6.3 ACCIDENT EVENT TIMES

Event	Time, minutes
Surry ABδ	
Core Uncover	0.5
Start Melt	27.0
Core Slump	56.0
Bottom Head Dry	58.0
Bottom Head Fail	81.0
Start Concrete Attack	81.0
Containment Fail	2540.9
End Calculation	3687.8
Surry ABγ	
Core Uncover	0.5
Start Melt	27.0
Core Slump	56.0
Bottom Head Dry	58.0
Bottom Head Fail	81.0
Start Concrete Attack	81.0
Containment Fail	81.0
End Calculation	684.8
Surry ABβ	
Containment Fail	0.0
Core Uncover	0.5
Start Melt	27.8
Core Slump	56.8
Bottom Head Dry	58.8
Bottom Head Fail	81.8
Start Concrete Attack	81.8
End Calculation	688.9

TABLE 6.3 (Continued)

	Surry TMLB'δ_l
Steam Generator Dry	83.0
Core Uncover	183.0
Start Melt	201.0
Core Slump	270.0
Core Collapse	273.0
Bottom Head Fail	275.0
Reactor Cavity Dry	277.3
Start Concrete Attack	389.9
Containment Fail	2830.8
End Calculation	2830.8

	Surry TMLB'δ_e
Steam Generator Dry	83.0
Core Uncover	183.0
Start Melt	201.0
Core Slump	270.0
Core Collapse	273.0
Bottom Head Fail	275.0
Containment Fail	276.0
Reactor Cavity Dry	283.5
Start Concrete Attack	389.9
End Calculation	994.7

	Surry S2D ϵ
Containment Heat Removal On	20.1
Containment Spray On	25.0
Core Uncover	31.7
Start Melt	50.1
Core Slump	77.3

(Continued)

TABLE 6.3 (Continued)

Surry S2D ε (Continued)	
Core Collapse	77.4
Bottom Head Fail	80.4
Reactor Cavity Dry	83.8
Start Concrete Attack	210.9
End Calculation	814.3
Surry S2D γ	
Containment Heat Removal On	20.1
Containment Spray On	25.0
Core Uncover	31.7
Start Melt	50.1
Core Slump	77.3
Core Collapse	77.4
Bottom Head Fail	80.4
Containment Fail	80.4
Reactor Cavity Dry	90.0
Start Concrete Attack	206.4
End Calculation	813.5
Surry V	
Core Uncover	4.9
Start Melt	37.2
Core Slump	64.4
Core Collapse	65.6
Bottom Head Fail	87.6
Start Concrete Attack	87.6
End Calculation	692.1

TABLE 6.4 CORE AND PRIMARY SYSTEM RESPONSE

Accident Event	Time, minutes	Primary System Pressure, psia	Primary System Water Inventory, lbm	Average Core Temperature, F	Peak Core Temperature, F	Fraction Core Melted	Fraction Clad Reacted
			Surry ABδ/γ				
Core Uncover	0.5	50.6	5.18×10^2	740	1175	0.	0.
Start Melt	27.0	25.5	5.74×10^4	1788	4130	0.0070	0.0110
Start Slump	56.0	24.5	5.30×10^4	4130	5477	0.75	0.3170
Bottom Head Dry	58.0	26.6	0.	3470	---	1.0	0.9984
Bottom Head Fail	81.0	29.6	0.	3846	---	1.0	0.9984
			Surry ABβ				
Core Uncover	0.5	50.4	5.13×10^2	740	1175	0.	0.
Start Melt	27.8	23.8	5.75×10^4	1678	4130	0.0487	0.0128
Start Slump	56.8	20.4	5.30×10^4	4022	5441	0.75	0.3123
Bottom Head Dry	58.8	22.2	0.	3465	---	1.0	0.9984
Bottom Head Fail	81.8	---	0.	---	---	1.0	0.9984
			Surry TMLB'δ_1				
Core Uncover	183.0	2515	1.31×10^5	672	677	0.	0.
Start Melt	201.0	2514	6.32×10^4	1399	4130	0.75	0.0148
Start Slump	270.0	2510	5.92×10^4	4130	5798	1.0	0.3225
Core Collapse	273.0	2513	1.88×10^4	4661	---	1.0	0.9984
Bottom Head Fail	275.0	---	0.	4130	---	1.0	0.9984

TABLE 6.4 CORE AND PRIMARY SYSTEM RESPONSE

Accident Event	Time, minutes	Primary System Pressure, psia	Primary System Water Inventory, lbm	Average Core Temperature, F	Peak Core Temperature, F	Fraction Core Melted	Fraction Clad Reacted
			Surry TMLB'δ_e				
Core Uncover	183	2515	1.31×10^5	672	677	0.	0.
Start Melt	201	2514	6.32×10^4	1399	4130	0.0688	0.0148
Start Slump	270	2510	5.92×10^4	4130	5798	0.75	0.3225
Core Collapse	273	2513	1.88×10^4	4661	---	1.0	0.9984
Bottom Head Fail	275	---	0.	4130	---	1.0	0.9984
			Surry S2Dϵ/γ				
Core Uncover	31.7	1459	1.06×10^5	596	604	0.	0.
Start Melt	50.1	1068	7.84×10^4	1277	4130	0.0031	0.0183
Start Slump	77.3	418	6.25×10^4	4130	7225	0.75	0.7089
Core Collapse	77.4	2171	2.35×10^4	3667	---	1.0	0.7089
Bottom Head Fail	80.4	---	$1.710. 10^5$	3652	---	1.0	0.9984
			Surry V				
Core Uncover	4.9	790	8.72×10^4	540	545	0.	0.
Start Melt	37.2	104	6.54×10^4	2057	4130	0.0554	0.0210
Start Slump	64.4	109	5.92×10^4	4130	6248	0.75	0.4223
Core Collapse	65.6	1807	0.	3686	---	1.0	0.9984
Bottom Head Fail	87.6	---	0.	3708	---	1.0	0.9984

TABLE 6.5 CONTAINMENT RESPONSE

Accident Event	Time, minutes	Containment Pressure, psia	Compartment Temperature, F	RWST or CST Water Mass, lbm	Sump Water Mass, lbm	Sump Water Temp., F	Reactor Cavity Water Mass, lbm	Reactor Cavity Water Temp., F	Steam Cond. on Walls lbm/min
				Surry ABδ					
Core Uncover	0.5	50.6	264	2.8×10^6	3.04×10^5	221	0.	---	55,110
Start Melt	27.0	25.2	208	2.8×10^6	4.82×10^5	208	0.	---	1,201
Start Slump	56.0	24.5	202	2.8×10^6	---	---	0.	---	0.
Bottom Head Dry	58.0	37.1	232	2.8×10^6	---	---	0.	---	4,629
Bottom Head Fail	81.0	29.6	211	2.8×10^6	5.19×10^5	203	0.	---	0.
Start Concrete Attack	81.0	103.2	2189	2.8×10^6	5.19×10^5	203	0.	---	0.
Containment Fail	2540.9	100.0	293	2.8×10^6	3.63×10^5	323	0.	---	386
End Calculation	3687.8	14.7	236	2.8×10^6	4.98×10^2	211	0.	---	0.
				Surry ABY*					
Containment Fail	81.0	102.8	2092	2.8×10^6	5.19×10^5	203	0.	---	0.
End Calculation	684.8	14.7	215	2.8×10^6	5.19×10^5	203	0.	---	0.

* Containment response same as Surry ABδ out to start of debris/water interaction.

TABLE 6.5 CONTAINMENT RESPONSE

Accident Event	Time, minutes	Compartment Pressure, psia	Containment Temperature, F	RWST or CST Water Mass, lbm	Sump Water Mass, lbm	Sump Water Temp., F	Reactor Cavity Water Mass, lbm	Reactor Cavity Water Temp., F	Steam Cond. on Walls lbm/min
				Surry ABβ					
Containment Fail	0.	14.9	154	2.8×10^6	2.15×10^5	152	0.	---	4,757
Core Uncover	0.5	49.0	262	2.8×10^6	---	---	0.	---	---
Start Melt	27.8	23.7	208	2.8×10^6	4.69×10^5	206	0.	---	997
Start Slump	56.8	20.5	207	2.8×10^6	4.71×10^5	200	0.	---	0.
Bottom Head Dry	58.8	32.8	237	2.8×10^6	---	---	0.	---	4,337
Bottom Head Fail	81.8	22.0	202	2.8×10^6	4.98×10^5	199	0.	---	0.
Start Concrete Attack	81.8	79.4	2294	2.8×10^6	4.98×10^5	199	0.	---	0.
End Calculation	688.9	14.7	219	2.8×10^6	4.98×10^5	199	0.	---	0.
				Surry TMLBδ$_1$					
Steam Generator Dry	83.0	11.5	114	3.0×10^6	6.08×10^3	104	0.	---	329
Core Uncover	183.0	25.2	208	3.0×10^6	2.08×10^5	164	0.	---	1816
Start Melt	201.0	24.3	205	3.0×10^6	2.38×10^5	170	0.	---	748
Start Slump	270.0	22.7	198	3.0×10^6	2.65×10^5	173	0.	---	528
Core Collapse	273.0	29.9	218	3.0×10^6	2.65×10^5	173	0.	---	---
Bottom Head Fail	275.0	57.6	402	3.0×10^6	2.65×10^5	173	0.	---	---

(Continued)

TABLE 6.5 CONTAINMENT RESPONSE

Accident Event	Time, minutes	Containment Pressure, psia	Compartment Temperature, F	RWST or CST Water Mass, lbm	Sump Water Mass, lbm	Sump Water Temp., F	Reactor Cavity Water Mass, lbm	Reactor Cavity Water Temp., F	Steam Cond. on Walls lbm/min
				Surry TMLBδ_1 (Continued)					
Start Debris/ Water Interaction	275.0	57.1	394	3.0×10^6	---	---	1.71×10^5	100	---
Cavity Dry	277.3	84.8	304	3.0×10^6	---	---	0.	---	1,723
Start Concrete Attack	389.9	45.9	255	3.0×10^6	4.48×10^5	218	0.	---	0.
End Calculation	2830.8	100.1	295	3.0×10^6	3.46×10^5	340	0.	---	385
				Surry TMLB'δ_e					
Steam Generator Dry	83.0	11.5	114	3.0×10^6	6.08×10^3	104	0.	---	328
Core Uncover	183.0	25.2	208	3.0×10^6	2.08×10^5	164	0.	---	1,816
Start Melt	201.0	24.3	205	3.0×10^6	2.38×10^5	170	0.	---	748
Start Slump	270.0	22.7	198	3.0×10^6	2.65×10^5	170	0.	---	528
Core Collapse	273.0	29.9	218	3.0×10^6	2.65×10^5	172	0.	---	---
Bottom Head Fail	275.0	57.6	402	3.0×10^6	2.56×10^5	173	1.71×10^5	100	---
Containment Fail	276.0	80.5	299	3.0×10^6	2.70×10^5	176	0.	---	1,723
Cavity Dryout	283.5	25.3	229	3.0×10^6	---	---	0.	---	0.
Start Concrete Attack	389.9	14.7	189	3.0×10^6	3.24×10^5	193	0.	---	0.
End Calculation	994.7	14.7	222	3.0×10^6	3.31×10^5	192	0.	---	0.

TABLE 6.5 CONTAINMENT RESPONSE

Accident Event	Time, minutes	Compartment Pressure, psia	Compartment Temperature, F	RWST or CST Water Mass, lbm	Sump Water Mass, lbm	Sump Water Temp., F	Reactor Cavity Water Mass, lbm	Reactor Cavity Water Temp., F	Steam Cond. on Walls lbm/min
				Surry S2Dε					
Containment Heat Removal On	20.1	19.1	182	2.89×10^6	1.89×10^5	162	0.	---	3,297
Containment Spray On	25.0	17.8	174	---	3.74×10^5	167	0.	---	---
Core Uncover	31.7	15.0	156	2.62×10^6	5.54×10^5	157	0.	---	294
Start Melt	50.1	13.2	105	2.08×10^6	1.12×10^6	139	0.	---	0.
Core Clump	77.3	13.6	120	---	---	---	0.	---	---
Core Collapse	77.4	13.7	119	---	1.86×10^6	121	0.	---	---
Bottom Head Fail	80.4	23.8	190	1.31×10^6	1.95×10^6	122	0.	---	---
Start Debris/ Water Interaction	80.4	23.9	190	---	---	---	1.71×10^5	100	---
Reactor Cavity Dry	83.8	52.7	270	---	---	---	0.	---	2,378
Start Concrete Attack	210.9	11.1	129	2.46×10^5	3.51×10^6	134	0.	---	0.
End Calculation	814.3	20.8	118	2.46×10^5	3.52×10^6	119	0.	---	0.
				Surry S2DY*					
Containment Fail	80.4	84.9	1906	1.31×10^6	1.95×10^6	122	1.71×10^5	100	--0.
Reactor Cavity Dry	90.0	14.5	200	1.31×10^6	2.0005×10^6	125	0.	---	364
Start Concrete Attack	206.4	14.7	210	1.31×10^6	2.02×10^6	126	0.	---	0.
End Calculation	813.5	14.7	210	1.31×10^6	2.03×10^6	126	0.	---	0.

* Containment response same as Surry S2Dε out to Start of Debris/Water Interaction.

TABLE 6.5 CONTAINMENT RESPONSE

Accident Event	Time, minutes	Compartment Pressure, psia 1	Compartment Pressure, psia 2	Compartment Temperature, F 1	Compartment Temperature, F 2	RWST or CST Water Mass, lbm	Sump Water Mass, lbm	Sump Water Temp., F	Reactor Cavity Water Mass, lbm	Reactor Cavity Water Temp., F	Steam Cond. on Walls lbm/min
					Surry V						
Core Uncover	4.9	14.7	14.7	---	---	3.0×10^6	0.	---	0.	---	0/109*
Start Melt	37.2	14.7	14.7	100	796	3.0×10^6	0.	---	0.	---	0/0
Start Slump	64.4	14.7	14.7	100	945	3.0×10^6	0.	---	0.	---	0/0
Core Collapse	65.6	14.7	14.7	100	350	3.0×10^6	0.	---	0.	---	-/-
Bottom Head Fail	87.6	14.7	14.7	100	316	3.0×10^6	0.	---	0.	---	-/-
Start Debris/ Water Interaction	87.6	14.7	14.7	100	314	3.0×10^6	0.	---	0.	---	-/-
Start Concrete Attack	87.6	14.7	14.7	109	218	3.0×10^6	0.	---	0.	---	0/0
End Calculation	692.1	14.7	14.7	150	214	3.0×10^6	0.	---	0.	---	0/0

* Volume 1/Volume 2

TABLE 6.6 CONTAINMENT LEAK RATES

Subsequence	CSIS Start, min	CSIS End, min	CSRS Start, min	CSRS End, min	Leakage Time Interval, min	Leakage Leak Rate, v/hr(a)	Pressure MPa	Pressure psia	Temp °F	Temp °C	Remarks
ABδ	--	--	--	--	0-0.4	4.2×10^{-4}	0.35	51	264	129	Blowdown
					0.4-57	4.2×10^{-4}	0.18	26	209	98	Core heating and melting
					57-81	4.2×10^{-4}	0.21	31	216	101	Vessel heating
					81	4.2×10^{-4}	0.43	63	1079	582	Bottom head fails
					81-82	4.2×10^{-4}	0.67	99	2101	1149	Hydrogen burn
					82-92	4.2×10^{-4}	0.34	50	791	422	Concrete decomposition
					92-150	4.2×10^{-4}	0.21	31	280	138	Concrete decomposition
					150-200	4.2×10^{-4}	0.27	39	399	204	Concrete decomposition
					200-432	4.2×10^{-4}	0.31	46	359	182	Concrete decomposition
					432-2541	4.2×10^{-4}	0.48	71	269	132	Concrete decomposition
					2541	4.2×10^{-4}	0.69	100	293	145	Containment fails
					2541-2558	0.11	0.29	43	239	115	Concrete decomposition
					2588-3496	0.06	0.10	15	253	123	Concrete decomposition
					3496-3688	4.2×10^{-4}	0.10	15	236	113	Concrete decomposition
ABY	--	--	--	--	0-0.4	4.2×10^{-4}	0.35	51	264	129	Blowdown
					0.4-57	4.2×10^{-4}	0.18	26	209	98	Core heating and melting
					57-81	4.2×10^{-4}	0.21	31	216	102	Vessel heating
					81	4.2×10^{-4}	0.42	62	1054	568	Bottom head fails
					81	0.18	0.69	102	2166	1186	Containment fails
					81-87	0.16	0.24	35	909	487	Initial concrete attack
					87-477	0.003	0.10	15	280	138	Concrete decomposition
					477-685	0.001	0.10	15	240	116	Concrete decomposition

(a) Normalized to a containment free volume of 1.8×10^6 ft^3 except for subsequence V. Units are volume fraction/hr.

TABLE 6.6 (Continued)

Subsequence	CSIS Start, min	CSIS End, min	CSRS Start, min	CSRS End, min	Leakage Time Interval, min	Leakage Leak Rate,(a) v/hr	Pressure MPa	Pressure psia	Temp. °F	Temp. °C	Remarks
$AB\beta$	--	--	--	--	0.02	4.2×10^{-4}	0.11	16	160	71	Containment failure
					0.02-0.4	5.7×10^{-3}	0.34	49	262	128	Blowdown
					0.4-28	5.7×10^{-3}	0.19	28	218	103	Core heating
					28-60	5.6×10^{-3}	0.15	22	204	96	Core melting
					60-81.8	6.0×10^{-3}	0.16	24	208	98	Vessel heating
					81.8	8.1×10^{-3}	0.33	49	1143	617	Bottom head fails
					81.8-82.5	0.01	0.48	70	1962	1072	Hydrogen burn
					82.5-83.8	0.01	0.37	54	1404	762	Concrete decomposition
					83.8-88.9	7.8×10^{-3}	0.20	30	597	314	Concrete decomposition
					88.9-172	5.3×10^{-3}	0.12	18	302	150	Concrete decomposition
					172-638	2.1×10^{-3}	0.10	15	270	132	Concrete decomposition
					638-689	4.2×10^{-4}	0.10	15	221	105	Concrete decomposition
$TMLB'\delta_1$	--	--	--	--	0-83	4.2×10^{-4}	0.07	10	100	39	Steam generator dryout
					83-183	4.2×10^{-4}	0.14	21	180	82	Core uncovery
					183-201	4.2×10^{-4}	0.17	25	206	97	Core heatup
					201-270	4.2×10^{-4}	0.17	25	200	93	Core melting
					270-275	4.2×10^{-4}	0.41	60	380	193	Vessel heating
					275	4.2×10^{-4}	0.59	85	452	233	Bottom head fails
					275-390	4.2×10^{-4}	0.37	54	269	132	Initial concrete attack
					390-1936	4.2×10^{-4}	0.37	55	266	130	Concrete decomposition
					1936-2388	4.2×10^{-4}	0.55	81	275	135	Concrete decomposition
					2388-2831	4.2×10^{-4}	0.64	94	289	143	Concrete decomposition
					2831	8.3	0.69	100	295	146	Containment fails

(a) Normalized to a containment free volume of 1.8×10^6 ft^3 except for subsequence V. Units are volume fraction/hr.

TABLE 6.6 (Continued)

Subsequence	CSIS Start, min	CSIS End, min	CSRS Start, min	CSRS End, min	Leakage Time Interval, min	Leakage Leak Rate,(a) v/hr	Pressure MPa	Pressure psia	Temp. °F	Temp. °C	Remarks
TMLB'δ_e	--	--	--	--	0-83	4.2×10^{-4}	0.07	10	100	39	Steam generator dryout
					83-183	4.2×10^{-4}	0.14	21	180	82	Core uncovery
					183-201	4.2×10^{-4}	0.17	25	206	97	Core heatup
					201-270	4.2×10^{-4}	0.17	25	200	93	Core melting
					270-276	4.2×10^{-4}	0.41	60	380	193	Vessel heating
					276	3.8	0.59	85	290	143	Containment fails
					276-390	0.16	0.10	15	225	107	Initial concrete attack
					390-400	0.16	0.10	15	205	96	Concrete decomposition
					400-1000	0.10	0.10	15	220	104	Concrete decomposition
S_2D-ε	20	130	20	815	0-77	4.2×10^{-4}	0.10	15	130	54	Core heating and melt thru
					77-80	4.2×10^{-4}	0.10	15	130	54	Reactor vessel melting
					80-90	4.2×10^{-4}	0.38	55	225	107	H_2O boil off
					90-210	4.2×10^{-4}	0.08	12	125	52	Initial concrete attack
					210-815	4.2×10^{-4}	0.14	21	118	48	Concrete decomposition
S_2D-γ	20	80	20	80	0-77	4.2×10^{-4}	0.10	15	100	38	Core heating and melting
					77-80	4.2×10^{-4}	0.10	15	140	60	Reactor vessel melting
					-80.4	9.01	0.14	20	140	60	Containment failure
					80.4-90	6.8	0.17	25	186	86	Boil off of H_2O
					90-218	0.08	0.10	15	166	86	Initial concrete attack

(a) Normalized to a containment free volume of 1.8×10^6 ft^3 except for subsequence V. Units are volume fraction/hr.

TABLE 6.6 (Continued)

Subsequence	CSIS Start, min	CSIS End, min	CSRS Start, min	CSRS End, min	Leakage Time Interval, min	Leak Rate, v/hr[a]	Pressure MPa	Pressure psia	Temp. °F	Temp. °C	Remarks
S_2D-Y (Continued)					218-300	0.003	0.10	15	176	80	Concrete decomposition
					300-785	0.5	0.10	15	181	83	Concrete decomposition
					785-814	0.09	0.10	15	181	83	Concrete decomposition
V					0+	4.2×10^{-4}[b]	0.10	15	100	38	Auxiliary bldg. failure
					0+-6.5	229[b]	0.10	15	100	38	Release thru auxiliary bldg.
					6.5-90	24[b]	0.10	15	100	38	Bypass containment
					90-220	1.6[b]	0.10	15	150	66	Concrete attack
					220-350	1.7[b]	0.10	15	185	85	Concrete decomposition
					350-690	0.9[b]	0.10	15	212	100	Concrete decomposition

(a) Normalized to a containment free volume of 1.8×10^6 ft^3 except for subsequence V. Units are volume fraction/hr.

(b) Normalized to an auxiliary building volume of 1.5×10^5 ft^3.

TABLE 6.7. DIMENSIONS OF PWR USED FOR CALCULATIONS

Containment Design	Compartment	Volume		Wall Area		Floor Area	
		ft^3	m^3	ft^2	m^2	ft^2	m^2
Large, high pressure	Containment	1.80×10^6	5.097×10^4	2.36×10^5	2.19×10^4	1.374×10^4	1.277×10^3
General, for V sequence	Containment	1.80×10^6	5.097×10^4	2.36×10^5	2.19×10^4	1.347×10^4	1.277×10^3
	Aux Building	1.50×10^5	4.248×10^3	5.25×10^3	4.88×10^2	1.875×10^3	1.742×10^2

TABLE 6.8. PWR CONTAINMENT SPRAY PARAMETERS

Pumps	Flow Rate		Height		Temperature		Droplet Diameter, μm
	lb/min	kg/s	ft	m	F	C	
Injection	2.60×10^4	1.966×10^2	90	27.4	120	48.89	400
Recirculation	5.80×10^4	4.385×10^2	90	27.4	120	48.89	400

TABLE 6.9. INITIAL FISSION PRODUCT INVENTORY FOR THE SURRY PLANT

Species	Inventory (kg)
Cs	130.6
I	12.4
Te	25.4
Xe	260.0
Kr	2.0
Sb	0.7
Ba	61.2
Ru	104.3
Zr	178.6
Sr	47.6
Mo	154.9

Group	Members	Inventory (kg)
1	Xe,Kr	262.0
2	Organic I	--
3	I,BR	13.2
4	Cs,Rb	147.7
5	Te,Se,Sb	28.8
6	Sr,Ba	109.1
7	Ru,Mo,Pd,Rh,Tc	362.2
8	La,Nd,Eu,Y,Ce,Zr Pr,Pm,Sm,Np,Pu,Nb	1217.8

TABLE 6.10. NONFISSION PRODUCT INVENTORY FOR THE SURRY PLANT

Species	Inventory (kg)
Ag	2750
Sn	262
Zr	16454
UO_2	79650
Fe	6486

TABLE 6.11. CORSOR PREDICTIONS OF PERCENT OF INVENTORY EMITTED BY CORE PRIOR TO CORE SLUMP FOR THE FOUR ACCIDENT SEQUENCES

Species	AB	TMLB'	V	S_2D	Core Inventory (kg)
Xe	88.35	99.45	94.82	78.38	260.
Kr	88.35	99.45	94.82	78.38	2.
I	88.23	99.44	94.75	78.09	12.4
Cs	88.55	99.46	94.92	78.84	131.
Te	76.52	94.88	88.10	71.04	25.
Sb	54.71	79.07	69.12	61.18	0.7
Sr	10.44	28.17	16.37	14.80	47.6
Ba	19.66	43.87	27.36	24.08	61.2
Ru	0.82	2.36	1.15	1.02	104.
Mo	6.85	17.10	8.84	7.44	155.
Zr (FP)	0.015	0.041	0.020	0.017	179.
Ag	76.52	94.88	88.10	71.04	3.
UO_2[(a)]	0.23	0.93	0.50	0.48	79650.
Sn[(a)]	54.73	79.07	69.12	61.17	262.
Zr[(a)] Clad	0.015	0.041	0.020	0.017	16462.
Fe[(a)]	1.51	4.01	1.93	1.66	6486.

(a) Nonfission product species.

TABLE 6.12. CORE RELEASE RATES INTO PRIMARY SYSTEM PREDICTED BY CORSOR FOR AB SEQUENCE

(Time Measured from Start of Core Melting)

Time (s)	Mass Release Rate (g/s)			
	Cs	I	Te	Aerosol
0	25.1	1.93	0.83	5.05
120	50.4	4.57	3.11	20.28
240	58.6	5.44	5.79	40.28
420	97.0	9.20	9.57	74.65
660	79.7	7.55	11.70	114.4
960	91.0	8.67	16.50	223.1
1260	52.1	5.13	13.67	485.2
1380	38.3	3.67	11.67	525.1
1500	31.4	3.17	11.67	554.2
1680	4.6	2.33	9.17	708.3

TABLE 6.13. CORE RELEASE RATES INTO PRIMARY SYSTEM PREDICTED BY CORSOR FOR TMLB' SEQUENCE

(Time Measured from Start of Core Melting)

Time (s)	Mass Release Rate (g/s)			
	Cs	I	Te	Aerosol
0	2.73	0.17	0.001	0.002
180	25.9	2.23	1.74	12.24
720	60.8	5.70	7.42	67.33
1440	78.9	7.67	10.32	218.4
1680	35.6	3.43	7.67	260.8
1980	24.2	2.31	5.86	325.2
2700	16.2	1.56	4.10	485.7
3360	8.33	0.82	2.43	743.3
3660	6.99	0.71	2.14	777.0

TABLE 6.14. CORE RELEASE RATES INTO PRIMARY SYSTEM PREDICTED BY CORSOR FOR S_2D SEQUENCE
(Time Measured from Start of Core Melting)

Time (s)	Mass Release Rate (g/s)			
	Cs	I	Te	Aerosol
0	3.55	2.89	1.45	8.94
174	43.9	4.17	5.04	21.08
396	68.9	6.74	6.75	52.67
828	94.2	8.62	17.88	459.6
1068	42.2	4.12	16.50	565.0
1374	26.5	2.58	7.17	611.6
1560	46.4	4.53	8.33	980.0

TABLE 6.15. CORE RELEASE RATES INTO PRIMARY SYSTEM PREDICTED BY CORSOR FOR V SEQUENCE

(Time Measured from Start of Core Melting)

Time (s)	Mass Release Rate (g/s)			
	Cs	I	Te	Aerosol
0	34.2	3.54	1.59	9.79
78	54.7	5.10	3.31	21.7
168	33.5	3.10	3.13	22.8
222	65.7	6.18	5.23	37.4
282	110	10.3	8.08	57.6
342	154	14.6	11.7	83.5
402	176	17.0	15.2	111
642	75.0	7.17	18.0	244
762	131	12.7	23.4	466
1002	61.3	4.27	15.7	642
1182	58.4	5.78	10.8	826
1332	40.0	3.33	9.90	824
1512	19.9	1.77	7.73	816
1696	16.4	1.59	7.16	824

TABLE 6.16. TEMPERATURES, PRESSURES, AND GAS MOLE RATIOS AS FUNCTIONS OF TIME DURING CORE MELTING FOR AB ACCIDENT SEQUENCE

t (s)	T_1 (a) (°C)	T_2 (b) (°C)	T_3 (c) (°C)	Ratio H/O	Ratio Cs/I	Ratio I/H_2O
0	708	567	557	2.91	12.43	1.43×10^{-4}
60	584	438		3.36	10.5	4.69×10^{-4}
180	636	439	649	5.51	10.3	1.03×10^{-3}
360	706	453	759	12.2	10.1	5.1×10^{-3}
600	715	433	840	33.4	10.1	1.54×10^{-2}
900	840	500	1055	555	10.0	.225
1200	803	463	1107	--	9.7	--
1320	809	463		--	9.97	--
1440	833	471	1101	--	9.56	--
1620	599	423		129	1.92	2.13×10^{-3}
1800	298	336		122	--	0

(a) T_1: The MERGE (Case 1) prediction of upper plenum, part 1, gas temperature.

(b) T_2: The MERGE (Case 1) prediction of upper plenum, part 2, gas temperature.

(c) T_3: The MERGE (Case 2) prediction of upper plenum gas temperature.

TABLE 6.17. TEMPERATURES, PRESSURES, AND GAS MOLE RATIOS AS FUNCTIONS OF TIME DURING CORE MELTING FOR TMLB' ACCIDENT SEQUENCE

t (s)	T_1 (a) (°C)	T_2 (b) (°C)	T_3 (c) (°C)	Ratio H/O	Ratio Cs/I	Ratio I/H_2O
0	746	625	506	2	14.9	1.25×10^{-5}
180	450	386	542	2.8	11.1	2.04×10^{-4}
720	499	374	613	11.5	10.2	4.49×10^{-3}
1440	618	394	796	105	9.82	5.44×10^{-2}
1680	632	396	829	985	9.93	.357
1980	647	398	847	--	10.0	--
2700	708	410	917	6577	9.92	19.5
3360	627	442	1006	1.07×10^5	9.74	15.0
3660	487	475	1040	--	9.55	--

(a) T_1: The MERGE (Case 1) prediction of upper plenum, part 1, gas temperature.

(b) T_2: The MERGE (Case 1) prediction of upper plenum, part 2, gas temperature.

(c) T_3: The MERGE (Case 2) prediction of upper plenum gas temperature.

TABLE 6.18. TEMPERATURES, PRESSURES, AND GAS MOLE RATIOS AS FUNCTIONS OF TIME DURING CORE MELTING FOR S_2D ACCIDENT SEQUENCE

t (s)	T_1 (a) (°C)	T_2 (b) (°C)	T_3 (c) (°C)	Ratio H/O	Ratio Cs/I	Ratio I/H_2O
0	746	589		2	11.2	6.11×10^{-6}
174	521	391		2.85	9.75	1.31×10^{-5}
396	517	351		4.94	9.66	5.51×10^{-5}
828	644	469		18.2	10.4	1.86×10^{-4}
1068	701	506		33.4	9.79	1.76×10^{-4}
1374	941	692		670	9.45	2.01×10^{-3}
1626	990	828		--	9.74	--

(a) T_1: The MERGE (Case 1) prediction of upper plenum, part 1, gas temperature.

(b) T_2: The MERGE (Case 1) prediction of upper plenum, part 2, gas temperature.

(c) T_3: The MERGE (Case 2) prediction of upper plenum gas temperature.

TABLE 6.19. TEMPERATURES, PRESSURES, AND GAS MOLE RATIOS AS FUNCTIONS OF TIME DURING CORE MELTING FOR V ACCIDENT SEQUENCE

t (s)	T_1(a) (°C)	T_2(b) (°C)	T_3(c) (°C)	Ratio H/O	Ratio Cs/I	Ratio I/H_2O
0	644	468	497	3.02	9.21	3.64×10^{-4}
78	461	294	603	2.99	10.2	3.31×10^{-4}
168	438	264		3.38	10.3	2.9×10^{-4}
228	458	262	739	5.26	10.1	1.17×10^{-3}
288	571	321		6.45	10.2	2.07×10^{-3}
348	658	368		7.95	10.1	2.43×10^{-3}
408	678	377	874	8.05	9.85	2.84×10^{-3}
648	744	397		16.2	10	3.44×10^{-3}
768	904	457	1175	27.8	9.82	7.69×10^{-3}
1008	937	491	1367	48.3	13.7	6.34×10^{-3}
1188	1031	336	1755	7847	9.65	1.58
1332	884	358	1605	1543	11.5	.275
1512	675	359	1122	--	9.55	--
1608	407	313	990	2.18	1	1.95×10^{-4}
1696	253	271	172	2.18	9.53	1.52×10^{-7}

(a) T_1: The MERGE (Case 1) prediction of upper plenum, part 1, gas temperature.

(b) T_2: The MERGE (Case 1) prediction of upper plenum, part 2, gas temperature.

(c) T_3: The MERGE (Case 2) prediction of upper plenum gas temperature.

TABLE 6.20. MELT COMPOSITION AT TIME OF RPV MELT-THROUGH, EXCLUSIVE OF BOTTOM HEAD MOLTEN MASS, DETERMINED FROM CORSOR PREDICTIONS

Species	Corium Inventory after RPV Failure (kg)			
	AB	TMLB'	S_2D	V
Xe	30	0	51.9	5.18
Kr	0.23	0	0.40	0.04
I	1.10	0	2.11	0
Cs	15.0	0	25.6	2.55
Te	5.90[b]	0.004	6.83	1.53
Sb	0.62	0.39	0.57	0.48
Sr	43.0	33.9	99.8	68.1
Ba	49.0	32.1	46.1	43.3
Ru	103.1	101.3	102.9	102.7
Mo	144.4	126.4	144.3	140.5
Zr (FP)	179.0	178.1	179.0	178.6
Ag	0.70	0.004	0.82	0.18
UO_2[a]	79471	78844	79261	79224
Sn[a]	119.0	33.9	99.8	68.1
Zr[a] Clad	16459	16455	16459	16459
Fe[a]	6748	6563	6738	6714

(a) Denotes nonfission product species.

(b) Also taken as 25 kg for parametric comparison of transport results.

References

(6.1) Technical Base for Estimating Fission Product Behavior During LWR Accidents, NUREG-0772, (June, 1981).

(6.2) Torgerson, D. F., et al., Fission Product Chemistry Under Reactor Accident Conditions, presented at the International Meeting on Thermal Nuclear Reactor Safety, Chicago, Illinois, U.S.A. (September 1982).

(6.3) Jordan, H., Schumacher, P. M., and Gieseke, J. A., "Comparison of QUICK Predictions with Results of Selected, Recent Aerosol Behavior Experiments", NUREG/CR-2922, BMI-2089 (September, 1982).

(6.4) Gieseke, J. A., et al, "Aerosol Source Term for Fast Reactor Safety Analysis", BMI-X-637 (August 11, 1972).

(6.5) Nuclear Aerosols in Reactor Safety, CSNI/SOAR No. 1 (June, 1979).

(6.6) Postma, A. K. and Zavodoski, R. W., Review of Organic Iodide Formation Under Accident Conditions in Water-Cooled Reactors, WASH-1233 (1972).

(6.7) Pelletier, C. A., et al., Preliminary Radioiodine Source Term and Inventory Assessment for TMI-2, SAI-139-82-12-RV (September, 1982).

(6.8) Lin, C. C., Chemical Effecs of Gamma Radiation on Iodine in Aqueous Solutions, J. Inorg. Nucl. Chem., 42, pp. 1101-1107 (1980).

(6.9) Reactor Safety Study: An Assessment of Accident Risks in U.S. Commercial Nuclear Power Plants, WASH-1400 (1974).

(6.10) Barnes, R. H., Kircher, J. F., and Townley, C. W., Chemical Equilibrium Studies of Organic Iodide Formation Under Nuclear Reactor Accident Conditions, BMI-1816 (1966).

7. RESULTS AND DISCUSSION

7.1 Introduction

Results of calculations for the transport and deposition of radionuclides are presented and discussed in this section. The plants and sequences selected for consideration were discussed in Chapter 4, the analytical and calculational methods were described in Chapter 5, and the assumptions and bases for the calculations were described in Chapter 6. Results presented in this chapter include the deposition and release to the containment of radionuclides leaving the core region. These results are based on TRAP-MELT code calculations. Also included as results are the masses of radionuclides airborne and deposited in the containment (or in the V sequence, the auxiliary building) as well as the airborne materials leaked to the environment.

There are five cases presented for radionuclide transport and deposition in the primary system. The calculations represent four sequences, AB (hot leg), TMLB', S_2D, and V, with assumptions leading to both "hot" and "cold" upper plenum conditions for the AB sequence with conditions of "hot" only used for the TMLB' and V, while "cold" only is used for Sequence S_2D in this report. An additional AB case termed AB-Te is implied in which there is assumed to be no tellurium release from the fuel within the primary system. The absence of Te is assumed to have no effect on primary system transport and deposition of other species.

Transport and deposition calculations for the containment are expanded to include parametric variation of containment failure time and include calculations performed with the CORRAL-2 and NAUA-4 codes. The codes for containment calculations are summarized in Table 7.1.

TABLE 7.1. PWR CONTAINMENT CASES

Sequence Designation	Upper Plenum	Containment Failure Time, min	Codes Used[a]
AB_γ	Cold	81	N,C
	Hot	81	N,C
AB_γ-Te	Cold	81	N
	Hot	81	N
$AB\delta_1$	Cold	2541	N,C
	Hot	2541	N,C
AB_β	Cold	0	N,C
	Hot	0	N,C
AB_ε	Cold	None	None -- same
	Hot	None	As $AB\delta_1$ to basemat melt-through
$TMLB'\delta_e$	Hot	276	N
$TMLB'\delta_1$	Hot	2830	N,C
S_2D_γ	Hot	80	N[b],C
S_2D_ε	Hot	None	N[b],C
V	Hot	None	N[c]

(a) C = CORRAL-2, N = NAUA-4.

(b) NAUA-4 modified by addition of spray removal of aerosols.

(c) Run for auxiliary building rather than containment.

7.2 Transport and Deposition in Primary System

The analyses of the transport and deposition within the RCS of materials released from the melting core have been performed using the TRAP-MELT code which was described in an earlier section of this report. The time frame of interest in the RCS for core meltdown accidents such as those considered here spans the period of time starting with the onset of core melting and ending with failure of the bottom head of the RPV. For accidents involving only minor fuel damage, the gap release term, which occurs prior to melting of fuel may be the major release and require careful consideration. For the accidents examined here, however, this release term is insignificant in comparison with the melt release and the period immediately prior to the onset of core melting is not considered. Rather, the gap releases calculated by CORSOR are added to the initial material emitted by the melting core.

When 75 percent of the core is predicted by MARCH to have become molten, it is assumed to slump into the lower plenum of the RPV, rapidly vaporizing the water which was present in that volume. For the low pressure sequences (AB and V), the volume of steam generated during this process is more than ample to quickly flush the RCS of its suspended materials. The higher pressure sequences (S_2D and TMLB') require further examination in this regard. In these latter sequences, however, there is a rapid depressurization of the RCS at the time of bottom head failure -- which requires only several minutes after slumping due to the pressure in the system. At the time of depressurization, the contents of the RCS are rapidly expelled into the containment by gas expansion. In both cases, i.e., flushing of the RCS due to the steam surge which accompanies core slumping and system depressurization, the results presented here are based on the assumption that the very short residence times which characterize these situations prevent retention of significant amounts of the materials suspended in the RCS at the time of core slumping. No reentrainment of deposited aerosol mass is considered, nor has evaporization of vapors condensed on surfaces been considered to occur during this phase of the accidents.

One further aspect of the time frame of the primary system analyses which should be noted is that the primary system is not considered in the analyses after the molten core has left the RPV. Air ingress into the RPV and deposition of materials evolved during the core-concrete interaction is not considered, nor is the primary system considered as a potential source of fission products due to reevolution of previously deposited materials.

The nature of the gas flow patterns in the control volumes of the RCS exert significant influence on the retention of the species of interest here. While the code used to perform the analyses presented here makes use of engineering correlations for the fluid flow properties, dependent upon the relevant thermal hydraulic parameters drawn from MERGE calculations, there exists some uncertainty as to whether flow through a region as complex as an upper plenum can be simulated using any simple approach. Both the degree of turbulence and the general sense of the flow in a volume affect the retention of material in the volume. The lack of detailed information regarding the geometry of the control volumes forces one to make simplifying assumptions which may turn out to be unjustified. It seems clear that detailed modeling of anticipated flow patterns in the upper plenum is required to reduce the uncertainties associated with the results which follow.

A significant source of uncertainty enters these analyses through the imprecision and uncertainties in the experimentally determined release rates and deposition velocities for the species under examination here. The influence of the release rate uncertainties on the CORSOR predictions of mass injected into the RCS is presented in Appendix B. The influence of these uncertainties on RCS transport and retention calculations has not been determined at this stage of the study.

Results are presented in this report using two assumptions regarding the fate of chemisorbed CsOH and Te. In one set of analyses, the material which deposited on system surfaces with the deposition velocity measured for chemisorption was permitted to evaporate as if no reaction took place. In a second set of analyses, the chemisorbed material was assumed to be irreversibly deposited. The actual situation in the RCS is likely to be closer to this latter case. The results presented below

indicate that, under the thermal hydraulic conditions which characterize the sequences studied, the fate of the chemisorbed material is only of significance for Te due to its deposition velocity, which is quite high in comparison with those of CsOH or I_2.

A further and potentially very important source of uncertainty in the analyses performed stems from the fact that the RCS structures' heatup caused by decay heat of the deposited fission products has not been taken into account. If one assumes an adiabatic heatup, one can estimate roughly that deposition of one-half of the core's inventory of I, Cs, and Te would impart sufficient decay heat to cause a temperature increase of about 800 C/hr in a 25,000 kg mass of steel. This mass and the deposited fraction of inventory stated are not out of the range of conditions which may characterize the upper plenum of the PWR considered here. This heatup would be expected to reduce the amount of vapor condensation on the surface and thereby limit the amount of condensible fission products which will deposit in a given location. The influence of this effect on primary system retention has not been investigated in this report.

In summary, the results presented below are subject to a number of uncertainties which require examination. These results are, however, based upon the best available information, and upon a methodology which represents a significant improvement over previous attempts at this type of analysis.

Results of the analyses of transport and deposition in the RCS for each of the four sequences, AB, 'MLB', S_2D, and V, are discussed separately in the following sections. The geometry describing the control volumes in the pathway to the containment for each case is found in Table 6.2, and the timing of the core melting portion of the sequences can be found in Table 6.3.

7.2.1 RCS Transport and Deposition for Sequence AB

The AB sequence was analyzed with the TRAP-MELT code using two different sets of RCS thermal hydraulic conditions provided by the MERGE code, as discussed in the previous chapter. The results from the MERGE

analysis which predicted lower system temperatures is referred to as the "Case 1" or "cold" case here. The results derived from the currently preferred estimates of the thermal hydraulic conditions are referred to as "Case 2" or "hot". The differences between these two sets of results are illustrated in Figures 6.2 and 6.3. The rates of emission of the various species into the RCS are, of course, the same for both sets of thermal hydraulics, and are specified in Table 6.9.

The TRAP-MELT predictions of primary system deposition of CsI, CsOH, Te, and aerosol are presented in Tables 7.2 through 7.5. The values in these tables denote the fractions of the material emitted from the core which are retained on RCS surfaces due to vapor condensation or chemisorption (Vap), the fraction which condenses on particles which are subsequently deposited (Aero), and the fraction of the core-emitted material which is suspended in the RCS at the stated times. For the aerosol in these tables, the fraction retained on the primary system surfaces (Ret) is listed along with the fraction suspended. Thus, the sum of the values for any species at a given time indicates how much of the material resides in the RCS, and the difference between this sum and unity is the fraction of the core-emitted material which has escaped the primary system. The numbers in these tables are cumulative in nature, and so the last entry can be interpreted as a primary system retention factor, integrated over the duration of core melting.

Several interesting features emerge from the results contained in Tables 7.2 through 7.5. The most obvious conclusion to be drawn is that the retention factors for the cesium species and aerosol are not great. Only about one quarter of the aerosol generated during core melting is retained in the Case 1 results, and still less is retained for the hot case. For the Case 1 MERGE conditions, approximately 25 percent of the CsI and CsOH are retained in the upper plenum, mostly due to vapor condensation on system surfaces. The extent of retention is, as one would expect, substantially reduced in the simulation performed using the hotter system temperatures which impede the vapor condensation. Tables 7.4 and 7.5 present results of TRAP-MELT calculations under the assumption that the chemisorption is an irreversible process. Clearly, only the Te is significantly affected by this change in the bases for the calculations.

TABLE 7.2. TRAP-MELT PREDICTIONS OF PRIMARY SYSTEM RETENTION DUE TO VAPOR DEPOSITION (VAP), AEROSOL DEPOSITION (AERO), AND THE AMOUNT REMAINING SUSPENDED IN RCS, EXPRESSED AS FRACTIONS OF THE SPECIES AVAILABLE FOR SEQUENCE AB (CASE 1)

Time	CsI			CsOH			Te			Aerosol	
(s)	Vap	Aero	Susp	Vap	Aero	Susp	Vap	Aero	Susp	Ret	Susp
200	.05	.03	.08	.09	.03	.07	.74	--	.06	.08	.11
400	.07	.03	.10	.09	.03	.09	.82	--	.05	.10	.12
600	.07	.04	.09	.10	.03	.09	.86	--	.05	.11	.15
800	.09	.04	.06	.11	.04	.06	.89	--	.04	.10	.12
1000	.14	.04	.04	.15	.04	.04	.92	--	.03	.10	.10
1200	.16	.04	.04	.17	.04	.04	.92	--	.03	.11	.15
1400	.16	.08	.03	.18	.08	.03	.93	--	.03	.26	.14
1600	.18	.09	--	.20	.09	--	.93	--	.01	.33	.02
1800	.16	.09	--	.17	.09	--	.50	--	.01	.26	--

TABLE 7.3. TRAP-MELT PREDICTIONS OF PRIMARY SYSTEM RETENTION DUE TO VAPOR DEPOSITION (VAP), AEROSOL DEPOSITION (AERO), AND THE AMOUNT REMAINING SUSPENDED IN RCS, EXPRESSED AS FRACTIONS OF THE SPECIES AVAILABLE FOR SEQUENCE AB (CASE 2)

Time	CsOH			CsI			Te			Aerosol	
(s)	Vap	Aero	Susp	Vap	Aero	Susp	Vap	Aero	Susp	Ret	Susp
200	.20	.01	.05	.11	.02	.06	.58	0	.05	.07	.08
400	.35	.01	.07	.33	.01	.08	.65	0	.05	.09	.09
600	.38	--	.05	.37	.01	.06	.71	0	.04	.09	.09
800	.38	--	.04	.35	--	.04	.73	0	.04	.09	.09
1000	.38	--	.04	.35	--	.04	.67	0	.04	.09	.08
1200	.34	--	.03	.30	--	.04	.53	0	.04	.08	.10
1400	.29	--	.04	.22	--	.05	.44	0	.05	.09	.13
1600	.21	--	.04	.07	--	.07	.34	0	.05	.15	.11
1800	.15	--	.04	0	--	.04	.28	0	.05	.17	.10

TABLE 7.4. TRAP-MELT PREDICTIONS OF PRIMARY SYSTEM RETENTION DUE TO VAPOR DEPOSITION (VAP), AEROSOL DEPOSITION (AERO), AND THE AMOUNT REMAINING SUSPENDED IN RCS, EXPRESSED AS FRACTIONS OF THE SPECIES AVAILABLE FOR SEQUENCE AB (CASE 1) WITH IRREVERSIBLE CHEMISORPTION

Time	CsOH			CsI			Te			Aerosol	
(s)	Vap	Aero	Susp	Vap	Aero	Susp	Vap	Aero	Susp	Ret	Susp
200	.05	.03	.08	.09	.03	.07	.74	--	.06	.08	.10
400	.07	.03	.10	.10	.03	.09	.82	--	.05	.08	.11
600	.07	.04	.09	.10	.03	.09	.86	--	.05	.10	.14
800	.09	.04	.06	.11	.04	.06	.89	--	.04	.10	.11
1000	.13	.04	.04	.15	.04	.04	.92	--	.03	.10	.10
1200	.16	.04	.04	.17	.04	.04	.92	--	.03	.10	.15
1400	.16	.08	.03	.18	.08	.03	.93	--	.03	.25	.15
1600	.17	.10	.02	.19	.10	.02	.94	--	.02	.36	.17
1800	.17	.11	.02	.19	.11	.02	.93	--	.03	.41	.11

TABLE 7.5 TRAP-MELT PREDICTIONS OF PRIMARY SYSTEM RETENTION DUE TO VAPOR DEPOSITION (VAP), AEROSOL DEPOSITION (AERO), AND THE AMOUNT REMAINING SUSPENDED IN RCS, EXPRESSED AS FRACTIONS OF THE SPECIES AVAILABLE FOR SEQUENCE AB (CASE 2) WITH IRREVERSIBLE CHEMISORPTION

Time	CsOH			CsI			Te			Aerosol	
(s)	Vap	Aero	Susp	Vap	Aero	Susp	Vap	Aero	Susp	Ret	Susp
200	.20	.01	.05	.11	.02	.06	.57	0	.05	.07	.08
400	.30	.01	.06	.26	.01	.06	.67	0	.05	.09	.09
600	.35	--	.05	.32	--	.05	.74	0	.04	.09	.09
800	.38	--	.04	.35	--	.04	.78	0	.04	.09	.09
1000	.37	--	.04	.35	--	.04	.81	0	.03	.09	.08
1200	.34	--	.03	.30	--	.04	.82	0	.02	.08	.10
1400	.29	--	.04	.22	--	.05	.84	0	.03	.09	.13
1600	.21	--	.04	.07	--	.07	.85	0	.02	.15	.11
1800	.15	--	.05	0	0	.04	.86	0	.02	.17	.10

These results demonstrate that, for irreversible chemisorption of Te, with a deposition velocity of 1 cm/sec, approximately 90 percent of this species is retained in the RCS, even for the AB sequence.

It is interesting to note also the dynamic nature of the retention factor, as its value reflects changing system conditions. As an example, in the Case 2 thermal hydraulics the temperatures of the upper plenum surfaces rise during the melt progression, rising noticeably at t = 1400 s. This is reflected in the reevolution of previously condensed CsI and, to a lesser extent, CsOH as indicated by the reduced value of "Vap" at this time. One can also detect the influence of the higher system gas temperatures for Case 2 in the lower values for "Aero", indicating reduced condensation on particle surfaces in the upper plenum. Figures 7.1 and 7.2 illustrate the total masses of the various species retained in the upper plenum for the cold and hot thermal hydraulics, along with aerosol retention in the core. The drop in the amount of CsOH and CsI retained late in the accident is perhaps more apparent here than in the tabular data. Another aspect of system response reflected in this figure is the increased aerosol deposition rate near the end of the melt period, due to the higher aerosol emission rate from the core. It is clear in these two figures that the lower temperatures used in the "cold" calculations bring about more retention in the RCS for all the species considered. (These figures are results of the analyses performed which permitted reevaporation of chemisorbed material.) Figures 7.3 and 7.4 put these calculations in terms of the amounts of the various species which escape the RCS prior to core slumping. It will be seen in the analyses here that the last portion of the core melting is quite important for the containment source term since this time period is characterized by the highest aerosol generation rates, and for most sequences, the shortest RCS residence times.

The relative importance of the different control volumes which form the pathway to the containment is frequently of interest since it gives insight into the aerosol behavior in the system. This is especially true in the more complex geometries which characterize some of the other accidents considered. Table 7.6 indicates the distribution of the retained aerosol between the core and the upper plenum volumes. Clearly, as the total amount of retention increases (as indicated by Table 7.3), the relative importance

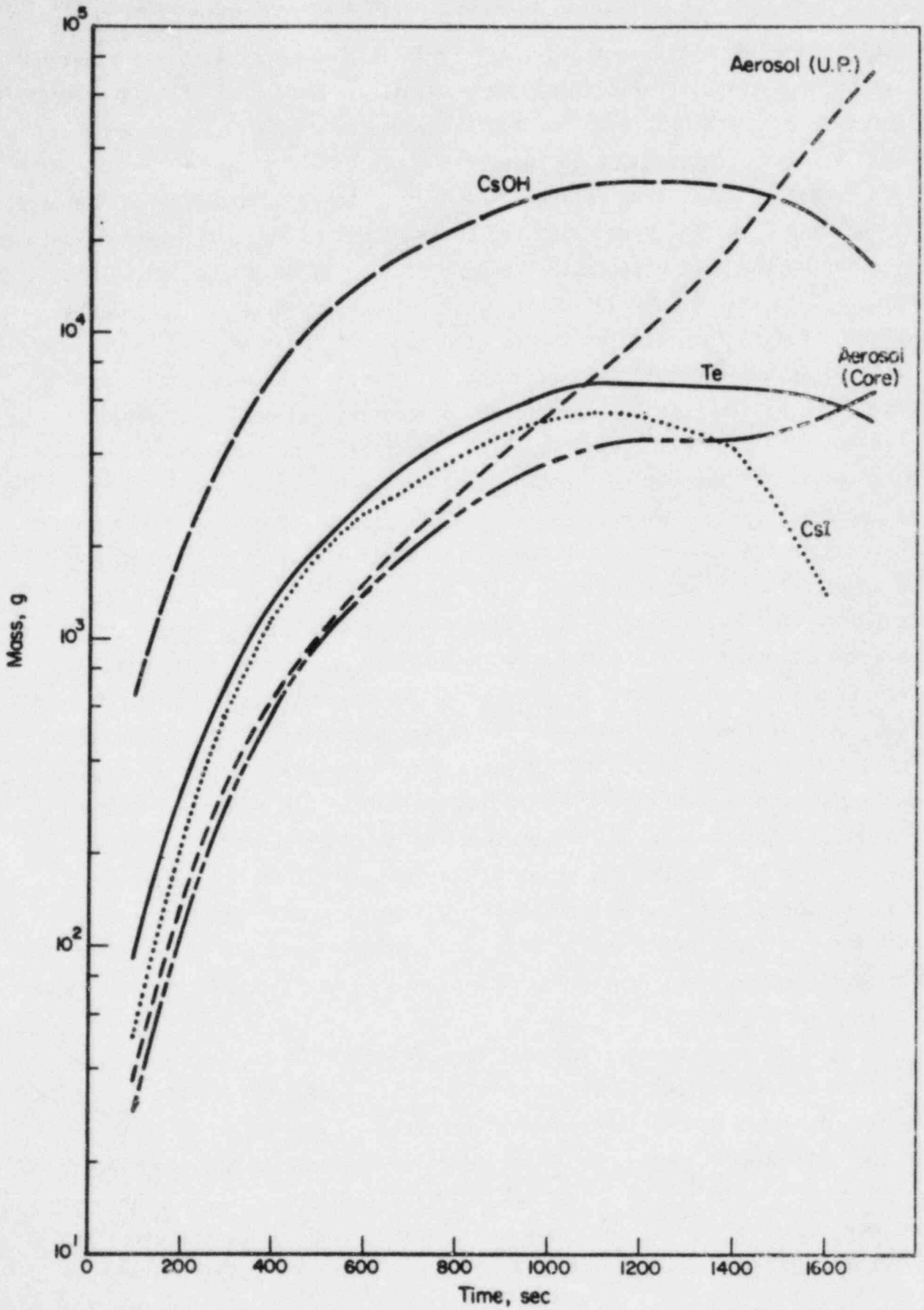

FIGURE 7.1. MASSES OF CsOH, CsI, Te, AND AEROSOL DEPOSITED IN UPPER PLENUM AND AEROSOL DEPOSITED IN CORE AS FUNCTIONS OF TIME AFTER START OF CORE MELTING FOR SEQUENCE AB (CASE 2)

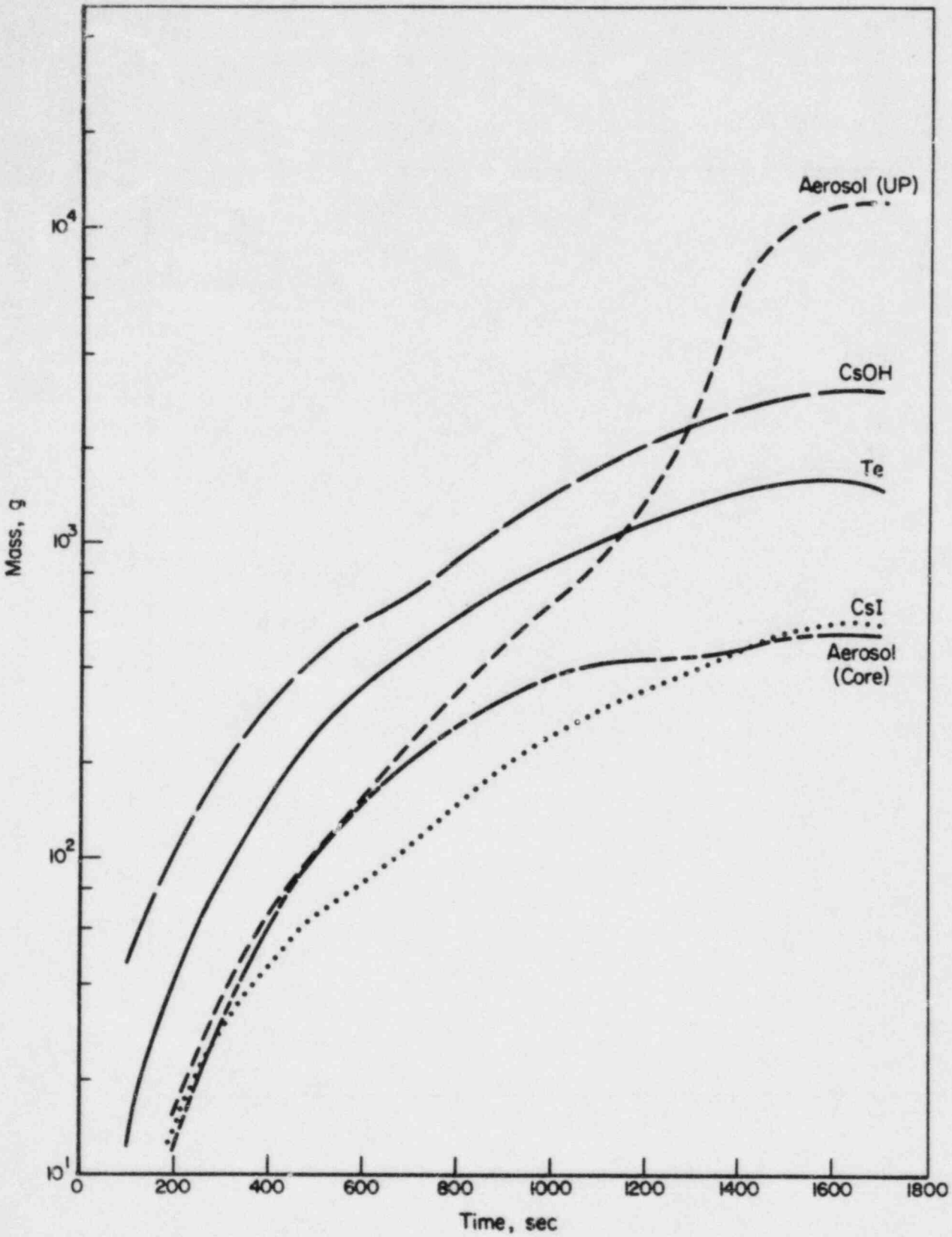

FIGURE 7.2. MASSES OF CsOH, CsI, Te, AND AEROSOL DEPOSITED IN UPPER PLENUM AND AEROSOL DEPOSITED IN CORE AS FUNCTIONS OF TIME AFTER START OF CORE MELTING FOR SEQUENCE AB (CASE 1)

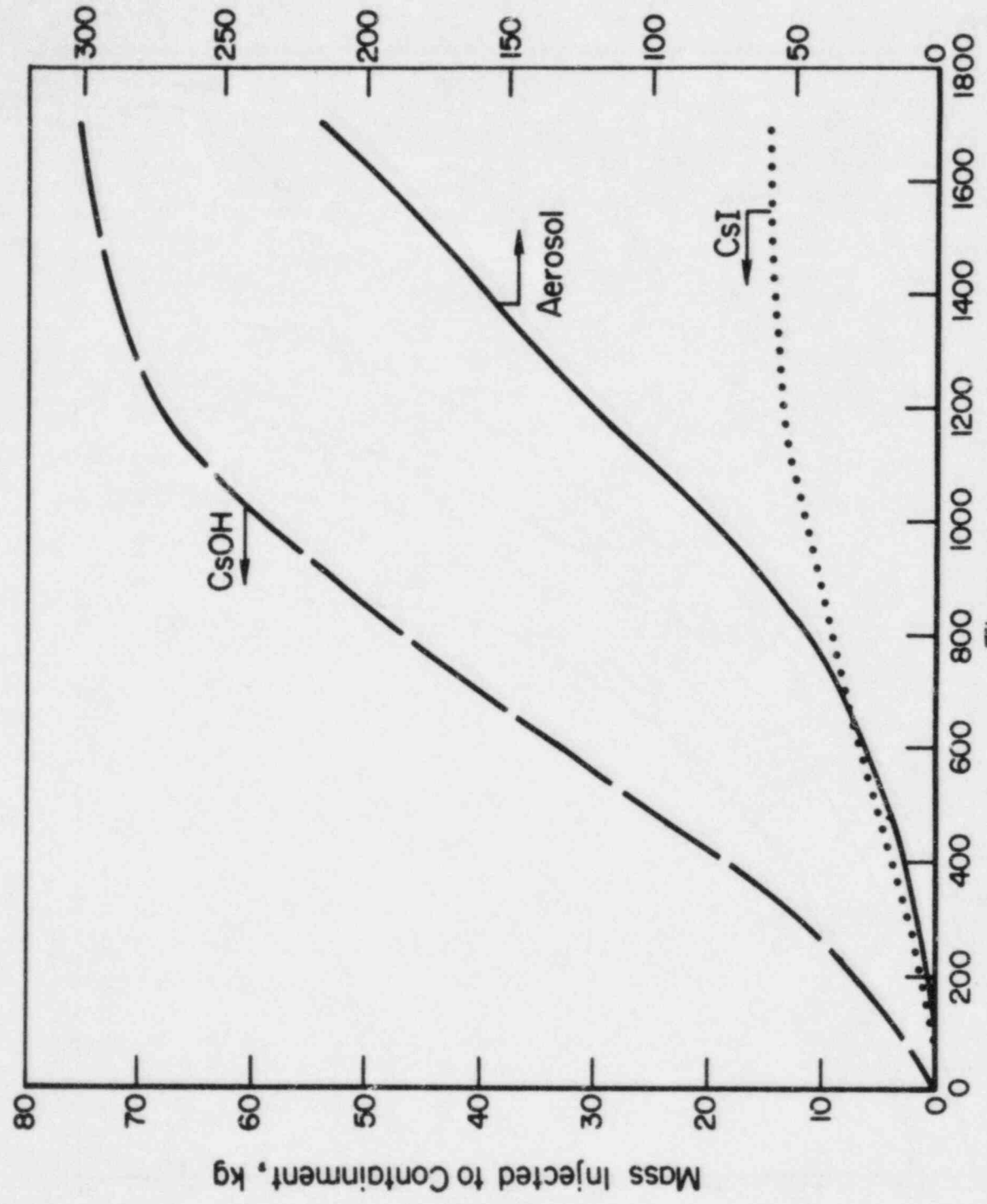

FIGURE 7.3. MASS OF CsOH, CsI AND AEROSOL INJECTED INTO CONTAINMENT DURING CORE MELTING IN AB COLD SEQUENCE

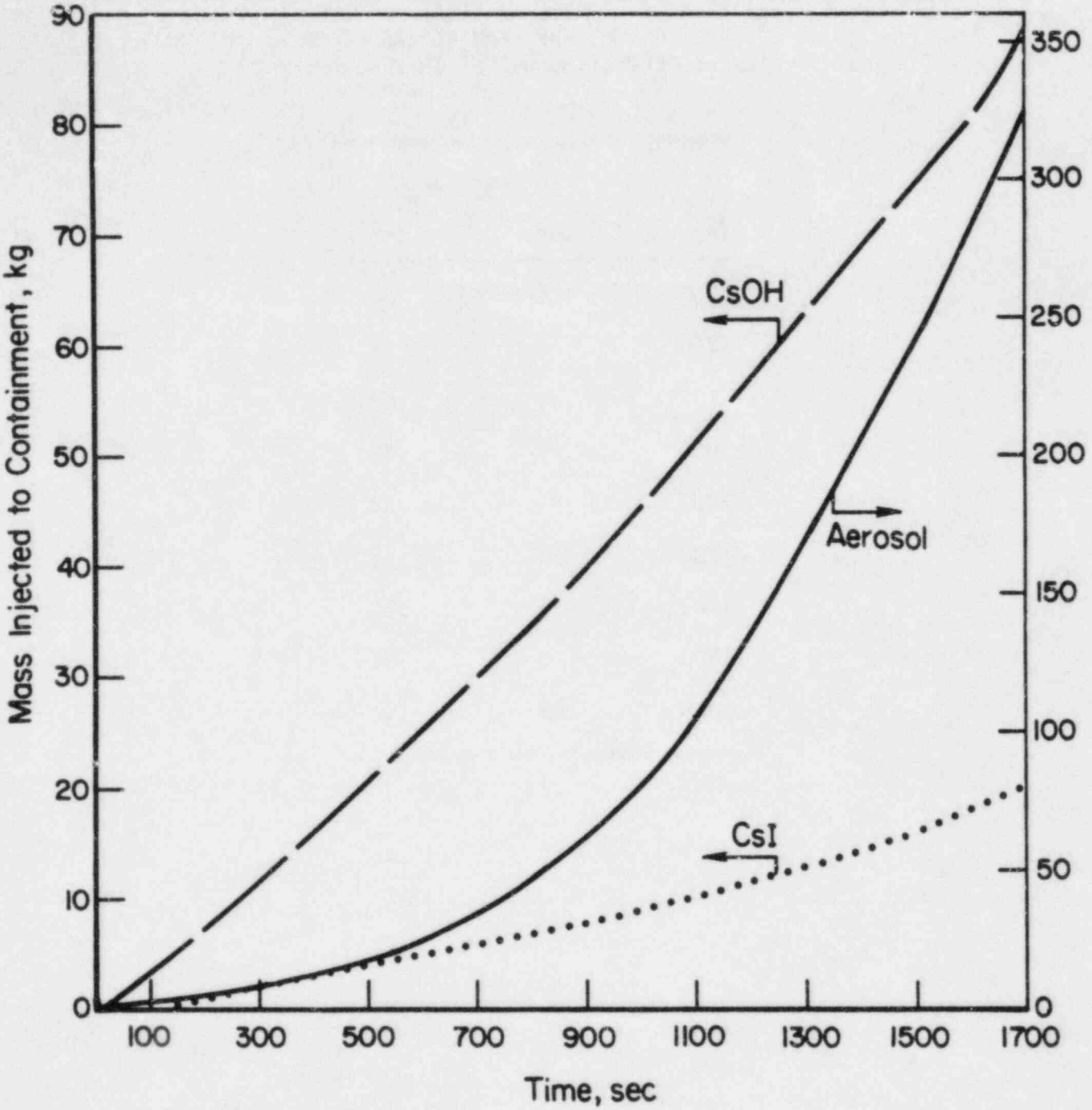

FIGURE 7.4. MASS OF CsOH, CsI, AND AEROSOL INJECTED INTO CONTAINMENT DURING CORE MELTING IN AB HOT SEQUENCE

TABLE 7.6. FRACTION OF AEROSOL MATERIAL RETAINED IN THE RCS CONTROL VOLUMES FOR SEQUENCE AB (CASE 2) (ALL VAPOR SPECIES DEPOSITION OCCURS IN UPPER PLENUM)

Time (s)	Aerosol	
	Core	Upper Plenum
200	.46	.54
400	.49	.51
600	.49	.51
800	.47	.53
1000	.41	.59
1200	.32	.68
1400	.19	.81
1600	.10	.90
1800	.08	.92

of the core as an aerosol receptor diminishes for this sequence. This is principally an effect of the residence time which determines the size to which the aerosol particles can grow. The extent of growth, in turn, greatly influences the retention due to gravitational settling of the particles.

It should be kept in mind when examining these results that the vapor concentrations in the RCS volumes at various times also influence the extent of retention, as does the residence time available for the mass transfer to occur. Due to the interactions between these various parameters, interpretation of the results of the transport analyses for the RCS is not so straightforward in some cases as for the relatively simple situation which characterizes the AB sequence.

7.2.2 RCS Transport and Deposition for Sequence TMLB'

The TRAP-MELT analysis of this sequence was performed using the MERGE Case 2 estimates of RCS thermal hydraulics and the core emission rates as presented in Table 6.10. It also assumes that chemisorption is irreversible. This sequence is different from any of the others considered in this report since the melt occurs in a sustained high pressure environment in addition to having a melt duration approximately twice as long as that of any of the other sequences.

Tables 7.7 and 7.8 summarize the results of the TRAP-MELT analyses of this sequence. It is apparent in Table 7.7 that even just prior to core slumping, essentially all of the material emitted from the core still resides in the RCS, in evidence of the extreme residence times which characterize this sequence. While this affords the aerosol material ample time to coagulate and thereby grow into the size regime where gravitational settling and removal become important, the low flow into the upper plenum prevents the condensation of much of the condensible CsI and CsOH on the surfaces of that volume. Thus, this sequence is characterized in these results by a retention factor of 0.93 for the aerosol, and only 0.27 for the CsOH and 0.17 for CsI.

The locations which dominate the retention fraction results are shown in Table 7.8. For the condensible species, CsI and CsOH, the trends

TABLE 7.7. TRAP-MELT PREDICTIONS OF PRIMARY SYSTEM RETENTION DUE TO VAPOR DEPOSITION (VAP), AEROSOL DEPOSITION (AERO), AND THE AMOUNT REMAINING SUSPENDED IN RCS, EXPRESSED AS FRACTIONS OF THE SPECIES AVAILABLE FOR SEQUENCE TMLB'

Time	CsOH			CsI			Te			Aerosol	
(s)	Vap	Aero	Susp	Vap	Aero	Susp	Vap	Aero	Susp	Ret	Susp
407	--	.01	.99	--	.01	.99	.15	0	.85	.03	.97
813	.01	.09	.90	--	.09	.91	.17	0	.83	.40	.60
1220	.01	.13	.86	--	.13	.86	.19	0	.81	.66	.33
1627	.03	.15	.82	.01	.15	.84	.20	0	.80	.79	.20
2033	.05	.15	.80	.01	.17	.82	.20	0	.80	.86	.14
2440	.07	.14	.78	.01	.17	.81	.20	0	.80	.90	.10
2847	.11	.13	.76	.01	.17	.81	.22	0	.78	.92	.08
3253	.12	.14	.74	--	.17	.82	.25	0	.75	.93	.07
3660	.13	.14	.73	--	.17	.82	.27	0	.73	.93	.07

TABLE 7.8. FRACTIONS OF RETAINED MATERIAL IN RCS IN THE VARIOUS CONTROL VOLUMES FOR TMLB' SEQUENCE

Time (s)	CsI		CsOH		Aerosol		
	Upper Plenum	Hot Leg	Upper Plenum	Hot Leg	Core	Upper Plenum	Hot Leg
203	.65	.19	.86	.09	.93	.04	.01
407	.60	.19	.70	.15	.79	.13	.03
610	.72	.12	.74	.12	.77	.17	.03
813	.80	.08	.81	.08	.84	.13	.01
1017	.82	.06	.83	.06	.88	.10	.01
1220	.83	.06	.84	.06	.90	.08	.01
1423	.84	.05	.85	.05	.92	.07	.01
1627	.84	.05	.85	.05	.93	.06	--
1830	.84	.05	.86	.04	.94	.05	--
2033	.84	.05	.86	.04	.95	.04	--
2237	.83	.05	.87	.04	.96	.03	--
2440	.83	.05	.87	.04	.97	.03	--
2643	.82	.05	.87	.04	.97	.02	--
2847	.81	.05	.87	.04	.97	.02	--
3050	.79	.05	.87	.04	.98	.02	--
3253	.76	.05	.87	.04	.98	.02	--

in the table indicate the obvious importance of the upper plenum as a receptor for the intermediate volatility species. The results of CsI also indicate a small amount of migration of this species from the site where it was initially deposited to a point further downstream as the surface temperatures rise and reevaporate a portion of the deposited mass. This effect can be shown to reduce the impact of uncertainties in upper plenum temperatures on RCS retention, since the material is redistributed but still retained if the downstream system temperatures remain relatively cool.

By far the dominant mechanism for aerosol retention in this sequence is gravitational settling in the core region. It is apparent that omission of this control volume from the analysis, or its incorrect treatment would greatly affect the results. It is assumed in all of these analyses that the aerosol settles against the flow in the core region (which, of course, reduces the settling velocity) and that material which settles onto the horizontal surface area available in this volume is permanently removed from the system.

The dominance of the gravitational settling mechanism for this sequence is explained in Figures 7.5 and 7.6. The aerosol mass distribution is depicted in Figure 7.5 for three of the RCS control volumes shortly before core slumping. The breadth of the distribution in the core is caused by the admixture of a strong source of very small particles with aerosol particles which have been aging, and undergoing coagulational growth for nearly an hour. The large particles in this volume are being removed via settling, while the smaller particles are being removed from the distribution through coagulation with the large particles. Thus, as the aerosol enters the hot leg of the system (after transiting the upper plenum), the aerosol distribution is greatly narrowed, as well as being reduced on an integral basis. This is depicted also in Figure 7.6 for three times during the core melting period, and illustrates the fact that even though the aerosol distribution in the vicinity of the core changes significantly during the course of the melt, the aerosol size distribution at the exit from the upper plenum does not. So, even though the TMLB' sequence affords the aerosol the longest period to grow, the sedimentation removes particles such that the mass median diameter of the particles is not significantly different from the latter portions of the other sequences.

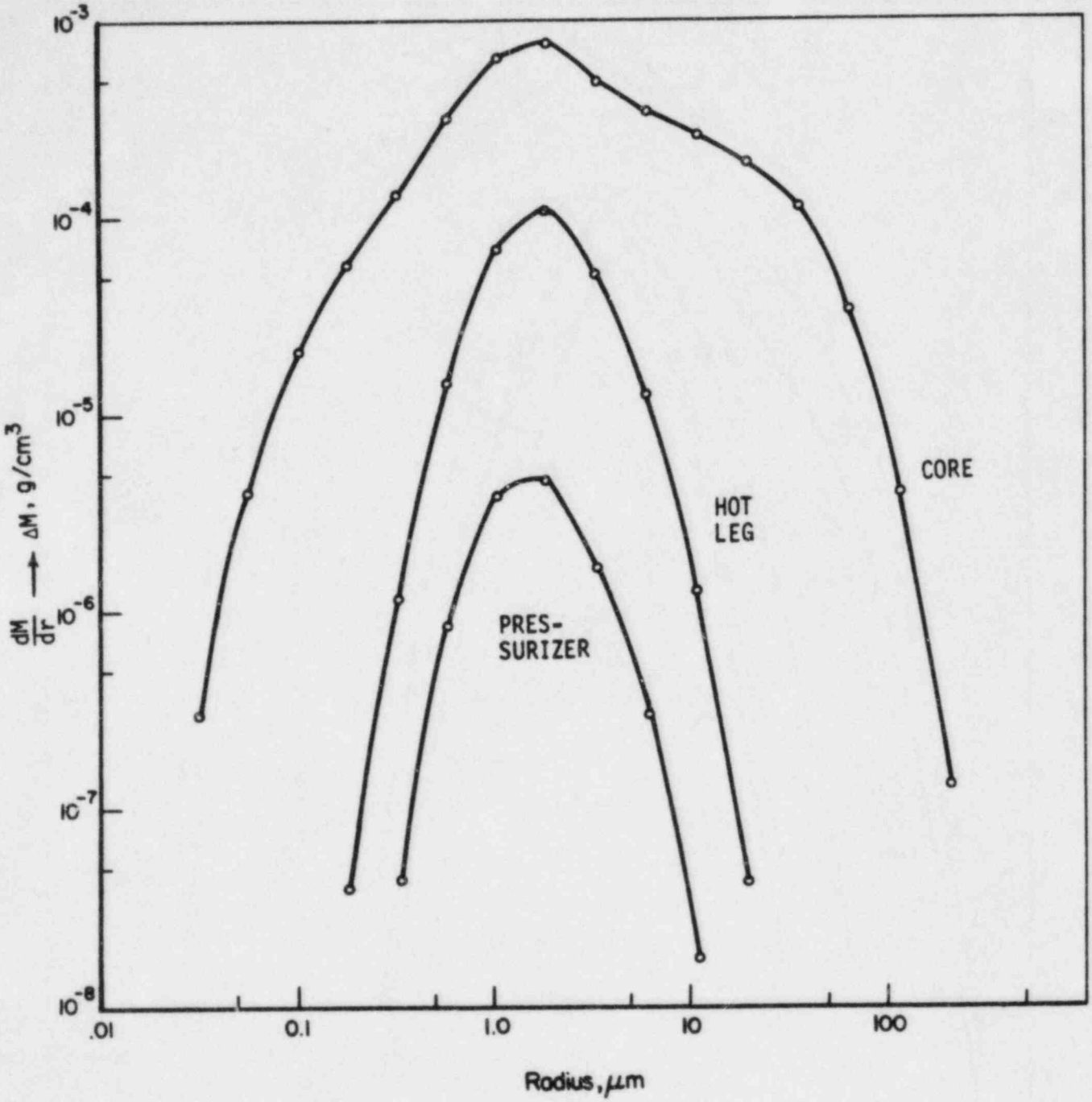

FIGURE 7.5. AEROSOL MASS DISTRIBUTIONS IN THE CORE, HOT LEG, AND PRESSURIZER AT t = 3253s AFTER START OF CORE MELT FOR SEQUENCE TMLB'

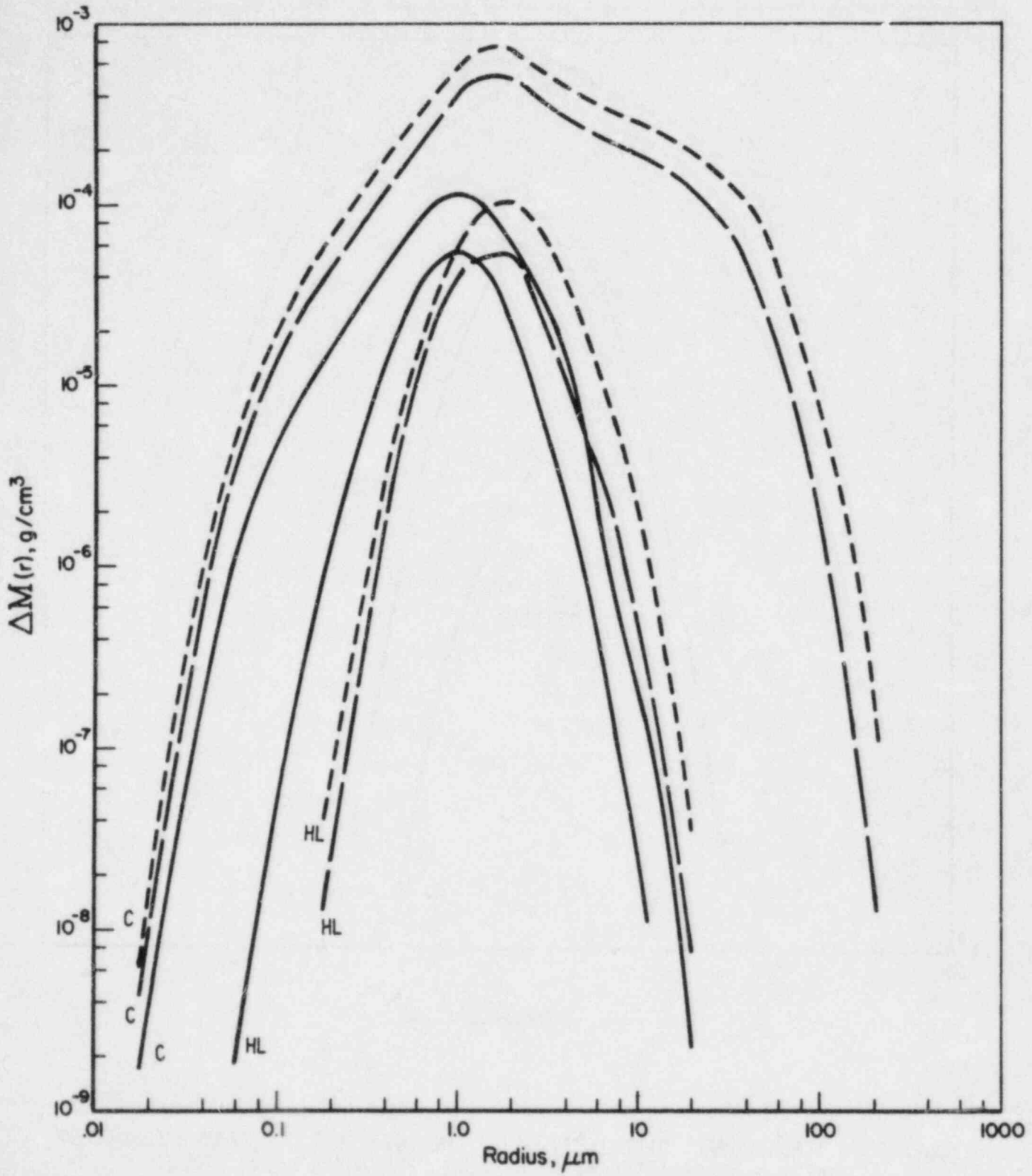

FIGURE 7.6. AEROSOL MASS DISTRIBUTIONS IN THE CORE (c) AND HOT LEG (HL) AT t = 400s (——), t = 2000s (— —), AND t = 3000s (---) FOR TMLB' SEQUENCE

7.2.3 RCS Transport and Deposition for Sequence S_2D

The S_2D sequence is characterized by intermediate pressure in the RCS and by the presence of a steam generator in the pathway to the containment. The analysis whose results are presented here used the Case 2 MERGE predictions of thermal hydraulic conditions and irreversible chemisorption of Te and CsOH. The primary system retention of the CsI and CsOH exceeds 60 percent, over 90 percent of the Te is expected to be retained and over 80 percent of the aerosol mass is predicted to be retained in this sequence as indicated in Table 7.9.

The RCS control volumes in which the retention of the cesium species and aerosol occurs are presented in Table 7.10. The importance of the steam generator for the retention of CsOH and CsI is apparent in the values in this table. It is perhaps less apparent that this component of the system is potentially quite important for aerosol retention. For although only 11 percent of the retained aerosol resides in the steam generator at the end of the melt period, this represents a very high efficiency of removal of the aerosol in this volume. Thus, even if the aerosol were to penetrate the upper plenum more than predicted in this analysis, the change in the mass injected into the containment would not be expected to be great.

One further point should be noted regarding the analysis of this sequence. It was assumed that flow to the containment occurs only through one of the two steam generators. The flow path through the other is considered to be effectively blocked. If this blockage does not occur, an additional flow pathway to the containment would be made available. This would result in longer residence times due to the reduced mass flow through each of the steam generators, and one would therefore expect yet higher retention efficiencies in the steam generators.

TABLE 7.9. TRAP-MELT PREDICTIONS OF PRIMARY SYSTEM RETENTION DUE TO VAPOR DEPOSITION (VAP), AEROSOL DEPOSITION (AERO), AND THE AMOUNT REMAINING SUSPENDED IN RCS, EXPRESSED AS FRACTIONS OF THE SPECIES AVAILABLE FOR SEQUENCE S_2D (CASE 2)

Time	CsOH			CsI			Te			Aerosol	
(s)	Vap	Aero	Susp	Vap	Aero	Susp	Vap	Aero	Susp	Ret	Susp
195	.02	.01	.92	.01	.01	.93	.57	0.0	.43	.04	.92
390	.04	.04	.79	.02	.05	.81	.69	0.0	.31	.09	.82
585	.12	.15	.57	.09	.15	.60	.72	0.0	.28	.16	.77
780	.18	.22	.47	.07	.23	.55	.73	0.0	.27	.41	.55
975	.18	.28	.42	.01	.34	.51	.77	0.0	.23	.62	.34
1170	.25	.35	.28	.02	.45	.39	.82	0.0	.18	.74	.24
1365	.28	.40	.19	.04	.54	.28	.88	0.0	.12	.80	.18
1560	.30	.43	.15	.04	.60	.22	.92	0.0	.08	.82	.16

TABLE 7.10. FRACTIONS OF RETAINED MATERIAL IN RCS IN THE VARIOUS CONTROL VOLUMES FOR S_2D (CASE 2) SEQUENCE

Time (s)	CsOH			CsI			Aerosol		
	Upper Plenum	Hot Leg	Steam Generator	Upper Plenum	Hot Leg	Steam Generator	Core	Upper Plenum	Steam Generator
195	.71	.21	.08	.59	.31	.10	.71	.12	.04
390	.67	.26	.07	.59	.33	.08	.49	.24	.05
585	.54	.15	.32	.47	.17	.36	.25	.27	.29
780	.49	.15	.36	.27	.22	.51	.31	.39	.17
975	.37	.18	.44	0.0	.30	.70	.38	.38	.14
1170	.37	.15	.47	0.0	.24	.76	.43	.36	.12
1365	.36	.14	.50	0.0	.20	.80	.46	.34	.11
1560	.36	.13	.51	0.0	.18	.82	.48	.33	.11

7.2.4 RCS Transport and Deposition for Sequence V

The V sequence has several features which distinguish it from the others analyzed in this report. With respect to primary system characteristics, it is a low pressure sequence like the AB discussed earlier. But unlike the AB, the materials released from the core must transit a large portion of the primary system, including a long small diameter pipe, before exiting to the auxiliary building. The availability of this much greater surface area and the somewhat greater residence times act to increase the amount of retention which occurs in the RCS. The extent of the increase in retention, compared to AB is apparent in Table 7.11.

This sequence is characterized by over 60 percent retention of both the cesium species, most of which occurs via vapor condensation on particles which are subsequently deposited. The retention of tellerium is due almost entirely to chemisorption of the vapor and accounts for 90 percent of that which was emitted from the core.

The aerosol retention increases throughout the sequence because of the ever increasing injection rate of aerosol mass into the flowing gas. The increasing mass concentration of aerosl emitted in the core region leads to larger particles as the melt period progresses so that eventually the aerosol achieves a settling velocity which results in aerosol removal from the gas at a significant rate. This is the principal mechanism for aerosol removal during the later stages of the melt period, which is when the majority of the mass removal occurs. Early in the melt period, thermophoretic deposition is the dominant aerosol removal mechanism.

In this analysis, nearly 80 kg of aerosol material is predicted to be retained in the 15-cm diameter pipe leading to the auxiliary building. Assuming that the deposited aerosol layer has a density of only one-fifth that of the bulk material of which it is composed, the predicted deposition would result in a layer approximately 3-mm thick on the lower half of the pipe surface. Resuspension of material from such a thick layer has not been considered in this analysis, nor have the possible effects of a very uneven distribution of this material in the pipe been analyzed.

TABLE 7.11. TRAP-MELT PREDICTIONS OF PRIMARY SYSTEM RETENTION DUE TO VAPOR DEPOSITION (VAP), AEROSOL DEPOSITION (AERO), AND THE AMOUNT REMAINING SUSPENDED IN RCS, EXPRESSED AS FRACTIONS OF THE SPECIES AVAILABLE FOR SEQUENCE V WITH IRREVERSIBLE CHEMISORPTION

Time	CsI			CsOH			Te			Aerosol	
(s)	Vap	Aero	Susp	Vap	Aero	Susp	Vap	Aero	Susp	Ret	Susp
200	.10	.16	.29	.14	.15	.28	.83	.01	.11	.34	.32
400	.25	.14	.31	.25	.14	.31	.86	.01	.10	.40	.33
600	.31	.23	.14	.33	.22	.14	.91	.02	.06	.46	.28
800	.24	.30	.15	.28	.29	.13	.93	.01	.04	.48	.30
1000	.01	.55	.11	.07	.47	.15	.96	.01	.02	.60	.21
1200	.01	.61	.06	.08	.56	.06	.96	.01	.03	.63	.22
1400	.01	.61	.09	.09	.56	.07	.91	.01	.07	.76	.14
1600	.01	.61	.09	.09	.56	.08	.90	--	.09	.83	.08

Table 7.12 clearly illustrates the importance of the steam generator and piping as retention sites for both the cesium species as well as the aerosol particles. Due to the formation of large particles towards the end of the melt period, retention of aerosol in the core region becomes a significant factor in the overall retention in the RCS. The masses of CsI, CsOH, and of aerosol which have escaped the primary system during the period of core melting are depicted in Figure 7.7.

7.2.5 Conclusions Regarding RCS Transport and Deposition

It is clear from the analyses discussed in this section that the retention of fission products in the primary system during the sequences considered must be considered on an individual basis. This is true because not only do the thermal hydraulic conditions and core emission rates vary among the sequences, but also what parts of the RCS constitute the pathway to the containment vary. There are, nevertheless, certain general features exhibited by all four of these accident sequences.

The aerosol mass concentrations in the core region as functions of time are presented in Figure 7.8. This represents the starting point for the aerosol transport calculations. Each sequence exhibits a very large increase in aerosol mass concentration as the generation rate increases with time. It is interesting to note that the natural aerosol removal processes, which become more effective at higher concentrations, act to limit the maximum concentration achieved. These removal processes, dominated by gravitational settling, act also to place an upper limit on the aerosol size distribution by removing larger particles much more effectively than the smaller ones. This is reflected in Figure 7.9, which presents the aerosol mass median diameter calculated by the TRAP-MELT code for the aerosol at the exit from the primary system. While these are clear differences among the sequences' results, the common upper bound on particle size, and general trend displayed by each of the sequences is readily apparent. Such results are useful for providing insight into sequences not analyzed here or for deducing likely effects of variations in conditions from those used in these analyses.

TABLE 7.12. FRACTIONS OF RETAINED MATERIAL IN RCS IN THE VARIOUS CONTROL VOLUMES FOR V SEQUENCE

Time (s)	CsI		CsOH		Aerosol				
	Steam Generator	Piping	Steam Generator	Piping	Core	Plenum	Hot Leg	Steam Generator	Piping
200	.34	.21	.29	.18	.63	.05	--	.20	.12
400	.17	.17	.17	.17	.65	.05	--	.15	.15
600	.16	.25	.16	.24	.4C	.05	.01	.17	.29
800	.23	.32	.22	.30	.31	.07	.01	.26	.35
1000	.50	.48	.45	.43	.13	.07	.01	.43	.36
1200	.54	.44	.51	.39	.08	.07	.01	.53	.30
1400	.56	.41	.52	.37	.23	.14	.02	.42	.19
1600	.56	.40	.51	.35	.42	.12	.02	.30	.13

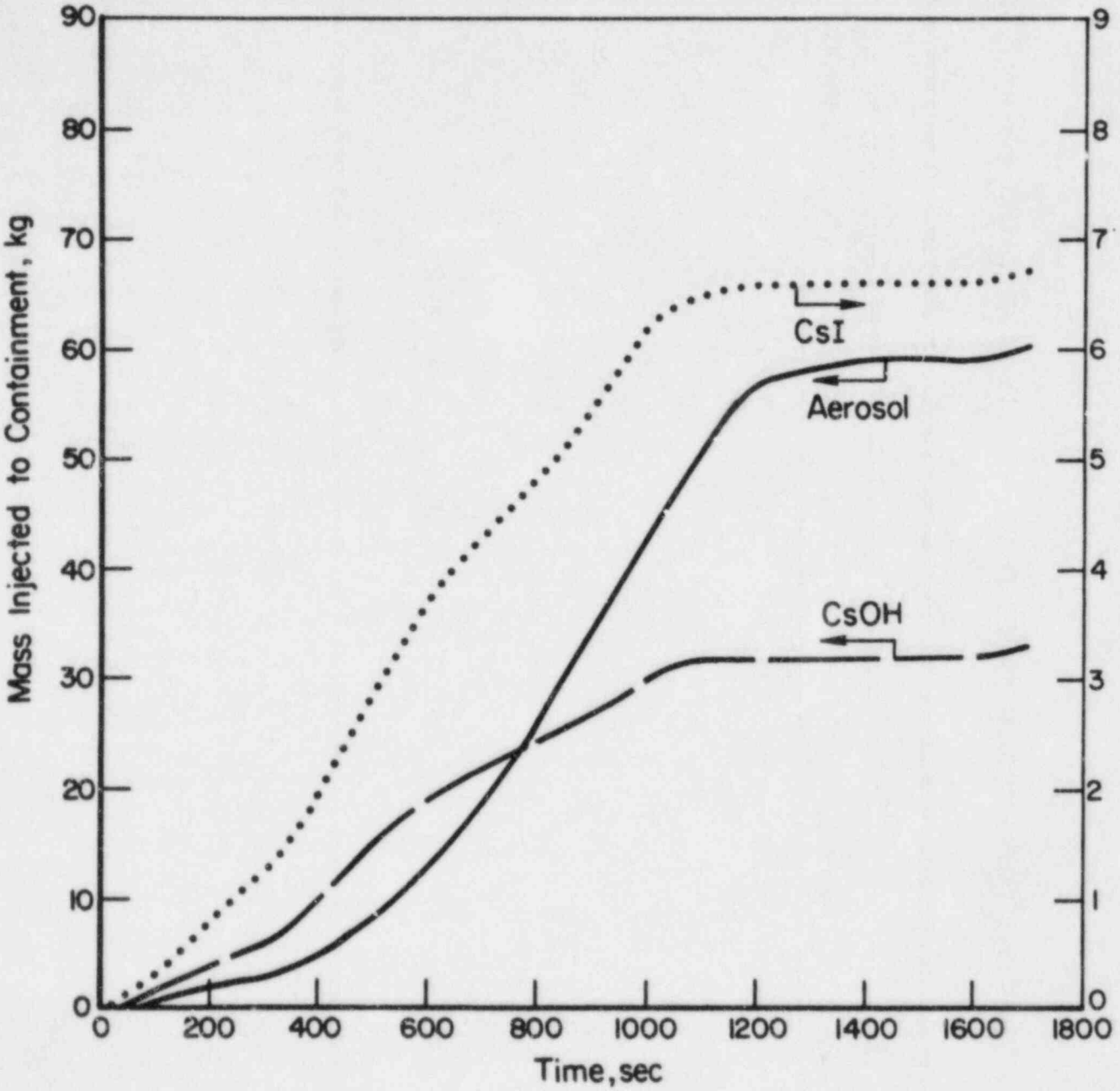

FIGURE 7.7. MASS OF CsOH, CsI, AND AEROSOL INJECTED INTO AUXILIARY BUILDING DURING CORE MELTING IN SEQUENCE V

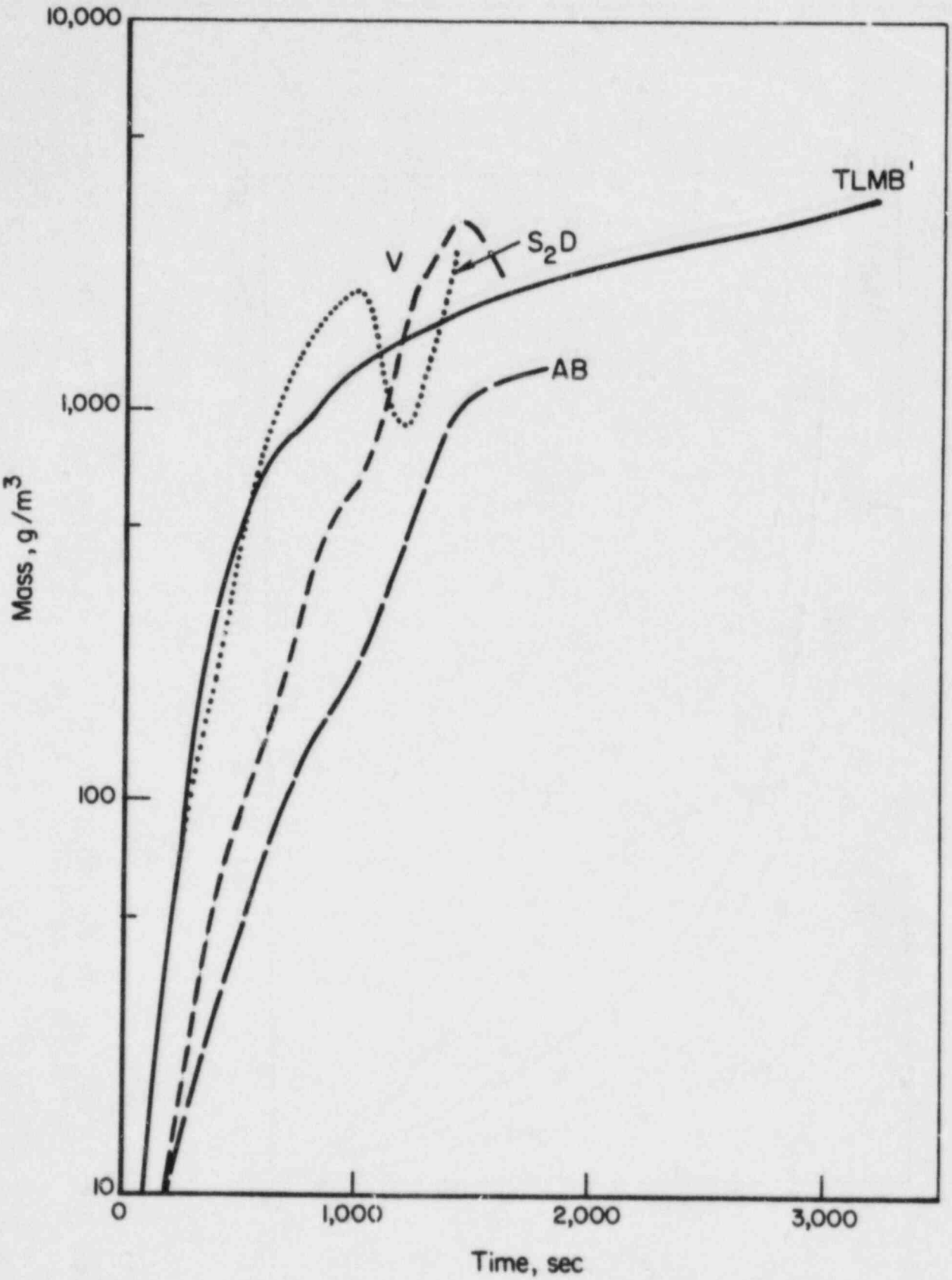

FIGURE 7.8. AEROSOL MASS CONCENTRATIONS IN CORE REGION AS FUNCTIONS OF TIME AFTER START OF CORE MELTING FOR SEQUENCES AB (CASE 2), TMLB', S_2D, AND V

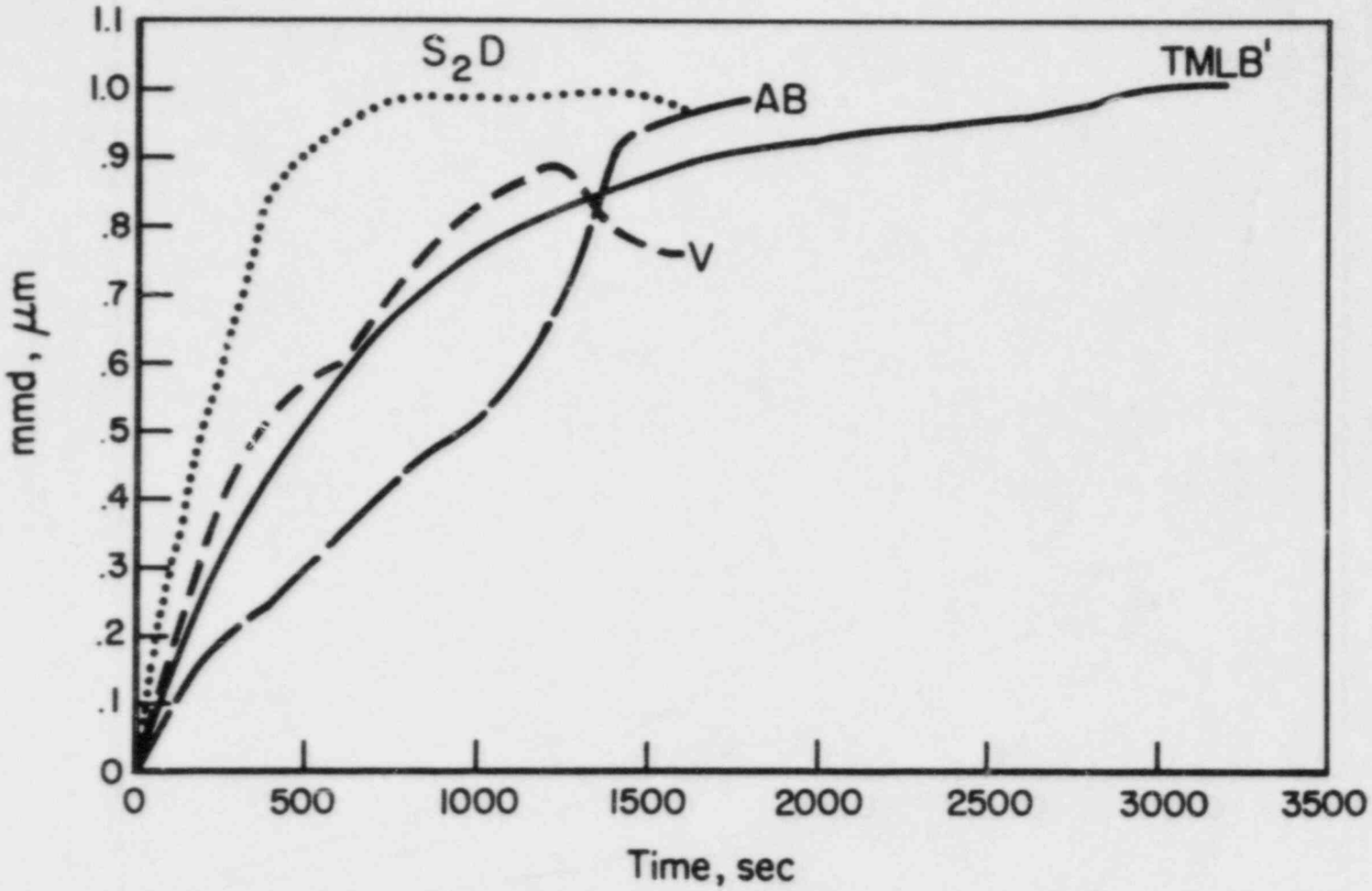

FIGURE 7.9. AEROSOL MASS MEDIAN DIAMETER AT EXIT FROM RCS AS FUNCTIONS OF TIME AFTER START OF CORE MELTING FOR SEQUENCES AB (CASE 2), TMLB', S_2D, AND V

...e importance of chemisorption as a primary system retention mechanism for CsOH and Te is illustrated in Table 7.13 for the sequences analyzed here. Clearly, this is the only mechanism of importance for the retention of Te due to its very high deposition velocity. The lower deposition velocity of CsOH makes the importance of this mechanism very much dependent on RCS residence times and thermal hydraulic conditions for this species. The difference between the chemisorbed fractions for AB hot and AB cold demonstrates that the upper plenum conditions and the deposition velocity are such that the competition between sorption and condensation is quite sensitive to changes in the system temperature.

An uncertainty contained in the results of these analyses stems from the assumption that all material suspended in the RCS at the time of core slumping or RPV failure is injected into the containment with no further attenuation. The potential impact of this assumption on the total mass predicted to be injected into the containment can be assessed using the information presented in Table 7.14. The aerosol, for example, ranges from 0.14 of that injected into the containment for the AB hot sequence to 0.5 for V, to over 0.99 for the TMLB' sequence. Clearly, the disposition of this material has an impact on the containment conditions.

The results of the TRAP-MELT analyses of the sequences discussed above are presented in Table 7.15, expressed in terms of release fractions for the primary system Since these values are the ratio of what is injected into the containment to the initial inventory of the stated species, they take into account the release from fuel, the gap release, melt release, and RCS retention factors. The values listed for I in this table assume all iodine in the RCS to be present in the form CsI. In general, the highest release fractions pertain to the AB sequences since the pathway to the containment affords the fission products little opportunity for retention in this case. The presence of the steam generator in the pathway is responsible for a significant part of the reduction in the values shown for the S_2D and V sequences. The values listed for the TMLB' sequence are believed to be influenced by two assumptions regarding this sequence, each of which would lead to greater releases than would actually be expected. Namely, the material suspended in the RCS at the time of RPV failure represents, for TMLB', nearly all the material ultimately injected into the containment.

TABLE 7.13. RELATIVE CONTRIBUTIONS OF CHEMISORPTION (Chem), VAPOR CONDENSATION (Cond), AND AEROSOL DEPOSITION (Aero) TO THE RETENTION OF CsOH AND Te IN THE RCS FOR THE SEQUENCES STUDIED

Sequence	CsOH			Te		
	Chem	Cond	Aero	Chem	Cond	Aero
AB hot	.47	--	.53	1.0	0.	0.
AB cold	.08	.55	.37	.99	.01	--
S_2D	.39	.03	.58	1.0	--	0.
TMLB'	.78	.01	.21	1.	0.	0.
V	.12	.02	.86	.99	--	.01

TABLE 7.14. MASSES SUSPENDED IN RCS AT TIME OF CORE SLUMPING

Sequence	CsI (kg)	CsOH (kg)	Te (kg)	Aerosol (kg)
AB hot	.95	5.3	2.0	45
AB cold	.43	2.7	.53	50
S_2D	4.9	18	2.0	72
TMLB'	20	91	14	63
V	2.2	9.6	1.8	58

TABLE 7.15. MELT RELEASE FRACTIONS FROM RCS CALCULATED USING TRAP-MELT CODE FOR THE PWR ACCIDENT SEQUENCES WITH IRREVERSIBLE CHEMISORPTION, EXPRESSED AS FRACTIONS OF CORE INVENTORY

Species	AB (1)	AB (2)	TMLB'	S_2D	V
Xe	.88	.88	.99	.77	.90
I	.61	.85	.83	.25	.36
Cs	.59	.72	.70	.19	.32
Te	.05	.10	.81	.05	.06
Sr	.06	.09	.01	.12	.02
Ru	4.8E-3	6.9E-3	1.2E-3	1.1E-3	1.8E-3
UO_2	1.3E-3	1.9E-3	4.5E-4	5.6E-4	7.7E-4

Further, the lack of circulation between the core and the upper plenum in this analysis prevents retention on upper plenum surface from affecting a large portion of the core emissions. If significant circulation were to exist, the amount of retention predicted for the CsI, CsOH, and Te would be expected to be significantly enhanced.

The results presented in this table and those throughout this discussion of RCS transport and deposition must be judged in light of the uncertainties which place limits on the analyses performed. The analyses reported here represent significant improvements over previous attempts to understand fission product behavior in the primary system, but it is clear that substantial, and as yet unquantified, uncertainties remain to be resolved.

7.3 Transport, Deposition and Leakage in Containment

Results are presented in this section for analyses performed to examine the transport and retention of various fission products in the containment. The NAUA code and the CORRAL code that were described previously were utilized in the analyses. The NAUA code deals exclusively with transport of the fission products that are in particulate form while the CORRAL code treats both vapors and particulates. Hand calculations were also made to supplement code calculations for certain cases as will be discussed shortly.

In general, the containment codes used here need information on the thermal hydraulic conditions of an accident of interest. The conditions provided by the MARCH computer calculation were used. The typical required thermal hydraulic conditions are time-dependent containment temperature, pressure, and wall temperature, and the rates at which steam enters the containment, condenses on the containment structure, and leaks from the containment.

Perhaps the most important and critical input tha tainment codes also need is the fission product source term for both vapor and particulates. The source rates calculated as release from the primary system (TRAP-MELT code) and the Sandia code calculations for release during the core-concrete interaction were taken for the melt and vaporization

releases, respectively. For the NAUA calculations, CsI, CsOH, Te, Ru, Sr, and UO_2 were distinguished. All these species were assumed to be in the particulate form in the containment atmosphere because the temperature and pressure under the containment conditions indicate that these species will remain as particulates for all practical circumstances. Although it is assumed in the calculation that individual species are distributed evenly over all sizes of particulates, differential amounts of these species at a given time due to different source timings were taken into consideration in the calculations.

As discussed in Chapter 6, it is reasonable to estimate that 0.05 percent of the containment inventory is maintained airborne as volatile forms of iodine (excluding particles) until the time of containment failure. After containment failure a release of these volatile forms to the containment atmosphere is taken to be at a rate of 2×10^{-7} fraction per hour. Some generalized considerations of the implications of these fractions lead to very simple conclusions.

On containment failure, it can be assumed that the 0.05 percent of containment iodine inventory is released during the period of pressure blowdown for the containment. This means that over a fairly short time period a fractional release for iodine is 0.0005. Up to the time of containment failure, the fractional release will be the airborne fraction multiplied by the fractional volumetric leak rate. For those cases when the containment fails, it fails in less than 100 hours and at 1 percent of the containment volume leaked per day, the fraction of the iodine inventory leaked up to this time will be only about 0.04×0.0005 which is negligible compared with the fraction 0.0005 released at containment failure. If the containment does not fail, the fraction of iodine leaked as volatile iodine will be 0.3×0.0005 at a time of 30 days. The time 30 days (720 hours) represents nearly 4 half-lives for I-131 and was the longest time period considered in WASH 1400.

The other alternative is the case of the release rate after containment failure of 2×10^{-7} fraction per hour. This rate is the maximum that could be released regardless of conainment leakage since it represents evolution from liquids and surfaces. The maximum from this release will then be the fraction 1.44×10^{-4} at 720 hours if the

containment fails immediately, and so at most this source into and therefore from the containment atmosphere is sufficient to produce only about one-third of the amount estimated to be released as a fairly short-term puff at containment failure. It can be concluded, therefore, that for all cases a total volatile iodine release will be no more than fraction of about 0.0005 with timing largely dependent on containment failure time. This fractional release must be compared with the iodine release in particulate form (as CsI) to determine its significance.

For comparative purposes, the CORRAL-2 code was utilized for certain cases. It was assumed in the analyses that iodine would transport in elemental form. All other species with the exception of the noble gases were assumed to transport as particulates. Further, all fission product sources used with the CORRAL-2 code were assumed to be at a constant rate for the melt release and at an exponentially decreasing rate for the vaporization release as imposed by the code. Although this type of treatment is not rigorous, the effects of such an allocation of source within a release period are probably not significant. This is particularly so if one is concerned with calculations for times after a source period is completed, since the CORRAL-2 code performs calculations based on the fractions of fission products released and does not account for the absolute magnitude of the source amount.

Four different accident sequences, AB, TMLB', S_2D, and V, were considered in the present calculations. The timing of the fission product source for the containment calculations was permitted to coincide with the prescribed accident sequence that was listed in Table 6.3. Thus, the melt release of aerosol mass occurs as the core starts melting and the vaporization release takes place as the core-concrete interaction begins. The time-dependent source rates in mass per unit time were provided as input to the NAUA calculations. In certain cases, effects of a different release timing of a particular fission product, notably Te, were further examined. The timing of source input and of accident sequences considered in the present calculations is summarized in Table 6.3. A leak rate of 1 percent of the containment volume per day was utilized in all containment calculations using the NAUA code as the design leakage rate until the containment failure occurs. Fractions of core inventory released to the environment

obtained with NAUA calculations for accident sequences and for different species are listed in Table 7.16. Similar results calculated with the CORRAL code are listed in Table 7.17. It should be noted that in NAUA calculations each species listed in Table 7.16 was assumed to be in aerosol form while in CORRAL calculations, Xe and I were treated as vapors.

7.3.1 AB Sequence

This accident represents the sequence in which a minimum retention of fission products is expected to occur in the primary system due to the presence of a relatively rapid steam flow conditions combined with a short transport pathway. For analysis of the AB sequence, four different containment failure modes were applied and these are identified using WASH 1400 nomenclature as AB-β, AB-γ, AB-δ_1, and AB-ε. The containment failure time corresponding to these sequences are shown in Table 7.1. The two melt releases designated as the cold and hot upper plenum cases which were discussed previously in Section 7.2 were used for the analyses of the AB sequences to investigate the effects of the assumed upper plenum conditions.

Table 7.16 summarizes the calculated fraction of core inventory released to the atmosphere as a function of both time and species for the mentioned AB cases. The values shown in the table are as calculated by the NAUA code and the CORRAL calculations results are shown in Table 7.17 for comparison. It should be noted that the calculated fraction of core inventory released to the atmosphere for AB-β shown in Tables 7.16 and 7.17 did not account for additional retention due to the presence of the safeguard building. These effects on the release fraction for AB-β will further be discussed in Section 7.4 under which release fractions of I and Cs are summarized.

It is seen that the containment failure time shows a pronounced effect on the amount of release to the environment as expected. It is also noted that the hot upper plenum condition causes the released fraction to change. However, this change is observed not to be significant probably because the retention factor of the primary system for the AB sequence is already very small.

TABLE 7.16. FRACTION OF INVENTORY RELEASED TO THE ATMOSPHERE (NAUA CALCULATIONS)

Time, hr	I	Cs	Te	Ru	Sr	UO_2
			AB-β Cold			
0.5	6.1×10^{-4}	6.1×10^{-4}	4.9×10^{-5}	6.9×10^{-7}	7.2×10^{-6}	3.3×10^{-8}
1	7.2×10^{-2}	6.9×10^{-2}	1.3×10^{-2}	4.2×10^{-4}	5.1×10^{-3}	9.5×10^{-5}
2	2.8×10^{-1}	2.6×10^{-1}	1.5×10^{-1}	2.4×10^{-3}	3.1×10^{-2}	1.2×10^{-3}
4	4.0×10^{-1}	3.9×10^{-1}	2.7×10^{-1}	3.5×10^{-3}	4.9×10^{-2}	3.1×10^{-3}
7	4.2×10^{-1}	4.0×10^{-1}	2.9×10^{-1}	3.6×10^{-3}	5.1×10^{-2}	3.7×10^{-3}
10	4.2×10^{-1}	4.0×10^{-1}	2.9×10^{-1}	3.6×10^{-3}	5.2×10^{-2}	3.7×10^{-3}
15	4.2×10^{-1}	4.0×10^{-1}	2.9×10^{-1}	3.6×10^{-3}	5.2×10^{-2}	3.7×10^{-3}
20	4.2×10^{-1}	4.0×10^{-1}	2.9×10^{-1}	3.6×10^{-3}	5.2×10^{-2}	3.7×10^{-3}
			AB-β Hot			
0.5	4.3×10^{-4}	4.0×10^{-4}	6.8×10^{-5}	5.1×10^{-7}	5.4×10^{-6}	2.7×10^{-8}
1	7.9×10^{-2}	6.8×10^{-2}	4.0×10^{-2}	5.0×10^{-4}	6.0×10^{-3}	1.2×10^{-4}
2	2.9×10^{-1}	2.5×10^{-1}	1.8×10^{-1}	2.1×10^{-3}	2.7×10^{-2}	1.1×10^{-3}
4	4.3×10^{-1}	3.7×10^{-1}	3.1×10^{-1}	3.0×10^{-3}	4.3×10^{-2}	2.9×10^{-3}
7	4.4×10^{-1}	3.8×10^{-1}	3.2×10^{-1}	3.1×10^{-3}	4.5×10^{-2}	3.5×10^{-3}
10	4.4×10^{-1}	3.8×10^{-1}	3.2×10^{-1}	3.1×10^{-3}	4.5×10^{-2}	3.6×10^{-3}
15	4.4×10^{-1}	3.8×10^{-1}	3.2×10^{-1}	3.1×10^{-3}	4.5×10^{-2}	3.6×10^{-3}
20	4.4×10^{-1}	3.8×10^{-1}	3.2×10^{-1}	3.1×10^{-3}	4.5×10^{-2}	3.6×10^{-3}
			AB-γ Cold			
0.5	8.5×10^{-7}	8.6×10^{-7}	7.1×10^{-8}	9.7×10^{-10}	1.0×10^{-8}	5.1×10^{-11}
1	8.2×10^{-5}	7.8×10^{-5}	1.3×10^{-5}	4.5×10^{-7}	5.4×10^{-6}	9.8×10^{-8}
2	2.8×10^{-1}	2.6×10^{-1}	1.6×10^{-1}	2.6×10^{-3}	3.4×10^{-2}	1.0×10^{-3}
4	2.9×10^{-1}	2.8×10^{-1}	1.8×10^{-1}	2.7×10^{-3}	3.6×10^{-2}	1.2×10^{-3}
7	3.0×10^{-1}	2.9×10^{-1}	1.9×10^{-1}	2.8×10^{-3}	3.7×10^{-2}	1.7×10^{-3}
10	3.0×10^{-1}	2.9×10^{-1}	1.9×10^{-1}	2.8×10^{-3}	3.7×10^{-2}	1.7×10^{-3}
20	3.0×10^{-1}	2.9×10^{-1}	1.9×10^{-1}	2.8×10^{-3}	3.7×10^{-2}	1.7×10^{-3}
			AB-γ Hot			
0.5	1.5×10^{-6}	1.5×10^{-6}	2.6×10^{-7}	2.2×10^{-9}	2.3×10^{-8}	1.2×10^{-10}
1	8.2×10^{-5}	7.2×10^{-5}	3.9×10^{-5}	4.9×10^{-7}	5.9×10^{-6}	1.1×10^{-7}
2	2.9×10^{-1}	2.4×10^{-1}	1.8×10^{-1}	2.1×10^{-3}	2.8×10^{-2}	8.7×10^{-4}
4	3.0×10^{-1}	2.6×10^{-1}	1.9×10^{-1}	2.2×10^{-3}	2.9×10^{-2}	1.1×10^{-3}
7	3.1×10^{-1}	2.6×10^{-1}	2.0×10^{-1}	2.3×10^{-3}	3.1×10^{-2}	1.6×10^{-3}
10	3.1×10^{-1}	2.6×10^{-1}	2.1×10^{-1}	2.3×10^{-3}	3.1×10^{-2}	1.6×10^{-3}
20	3.1×10^{-1}	2.6×10^{-1}	2.1×10^{-1}	2.3×10^{-3}	3.1×10^{-2}	1.6×10^{-3}

TABLE 7.16. (Continued)

Time, hr	I	Cs	Te	Ru	Sr	UO_2
			AB-Y Cold Te			
0.5	8.5×10^{-7}	8.6×10^{-7}	0.0	9.7×10^{-10}	1.0×10^{-8}	5.1×10^{-11}
1	8.2×10^{-5}	7.8×10^{-5}	0.0	4.5×10^{-7}	5.4×10^{-6}	9.8×10^{-8}
2	2.8×10^{-1}	2.6×10^{-1}	3.0×10^{-2}	2.6×10^{-3}	3.4×10^{-2}	1.0×10^{-3}
4	2.9×10^{-1}	2.8×10^{-1}	5.9×10^{-2}	2.7×10^{-3}	3.6×10^{-2}	1.2×10^{-3}
7	3.0×10^{-1}	2.9×10^{-1}	1.0×10^{-1}	2.8×10^{-3}	3.7×10^{-2}	1.7×10^{-3}
10	3.0×10^{-1}	2.9×10^{-1}	1.0×10^{-1}	2.8×10^{-3}	3.7×10^{-2}	1.7×10^{-3}
20	3.0×10^{-1}	2.9×10^{-1}	1.0×10^{-1}	2.8×10^{-3}	3.7×10^{-2}	1.7×10^{-3}
			AB-Y Hot Te			
0.5	1.5×10^{-6}	1.5×10^{-6}	0.0	2.2×10^{-9}	2.3×10^{-8}	1.2×10^{-10}
1	8.2×10^{-5}	7.2×10^{-5}	0.0	4.9×10^{-7}	5.9×10^{-6}	1.1×10^{-7}
2	2.9×10^{-1}	2.4×10^{-1}	3.0×10^{-2}	2.1×10^{-3}	2.8×10^{-2}	8.7×10^{-4}
4	3.0×10^{-1}	2.6×10^{-1}	5.9×10^{-2}	2.2×10^{-3}	2.9×10^{-2}	1.1×10^{-3}
7	3.1×10^{-1}	2.6×10^{-1}	1.0×10^{-1}	2.3×10^{-3}	3.1×10^{-2}	1.6×10^{-3}
10	3.1×10^{-1}	2.6×10^{-1}	1.1×10^{-1}	2.3×10^{-3}	3.1×10^{-2}	1.6×10^{-3}
20	3.1×10^{-1}	2.6×10^{-1}	1.1×10^{-1}	2.3×10^{-3}	3.1×10^{-2}	1.6×10^{-3}
			AB-δ_1 Cold			
0.5	3.4×10^{-7}	3.4×10^{-7}	2.7×10^{-8}	3.8×10^{-10}	4.0×10^{-9}	2.0×10^{-11}
1	7.2×10^{-5}	6.8×10^{-5}	1.8×10^{-5}	5.0×10^{-7}	6.2×10^{-6}	1.3×10^{-7}
2	1.4×10^{-4}	1.4×10^{-4}	7.3×10^{-5}	1.1×10^{-6}	1.5×10^{-5}	8.5×10^{-7}
4	2.1×10^{-4}	2.1×10^{-4}	1.6×10^{-4}	1.5×10^{-6}	2.5×10^{-5}	3.0×10^{-6}
7	2.3×10^{-4}	2.3×10^{-4}	2.0×10^{-4}	1.6×10^{-6}	2.9×10^{-5}	4.7×10^{-6}
10	2.3×10^{-4}	2.3×10^{-4}	2.1×10^{-4}	1.6×10^{-6}	2.9×10^{-5}	4.9×10^{-6}
20	2.3×10^{-4}	2.3×10^{-4}	2.1×10^{-4}	1.6×10^{-6}	2.9×10^{-5}	5.0×10^{-6}
50	2.3×10^{-4}	2.3×10^{-4}	2.1×10^{-4}	1.6×10^{-6}	2.9×10^{-5}	5.0×10^{-6}
70	2.3×10^{-4}	2.3×10^{-4}	2.1×10^{-4}	1.6×10^{-6}	2.9×10^{-5}	5.0×10^{-6}
			AB-δ_1 Hot			
0.5	3.1×10^{-7}	2.9×10^{-7}	4.8×10^{-8}	3.7×10^{-10}	3.9×10^{-9}	1.9×10^{-11}
1	7.8×10^{-5}	6.8×10^{-5}	4.1×10^{-5}	5.0×10^{-7}	6.1×10^{-6}	1.2×10^{-7}
2	1.8×10^{-4}	1.6×10^{-4}	1.1×10^{-4}	1.1×10^{-6}	1.6×10^{-5}	9.1×10^{-7}
4	2.6×10^{-4}	2.4×10^{-4}	2.0×10^{-4}	1.5×10^{-6}	2.5×10^{-5}	3.0×10^{-6}
7	2.8×10^{-4}	2.6×10^{-4}	2.4×10^{-4}	1.6×10^{-6}	2.9×10^{-5}	4.6×10^{-6}
10	2.8×10^{-4}	2.6×10^{-4}	2.5×10^{-4}	1.6×10^{-6}	2.9×10^{-5}	4.9×10^{-6}
20	2.8×10^{-4}	2.6×10^{-4}	2.6×10^{-4}	1.6×10^{-6}	3.0×10^{-5}	5.0×10^{-6}
50	2.8×10^{-4}	2.6×10^{-4}	2.6×10^{-4}	1.6×10^{-6}	3.0×10^{-5}	5.0×10^{-6}
70	2.8×10^{-4}	2.6×10^{-4}	2.6×10^{-4}	1.6×10^{-6}	3.0×10^{-5}	5.0×10^{-6}

TABLE 7.16. (Continued)

Time, hr	I	Cs	Te	Ru	Sr	UO_2
			TMLB'-δ_e			
4	2.4×10^{-7}	2.4×10^{-7}	6.9×10^{-1}	3.7×10^{-10}	4.2×10^{-9}	5.8×10^{-11}
7	6.6×10^{-1}	5.5×10^{-1}	4.5×10^{-1}	7.5×10^{-4}	9.2×10^{-3}	5.5×10^{-4}
9	6.6×10^{-1}	5.5×10^{-1}	4.5×10^{-1}	7.5×10^{-4}	1.1×10^{-2}	1.6×10^{-3}
10	6.6×10^{-1}	5.5×10^{-1}	4.5×10^{-1}	7.5×10^{-4}	1.1×10^{-2}	1.8×10^{-3}
15	6.6×10^{-1}	5.5×10^{-1}	4.5×10^{-1}	7.5×10^{-4}	1.2×10^{-2}	2.2×10^{-3}
20	6.6×10^{-1}	5.5×10^{-1}	4.5×10^{-1}	7.5×10^{-4}	1.2×10^{-2}	2.2×10^{-3}
			TMLB'-δ_l			
4	2.4×10^{-7}	2.4×10^{-7}	6.9×10^{-10}	3.7×10^{-10}	4.2×10^{-9}	5.8×10^{-11}
7	6.2×10^{-4}	5.3×10^{-4}	4.3×10^{-4}	7.1×10^{-7}	9.0×10^{-6}	7.1×10^{-7}
9	8.6×10^{-4}	7.3×10^{-4}	5.9×10^{-4}	9.8×10^{-7}	1.7×10^{-5}	3.4×10^{-6}
10	9.0×10^{-4}	7.6×10^{-4}	6.2×10^{-4}	1.0×10^{-6}	1.8×10^{-5}	4.2×10^{-6}
15	9.3×10^{-4}	7.9×10^{-4}	6.4×10^{-4}	1.1×10^{-6}	2.1×10^{-5}	5.8×10^{-6}
20	9.4×10^{-4}	7.9×10^{-4}	6.4×10^{-4}	1.1×10^{-7}	2.1×10^{-5}	6.0×10^{-6}
70	9.9×10^{-4}	8.4×10^{-4}	6.8×10^{-4}	1.1×10^{-6}	2.6×10^{-5}	9.4×10^{-6}
			S_2D-Y Hot			
1	5.5×10^{-9}	5.3×10^{-9}	3.2×10^{-13}	6.3×10^{-12}	7.6×10^{-11}	1.2×10^{-12}
1.5	7.7×10^{-2}	5.3×10^{-2}	2.7×10^{-2}	1.8×10^{-11}	8.2×10^{-3}	3.3×10^{-4}
2	8.6×10^{-2}	5.9×10^{-2}	3.1×10^{-2}	1.8×10^{-11}	9.2×10^{-3}	3.7×10^{-4}
4	8.6×10^{-2}	5.9×10^{-2}	3.1×10^{-2}	1.2×10^{-10}	9.2×10^{-3}	3.7×10^{-4}
10	8.6×10^{-2}	5.9×10^{-2}	3.1×10^{-2}	4.3×10^{-9}	9.2×10^{-3}	3.8×10^{-4}
20	8.7×10^{-2}	6.0×10^{-2}	3.2×10^{-2}	6.1×10^{-8}	9.3×10^{-3}	4.1×10^{-4}
50	8.7×10^{-2}	6.0×10^{-2}	3.2×10^{-2}	7.8×10^{-8}	9.3×10^{-3}	4.2×10^{-4}
			S_2D-ε Hot			
1	5.5×10^{-9}	5.3×10^{-9}	3.2×10^{-13}	6.3×10^{-12}	7.6×10^{-11}	1.2×10^{-12}
1.5	3.0×10^{-8}	2.2×10^{-8}	6.2×10^{-9}	1.8×10^{-11}	2.2×10^{-9}	8.4×10^{-11}
2	3.0×10^{-8}	2.2×10^{-8}	6.2×10^{-9}	1.8×10^{-11}	2.2×10^{-9}	8.4×10^{-11}
4	5.7×10^{-7}	5.9×10^{-7}	3.6×10^{-7}	2.0×10^{-11}	2.3×10^{-8}	9.6×10^{-9}
10	5.7×10^{-7}	5.9×10^{-7}	1.2×10^{-6}	3.2×10^{-11}	6.0×10^{-8}	2.7×10^{-8}
20	5.7×10^{-7}	5.9×10^{-7}	1.2×10^{-6}	3.2×10^{-11}	6.0×10^{-8}	2.7×10^{-8}
50	5.7×10^{-7}	5.9×10^{-7}	1.2×10^{-6}	3.2×10^{-11}	6.0×10^{-8}	2.7×10^{-8}

TABLE 7.16. (Continued)

Time, hr	I	Cs	Te	Ru	Sr	UO_2
			V			
1	1.7×10^{-1}	1.6×10^{-1}	2.1×10^{-2}	5.4×10^{-4}	6.3×10^{-3}	7.8×10^{-5}
2	1.8×10^{-1}	1.7×10^{-1}	3.6×10^{-2}	6.5×10^{-4}	8.5×10^{-3}	4.5×10^{-4}
4	1.8×10^{-1}	1.7×10^{-1}	4.2×10^{-2}	6.5×10^{-4}	9.6×10^{-3}	9.0×10^{-4}
7	1.8×10^{-1}	1.7×10^{-1}	4.7×10^{-2}	6.6×10^{-4}	1.1×10^{-2}	2.2×10^{-3}
10	1.8×10^{-1}	1.7×10^{-1}	4.7×10^{-2}	6.6×10^{-4}	1.1×10^{-2}	2.2×10^{-3}
15	1.8×10^{-1}	1.7×10^{-1}	4.7×10^{-2}	6.6×10^{-4}	1.1×10^{-2}	2.2×10^{-3}
20	1.8×10^{-1}	1.7×10^{-1}	4.7×10^{-2}	6.6×10^{-4}	1.1×10^{-2}	2.2×10^{-3}
40	1.8×10^{-1}	1.7×10^{-1}	4.7×10^{-2}	6.6×10^{-4}	1.1×10^{-2}	2.2×10^{-3}

TABLE 7.17. FRACTION OF CORE INVENTORY RELEASED TO THE ATMOSPHERE (CORRAL CALCULATIONS)

Time, hr	Xe	I	Cs	Te	Ru	Sr	La	Cumulative Containment Release Energy (10^6 Btu)
				AB-6_1 Cold				
0.5	5.7×10^{-7}	3.0×10^{-7}	3.4×10^{-7}	8.4×10^{-7}	1.2×10^{-9}	2.0×10^{-8}	3.5×10^{-10}	---
1.0	1.2×10^{-5}	9.5×10^{-6}	7.7×10^{-6}	4.4×10^{-6}	7.3×10^{-8}	9.4×10^{-7}	2.1×10^{-8}	---
2.0	5.2×10^{-5}	1.4×10^{-5}	2.9×10^{-5}	1.7×10^{-5}	2.6×10^{-7}	3.4×10^{-6}	1.2×10^{-7}	---
4.0	1.3×10^{-4}	1.6×10^{-5}	6.6×10^{-5}	3.8×10^{-5}	5.0×10^{-7}	7.0×10^{-6}	4.4×10^{-7}	---
7.0	2.5×10^{-4}	1.8×10^{-5}	1.1×10^{-4}	6.3×10^{-5}	7.4×10^{-7}	1.1×10^{-5}	8.9×10^{-7}	---
20.0	8.0×10^{-4}	2.3×10^{-5}	2.4×10^{-4}	1.4×10^{-4}	1.5×10^{-6}	2.2×10^{-5}	2.2×10^{-6}	---
50.0	9.6×10^{-1}	8.6×10^{-3}	3.2×10^{-2}	1.8×10^{-2}	1.8×10^{-4}	2.8×10^{-3}	3.2×10^{-4}	34.8
240.0	9.9×10^{-1}	8.9×10^{-3}	3.2×10^{-2}	1.8×10^{-2}	1.8×10^{-4}	2.9×10^{-3}	3.2×10^{-4}	44.0
				AB-6_1 Hot				
0.5	3.7×10^{-7}	3.0×10^{-7}	3.6×10^{-7}	1.2×10^{-7}	1.4×10^{-9}	2.3×10^{-8}	3.9×10^{-10}	---
1.0	1.2×10^{-5}	9.5×10^{-6}	8.8×10^{-6}	6.3×10^{-6}	8.4×10^{-8}	1.1×10^{-6}	2.3×10^{-8}	---
2.0	5.2×10^{-5}	1.4×10^{-5}	3.2×10^{-5}	2.3×10^{-5}	3.0×10^{-7}	3.9×10^{-6}	1.2×10^{-7}	---
4.0	1.3×10^{-4}	1.6×10^{-5}	7.0×10^{-5}	5.1×10^{-5}	5.7×10^{-7}	8.0×10^{-6}	4.6×10^{-7}	---
7.0	2.5×10^{-4}	1.8×10^{-5}	1.1×10^{-4}	8.3×10^{-5}	8.5×10^{-7}	1.2×10^{-5}	9.2×10^{-7}	---
20.0	8.0×10^{-4}	2.3×10^{-5}	2.4×10^{-4}	1.8×10^{-4}	1.7×10^{-6}	2.5×10^{-5}	2.2×10^{-6}	---
50.0	9.6×10^{-1}	8.6×10^{-3}	3.1×10^{-2}	2.3×10^{-2}	2.1×10^{-4}	3.2×10^{-3}	3.2×10^{-4}	34.8
240.0	9.9×10^{-1}	8.9×10^{-3}	3.2×10^{-2}	2.3×10^{-2}	2.1×10^{-4}	3.2×10^{-3}	3.3×10^{-4}	44.0
				AB-Y Cold				
0.5	3.7×10^{-7}	2.9×10^{-7}	3.4×10^{-7}	8.4×10^{-8}	1.2×10^{-9}	2.0×10^{-8}	3.5×10^{-10}	---
1.0	1.2×10^{-5}	9.1×10^{-6}	7.7×10^{-6}	4.4×10^{-6}	7.3×10^{-8}	9.4×10^{-7}	2.1×10^{-8}	---
2.0	8.7×10^{-1}	3.7×10^{-1}	4.9×10^{-1}	2.9×10^{-1}	4.6×10^{-3}	6.0×10^{-2}	1.7×10^{-3}	29.9
4.0	8.9×10^{-1}	3.8×10^{-1}	5.2×10^{-1}	3.1×10^{-1}	4.6×10^{-3}	6.1×10^{-2}	2.5×10^{-3}	31.4
7.0	9.2×10^{-1}	3.8×10^{-1}	5.6×10^{-1}	3.3×10^{-1}	4.6×10^{-3}	6.3×10^{-2}	3.2×10^{-3}	32.8
20.0	9.5×10^{-1}	3.8×10^{-1}	5.9×10^{-1}	3.5×10^{-1}	4.6×10^{-3}	6.4×10^{-2}	3.8×10^{-3}	34.5 (11.4 hr)
240.0	9.6×10^{-1}	3.8×10^{-1}	5.9×10^{-1}	3.5×10^{-1}	4.6×10^{-3}	6.4×10^{-2}	3.8×10^{-3}	---

TABLE 7.17. (Continued)

Time, hr	Xe	I	Cs	Te	Ru	Sr	La	Cumulative Containment Release Energy (10^6 Btu)
				AB-Y Hot				
0.5	3.7×10^{-7}	2.9×10^{-7}	3.6×10^{-7}	1.2×10^{-7}	1.4×10^{-9}	2.3×10^{-8}	3.9×10^{-10}	---
1.0	1.2×10^{-5}	9.1×10^{-6}	8.8×10^{-6}	6.3×10^{-6}	8.4×10^{-8}	1.1×10^{-6}	2.3×10^{-8}	---
2.0	8.7×10^{-1}	3.7×10^{-1}	5.5×10^{-1}	4.1×10^{-1}	5.3×10^{-3}	6.9×10^{-2}	1.9×10^{-3}	29.9
4.0	8.9×10^{-1}	3.8×10^{-1}	5.8×10^{-1}	4.3×10^{-1}	5.3×10^{-3}	7.1×10^{-2}	2.6×10^{-3}	31.4
7.0	9.2×10^{-1}	3.8×10^{-1}	6.1×10^{-1}	4.5×10^{-1}	5.3×10^{-3}	7.2×10^{-2}	3.4×10^{-3}	32.8
20.0	9.5×10^{-1}	3.8×10^{-1}	6.3×10^{-1}	4.7×10^{-1}	5.3×10^{-3}	7.3×10^{-2}	3.9×10^{-3}	34.5 (11.4 hr)
240.0	9.6×10^{-1}	3.8×10^{-1}	6.3×10^{-1}	4.7×10^{-1}	5.3×10^{-3}	7.3×10^{-2}	3.9×10^{-3}	---
				AB-8 Cold				
0.5	3.0×10^{-3}	2.3×10^{-3}	2.7×10^{-3}	6.8×10^{-4}	1.0×10^{-5}	1.6×10^{-4}	2.9×10^{-6}	1.1
1.0	9.6×10^{-2}	7.3×10^{-2}	5.9×10^{-2}	3.4×10^{-2}	5.7×10^{-4}	7.3×10^{-3}	1.6×10^{-4}	1.9
2.0	3.4×10^{-1}	1.2×10^{-1}	1.9×10^{-1}	1.1×10^{-1}	1.8×10^{-3}	2.4×10^{-2}	6.9×10^{-4}	5.4
4.0	5.5×10^{-1}	1.3×10^{-1}	3.1×10^{-1}	1.8×10^{-1}	2.4×10^{-3}	3.4×10^{-2}	2.0×10^{-3}	7.9
7.0	7.1×10^{-1}	1.3×10^{-1}	3.9×10^{-1}	2.2×10^{-1}	2.7×10^{-3}	3.8×10^{-2}	3.0×10^{-3}	11.2 (11.5 hr)
20.0	8.7×10^{-1}	1.3×10^{-1}	4.4×10^{-1}	2.5×10^{-1}	2.9×10^{-3}	4.3×10^{-2}	3.6×10^{-3}	---
240.0	1.0	1.4×10^{-1}	4.5×10^{-1}	2.6×10^{-1}	3.0×10^{-3}	4.4×10^{-2}	3.8×10^{-3}	---
				AB-8 Hot				
0.5	3.0×10^{-3}	2.3×10^{-3}	2.8×10^{-3}	9.5×10^{-4}	1.2×10^{-5}	1.8×10^{-4}	3.2×10^{-6}	1.1
1.0	9.6×10^{-2}	7.3×10^{-2}	6.8×10^{-2}	4.9×10^{-2}	6.5×10^{-4}	8.4×10^{-3}	1.8×10^{-4}	1.9
2.0	3.4×10^{-1}	1.2×10^{-1}	2.2×10^{-1}	1.6×10^{-1}	2.1×10^{-3}	2.7×10^{-2}	7.5×10^{-4}	5.4
4.0	5.5×10^{-1}	1.3×10^{-1}	3.3×10^{-1}	2.4×10^{-1}	2.8×10^{-3}	3.8×10^{-2}	2.0×10^{-3}	7.9
7.0	7.1×10^{-1}	1.3×10^{-1}	4.0×10^{-1}	3.0×10^{-1}	3.1×10^{-3}	4.5×10^{-2}	3.0×10^{-3}	11.2 (11.5 hr)
20.0	8.7×10^{-1}	1.3×10^{-1}	4.5×10^{-1}	3.3×10^{-1}	3.4×10^{-3}	4.9×10^{-2}	3.8×10^{-3}	---
240.0	1.0	1.4×10^{-1}	4.6×10^{-1}	3.4×10^{-1}	3.4×10^{-3}	5.0×10^{-2}	3.9×10^{-3}	---

TABLE 7.17. (Continued)

Time, hr	Xe	I	Cs	Te	Ru	Sr	La	Cumulative Containment Release Energy (10^6 Btu)
				S_2D-Y Hot				
0.4	0	0	0	0	0	0	0	---
1.0	1.4×10^{-5}	1.7×10^{-6}	3.2×10^{-7}	8.8×10^{-8}	3.2×10^{-9}	4.6×10^{-8}	1.5×10^{-9}	---
2.0	6.7×10^{-1}	2.8×10^{-3}	$\times 10^{-4}$	1.1×10^{-4}	3.9×10^{-6}	5.6×10^{-5}	1.9×10^{-6}	19.4
4.0	6.9×10^{-1}	3.1×10^{-3}	7.5×10^{-4}	4.6×10^{-4}	3.9×10^{-6}	7.7×10^{-5}	1.4×10^{-5}	19.8
7.0	8.5×10^{-1}	1.6×10^{-2}	5.3×10^{-2}	5.2×10^{-2}	6.1×10^{-6}	3.0×10^{-3}	1.7×10^{-3}	48.2 (13.6 hr)
20.0	1.0	1.9×10^{-2}	1.0×10^{-1}	1.0×10^{-1}	8.0×10^{-6}	5.7×10^{-3}	3.4×10^{-3}	48.2
720.0	1.0	1.9×10^{-2}	1.0×10^{-1}	1.0×10^{-1}	8.1×10^{-6}	5.8×10^{-3}	3.4×10^{-3}	48.2
				S_2D-ϵ Hot				
0.4	0	0	0	0	0	0	0	---
1.0	1.4×10^{-5}	1.7×10^{-6}	4.0×10^{-7}	1.1×10^{-7}	4.0×10^{-9}	5.8×10^{-8}	1.9×10^{-9}	---
2.3	4.6×10^{-4}	5.3×10^{-6}	9.8×10^{-7}	2.7×10^{-7}	9.8×10^{-9}	1.4×10^{-7}	4.7×10^{-9}	---
4.0	1.1×10^{-3}	6.9×10^{-6}	1.4×10^{-6}	7.1×10^{-7}	1.0×10^{-8}	1.7×10^{-7}	1.9×10^{-8}	---
7.0	2.3×10^{-3}	9.3×10^{-6}	3.0×10^{-6}	2.3×10^{-6}	1.0×10^{-8}	2.6×10^{-7}	7.1×10^{-8}	---
20.0	7.7×10^{-3}	1.4×10^{-5}	3.5×10^{-6}	2.7×19^{-6}	1.0×10^{-8}	2.8×10^{-7}	8.6×10^{-8}	---
720.0	2.6×10^{-1}	4.7×10^{-5}	3.5×10^{-6}	2.7×10^{-6}	1.0×10^{-8}	2.8×10^{-7}	8.6×10^{-8}	---
				TMLB'-δ_1 Hot				
4.0	1.1×10^{-4}	5.1×10^{-5}	7.5×10^{-5}	5.0×10^{-5}	1.3×10^{-7}	1.6×10^{-6}	5.3×10^{-8}	---
7.0	1.3×10^{-3}	1.5×10^{-4}	5.3×10^{-4}	4.2×10^{-4}	1.1×10^{-6}	1.4×10^{-5}	7.5×10^{-7}	---
9.0	2.2×10^{-3}	1.8×10^{-4}	8.1×10^{-4}	5.8×10^{-4}	1.5×10^{-6}	2.3×10^{-5}	3.7×10^{-6}	---
10.0	2.6×10^{-3}	1.9×10^{-4}	9.3×10^{-4}	6.4×10^{-4}	1.7×10^{-6}	2.7×10^{-5}	5.2×10^{-6}	---
15.0	4.7×10^{-3}	2.2×10^{-4}	1.4×10^{-3}	9.2×10^{-4}	2.4×10^{-6}	4.6×10^{-5}	1.2×10^{-5}	---
20.0	6.8×10^{-3}	2.4×10^{-4}	1.8×10^{-3}	1.1×10^{-3}	3.0×10^{-6}	5.8×10^{-5}	1.6×10^{-5}	---
240.0	2.6×10^{-1}	2.5×10^{-3}	2.8×10^{-3}	1.6×10^{-3}	4.3×10^{-6}	9.1×10^{-5}	2.8×10^{-5}	---

Figure 7.11 shows the calculated amounts of each species that is leaked into the environment. The rapid rise of the leaked amount seen at times of 27 and 81 minutes in the figure represent, of course, the melt release and the vaporization release, respectively. As in the case of airborne mass shown in Figure 7.12, the time-dependent leaked amounts of various species do not increase proportionally to that for the total particulates due to different timings of release from the primary system.

Figure 7.13 shows the time-dependent airborne masses of particulates for the AB-δ_1 hot case. Additionally shown in the figure are the masses including the amount of water that condensed onto particles. It is seen that the airborne particulates are dominated by the condensed water during the melt release period and then the condensed water evaporates rapidly at a time of 80 minutes as the vaporization release takes place. To demonstrate further the effect of steam condensation on the particle transport, Figure 7.14 was prepared showing the particle size distribution of the total airborne masses including water at different times. The particular sequence used in the figure is the AB-δ_1 hot case. While the size distribution was approximately lognormal for the source aerosol released during the melt release, it is shown to become bimodal, showing the effects of steam condensation. Figure 7.15 illustrates the particle size distribution in each size class that is further divided into various species and condensed water as an example.

It should be noted from Figures 7.14 through 7.15, that the mass of water condensed on the particulates is considerably larger than the solid particulate mass. Thus, the settling velocity of such a condensed aerosol will increase substantially causing the particle to settle out rapidly. In general, the particle growth rate by condensation depends upon the size of the primary particles. The particles whose sizes are smaller than the critical size tend not to be condensed while particles exceeding the critical size grow at a rapid rate and are subject to various aerosol removal mechanisms such as sedimentation as a result of their increased size. The critical size for the aerosol illustrated in Figures 7.14 and 7.15 is seen to be approximately 0.6 μm. Thus, the steam condensation mechanism can substantially alter the picture of overall airborne mass amounts as demonstrated. A situation in which particulates whose size exceeds the critical

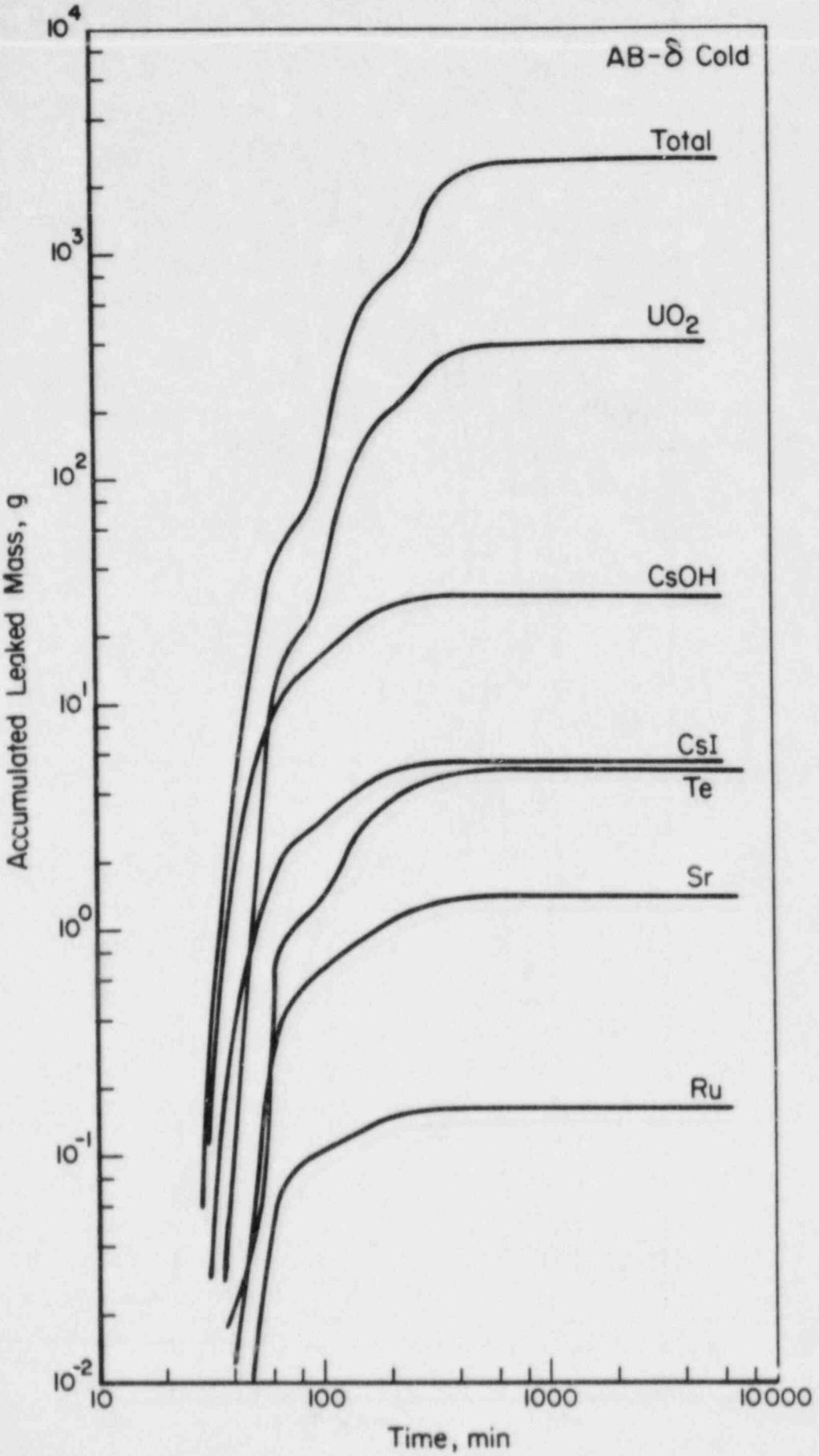

FIGURE 7.11. ACCUMULATED LEAKED MASS OF EACH SPECIES FOR AB-δ_1 COLD

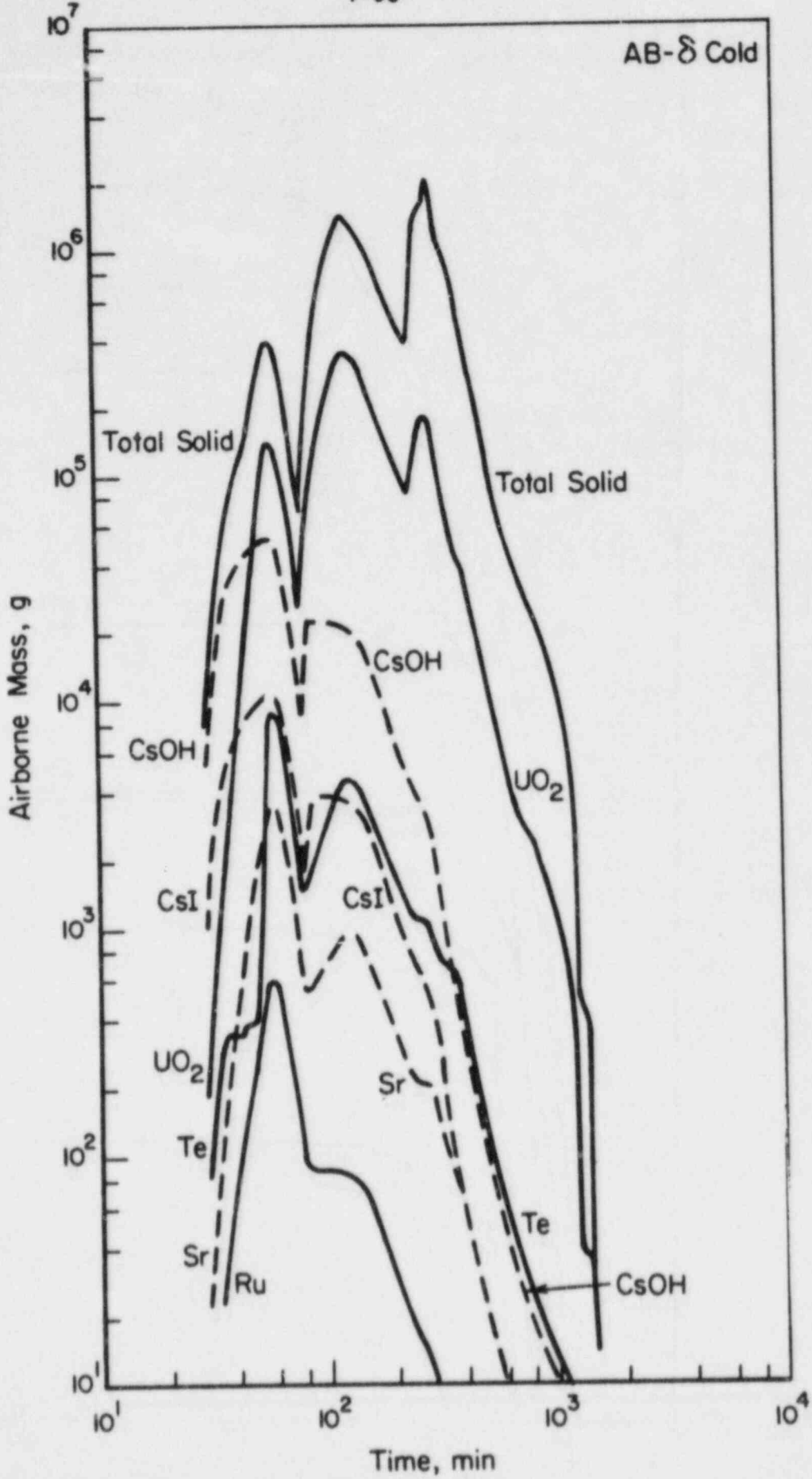

FIGURE 7.12. AIRBORNE MASS OF EACH SPECIES AS A FUNCTION OF TIME FOR AB-δ_1 COLD

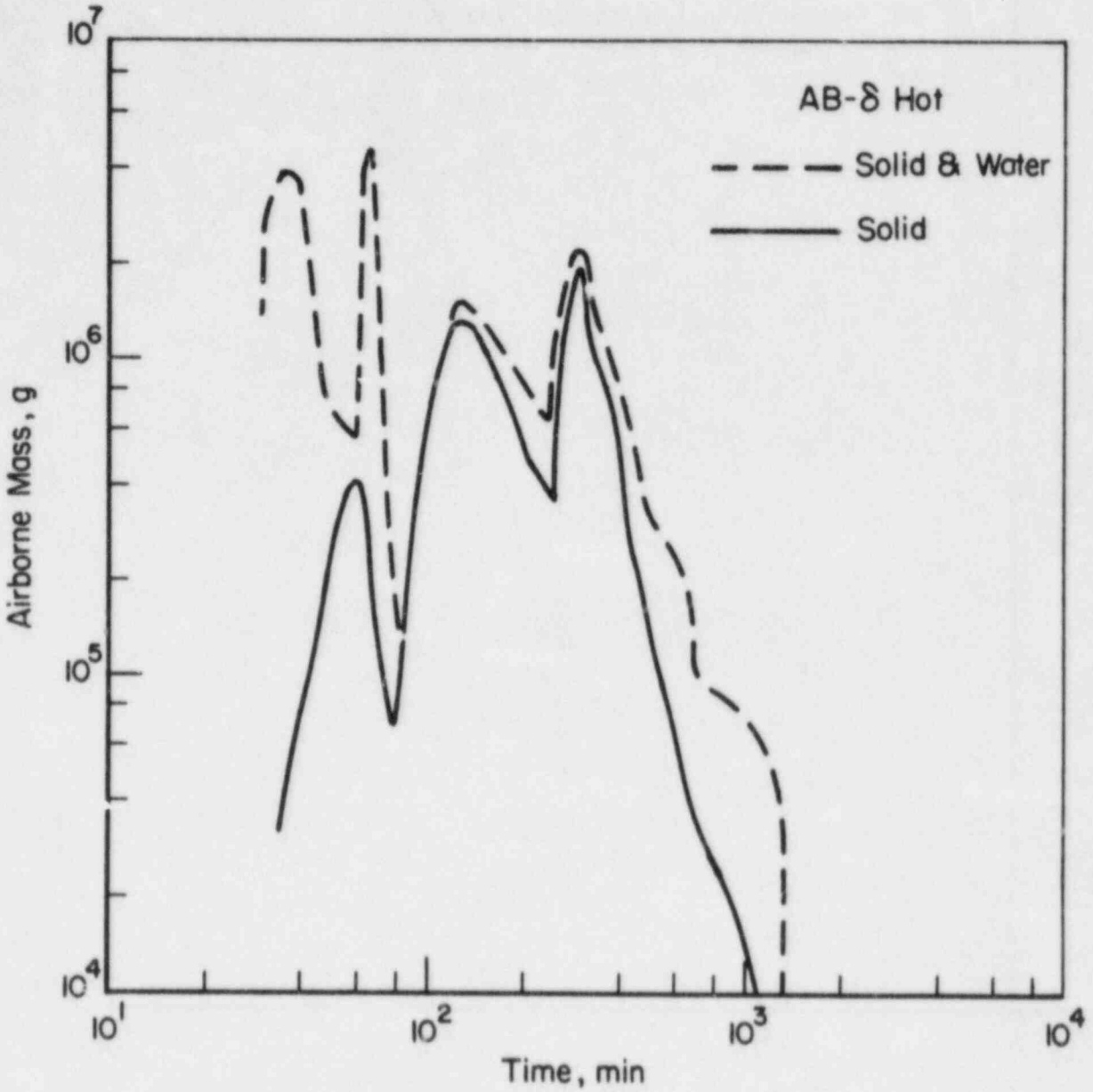

FIGURE 7.13. AIRBORNE MASS OF PARTICULATES FOR AB-δ_1 SHOWING THE AMOUNT OF STEAM CONDENSED

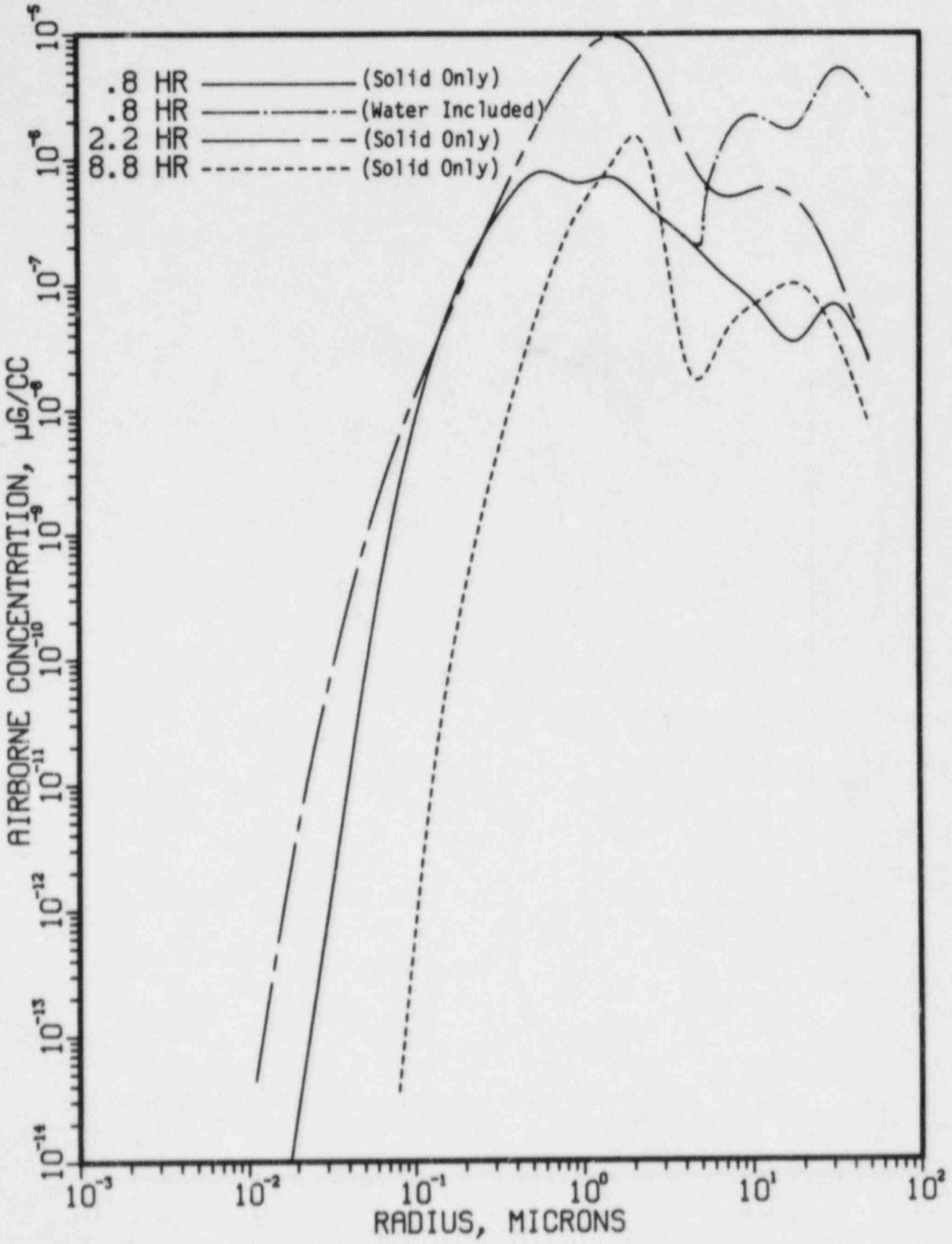

FIGURE 7.14. CHANGE OF AIRBORNE PARTICLE SIZE DISTRIBUTION

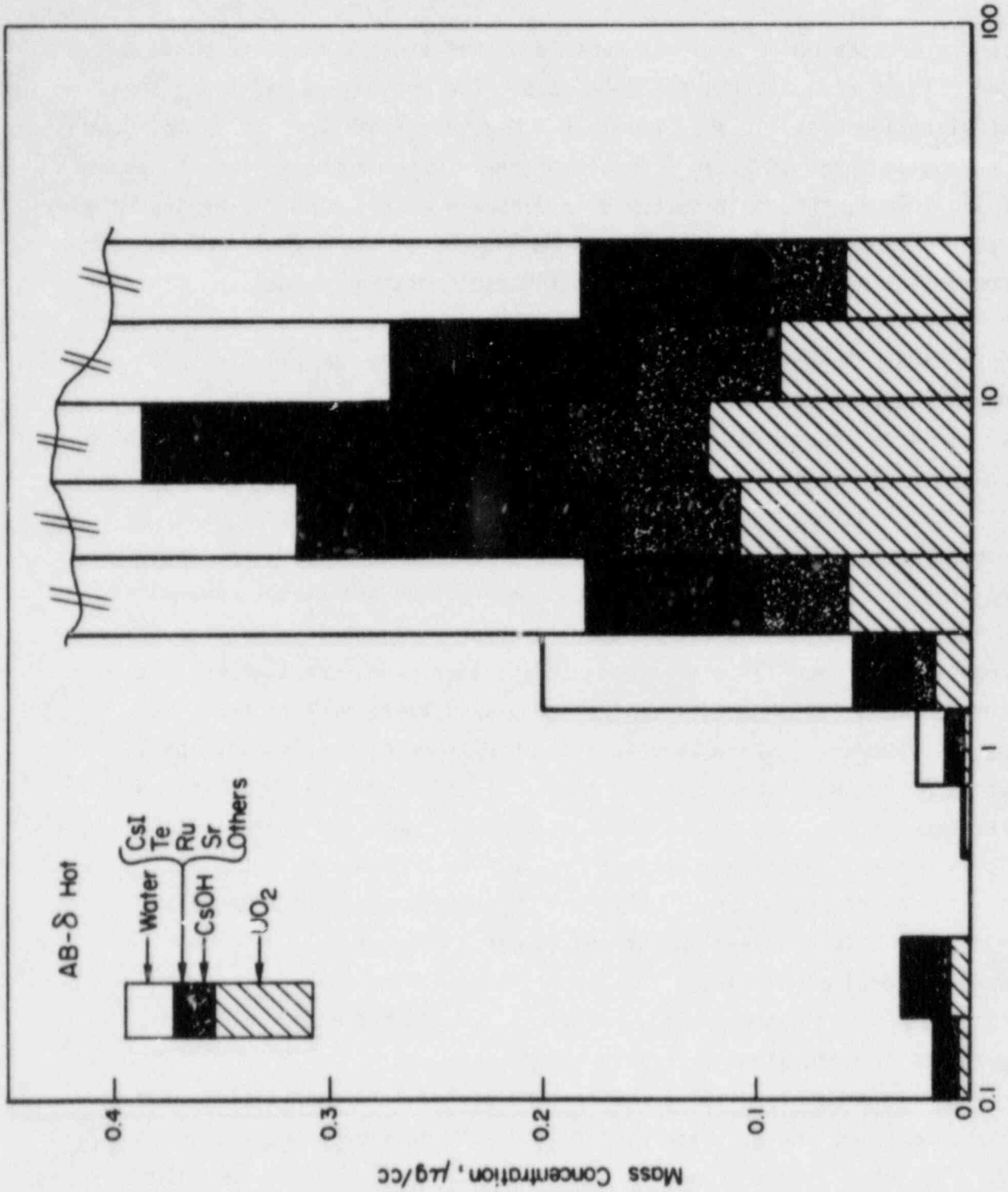

FIGURE 7.15. AIRBORNE PARTICLES SIZE DISTRIBUTION SHOWING FRACTION OF SPECIES

size are present under a highly supersaturated steam atmosphere plays a major role in reducing the airborne mass. The present calculations show this situation prevails approximately 3 minutes after the core slumps due to a massive surge of steam from the primary system representing the end of boiling. Thus, the rapid decrease in airborne mass during the period between 57 and 80 minutes in Figure 7.12 can be interpreted as a result of the steam condensation mechanism combined with the sedimentation mechanism. This type of dynamics is not considered in CORRAL calculations and this is the reason NAUA calculations generally show considerably low released fractions. Figure 7.16 compares the present calculation for the AB-δ_1 hot case with a similar sequence without including the steam condensation mechanism. Also shown in Figure 7.16 is the effect of diffusiophoresis. Although an initial calculation result has demonstrated a rather dramatic effect of steam on particulate mechanics, it should be cautioned that the demonstrated magnitude of the role played by steam condensation and diffusiophoresis should, of course, be carefully studied and experimentally verified. Having recognized the importance of steam condensation, the work that would also be needed in this connection will be realistic assessment of the time-dependent amount of steam that is available for condensation onto particulates. Accurate estimates of the amount of water condensing to the containment structure and the inclusion of effects of noncondensible gases on calculation of supersaturation ratio should be considered.

As discussed previously, the containment failure time plays a dominant role in determining the leaked mass. Figure 7.17 compares the amount of total particulates that is released to the environment for AB-β, AB-γ, and AB-δ_1. Again, rapid increase in the leaked mass, of course, represents the containment failure times.

In order to examine how aerosol particulates are distributed at various accident phases, Figures 7.18 and 7.19 have been prepared. In general, the total amount of source particulates may be divided into those airborne, leaked outside the containment, plated on the walls and settled on the floor. The distribution among these locations depends upon various aerosol behavior mechanisms prevailing in the containment. In both figures, it is observed that the distribution of material is governed mainly by accident events including the source timing and mass and the containment

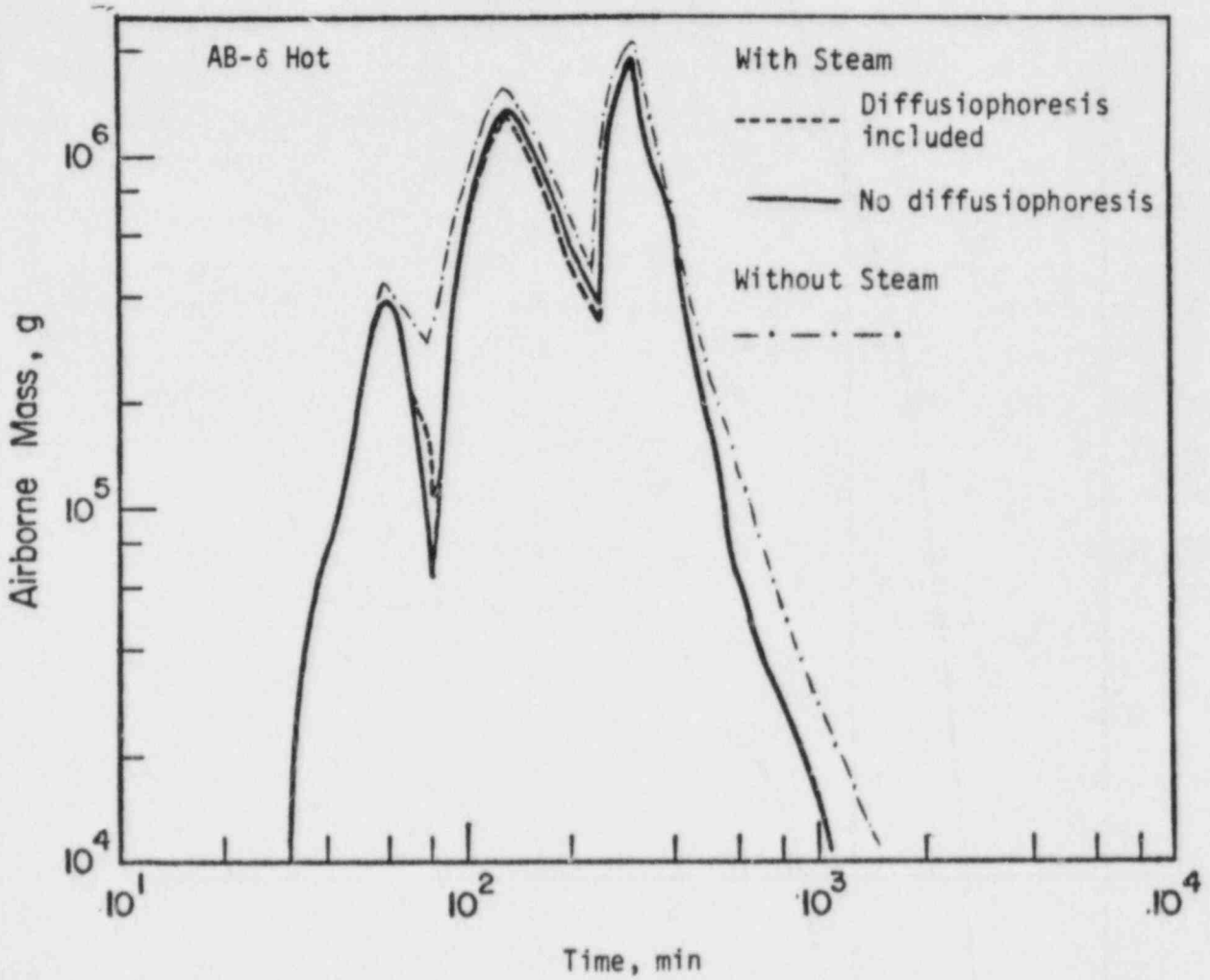

FIGURE 7.16. AB-δ SHOWING EFFECTS OF STEAM CONDENSATION AND DIFFUSIOPHORESIS ON AIRBORNE MASS OF SOLID PARTICULATES

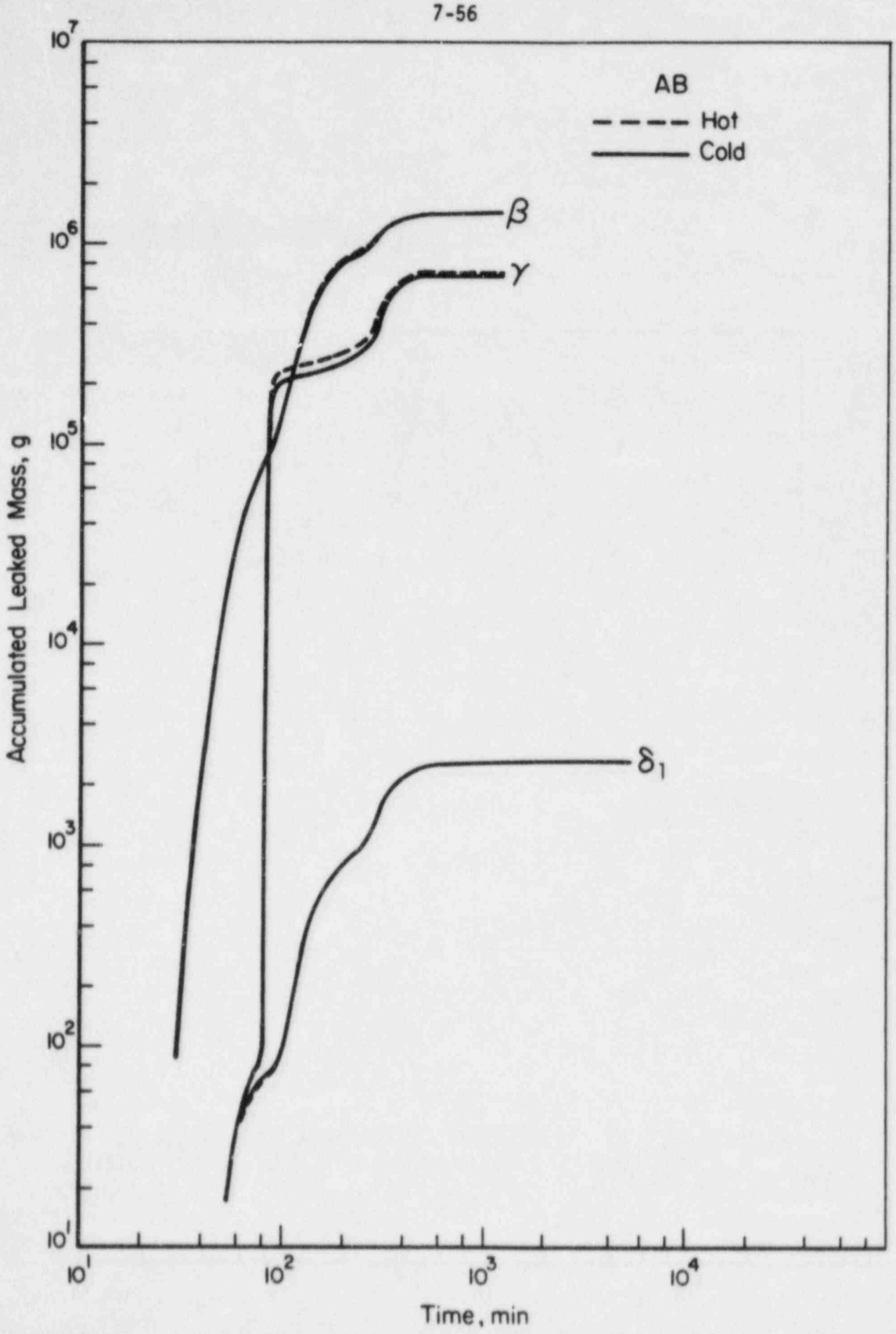

FIGURE 7.17. COMPARISON OF ACCUMULATED LEAKED MASS FOR AB-β, -γ, AND δ_1 SEQUENCES

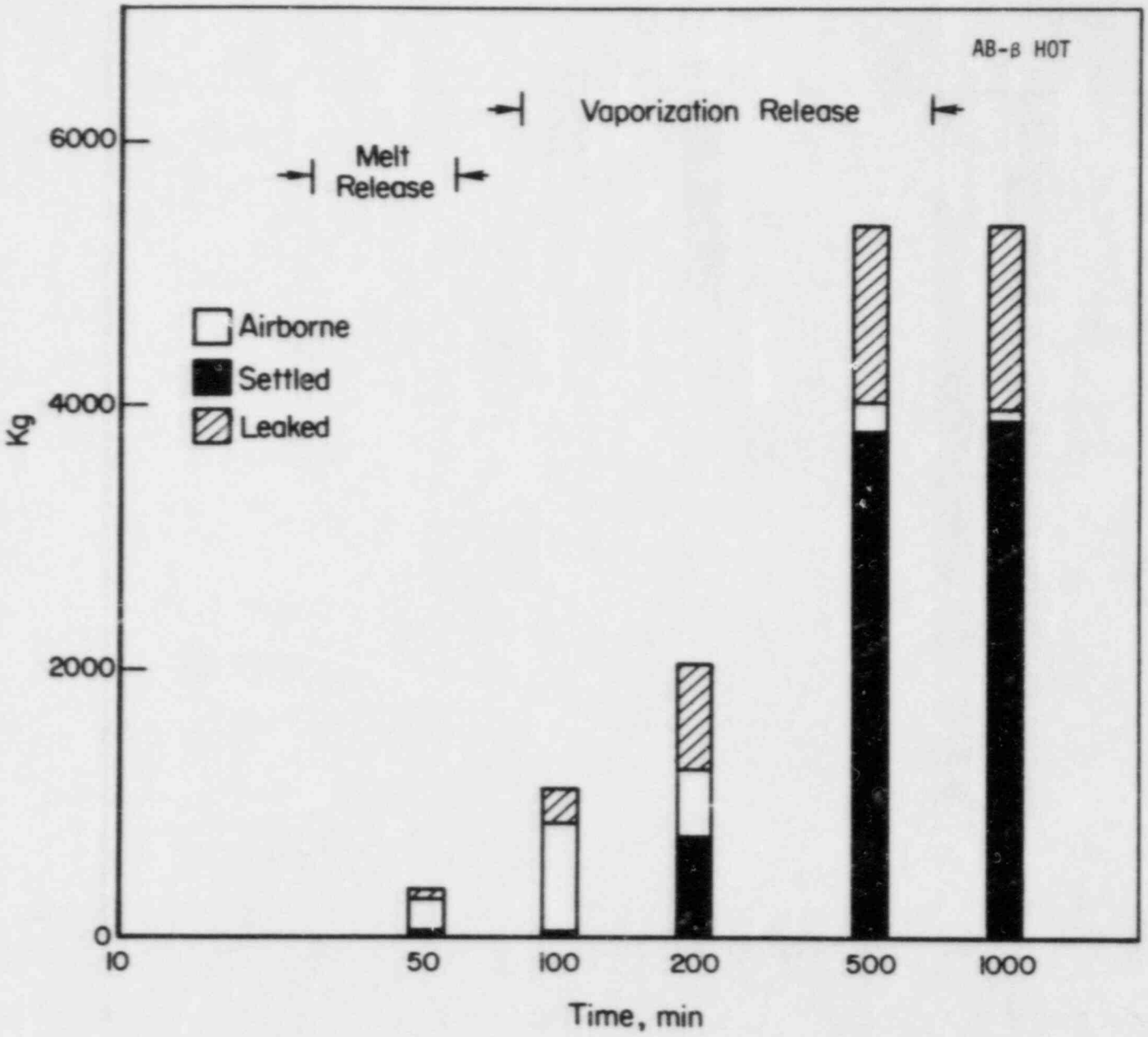

FIGURE 7.18. DISTRIBUTION OF PARTICULATE MASS FOR AB-β HOT

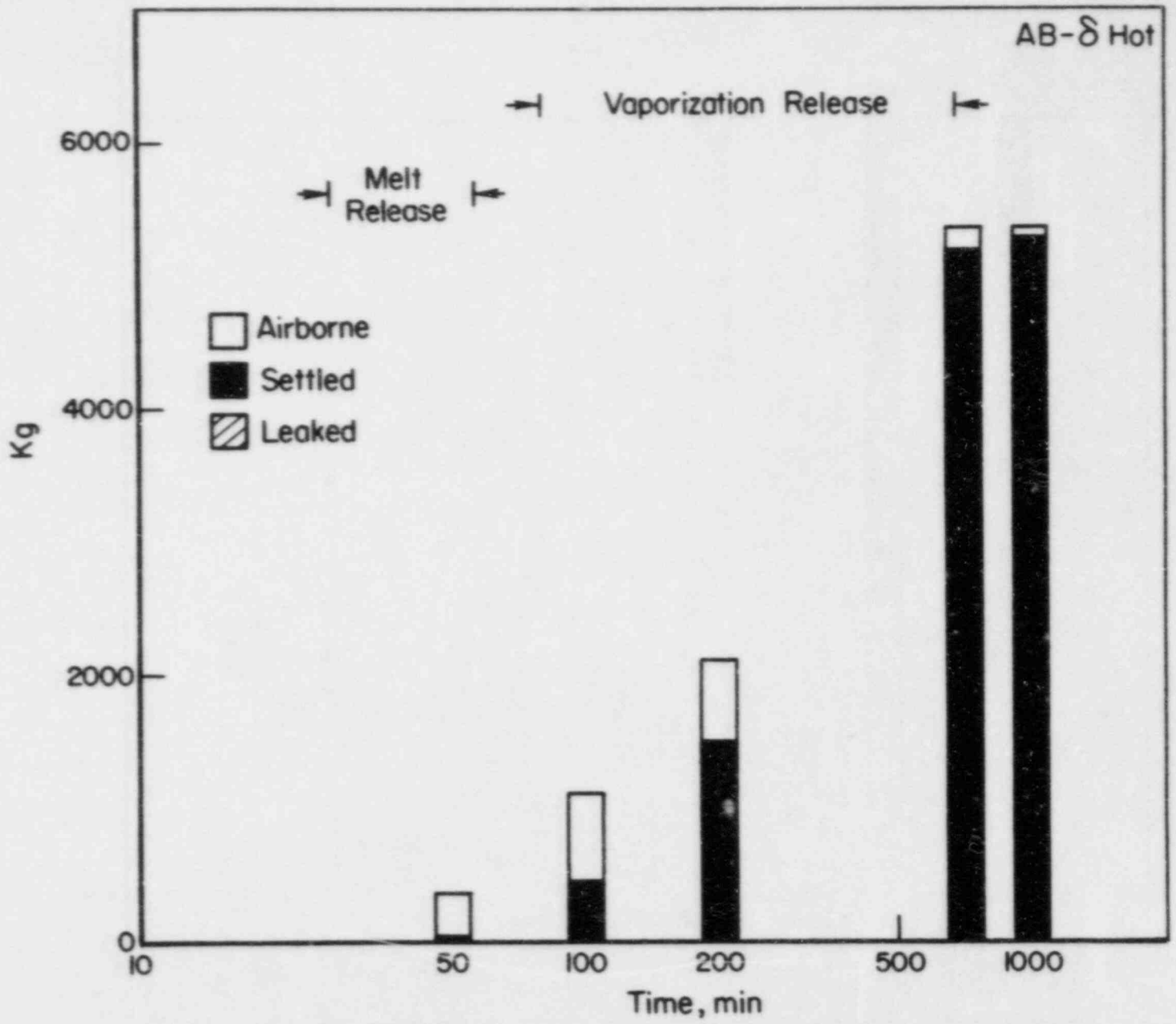

FIGURE 7.19. DISTRIBUTION OF PARTICULATE MASS FOR AB-δ_1 HOT

failure time. Among various aerosol behavior mechanisms, sedimentation, as influenced by agglomeration and condensation, is seen to be the most dominant mechanism in determining the location of the aerosol particulates. As will further be discussed later for the TMLB' sequences, the amount plated on walls by the diffusion mechanism is too small to appear in Figures 7.18 and 7.19 and this is true for all the accident sequences.

7.3.2 TMLB' Sequence

Two containment failure modes were examined for the subject accident sequence. In the first failure mode designated TMLB'-δ_e the containment fails 276 minutes after the core uncovers and this time coincides with the event the bottom head fails. At this point, the containment pressure reaches 89 psi. In the second mode designated TMLB'-δ_1, the containment fails at a time of 42 hours with a containment pressure of 100 psi. Figure 7.20 shows the distribution of dry particulates as settled and airborne in the containment or as leaked to the environment at various times for TMLB'-δ_e. The amount plated on the containment inner wall is too small to be shown in the figure. The location distribution of material that is further broken down into various species is listed in Table 7.18. The fraction of core inventory that is released to the environment is listed in Table 7.16. CORRAL calculations for TMLB'-δ_1 are listed in Table 7.17 for comparison.

Compared with other accident sequences listed in Table 7.16, the TMLB'-δ_e sequence represents an accident that permits a maximum amount of fission product to escape to the atmosphere. This is, of course, due to the fact that in this accident, the containment fails in a relatively short time ($\sim$5 minutes) after the core slumps. Thus, the source particulates released from the primary system tend to escape the containment before they are subject to any natural retention mechanisms such as agglomeration, steam condensation, and sedimentation. It is also interesting to note that for this reason, the predicted fractions of core inventory of I and Cs released to the environment are about the same as that calculated in the previous WASH 1400 study.

TMLB'-δ_1 is similar to TMLB'-δ_e except that the containment fails at a later time. Therefore, it is expected that the leaked amount shown in

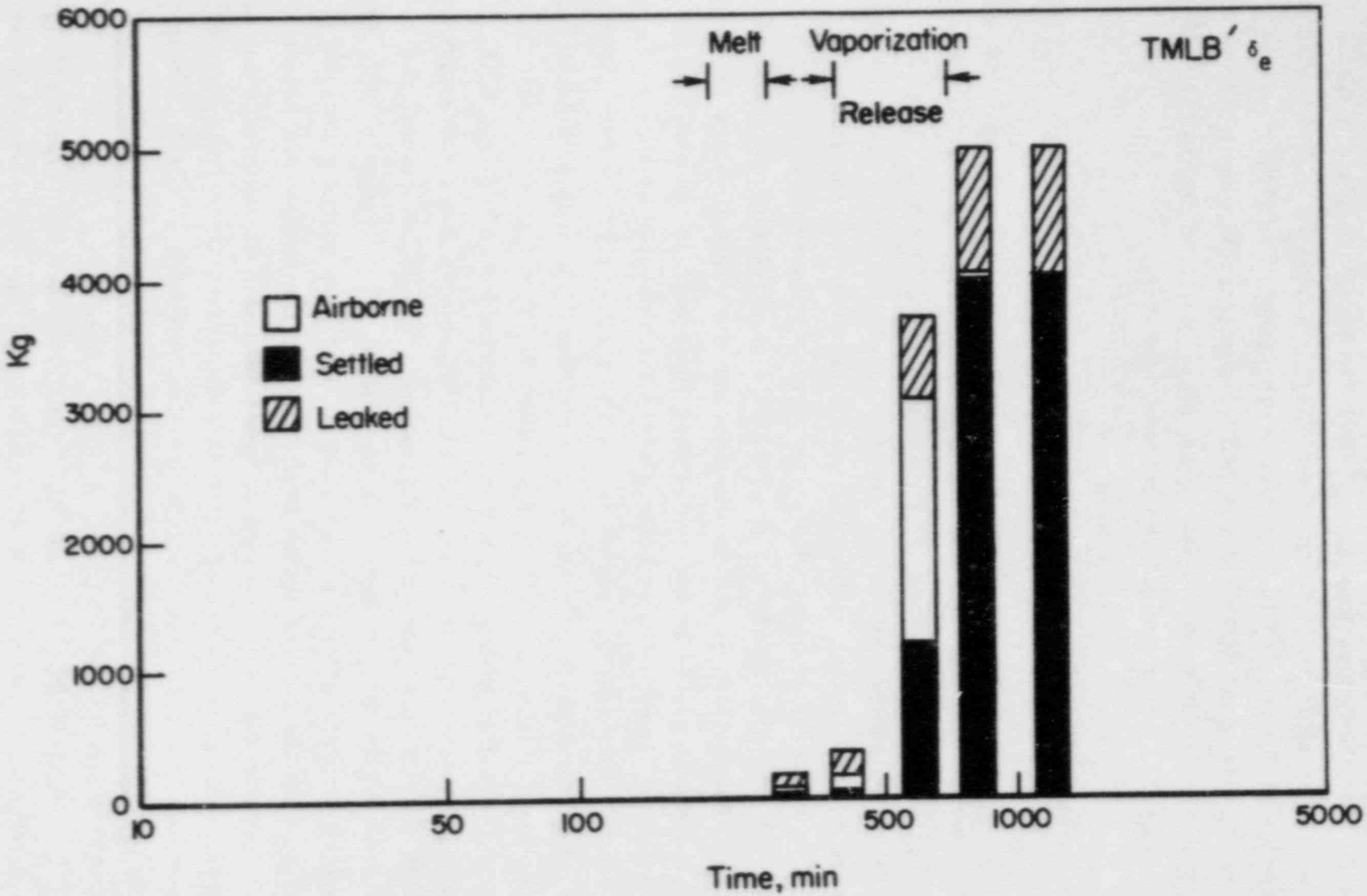

FIGURE 7.20. DISTRIBUTION OF PARTICULATE MASS FOR TMLB'-δ_e

TABLE 7.18. LOCATION DISTRIBUTION OF SPECIES AT VARIOUS TIMES FOR TMLB'-δ_e

Species	Leaked, g	Airborne, g	Plated, g	Settled, g	Total, g
		t = 300 min (5 hr)			
Total particulate	1.4×10^5	32000	6	13000	1.8×10^5
CsI	16000	3400	0.7	1500	21000
CsOH	70000	16000	3	6500	93000
Te	11000	2400	0.4	1000	14000
Ru	75	17	.003	7	99
Sr	410	91	.02	39	540
UO_2	29000	6300	1	2700	38000
		t = 400 min (6.7 hr)			
Total particulate	1.5×10^5	1.8×10^5	22	41000	3.7×10^5
CsI	16000	34	0.7	4400	21000
CsOH	73000	15	3	20000	93000
Te	11000	3	0.5	3100	14000
Ru	77	.05	.004	21	98
Sr	430	110	.03	120	660
UO_2	32000	1.1×10^5	1.2	8400	1.5×10^5
		t = 600 min (10 hr)			
Total particulate	6.3×10^5	1.9×10^6	550	1.2×10^6	3.7×10^6
CsI	16000	.45	.72	4400	21000
CsOH	73000	2	3.3	20000	93000
Te	11000	1	0.5	3100	14000
Ru	78	0.5	.004	22	100
Sr	540	105	.16	380	1000
UO_2	1.4×10^5	1.9×10^5	140	2.6×10^5	5.9×10^5

7.18. (Continued)

Species	Leaked, g	Airborne, g	Plated, g	Settled, g	Total, g
		t = 800 min (13.3 hr)			
Total particulate	9.3×10^5	140	950	4.0×10^6	4.9×10^6
CsI	16000	1.5×10^{-5}	0.7	4400	21000
CsOH	73000	6.6×10^{-5}	3.3	20000	93000
Te	11000	8.7×10^{-5}	0.5	3100	14000
Ru	76	2.6×10^{-5}	.004	22	98
Sr	560	.01	0	540	1100
UO_2	1.7×10^5	13	180	5.2×10^5	6.9×10^5
		t = 1200 min (20 hr)			
Total particulate	9.3×10^5	18	950	4.0×10^6	4.9×10^6
CsI	16000	1.9×10^{-6}	0.7	4400	21000
CsOH	73000	8.4×10^{-6}	3.3	20000	93000
Te	11000	1.1×10^{-5}	0.5	3100	14000
Ru	78	3.2×10^{-6}	.004	22	100
Sr	560	.001	0.2	540	1100
UO_2	1.7×10^5	1.6	180	5.2×10^5	6.9×10^5

Figure 7.20 is substantially reduced for this containment failure mode and this is shown in Figure 7.21.

Figure 7.22 shows the mass of airborne particulates of selected species for TMLB'-δ_1. Generally a time-dependent airborne mass similar to that observed for the AB-δ_1 case is observed in that increase or decrease of the airborne mass follows closely the timings of the two release periods and the containment failure. In fact, the calculated fractions of core inventory released to the atmosphere for the TMLB'-δ_1 and the AB-δ_1 cases are found to be on the same order of magnitude for I and Cs as listed in Table 7.16. It should be noted that these numbers are, however, considerably lower than the corresponding values from CORRAL calculations as listed in Table 7.17.

7.3.3 S_2D Sequence

The S_2D sequence is a small pipe break accident as already discussed. As shown in Table 7.1, two different containment failure times were examined and the melt release source for the cold upper plenum was utilized. Unlike the AB and TMLB' accident sequences, containment spray systems operate during this sequence in order to condense steam and to reduce the containment pressure. Fraction of core inventory released to the environment as calculated by the NAUA code is shown in Table 7.16.

Since the NAUA code does not have any provision for engineered safeguard, calculations were made by adding the removal mechanism of aerosol particles due to spraying. Details on modification of the NAUA code have already been discussed in Section 5.3.2. One of the most important parameters that influence substantially the particulate removal efficiency by spraying is the water drop size. The drop size, of course, depends upon the type of commercial nozzle in use, the operating pressure, and on the operating flow rate. The drop size used in the past ranges from 400 to 1000 μm. The surface mean diameter computed based on the data provided by manufacturers is about 800 μm for the top header-containment spray and about 1000 μm for the lower header-recirculation spray.(7.1) Since there is a wide range of optimum values, a simple sensitivity calculation was performed also.

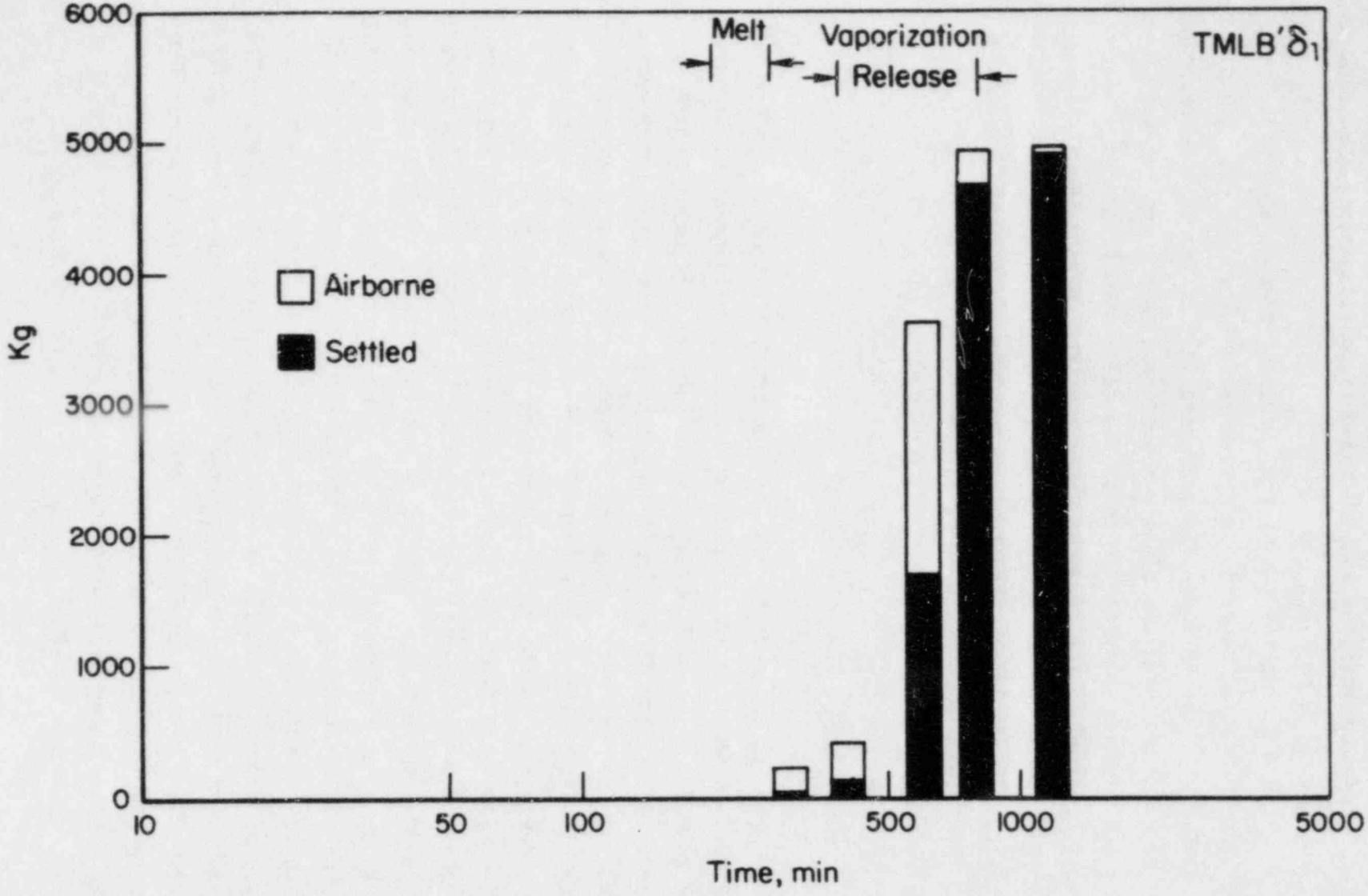

FIGURE 7.21. DISTRIBUTION OF PARTICULATE MASS FOR TMLB-δ_1

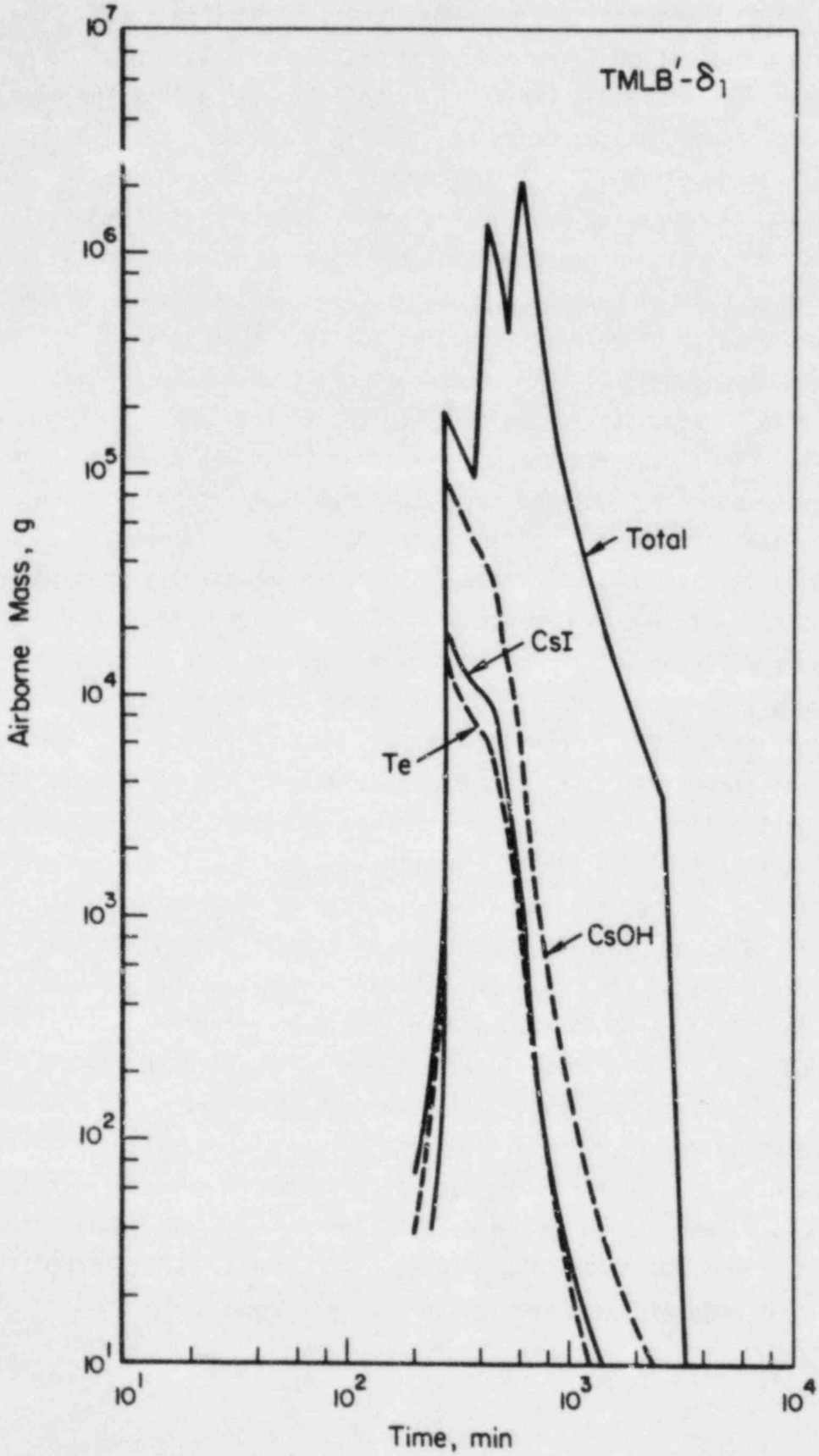

FIGURE 7.22. AIRBORNE MASS OF SELECTED SPECIES AS A FUNCTION OF TIME FOR TMLB'-δ_1

Two containment failure modes were examined in this study. The accident events are shown in Table 6.3. The calculated fraction of core inventory released is listed in Tables 7.16 and 7.17. Note that the core primary system transport calculations for the S_2D cases were based on the "hot" upper plenum conditions.

In general, spraying systems are highly effective in removing aerosol particles, and it is expected that the spraying mechanism will dominate all other natural retention mechanisms in the case of S_2D sequence. The calculation results of released fraction for the S_2D-ε in which spraying systems operate throughout all the accident events show that very small fractions of fission products are released to the environment. When compared with the CORRAL calculation results, the released fractions calculated by the NAUA computer code are observed to be somewhat lower for all the species, perhaps due to the difference in defining the collision efficiency, ε. While Equation (5.2) is utilized in NAUA calculations, an empirical expression is used in CORRAL calculations regardless of sizes of particle and spray drop.

Figure 7.23 shows the time-dependent airborne mass for both containment failure modes. In Figure 7.23, it is seen as expected that the airborne mass remains below 10 grams during the melt release period due to the high removal effectiveness of spraying coupled with the relatively high retention of particulates in the primary system. However, the airborne mass is seen to increase to a higher concentration at around 80 minutes showing the release of additional source materials as the bottom head fails. At a time of 200 minutes, when the vaporization release starts, the airborne mass increased rapidly in $S_2D\gamma$ in which it was assumed the spray ceases operating as the containment fails. However, in $S_2D\varepsilon$ where the spray continues to operate throughout the accident event, the airborne concentration reaches a relatively low level. It should be noted that in the S_2D calculation shown in Figure 7.23, a drop size of 400 μm was used. In order to examine the effects of water drop size on the airborne concentration, the water drop size was varied in the calculation and the results are shown in Figure 7.24. It is seen that the effects are rather dramatic demonstrating the important role of spray removal in the S_2D case.

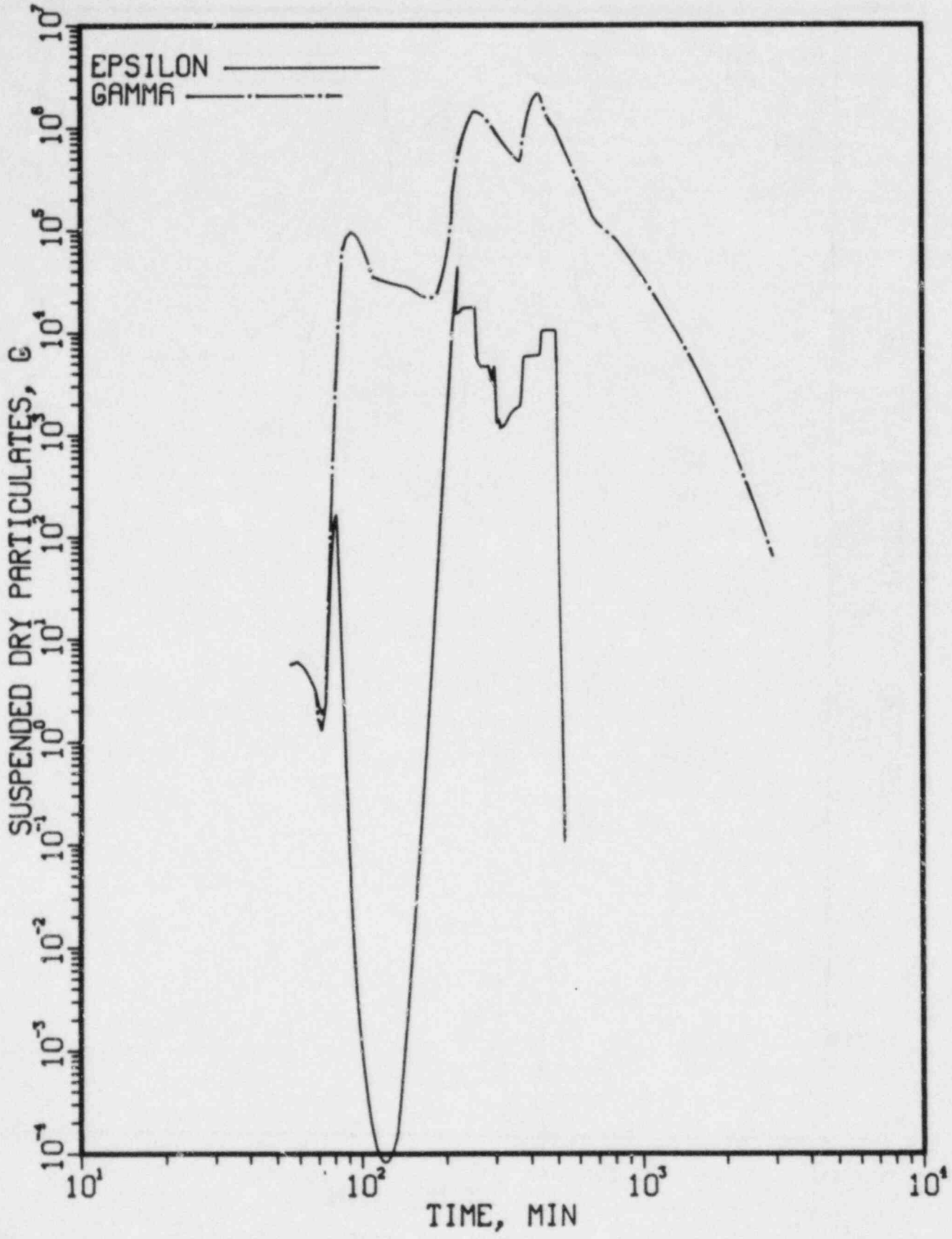

FIGURE 7.23. AIRBORNE MASS OF PARTICULATE AS FUNCTION OF TIME FOR S_2D

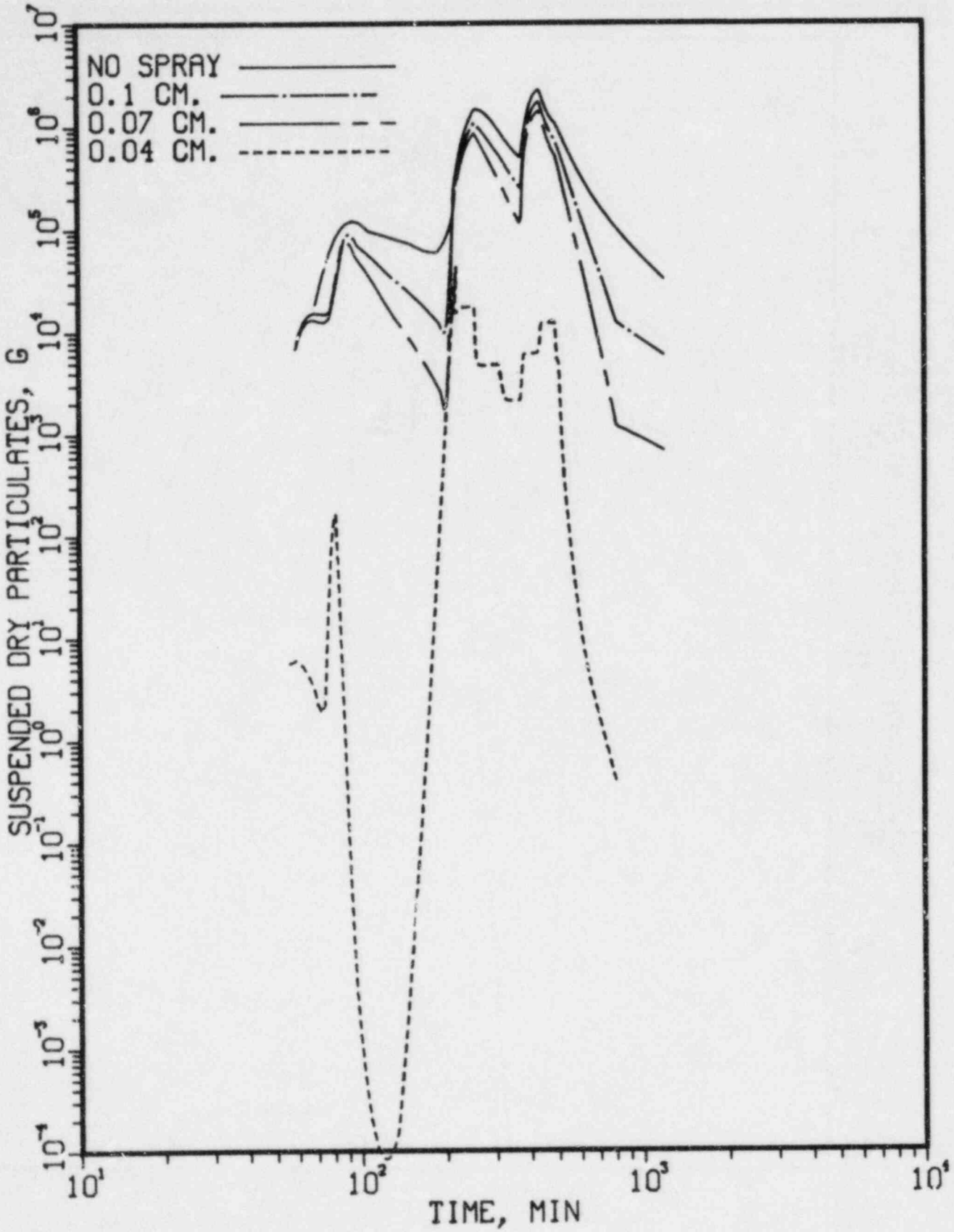

FIGURE 7.24. ACCUMULATED LEAKED MASS FOR S_2O

7.3.4 V Sequence

In the event check valves that provide a barrier between the RCS piping and the low pressure ECC system should fail, the fission products can bypass the containment safety feature and be released to the auxiliary building. If the auxiliary buildling is treated as a containment for modeling purposes, calculational methods identical to those used for the other accident sequences can be applied. Results calculated with the TRAP-MELT code were used for the melt release source for NAUA containment calculations. In treating the vaporization release, it was assumed that no attenuation of particulates occurs in their passage from the reactor cavity through the primary system. This simplification is expected to overestimate the amount of fission products released to the environment. It is planned in the next phase of the present study to simulate this sequence by using a multi-volume approach to assess the effects of retention of particulate material in the primary system for the vaporization release term. Two separate TRAP-MELT calculations will be necessary in that approach.

The fractions of core inventory of various species released to the atmosphere as predicted by the NAUA code are listed in Table 7.16. As expected, the calculated results show that this accident sequence still remains as one of the most important sequences in terms of total release with the fractions being about 15 percent of the Cs and I inventories. Accumulated leaked mass of each species for V is shown in Figure 7.25.

7.3.5 General Observations

The results of 13 NAUA calculations and 9 CORRAL calculations have been presented. Based on results of the present calculation, the following conclusions can be made on transport and retention of fission products in the containment. The amount of particulates escaping the containment is largely dependent upon timings of the two releases from fuel (melt and vaporization) and upon containment failure time. As demonstrated in calculations for the sequences involving an early containment failure (AB-β, AB-γ, TMLB-δ_e, and V), these accidents lead to the highest release fractions.

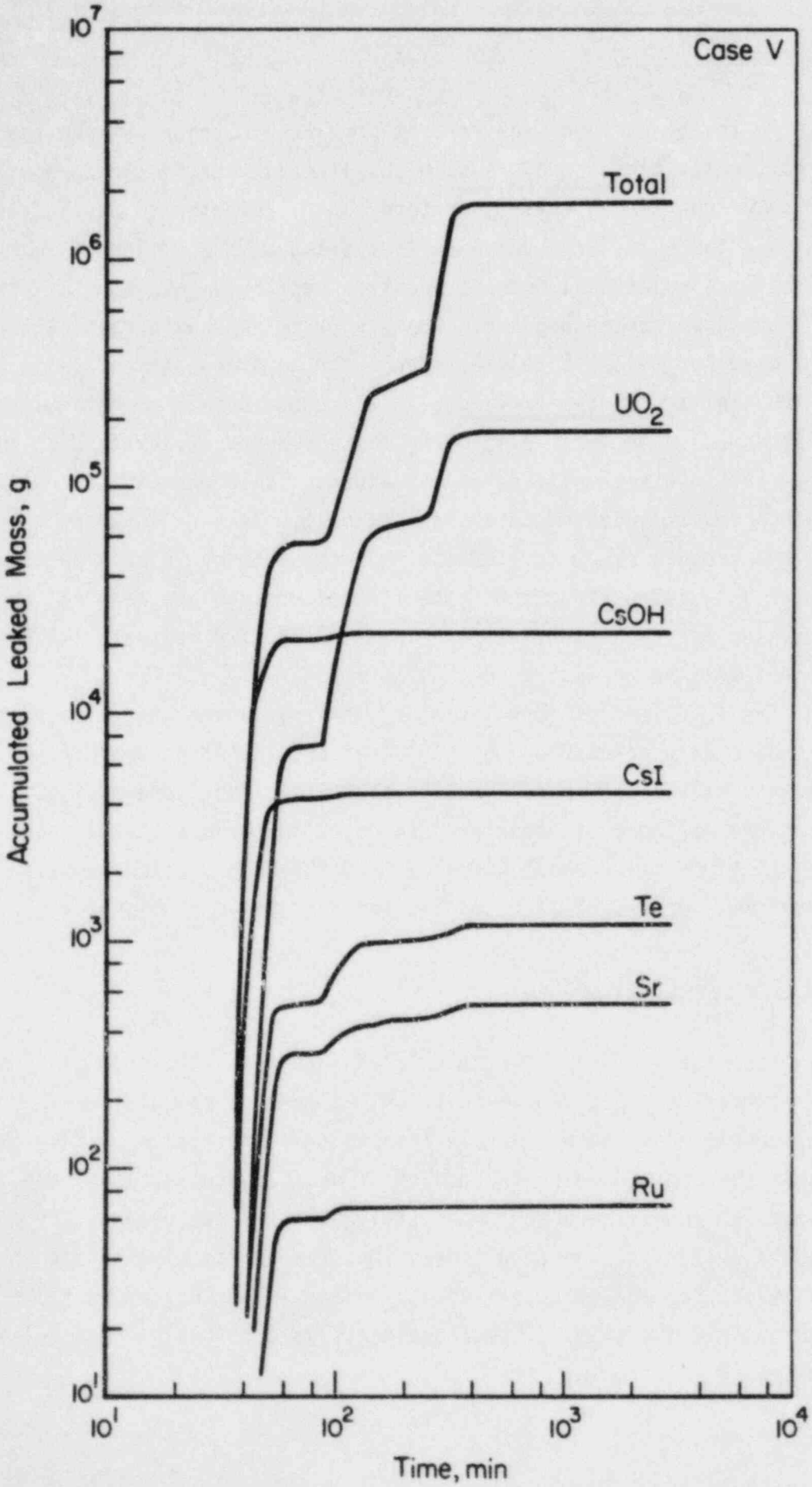

FIGURE 7.25. ACCUMULATED LEAKED MASS OF EACH SPECIES FOR V

The particle growth rate used in the present study is based on Mason's equation as utilized in the NAUA computer code. His expression does not account for the gas slip effects and therefore might not give an accurate steam condensation rate for the case in which very small particles are considered. However, the size of particles dealt with in this study is generally much larger than the free path length of gas molecules, causing the resulting Knudsen number to become small. This is particularly true if one considers that the mean free path length of gas molecules will further reduce as the containment pressure reaches a high of 55 psi in accident sequences such as AB-δ_1 and TMLB'-δ_1.

In conjunction with the steam condensation onto particulate matter, another particle retention mechanism, diffusiophoresis, may also be considered. Particle deposition takes place by this mechanism since the particles suspended in a hot steam-air atmosphere can migrate along with the steam flux toward the containment walls. Importance of this mechanism depends, of course, upon the saturation water vapor pressure at the prevailing containment atmosphere and upon the saturation vapor pressure of water near the wall. The accident cases examined in the present study generally show that during the time period between the melt release and the containment failure time, a relatively small amount of steam is found to condense onto the walls when compared with the steam amount contained in the air as vapor and with the amount condensing onto particles. Therefore, this mechanism has not been considered here. For inclusion of this mechanism in the future, it will be necessary to validate existing theories on this mechanism and more importantly to perform accurate calculations on the time-dependent steam flux which will be determined by the temperatures of both the containment atmosphere and the wall and the boundary layer thickness.

It is worthwhile to note that the retention of fission products that takes place in the flow path of the primary system reduces the source term to the containment and subsequently will reduce the amount of fission products that escape the containment. However, the retention effects of the primary system on the release to the environment would not be so apparent for accidents involving a late containment failure mode. In such accident sequences, the fission products that are not retained in the primary system will be retained in the containment due to prolonged residence times. One

can then conclude that alteration of the melt release rate would not significantly change the final release fraction in such sequences.

7.4 Discussion

In the following discussion the "best estimate" reslts of this study are compared with release assumptions made in WASH 1400. Although the models used in these analyses represent major improvements over WASH 1400, it should be recognized that the uncertainties in the current "best estimates" are still quite large. Some of the principal uncertainties and approximations made in these analyses are identified in earlier sections. Additional model improvement and experimental data could result in significant changes in these "best estimate" values.

The results obtained for the release of fission products from the fuel are quite similar to the release fractions used in WASH 1400. These are compared in Table 7.19 for the TMLB' sequence, which has slightly higher melt release fractions than the other sequences due to the longer melt period. For the volatile groups nearly all of the core inventory would be released during heat-up and melting in the vessel. The releases for the less volatile groups estimated in this study are also similar to the release values used in WASH 1400. The mass of aerosols released from the fuel in WASH 1400 was much smaller than in the current study, which accounts for sources of inert aerosols, but the mass of aerosols was not a factor in the simplified WASH 1400 analysis methods.

No credit was taken for primary systems retention of fission products in WASH 1400. The results obtained in this study with the TRAP-MELT code show a wide range for the potential retention as a function of the accident sequence. For example, the predicted transmission fraction for CsI in the primary system varies from about 0.85 for the AB sequence to approximately 0.15 for the S_2D sequence. In some of the analyses the predicted retention of less volatile species associated with the aerosols is very large, resulting in more than an order of magnitude reduction in the source to the containment. Of the major areas where retention could be significant, the status of methods for analyzing the primary system is the least well developed and supported by experimental data. Even though the

TABLE 7.19. FISSION PRODUCT RELEASE FROM FUEL

	Xe	I	Cs	Te	Sr	Ru	La
				Current Study			
Gap/Melt	0.86	0.86	0.87	0.79	0.26	.022	8.5×10^{-3}
Vaporization	0.14	0.14	0.13	1.6×10^{-4}	0.011	--	8.2×10^{-3}
Total	1.0	1.0	1.0	0.79	0.27	.022	0.017
				WASH 1400			
Gap/Melt	0.90	0.90	0.81	0.15	0.10	0.030	0.003
Vaporization	0.10	0.10	0.19	0.85	0.01	0.003	0.010
Total	1.0	1.0	1.0	1.0	0.11	0.033	0.013

individual deposition mechanisms incorporated into the TRAP-MELT code are based on verified models, their incorporation into a flow scheme and combination into an integral analysis have not been verified. Therefore, the results provided in this report must be considered tentative.

As recognized in NUREG-0772, the CORRAL code tends to underestimate the natural removal processes for airborne aerosols and as a result overestimates the release of radioactive material in accidents in which the containment fails after an extended period of time. The differences between the NAUA and CORRAL predictions for the release fractions in the AB-δ_1 and TMLB'-δ_1 sequences are approximately two orders of magnitude. In general, in the cases for which the containment is predicted to fail early in the accident (e.g., containment isolation failure (β) or early overpressure failure (γ or δ_e) the differences between the NAUA and CORRAL results are small. This is because the time constant for natural deposition in the containment is small relative to the residence time for these cases.

In CORRAL, iodine is treated as being in elemental form whereas in NAUA the iodine was treated as a condensed iodide form associated with the aerosols. A separate calculation was performed by hand for the volatile iodine species, assuming that these forms are primarily produced in the containment after being released from the primary system as less volatile species. The predicted release fractions for I_2 in the CORRAL analyses performed in this study are lower than those obtained with CORRAL in WASH 1400 because the input thermal hydraulic conditions obtained from MARCH are more realistic than the flow assumptions made in WASH 1400.

In Tables 7.20 and 7.21 direct comparisons are made between the results of this study to date and WASH 1400 results for the releases from containment of the important volatile fission products, iodine and cesium. In WASH 1400, accident sequences were grouped into categories for the analysis of ex-plant consequences. The values shown for WASH 1400 are therefore the release fractions for the associated WASH 1400 release categories rather than those for specific accident sequences.

The extent to which volatile fission products are predicted to be retained in the primary system varies over a decade depending on the accident sequence analyzed. For some accident conditions and release pathways, the amount of retention predicted is minor, however, at least when compared

TABLE 7.20. RELEASE FRACTIONS FOR IODINE

Sequence	Primary[a]	Containment[a]	Total[a]	WASH 1400 Total
AB-γ	1.0	0.3	0.3	0.7
δ_1	1.0	3×10^{-4}	3×10^{-4}	0.7
β	1.0	0.4	0.4[b]	0.7
ε	1.0	3×10^{-4}	3×10^{-4}	8×10^{-4}
TMLB'-δ_e	0.8	0.8	0.7	0.7
δ_1	0.8	1×10^{-3}	1×10^{-3}	0.7
S_2D-ε	0.4	1.5×10^{-6}	6×10^{-7}	2×10^{-5}
V	0.4	0.5	0.2	0.7

(a) Assuming iodine is present only as CsI.

(b) No credit was taken for retention in the building into which the leakage from containment is assumed to occur.

TABLE 7.21. RELEASE FRACTIONS FOR CESIUM

Sequence	Primary	Containment	Total	WASH 1400 Total
AB-γ	0.85	0.4	0.3	0.5
δ_1	0.85	4×10^{-4}	3×10^{-4}	0.5
β	0.85	0.5	0.4[a]	0.5
ϵ	0.85	4×10^{-4}	3×10^{-4}	8×10^{-4}
TMLB'-δ_e	0.7	0.8	0.6	0.5
δ_1	0.7	1×10^{-3}	8×10^{-4}	0.5
S_2D-ϵ	0.3	2×10^{-6}	6×10^{-7}	1×10^{-5}
V	0.4	0.5	0.2	0.5

(a) No credit was taken for retention in the building into which the leakage from containment is assumed to occur.

to the predicted retention of aerosols. Some aspects of the analyses used in this table may tend to underestimate the actual retention, in particular:

(1) The simple thermal hydraulic analyses performed may not adequately represent the actual flow patterns in the upper plenum and primary system which could result in greater deposition.

(2) The hot upper plenum results are used which probably underestimate the mass and surface areas of structures in the upper plenum contacted by the flow.

(3) Volatile species were allowed to evolve from hot surfaces without allowance for reaction of condensed vapors with surface materials.

It should be recognized, however, that heating of the structures by decay of deposited radionuclides was not accounted for in the analyses. Decay heating would tend to drive the volatiles farther along the flow path and possibly from the primary system. Each of these effects will be accounted for in some manner later in the program.

The most significant difference observed in these tables is the effect of delay in containment failure. If containment is able to remain intact for a number of hours, the eventual release to the environment would be much smaller than implied in WASH 1400. The table does, however, show some specific sequences in which the release fractions could be comparable to WASH 1400 values. In the event of containment isolation failure in conjunction with the unavailability of containment sprays, inadequate time is available to effectively remove fission products from the containment atmosphere prior to leakage. In the analysis that was performed, deposition within the building into which the leakage occurs was not taken into account. Thus, an additional decontamination factor of two or greater would probably be applied to the release fractions in a more complete analysis involving a specification of the isolation failure. In the V sequence the containment is bypassed and the small low pressure safeguards building, into which the fission products would be released, is comparatively ineffective in fission product removal.

The large transmission factor for the containment in the TMLB'-δ_e sequence is the result of an adverse combination of event timings. In the TRAP-MELT analyses a large fraction of the volatile fission products are

predicted to be airborne in the primary system at the time the lower head of the vessel is predicted to fail. The pressure pulse that is assumed to lead to containment failure immediately follows bottom head failure. Thus, the containment fails and depressurizes to the environment at essentially the same time that the fission products are released to the containment atmosphere.

The iodine fractions indicated in Table 7.20 are associated with the component of the iodine that is assumed to be in the iodide form. An additional component of more volatile chemical forms (e.g., organic and elemental iodine) would also be released which is on the order of 5×10^{-4} of core inventory. This term can be compared with the assumed release of approximately 7×10^{-3} organic iodine in WASH 1400.

In Table 7.22 release fractions are compared between the WASH 1400 release category PWR 2 and each of the accident sequences analyzed in this study that were assigned to that group. In this table, all of the fission product groups are represented. In general, the same trends are shown for the less volatile fission products as for iodine and cesium.

Because of the large consequences associated with a PWR 2 category release, the sequences assigned to this category tended to dominate the risk predicted for the Surry plant in WASH 1400. The results of the current study indicate that, although the consequences of some of the sequences were significantly overestimated in WASH 1400, the possibility of specific sequences with consequences comparable to the PWR 2 releases cannot be precluded based on current understanding of fission product retention mechanisms. The greatest conservatism in the WASH 1400 treatment treatment appears to be in the treatment of accident sequences that involve delayed containment failure. Thus, the impact of the results of the current study on the predicted risk is very sensitive to the relative likelihoods of the early and delayed containment failure modes and in particular to the timing of containment failure relative to the timing of the melt and vaporization releases of fission products. Improved understanding of containment strength and the phenomena that could lead to early failure of the containment (rapid steam generation, steam explosions and hydrogen burning) indicates that the likelihood of early containment failure is very small and in some cases in which failure has been assumed it may not be physically

TABLE 7.22. RELEASE FRACTIONS FOR SEQUENCES IN CATEGORY PWR 2

	Xe	I	Cs	Te	Sr	Ru	La
WASH 1400	0.9	0.7	0.5	0.3	0.06	0.02	4×10^{-3}
TMLB-δ_e	1.0	0.7	0.6	0.5	0.01	8×10^{-4}	2×10^{-3}
TMLB-δ	1.0	1×10^{-3}	8×10^{-4}	7×10^{-4}	3×10^{-5}	1×10^{-6}	9×10^{-6}
AB-γ	1.0	0.3	0.3	0.2	0.03	2×10^{-3}	2×10^{-3}
AB-δ_l	1.0	3×10^{-4}	3×10^{-4}	3×10^{-4}	3×10^{-5}	2×10^{-6}	5×10^{-6}
AB-β[a]	1.0	0.4	0.4	0.3	0.05	3×10^{-3}	4×10^{-3}
V	1.0	0.2	0.2	5×10^{-2}	1×10^{-2}	7×10^{-4}	2×10^{-3}

(a) No credit was taken for retention in the building into which the leakage from containment is assumed to occur.

possible. In a separate effort the NRC is re-evaluating the likelihood of the different failure modes in these accident sequences.

References

(7.1) Pasedag, W., private communication (1983).

APPENDIX A

THE MERGE CODE

APPENDIX A

THE MERGE CODE

MERGE is an interface computer code which utilizes data generated by MARCH 1.1 to calculate thermal-hydraulic data for input to TRAP-MELT. The code employs MARCH 1.1 output parameters to perform a gas-to-structures heat transfer analysis and converts its calculations into a form acceptable as input to TRAP-MELT. Two MARCH 1.1 output data files (TAPE10 and TAPE15) containing parameters necessary for the heat transfer analysis are attached to the MERGE code. One other MARCH 1.1 output data file can be attached to the code and listed upon user request. The MARCH 1.1 code can generate data at several hundred intervals with each timestep identified by a timestep index. The TRAP-MELT code, however, presently accepts only a maximum of 20 intervals of parametric change. In order to accommodate the data input limitations of TRAP-MELT, MERGE additionally performs data reduction by using a numerical averaging routine.

For most applications, two MERGE runs are performed to process the MARCH output data files. Parameters from the MARCH accident analysis required for the gas-to-structure heat transfer are input to the MERGE code. A user-supplied print index is also input to the code in order to list these parameters. Using the list as a guide, a maximum of 21 MARCH timestep indexes can be selected for use as limits of a maximum of 20 intervals of averaging for the MARCH results. The interval values are selected such that they adequately represent the MARCH output data and, thus, the MERGE output data, over the intervals of interest.

The MERGE gas-to-structures heat transfer analysis calculates thermal-hydraulic data for control volumes in the core exit gas flow path. To account for escape from the primary system through pipe breaks, a fictitious control volume is added to represent the outer containment. Flow between control volumes is identified in a control volume flow matrix which consists of source volumes to indicate flow exiting a volume and receiver volumes to indicate flow entering a volume.

The control volume flow matrix is input to show the path of the gas from source volume J to control volume I. A value of 1 or 0 is assigned to each matrix member to indicate flow/no flow from J to I. Each row and column in the matrix is summed and the values are used as limits for the number of flow paths to/from each control volume. Thus, the matrix setup allows for easy handling of multiple flow paths.

Required geometric data for each control volume include heat transfer area, cross-flow area, hydraulic diameter, length along line of flow, and vertical height. Additional required inputs include initial control volume gas and wall temperatures, heat capacities, number of heat transfer structures within a control volume, and percentage of flow entering each volume. For a control volume containing more than one structure, each structure must be identified with its own geometry, wall temperature, and heat capacity. For a control volume with a change in flow percentage, a flag must be set (e.g., FLAG2 = .TRUE). If this flag has been set to change, the time at which the change occurs (e.g., FTIME(2)) and the new flow percentage to the volume (e.g., FF(2)) are required inputs.

Figure A.1 is a diagram showing the sequential flow of the calculations in the MERGE code. It should be noted that calculations begin at the start of core uncovery or core melt and end at failure of the reactor pressure vessel. A description of each subroutine in the code is given below.

Subroutine EXITQ. In the MERGE code, the subroutine EXITQ and its associated subroutines analyze the thermal-hydraulic processes. EXITQ is the main subroutine for the gas-to-structures heat transfer analysis and is the largest subroutine in the code.

The approach used in solving for the thermal-hydraulic conditions in each volume involves an explicit finite difference solution to the flow equations. Conditions within each volume are obtained by moving consecutively from volume to volume downstream of the core. In each case the givens for a particular volume are the initial gas temperature, mass, ratio of hydrogen to steam, and rate of heat addition to structures. Also known from the MARCH calculation are the total pressure, the temperature of the

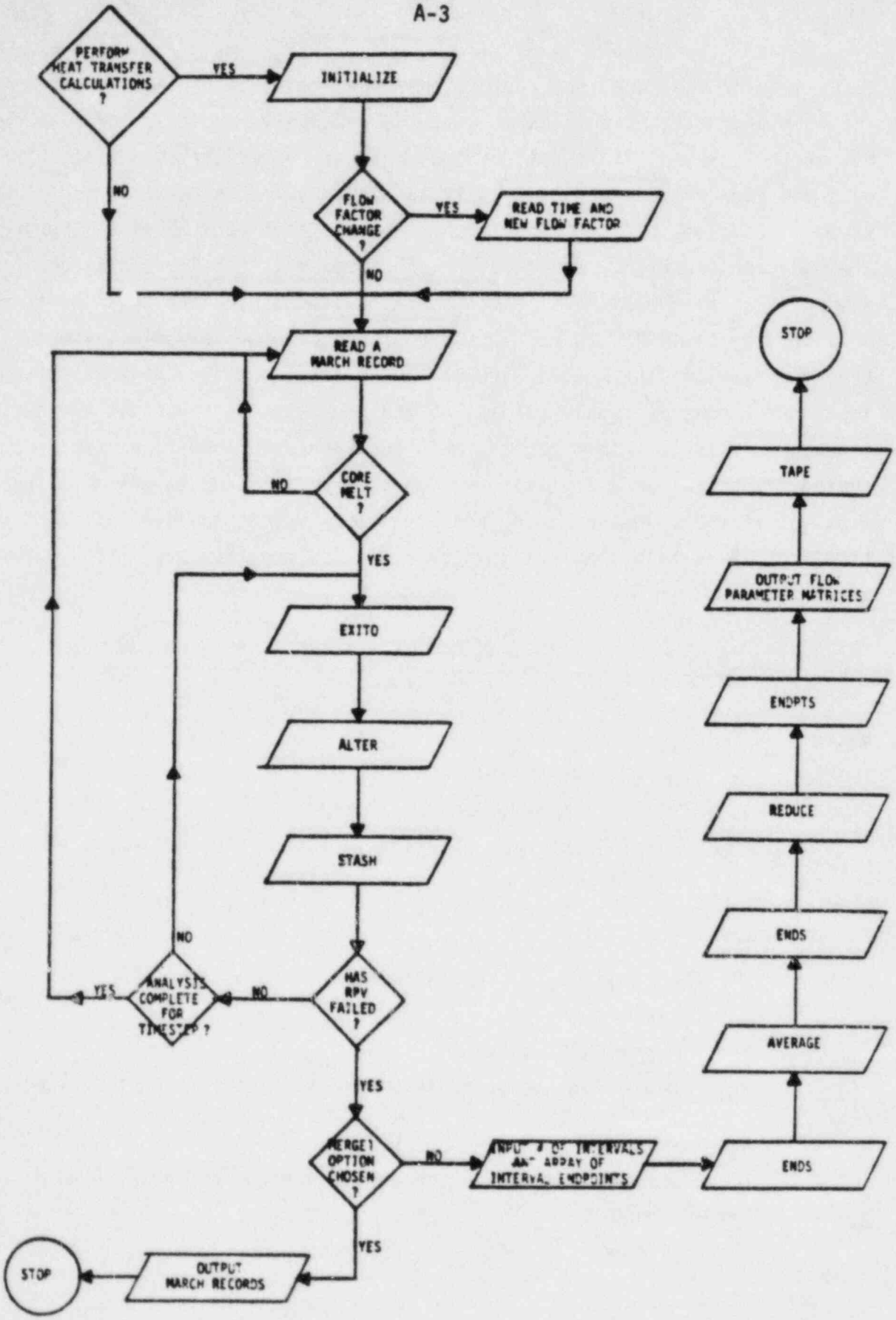

FIGURE A.1. FLOW CHART OF THE MERGE CODE

gases leaving the core, the ratio of hydrogen to steam of these gases, and the mass flow rate. For each volume, the unknown variable is the flow rate out of the volume. The equations that must be solved are conservation of mass and conservation of energy. It is also assumed that the hydrogen and steam in a volume has the same temperature and that each obeys an appropriate equation of state. Conservation of momentum is not imposed since it is assumed that at a particular timestep, all volumes have the total pressure predicted by the MARCH code. These equations can then be solved iteratively by varying the outlet flow until the total pressure is equal to the input MARCH pressure while satisfying the conservation equations and the equations of state. In practice, this approach was found to be time consuming. Instead, an approximate method is used in MERGE to estimate the flow out of the volume assuming that the gases act as an ideal gas over the timestep. This allows an analytic solution for the flow out of the volume given by

$$W_n = \frac{H_n^0 + W_{n-1}\Delta t(h_{n-1} + 460\,C_0 - C_1) - \frac{(144)C_0PV_n}{R} + M_{totn}(460\,C_0 - C_1) - Q\Delta t + (144/778)(P - P_0)V_n}{(h_n + 460\,C_0 - C_1)\Delta t} \qquad (A.1)$$

where

W_n = flow out of volume n, lbm/min

W_{n-1} = flow out of volume n-1, lbm/min

H_n^0 = total enthalpy of gases in volume n at beginning of timestep, Btu

h_n = specific enthalpy of gases in volume n, Btu/lbm

h_{n-1} = specific enthalpy of gases in volume n-1, Btu/lbm

M_{totn} = total mass of gases in volume n, lbm

t = timestep, min

P = pressure, psia

P_0 = pressure of gases in volume at beginning of timestep, psia

V_n = gas volume for the control volume, ft^3

Q = heat transferred between volume gas and wall, Btu/min,

and it is assumed that

$$h_n = C_0T + C_1$$

where

T = temperature in F

C_0, C_1 = coefficients recalculated at each timestep based on the equations of state for steam and hydrogen.

Given the estimated value for the outflow, the gases are then required to satisfy realistic equations of state for steam and hydrogen. The result of the approximation is to yield a slightly different value of the pressure at the end of the timestep than the MARCH calculated value. Because of the crudeness of the one-volume solution that led to the MARCH calculated pressure, this discrepancy is considered minor.

It should be noted that this subroutine also regulates control volume flow throughput by dividing the MARCH timestep into subintervals in order to prevent the total evacuation of the mass in a volume within a timestep. The subinterval timesteps are determined by first examining each control volume to obtain the one having the least gas volume; second, treating the mixture exiting the top of the core as an ideal gas to determine an approximate volumetric flow rate; and third, subdividing the MARCH timestep until the volumetric flow rates times the subinterval time is less than or equal to 25 percent of the volume having the least gas volume. Furthermore, the heat transfer analysis is completed for each control volume over the MARCH timestep, and thus, all subintervals, before proceeding to the analysis for the next control volume at the same MARCH timestep.

The Newton-Raphson[A-1] method of iteration is then employed to solve control volume steam temperature, pressure, and enthalpy. The following three simultaneous equations are used:

$$HST = (HH - H2M*HH2)/STMM \quad , \tag{A.2}$$

$$T = f(PSTM, HST)(2) \tag{A.3}$$

$$V = f(PSTM, HST)(3) \tag{A.4}$$

where

HST = specific enthalpy of steam in the control volume, BTU/lbm

T = temperature of steam in the control volume, F

V = specific volume of steam in the control volume, ft^3/lbm

PSTM = partial pressure of steam in the control volumes, psia

HH2 = specific enthalpy of hydrogen in the control volume, BTU/lbm

HH = total enthalpy of the steam-hydrogen mixture in the control volume, BTU

H2M = mass of hydrogen in the control volume, lbm

STMM = mass of steam in the control volume, lbm.

The method uses initial guesses of steam temperature, pressure, and enthalpy to calculate new values of each. This interactive process continues until values are found to satisfy the three equations. Once solutions to the simultaneous equations have been found, a heat balance between the gas and each structure within the control volume is performed. The heat transferred from the steam-hydrogen mixture exiting the top of the core to each control volume through an internally calculated heat transfer coefficient.

In determining the heat transfer coefficient between the gas and structure, the Reynolds Number is first calculated and depending on whether the flow is in the laminar or turbulent regime, the coefficient is calculated as:(A-4)

Laminar

$$h_c = \frac{k_m}{d} Nu_d \quad , BTU/hr/ft^2/F \qquad (A.5)$$

Turbulent

$$h_c = 0.0144\ Cpm\ \frac{G^{0.8}}{d^{0.2}} \quad , BTU/hr/ft^2/F \qquad (A.6)$$

where

k_m = thermal conductivity of the gas mixture, $BTU/hr/ft^2/F$

$$Nu_d = 3.66 + \frac{0.0688(d/L)Re_dPr}{1 + 0.04\ (d/L)RedPr\ 2/3}$$

d = hydraulic diameter, ft

C_{pm} = specific heat of the gas mixture, BTU/lb/F

G = mass velocity, $lb/hr/ft^2$.

A natural convection coefficient is also calculated depending on the Rayleigh Number regime:(A-4)

for X 10^9

$$h_c = 0.59 \frac{k}{L} X^{0.25} \quad , BTU/hr/ft^2/F \tag{A.7}$$

for X 10^9

$$h_c = 0.10 \frac{k}{L} X^{0.33} \quad , BTU/hr/ft^2/F \tag{A.8}$$

where

k_m = thermal conductivity of the gas mixture, $BTU/hr/ft^2/F$

L = length, ft

X = Rayleigh Number.

The larger of the natural and forced convection coefficients is used in the analysis.

Since the average structure temperature rather than the surface temperature is used in calculating the heat flux, a conduction term is used to modify the heat transfer coefficient. In addition a radiative term is added to the resulting coefficient based upon the analysis of radiation to steam provided in the MARCH code.

$$h_c^* = \frac{2k/\Delta x(h_c + hrad)}{h_c + hrad + 2k/\Delta x}$$

where

k = thermal conductivity of the structure

Δx = thickness of structure with one insulated boundary

hrad = radiation contribution.

The first control volume above the core also receives radiation heat transfer from the top of the core. The inlet gas temperature for this

volume is the gas temperature exiting the top of the core. For other volumes, the inlet temperature is the gas temperature at the outlet of the previous volume.

A flow diagram showing the calculations in subroutine EXITQ is given in Figure A.2. It should also be noted that for a control volume with an inlet gas-wall temperature difference of three degrees C or less, the calculations are skipped. Thus, the outlet gas and wall temperatures of the control volume remain unchanged and outlet flow rate is equated to inlet flow rate.

Subroutine ALTER. Subroutine ALTER saves control volume thermal-hydraulic data as a function of timestep index N. It also serves to redefine output parameters for total mass flow rates less than 10^{-10} lb/sec. For any timestep index if the flow meets this criterion: (1) total, hydrogen, and steam mass flow rates are set to zero, and (2) control volume inlet, outlet, and wall temperatures remain unchanged.

Subroutine STASH. Subroutine STASH stores MERGE output data required by TRAP-MELT in a flow parameter matrix for each volume. In addition, it sums input flow rates and averages temperatures for control volumes with more than one source.

Subroutine AVERAGE. Subroutine AVERAGE is a numerical averaging routine used to reduce MERGE input data from the MARCH code. It gives a sequence of up to 20 values at preselected event timestep indexes of all MARCH parameters required for the heat transfer analysis. These interval values are stored on MERGE output file TAPE5.

Subroutine ENDS. Subroutine ENDS stores the MERGE input data from the MARCH code at the first and final timestep indexes.

Subroutine REDUCE. Subroutine REDUCE uses a numerical averaging routine to reduce the flow parameter matrices created in subroutine STASH into a form acceptable for input to the TRAP-MELT code. It uses the

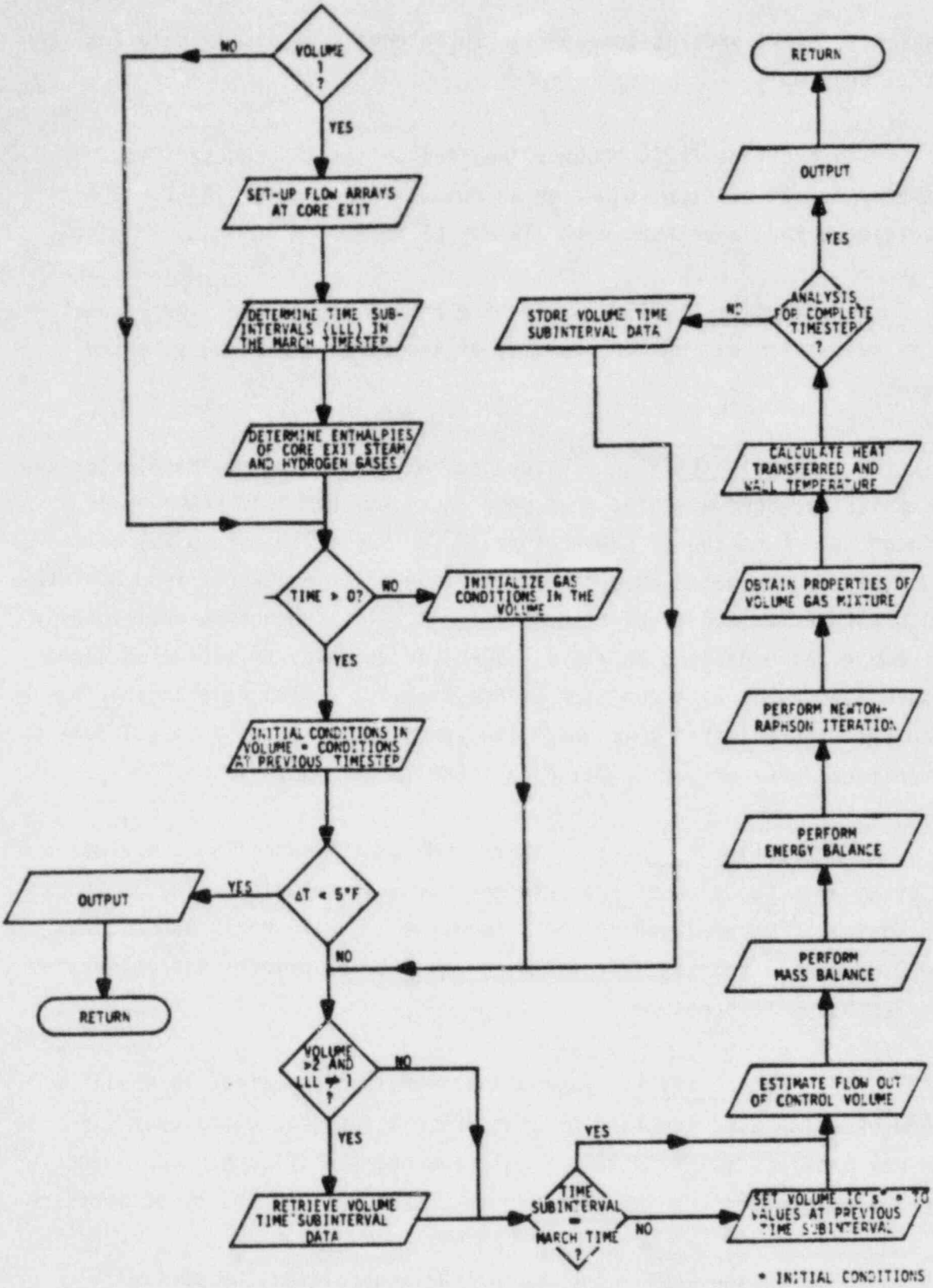

FIGURE A.2. FLOW CHART OF SUBROUTINE EXITQ

preselected event indexes to generate 20 intervals of matrix data for each control volume.

Subroutine TAPE. Subroutine TAPE writes the reduced flow parameter matrix of each volume on an output file labeled TAPE2. The file is cataloged for later use in the TRAP-MELT code.

Subroutine ENDPTS. Subroutine ENDPTS stores the flow parameter matrix values for all control volumes at the first and final timestep indexes.

Subroutine ENTHAL. Subroutine ENTHAL uses an empirical equation to express hydrogen specific heat; and thus, the specific enthalpy of hydrogen as a function of temperature.(A-5) The relationship may be adequately approximated throughout the range of temperatures from 80 F to 5840 F with a maximum error of 0.60 percent. The subroutine additionally uses empirical equations to express specific enthalpy of saturated liquid or saturated vapor as a function of pressure.(A-6) The relationship may be adequately approximated throughout the range of pressures from 1.1 psia to the critical pressure of 3208.2 psia (PCRIT).

Subroutine TEMP. Subroutine TEMP approximates the temperature of the steam as a function of pressure and specific enthalpy. The empirical relationship(A-2) employed in the subroutine is valid for pressure less than 3208.2 psia and specific enthalpy equal to or greater than saturated vapor enthalpy at pressure.

Subroutine SPVOL. Subroutine SPVOL approximates the specific volume of steam as a function of pressure and specific enthalpy.(A-3) The critical pressure value is 3208.2 psia and the specific enthalpy boundary is enthalpy greater than or equal to saturated vapor enthalpy at pressure.

Subroutine PART. Subroutine PART calculates the partial derivatives of temperature and specific volume with respect to both steam

pressure and enthalpy for use in the Newton-Raphson iterative calculations. The subroutine differentiates the empirical relationships previously established for temperature and specific volume.

Subroutine SUBTIME. Subroutine SUBTIME stores time subinterval MERGE control volume source parameters for later use as inputs to the receiver volumes at corresponding time intervals.

Subroutine HRSTM. Subroutine HRSTM calculates steam emissivity by using the product of steam partial pressure and control volume hydraulic diameter in conjunction with a plot of gas emissivity versus gas temperature given in McAdam's Figure 4.15.[A-7] The resulting emissivity is used to calculate a radiant heat transfer coefficient between the control volume and wall surface.

Subroutine PROP. Subroutine PROP is a routine written and supplied by Sandia to evaluate hydrogen and water properties.[A-8] The routine is specifically used in the MERGE code to obtain hydrogen and steam specific heats, conductivities, and viscosities for use in the gas-to-structures heat transfer analysis.

Subroutine INTERP. Subroutine INTERP is a routine also written and supplied by Sandia. It is used in conjunction with subroutine PROP and performs required properties interpolation.

References

(A-1) Stark, P. A., Introduction to Numerical Methods, MacMillan Publishing Company, Inc., 1970.

(A-2) McFadden, J. H., et al, "RETRAN-02--A Program for Transient Thermal-Hydraulic Analysis of Complex Fluid Flow Systems Volume 1: Equations and Numerics", EPRI NP-1850, Equation III.1-12, p. III-7, May 1981.

(A-3) McFadden, J. H., et al, "RETRAN-02--A Program for Transient Thermal-Hydraulic Analysis of Complex Fluid Flow Systems Volume 1: Equations and Numerics", EPRI NP-1850, Equation III.1-16, p. III-8, May 1981.

(A-4) Holman, J. P., Heat Transfer, Third Edition, McGraw-Hill Book Company.

(A-5) Van Wylen, G. J., and Sonntag, R. E., Fundamentals of Classical Thermodynamics, Second Edition, John Wiley and Sons, Inc., New York, 1973.

(A-6) McFadden, J. H., et al, "RETRAN-02--A Program for Transient Thermal-Hydraulic Analysis of Complex Fluid Flow Systems Volume 1: Equations and Numerics", EPRI NP-1850, Equations III.1-4 through III.1-9, pp. III-3, -4, May 1981.

(A-7) McAdams, W. H., Heat Transmission, Third Edition, McGraw-Hill Book Company, New York, 1954.

(A-8) Sandia National Laboratories, Private Communication from Eric Haskin, 1982.

APPENDIX B

CORSOR SENSITIVITY

APPENDIX B

CORSOR SENSITIVITY

To better assess the sensitivity of the CORSOR code predictions of release rates of the various species from the core region, a simple parametric study was performed in which certain assumptions and uncertainties contained in the code and its input data were examined.

First among these is the temperature at which the fuel rod cladding is predicted to burst. It is recognized that a distribution of burst temperatures will better characterize actual rods under severe accident conditions, but for use in CORSOR, a single temperature is used as the criterion to determine when any portion of a fuel rod will burst. For the analyses in this study, 900 C was taken to be the temperature at which fuel rods will burst, in accordance with the average burst temperature cited in the "Technical Bases Report". Figures B-1 and B-2 indicate the core release as a function of time for cladding burst temperatures of 750 C, 900 C, and 1100 C. The lack of sensitivity of the system to this parameter's value is apparent in these figures.

The maximum allowable temperature in the core is another parameter built into the CORSOR code. Temperatures, as calculated by the MARCH code, at some of the core nodes can exceed 3316 C (6000 F). An upper limit for the temperatures is set at 2760 C (5000 F) or the approximate melting point of uranium dioxide. Figures B-3 through B-5 depict the core release as a function of time using this maximum temperature and two other cases, 2260 C (4100 F) and 3038 C (5500 F). The case utilizing 2260 C (4100 F) was chosen since it is a value that approximates the UO_2-ZrO_2 eutectic point. Highly volatile species demonstrate an insensitivity to this parameter, whereas the release of the less volatile nonfission product aerosol is much more sensitive.

Figures B-6 through B-8 demonstrate the sensitivity of the release rate calculations to the core temperatures as predicted by the MARCH code. The release rates are extremely sensitive to temperature, as would be

expected since the fraction released is an exponential function of the temperature. The different releases apparent in these figures is caused by only a ±25 percent variation in the predicted core temperatures (C). In Figures B-9 through B-11, instead of adjusting the temperature, the computed release rate was adjusted up or down by one order of magnitude. Once again the results are anticipated and the variation is somewhat greater than when the temperature was adjusted by only ±25 percent. Clearly, the release rate of the areosol material from the core is quite sensitive to uncertainties in release rate data and in the high temperature values reached in the core.

Figures B-12 and B-13 provide a concise summary of the sensitivity of cladding rupture temperature, maximum allowable core temperature, and precision of temperature and release coefficients to the release of cesium from the core. Cesium was used here since it is representative of the intermediate volatility species, and because its release is believed to be better understood than the collection of substances comprising the aerosol. It is quite evident that the most sensitive factors here are the precision of the numbers which make up the release rate calculation and that fuel rod burst temperature and maximum core temperatures are not very sensitive parameters for the release of cesium. This is because the gap release represents such a small portion of the total release, and because the cesium inventory is released from a fuel rod considerably before the maximum temperatures are approached.

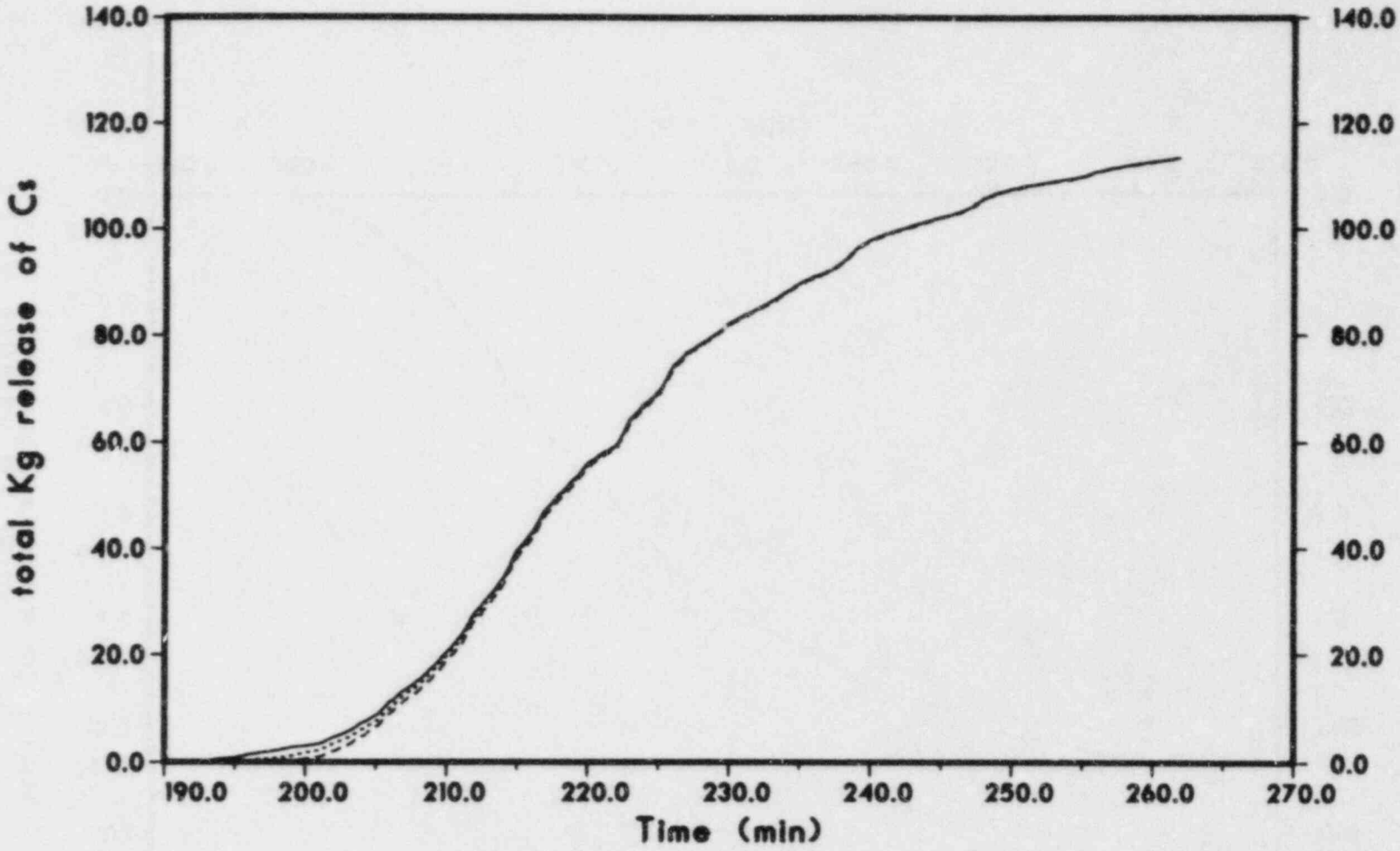

FIGURE B.1. CORSOR PREDICTIONS OF Cs RELEASE FROM CORE DURING TMLB' SEQUENCE FOR CLADDING BURST TEMPERATURES OF 750 °C (——), 900 °C (...) AND 1100 °C (---)

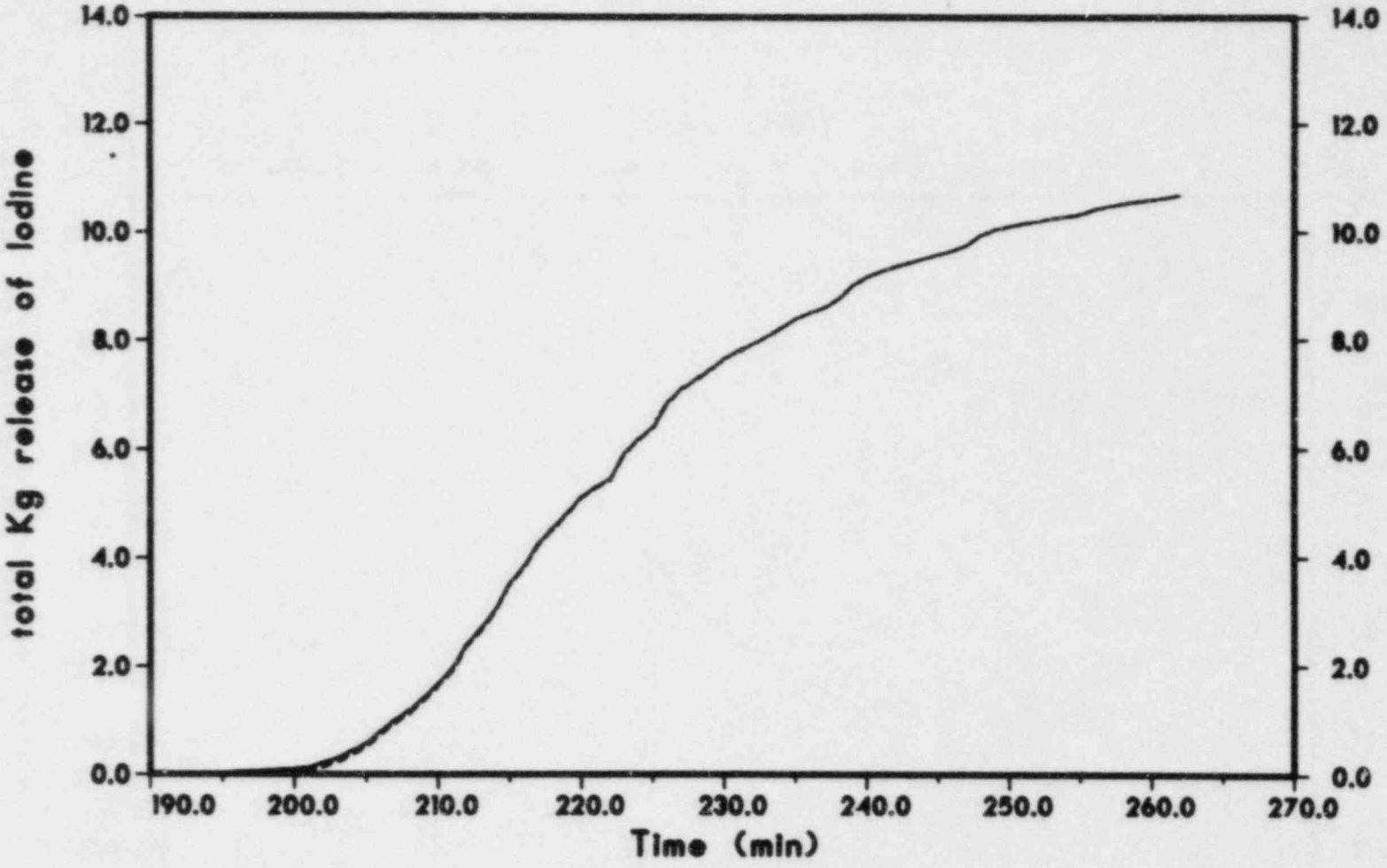

FIGURE B.2. CORSOR PREDICTIONS OF I RELEASE FROM CORE DURING TMLB' SEQUENCE FOR CLADDING BURST TEMPERATURES OF 750 °C (——), 900 °C (...) AND 1100 °C (---)

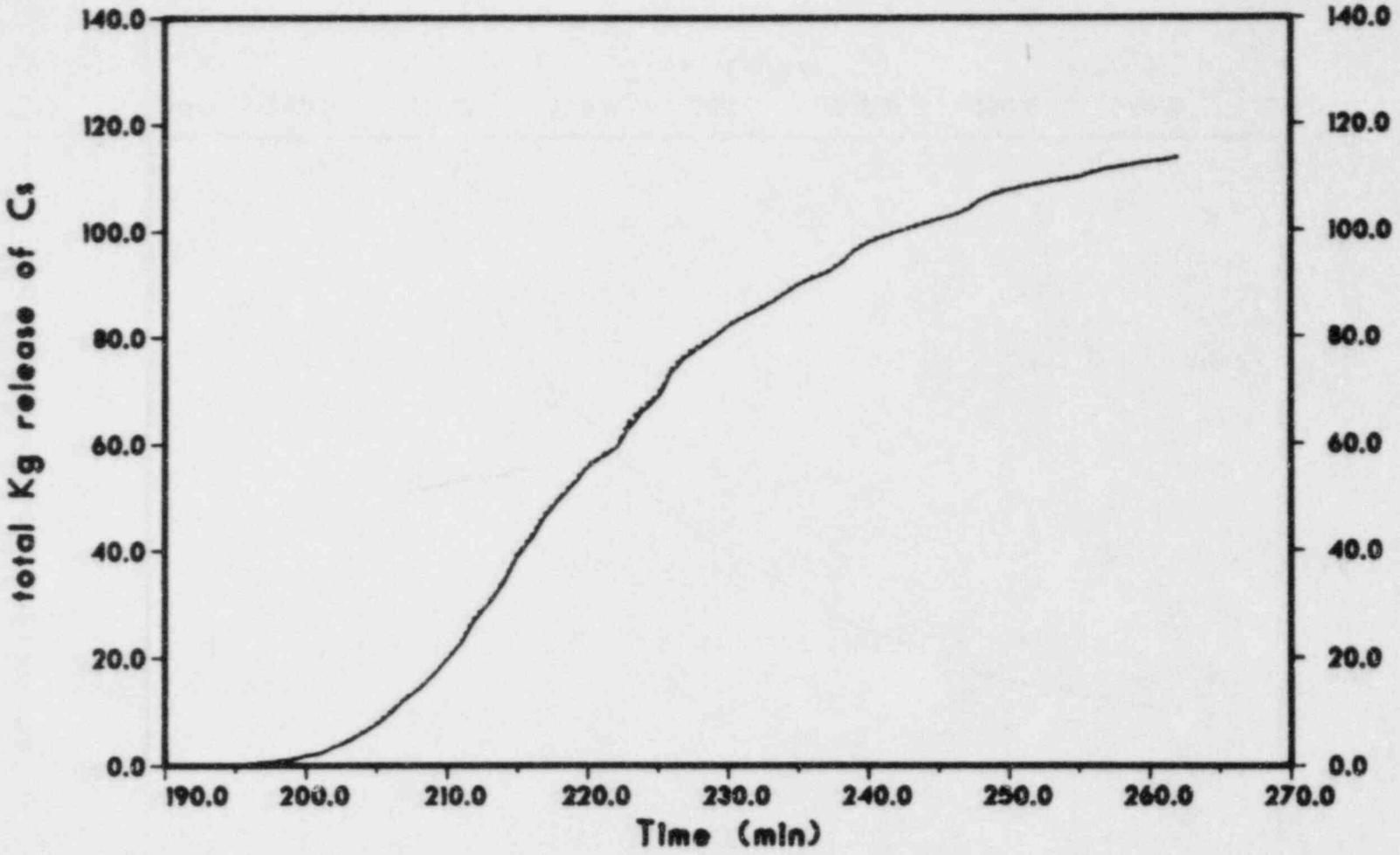

FIGURE B.3. CORSOR PREDICTIONS OF Cs RELEASE FROM CORE DURING TMLB' SEQUENCE FOR MAXIMUM TEMPERATURES OF 2260 °C (——), 2760 °C (...) AND 3038 °C (---)

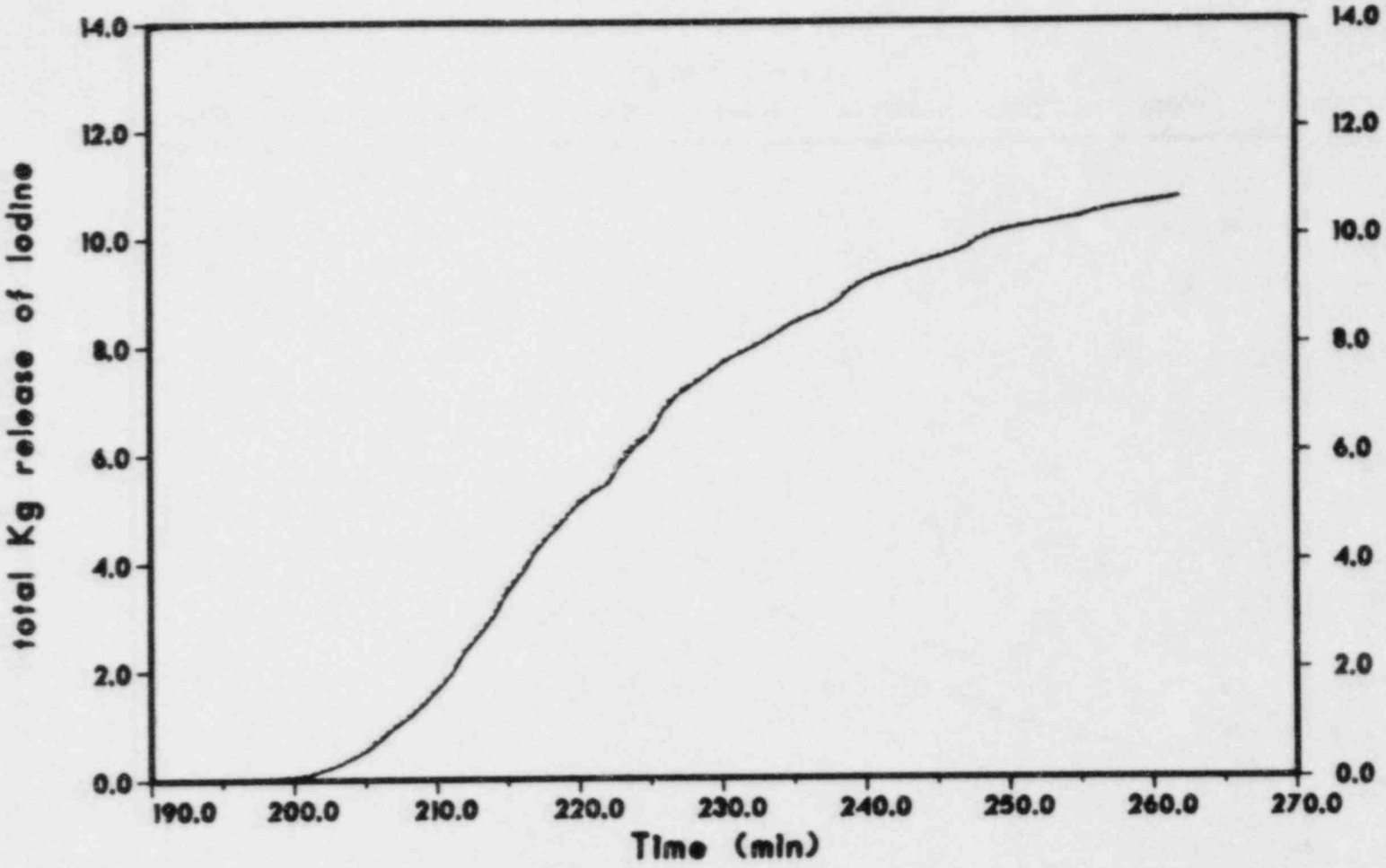

FIGURE B.4. CORSOR PREDICTIONS OF I RELEASE FROM CORE DURING TMLB' SEQUENCE FOR MAXIMUM TEMPERATURES OF 2260 °C (——), 2760 °C (...) AND 3038 °C (---)

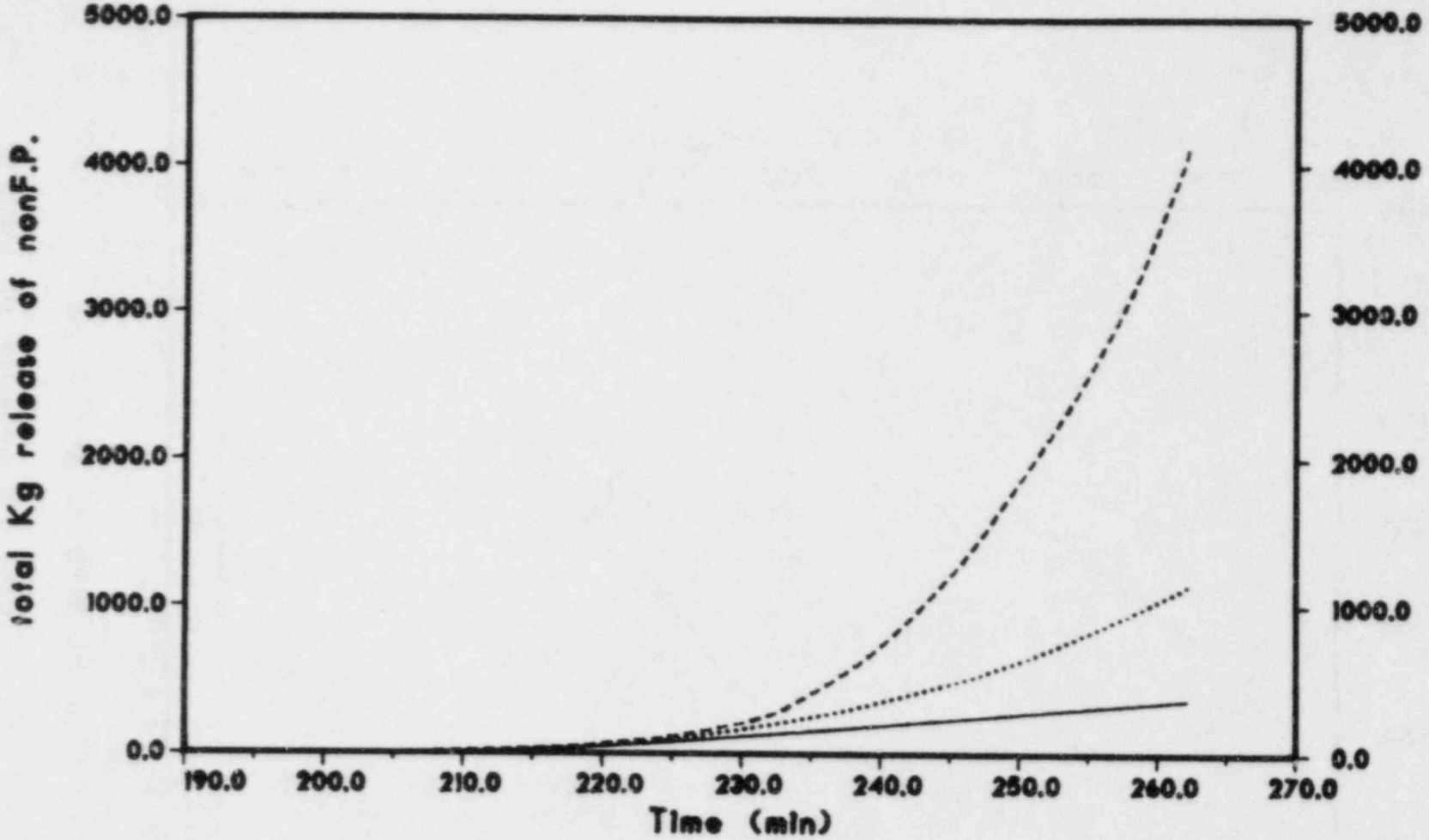

FIGURE B.5. CORSOR PREDICTIONS OF NONFISSION PRODUCT AEROSOL RELEASE FROM CORE DURING TMLB' SEQUENCE FOR MAXIMUM TEMPERATURES OF 2260 °C (——), 2760 °C (...) AND 3038 °C (---)

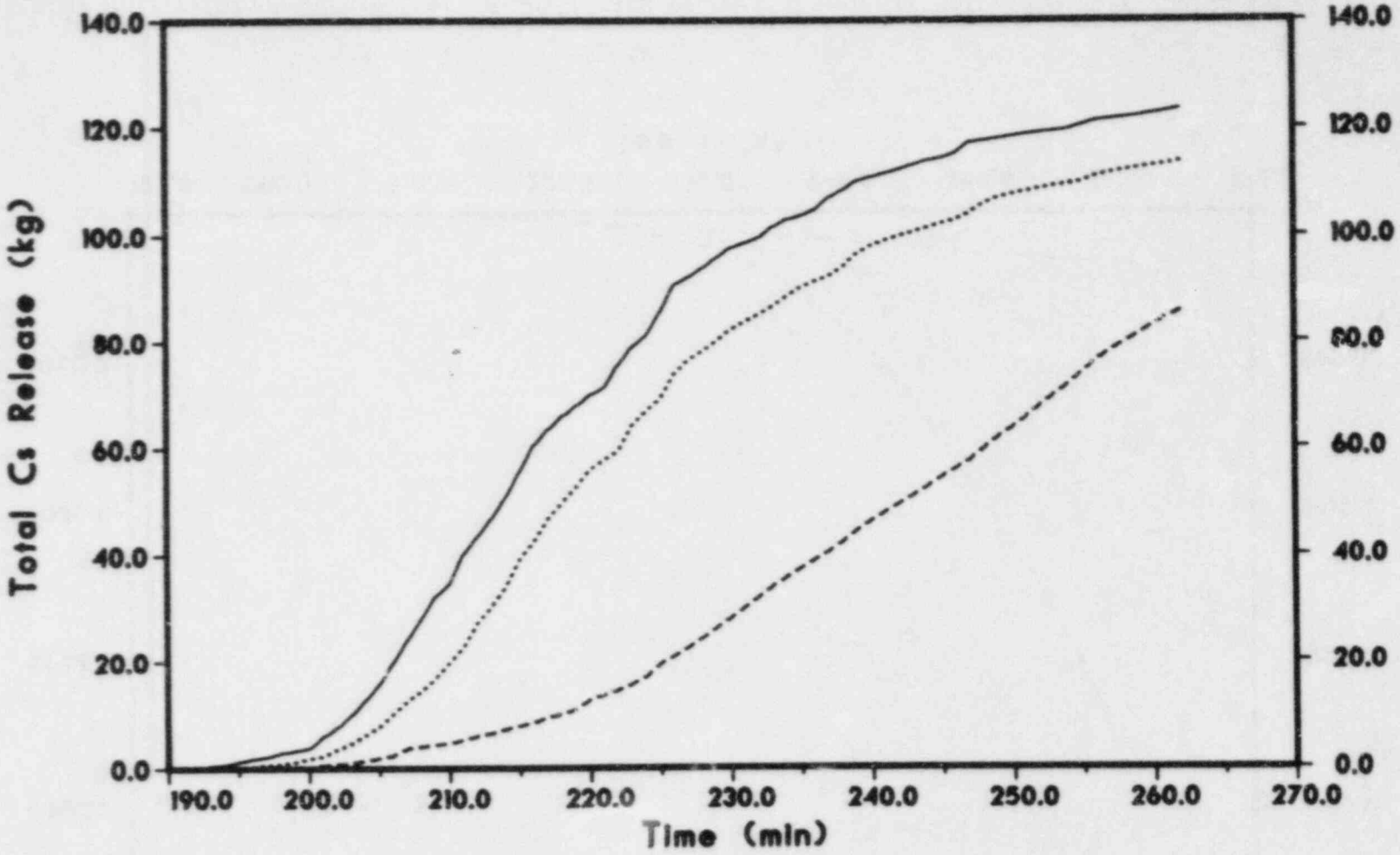

FIGURE B.6. CORSOR PREDICTIONS OF Cs RELEASE FROM THE CORE DURING TMLB' SEQUENCE FOR CALCULATED MARCH TEMPERATURES (...), CALCULATED TEMPERATURES +25% (——) AND TEMPERATURES -25% (---)

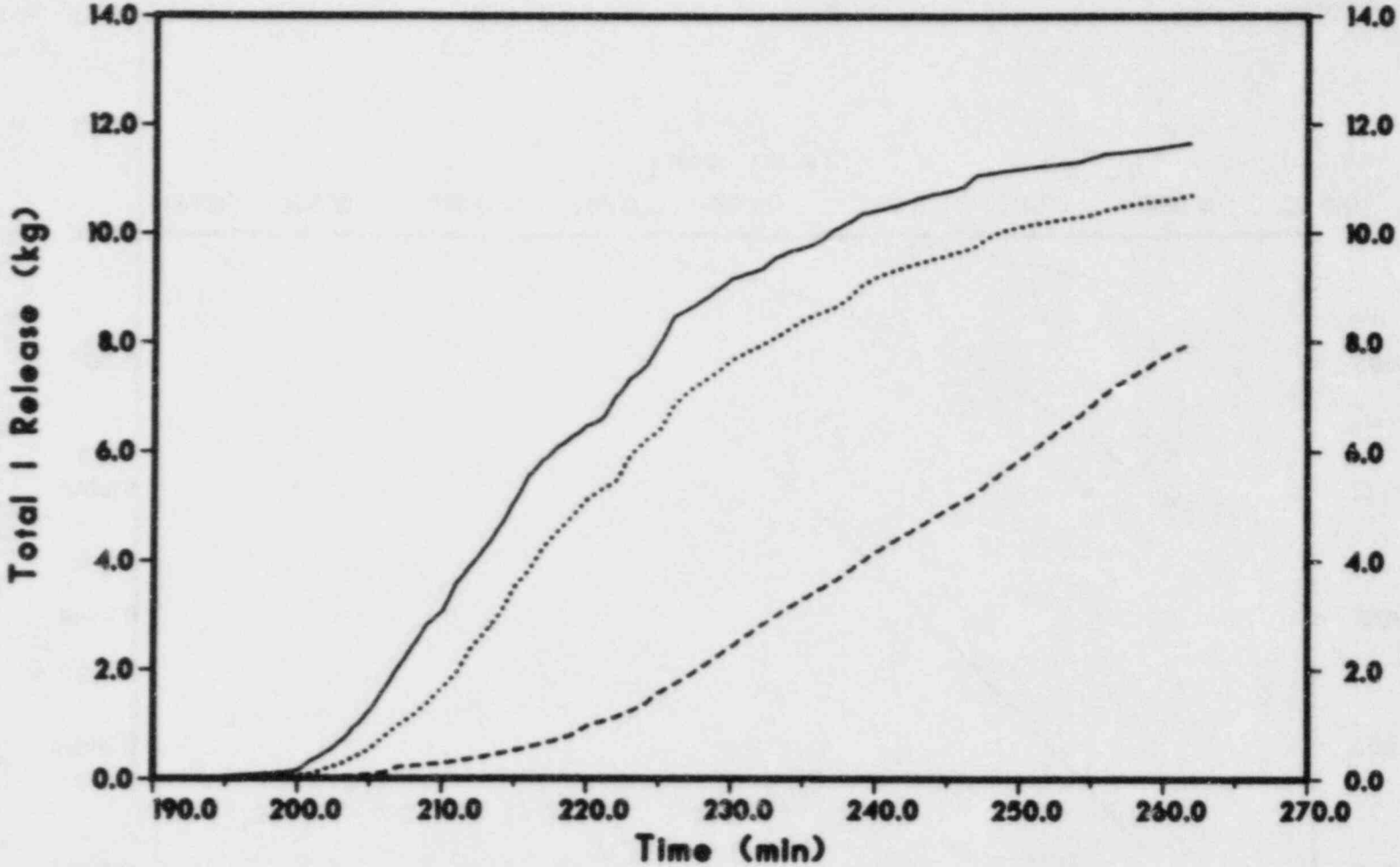

FIGURE B.7. CORSOR PREDICTIONS OF I RELEASE FROM THE CORE DURING TMLB' SEQUENCE FOR CALCULATED MARCH TEMPERATURES (...), CALCULATED TEMPERATURES +25% (——) AND TEMPERATURES -25% (---)

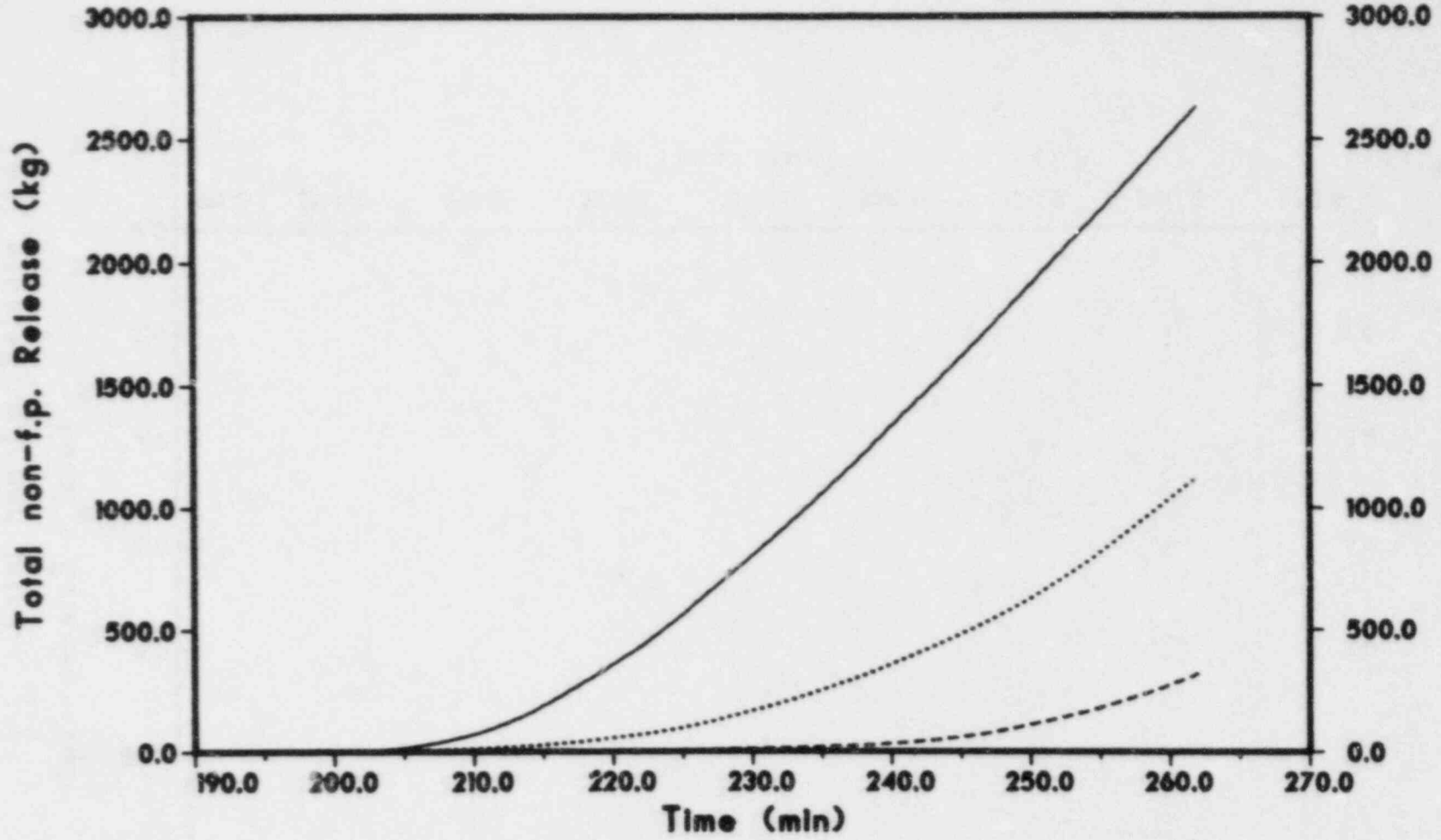

FIGURE B.8. CORSOR PREDICTIONS OF NONFISSION PRODUCT AEROSOL RELEASE FROM THE CORE DURING TMLB' SEQUENCE FOR CALCULATED MARCH TEMPERATURES (...), CALCULATED TEMPERATURES +25% (——) AND TEMPERATURES -25% (---)

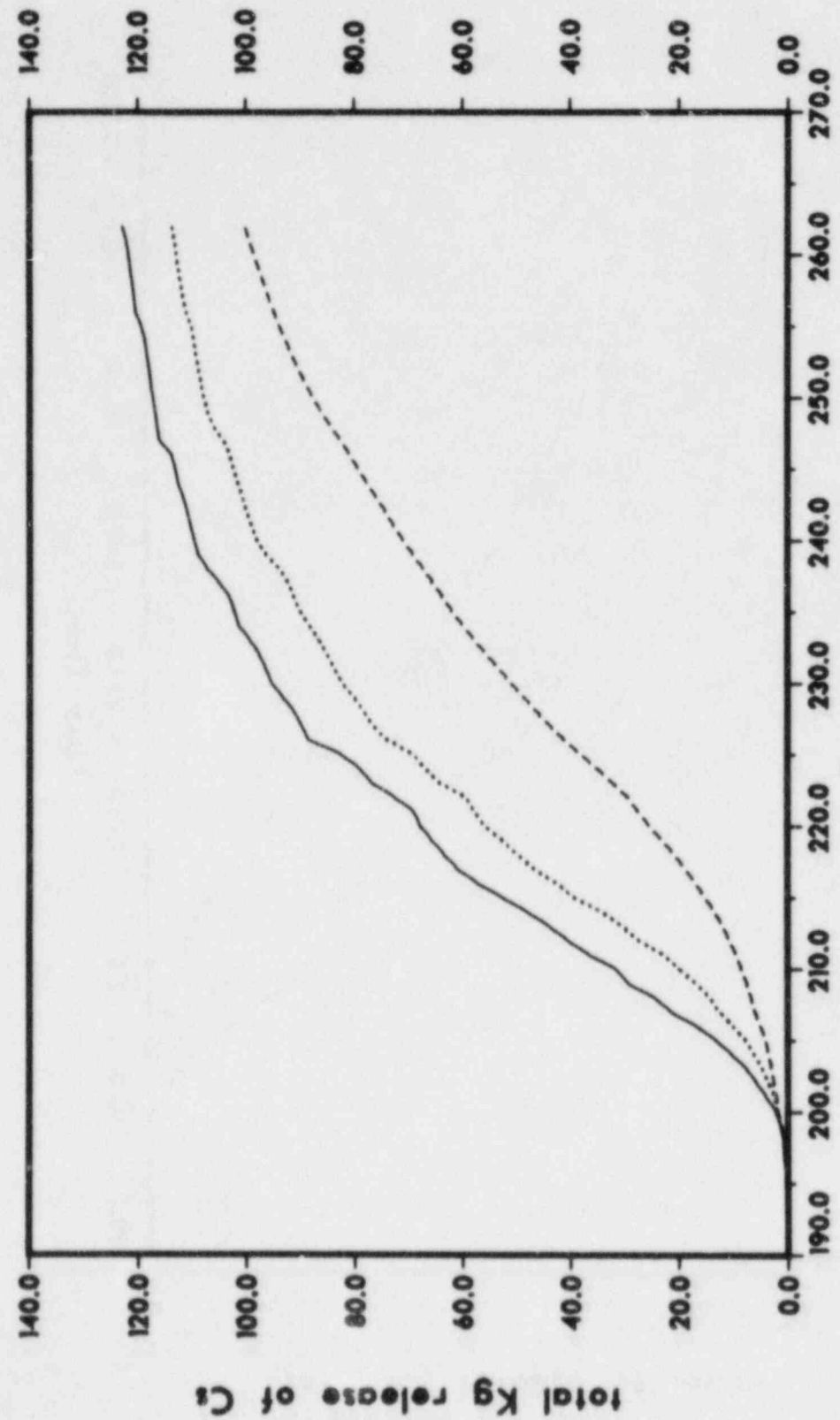

FIGURE B.9. CORSOR PREDICTIONS OF Cs RELEASE FROM THE CORE DURING TMLB' SEQUENCE FOR RELEASE RATE DETERMINED FROM EQUATION RATE = AeBT (...), 0.1xA (---) AND 10.xA (——)

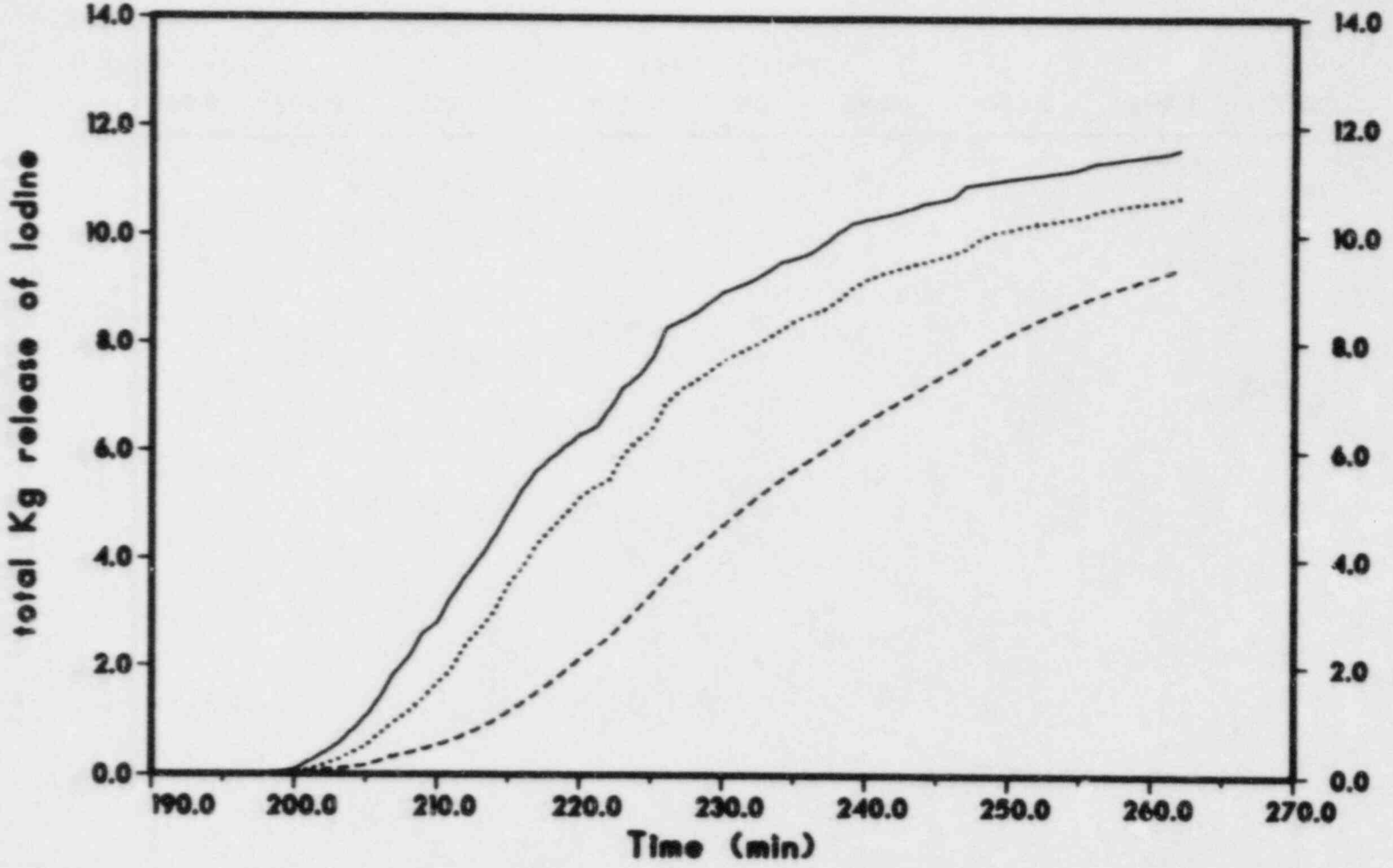

FIGURE B.10. CORSOR PREDICTIONS OF I RELEASE FROM THE CORE DURING TMLB' SEQUENCE FOR RELEASE RATE DETERMINED FROM EQUATION RATE = Ae^{BT} (...), 0.1xA (---) AND 10.xA (——)

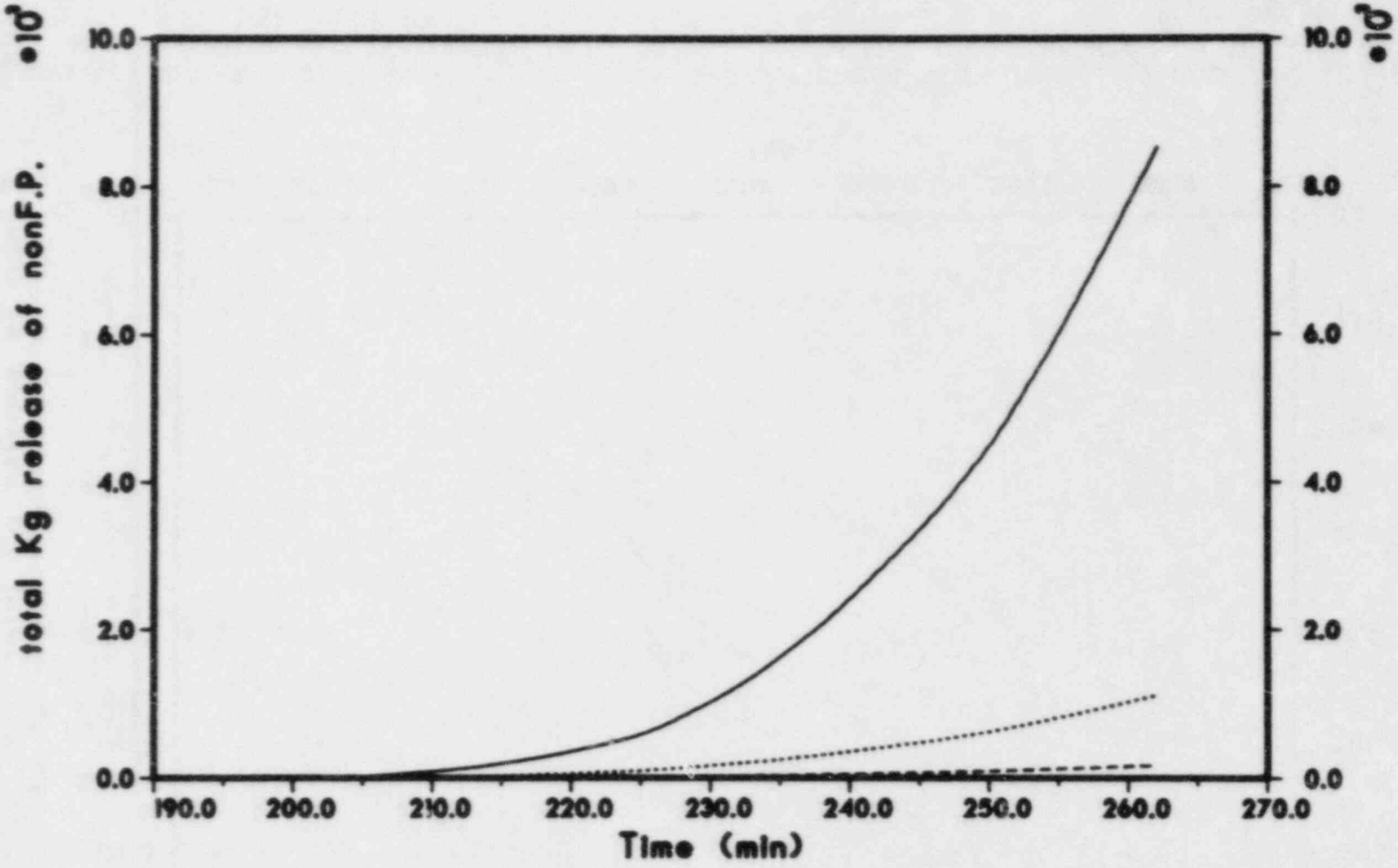

FIGURE B.11. CORSOR PREDICTIONS OF NONFISSION PRODUCT AEROSOL RELEASE FROM THE CORE DURING TLMB' SEQUENCE FOR RELEASE RATE DETERMINED FROM EQUATION RATE = Ae^{BT} (...), 0.1xA (---) AND 10.xA (——)

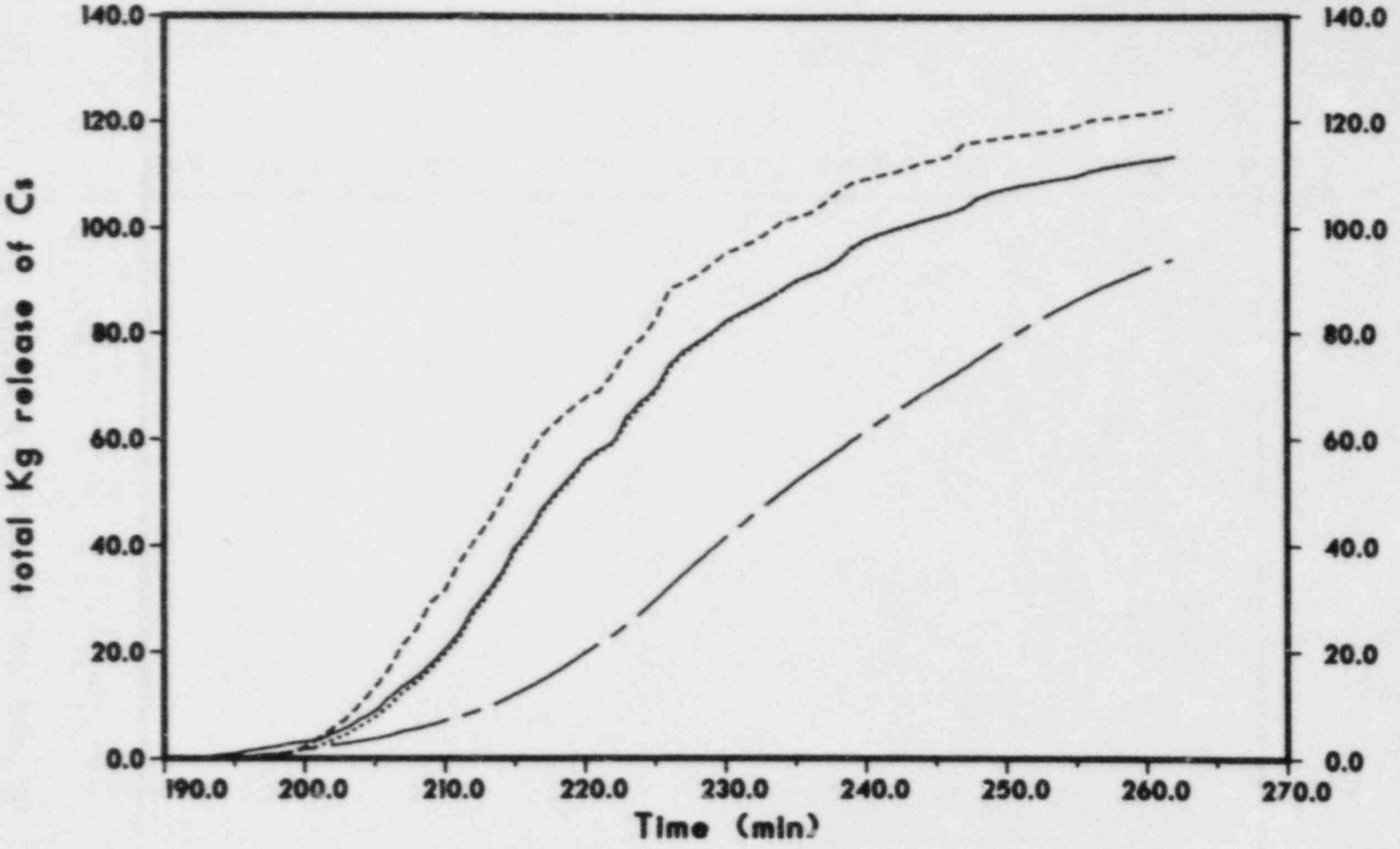

FIGURE B.12. CORSOR PREDICTIONS OF Cs RELEASE FROM THE CORE DURING TMLB' SEQUENCE FOR BASE CASE (...) CLADDING BURST TEMPERATURE OF 750 °C (——), CALCULATED MARCH TEMPERATURES -25% (— – —) AND RELEASE RATE INCREASED BY FACTOR OF TEN (---)

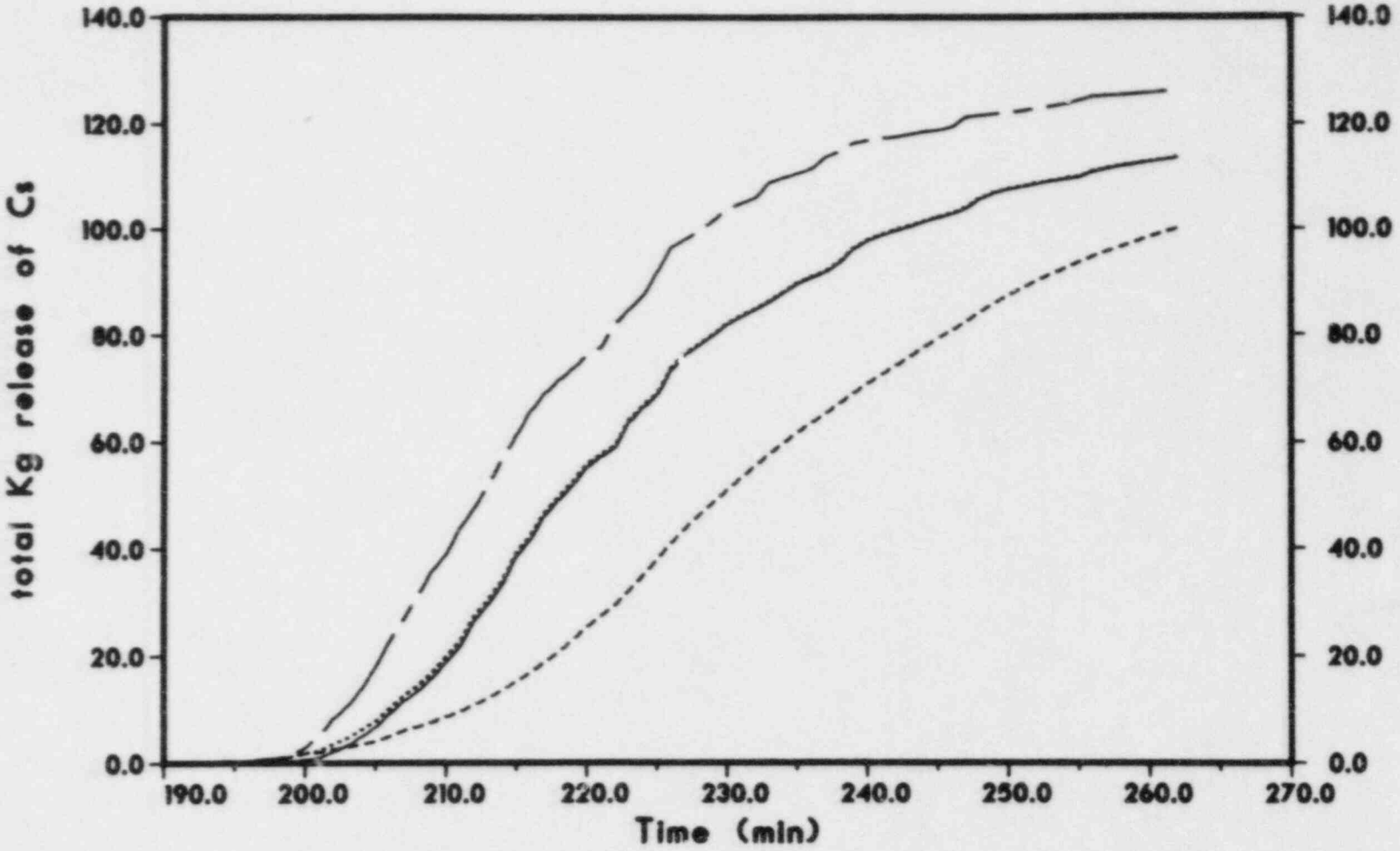

FIGURE B.13. CORSOR PREDICTIONS OF Cs RELEASE FROM THE CORE DURING TMLB' SEQUENCE FOR BASE CASE (...), CLADDING BURST TEMPERATURE OF 1100 °C (——), CALCULATED MARCH TEMPERATURES +25% (— – —) AND RELEASE RATE DECREASED BY FACTOR OF TEN (---)

APPENDIX C

RELEASE OF FISSION PRODUCTS AND GENERATION OF AEROSOLS OUTSIDE THE PRIMARY SYSTEM

Dana Powers
John Brockmann

Sandia National Laboratory

APPENDIX C

RELEASE OF FISSION PRODUCTS AND GENERATION OF AEROSOLS OUTSIDE THE PRIMARY SYSTEM

Progression of a severe reactor accident will eventually lead to the point where the molten core debris penetrates the primary vessel and falls into the reactor cavity. The interactions of molten core debris with structural concretes are known to produce copious amounts of aerosol and release of fission products.[1] Figure 1 is a photograph of an experiment in which about 200 Kg of furnace-prepared melt at 1700 C was poured into a concrete crucible. This photograph shows how dramatic aerosol generation during melt/concrete interactions can be. Much of the discussion of ex-vessel aerosol generation in this appendix is based on experiments such as the one shown in this figure.

The experimental data base on aerosol production and fission product release during core debris interactions with concrete is not as extensive as that for other phases of a severe reactor accident. The data that are available have been used in the past to formulate empirical models of the fission product release in a severe accident. For this work a more mechanistic model was formulated from the available data and data for analogous situations in the process metallurgy industry. A detailed description of this model is to be found in Reference 3. The major features of the model as well as some of the more important predictions and sensitivities of the model are described here.

A). MECHANISMS OF AEROSOL GENERATION DURING MELT/CONCRETE INTERACTIONS

Experimental investigations of melts interacting with concrete have shown that the concrete is aggressively attacked.[4] A most important aspect of this attack is that hydrates and carbonates within the concrete are thermally decomposed to produce steam and carbon dioxide. The experimental studies have conclusively demonstrated that these gaseous products

of concrete decomposition sparge up freely through the melt[4,5] rather than circulate around the perimeter of the melt as hypothesized in some analyses of core debris interactions with concrete.[6] As the gases pass through the melt there is significant generation of aerosols. These aerosols typically have mean sizes of about 1 μm with a geometric standard deviation of about 2. The aerosols are composed of chemical species from the concrete, the main constituents of the melt, and any fission products doped into the melts.

Somewhat analogous situations of high temperature melts being sparged with reactive gases arise in the process metallurgy industry[7,8] and in arc welding.[9] Aerosol generation also occurs in these situations. Aerosol generation during the "carbon boil" phase of oxygen steelmaking is particularly well-known.

Studies of the metallurgical processes and indications from the experimental investigations of high temperature melts interacting with concrete suggest there are two main mechanisms of aerosol generation:

(1) Vaporization: Because of their relatively high vapor pressures, species in the melt evaporate into the gas stream. When the gas stream cools these vapors condense to form aerosols.

(2) Mechanical: Violent agitation of the melt by sparging gases leads to formation of particulate melt in the gas stream.

Vaporization of species from the melts can be enhanced because the gases sparging through the melt are quite reactive. The importance of oxidation to yield volatile species has been recognized in previous analyses as a mechanism of fission product release. It was not recognized that this chemical enhancement of vaporization would occur during core debris interactions with concrete until it was determined gaseous products of concrete decomposition pass freely through the melt. More subtle than simple oxidation to yield volatile oxides of fission products is the fact that water vapor can react with fission products to yield volatile hydroxides.[10]

Mechanical generation of aerosols occurs by two means. The first develops when melts first contact concrete and there is a period of exceptionally violent gas generation. During this period droplets of melt are

thrown up into the gas. Inertial forces cause the particles to disintegrate until they become small enough that surface tension stops the breakup. Evidence with simulant fluids has shown this disintegration process continues until a critical Weber number is reached:[11]

$$We(critical) = \frac{\rho V^2 d}{\sigma} = 12$$

ρ = density of the melt

V = relative velocity between gas and melt droplet

d = diameter of the particle

σ = surface tension of the melt.

This mechanical process seldom yields particles with mean sizes less than about 50 μm.

The second mechanism of mechanical aerosol generation is associated with the bursting of bubbles at the surface of the melt. As the bubble breaks, the melt film over the bubble is thrown off in the form of the fine particles. For isolated air bubbles in aqueous sodium chloride solutions the mean particle size of aerosols formed by this process lies between 0.5 and 10 μm (12). Though it is generally recognized this process of aerosol formation occurs during many metallurgical processes, the aerosol products have only been poorly characterized.

The composition of aerosol produced by vaporization depends on the vapor pressure and chemical reactivity of the constituents of the melt. Consequently, the aerosol composition need not be similar to the melt composition. The composition of aerosols produced by mechanical processes is very nearly the same as that of the melt.

FORMATION OF THE MODEL

Several computer models exist that describe melt temperature, concrete erosion, and gas generation during core debris interactions with concrete. One of these, the CORCON code,[13] was used as the basis of the model. Output from this code used in the analyses described below is listed in Table 1. These input data included mean melt temperature, molar gas

generation rates, and the rate at which condensed products of concrete decomposition were incorporated into the melt.

Gases bubbling through the melt were assumed to be one cm ellipsoids based on evidence from melt/concrete interaction tests monitored by X-rays[5] and bubbles frozen in solidified melts following melt/concrete interactions.[4] The bursting of bubbles at the melt surface was assumed to be the sole source of mechanically generated aerosols. The size of these aerosol particles and the number of mechanically generated aerosol particles per bubble were taken to be the same as that observed in experiments with 0.55 cm air bubbles passing through aqueous sodium chloride solutions.[12] Evidence from the steel industry suggests a more vigorous aerosol generation should be attributed to bubble bursting. Studies of bubble-bursting during steelmaking have not adequately characterized aerosol production for the purposes of this model.

By far the greatest attention was paid in developing the model to the process of aerosol generation by vaporization. The diversity of chemical species that can form in the vapor state when reactive gases sparge through high temperature melts is better appreciated now than it was in previous analyses. About 200 vapor species were considered in this model. These species are listed in Table 2.

The equilibrium vapor pressures of these species are readily calculated by conventional thermochemical methods taking into account mass balance constraints. For this model, a Brinkley equilibrium constant technique was used.[14] Vapors were assumed to be ideal gases. The melts were assumed to be ideal so activity coefficients were all unity. As will be noted below, this assumption is the source of great uncertainty in the computed rates of vaporization from the melt.

In previous analyses of vaporization the computation of equilibrium vapor pressures was taken to be sufficient to compute vaporization rate. Had this been done in this model, much higher vaporization rates would have been computed because of the greater variety of chemical species recognized by the model. In reality, the melt never fully equilibrates with the gas phase. Consequently, the gases do not carry off as much material as would be estimated from equilibrium thermodynamics. To obtain more realistic

estimates of the rate of vaporization it is necessary to consider kinetic barriers to the approach to the thermodynamic limit to vaporization. The most significant technical development in this model of aerosol generation during core debris interactions with concrete is that it mechanistically accounts for the kinetic barriers to vaporization.

Specific barriers to vaporization recognized in the model are:

(1) Mass transport of species to the melt interface with gas.
(2) Kinetic limits to vaporization at the gas/melt interface.
(3) Mass transport in the gas phase once vaporization occurs.
(4) Residence time of bubbles in the melt.

A fifth barrier, that posed by the caloric cost of vaporization, was not included in the model. Aerosol generation never becomes intense enough to affect the melt temperature so this barrier does not arise.

Finally, the model crudely calculates the mean particle size of aerosols produced by condensation of vapors. This size is given by an empirical formula developed from experimental data taken during core debris/concrete interaction tests:

$$d = 0.2657 \left(\frac{A}{\rho}\right)^{1/3}$$

where

d = mass mean aerosol particle size in μm
ρ = mean density of the material that makes up the aerosol
A = concentration of the aerosol in the evolved gas (g/m^3)

ACCIDENT ANALYSES AND SENSITIVITIES OF THE MODEL

Five accident scenarios were analyzed with the model. These scenarios were assumed to differ, for the purpose of core debris/concrete interactions, only in the compositions of the melts. The melt compositions at the onset of core debris/concrete interaction are listed in Table 3. As the interaction progressed, the compositions of the melts were allowed to change as a result of:

(1) Oxidation of the metallic phase,

(2) Incorporation of the condensed products of concrete decomposition into the oxide phase, and

(3) Aerosol production.

Results of the accident analyses are collected in Tables 4-13. For each accident there are estimates of:

(1) Mass rate of aerosol generation

(2) Concentration of aerosol in the evolved gas

(3) Material density of the aerosol

(4) Mean particle size of the aerosol

(5) Chemical composition of the aerosol.

Some observations that can be made from the results of these accident analyses are:

(1) Initially the aerosol is predominantly made up of core debris constituents. Once concrete is incorporated in the melt, constituents of the concrete make up a large fraction of the aerosol. One consequence of this is the material density of the areosol changes very rapidly at the start of melt interactions with concrete but quickly achieves a nearly constant value of 2.5-3.0 g/cm^3.

(2) Aerosol production becomes similar for all accident sequences. Initial differences in melt composition are changed by the vaporization process so that after about 5 hours all the melts have very similar compositions. Once the melts are similar in composition the rate of aerosol production depends on the nature of the core debris interactions and becomes independent of the history of the accident except insofar as this history affects the interaction.

(3) The fission product release during core debris interactions with concrete can compensate for differences in the assumed release of fission products during the in-vessel phase of an accident. For instance, the AB and the AB-tellurium sequences differ only by the inventory of tellurium in the core debris when it contacts concrete (6 and 25 Kg, respectively). The inventory of tellurium in the melts for these two sequences is shown in Figure 2. The rate of tellurium release decreases with decreasing inventory. Consequently, after about 6 hours the amount of tellurium left in the melt is about the same for both the AB and AB-tellurium sequences.

(4) The concentration of aerosols in the gases evolved during melt/concrete interactions varies over a wide range (9 -1300 g/m^3). As expected, based on experimental data, the particle size of the aerosol increases with concentration. When mass input rates are high, particle sizes are large and there is a stronger tendency for these larger particles to settle out.

SENSITIVITIES OF THE MODEL

Work with this relatively new model has been quite limited. Sources of output sensitivity have been identified:

(1) Melt temperature

(2) Gas flow rate

(3) Melt chemistry.

The rate of aerosol mass generation at a fixed gas flow rate and varying melt temperatures is shown in Figure 3. The aerosol generation rate is exponentially dependent on melt temperature. Errors in estimates of melt temperature yield magnified errors in the estimated aerosol generation rates.

The effect of the flow rate of gases through the melt on the aerosol production rate is shown in Figure 4. Except for very large and very small flow rates, the aerosol production rates are lineraly dependent on gas flow rates. Errors in the estimates of gas generation during core debris interactions with concrete lead to proportional errors in the estimates of aerosol production.

The sensitivity to temperature and gas flow rate means that accurate predictions of core debris/concrete interactions are essential to accurate estimates of aerosol generation.

The composition of the aerosols is sensitive to the thermochemical description of the melt. For these calculations, activity coefficients of melt constituents were assumed to be unity. In reality, activity coefficients can be either greater or less than one. Consequently, the rate of vaporization of a melt constituent can be either greater or less than predicted. To a first approximation activity coefficients are given by

$$RT \ln \gamma = A (1-X)^2$$

where

R = gas constant

T = absolute temperature

γ = activity coefficient of the species in question

A = interaction constant peculiar to the species in question

X = mole fraction of the species in the melt.

By varying the interaction constant, A, the effects on vaporization of varying activity coefficients for a species in the melt can be seen. Results for vaporization of lanthanum assuming various values of the interaction coefficient are shown in Figure 5. Quite clearly, assumptions about the interaction coefficient can have serious effects on the extent of species release.

Comparison of model predictions to the limited data available on aerosol production during core debris/concrete interactions shows that the model predicts trends in release well;[3] that is, the assumption of unit activity coefficients is not radically wrong. This assumption leads to correct estimates of the qualitative volatility of species from the melt. Quantitative accuracy in the relative volatilities can be achieved only by having accurate estimates of the activity coefficient of species in real melts.

OTHER SOURCES OF AEROSOLS

Recently, small-scale tests have shown there is another source of ex-vessel aerosols that could arise in certain accident sequences. Recent probabilistic risk assessments have shown that core melts produced in accidents initiated by transient events can penetrate the reactor pressure vessel when the vessel is still pressurized.[15] Were this to happen, melt would be ejected into the reactor cavity at high velocity. This is quite a different situation than has been hypothesized in the past.

Recent tests have shown that when small-scale melts (10 Kg) are ejected from pressure vessels at pressures of 600 to 1500 psi tremendous

quantities of aerosol are yielded. Figure 6 is a series of photographs from one of these tests.

Aerosol sampling during these tests has shown the aerosols to be bimodal or perhaps trimodal with means at about 0.5, 5, and perhaps 60 μm. No measurements of the amount of melt aerosolized were made. The basis for scaling the test observations to real accident situations has been found. Consequently, it has not been possible to formulate models adequate to incorporate these potential phenomena into this work.

REFERENCES

(1) D. A. Powers, "Aerosol Generation During Melt/Concrete Interactions", 7th International Light Water Reactor Safety Information Meeting, Gaithersburg, MD.

(2) W. B. Murfin and D. A. Powers, "Interaction of the Melt with Concrete and MgO", Chapter 5 in Report of the Zion/Indian Point Study, Volume 1; W. B. Murfin, Ed., NUREG/CR-1410; SAND80-0617/1, Sandia National Laboratories, Albuquerque, NM, August, 1980.

(3) D. A. Powers and J. E. Brockmann, A Mechanistic Model of Aerosol Generation During Core Debris Interactions with Concrete, Sandia National Laboratories, Albuquerque, NM.

(4) D. A Powers and F. E. Arellano, NUREG/CR-2282; SAND81-1753, Sandia National Laboratories, Albuquerque, NM, January, 1982.

(5) D. A. Powers and F. E. Arellano, NUREG/CR-2283; SAND81-1754, Sandia National Laboratories, Albuquerque, January, 1982.

(6) Reactor Safety Study: An Assessment of Accident Risks in U.S. Commercial Nuclear Power Plants, Appendix VII, "Release of Radioactivity in Reactor Accidents", U.S. Nuclear Regulatory Commission WASH1400 PB-248 207, October, 1975.

(7) A. F. Ellis and J. Glover, J. Iron and Steel Institute, p. 593, August, 1971.

(8) J. Szekely and N. J. Thermelis, Rate Phenomena in Process Metallurgy, Wiley Interscience, 1971.

(9) V. Berner and A. Berner, The Annual Conference of the GAeF, 1981, p. 191.

(10) D. D. Jackson, UCRL-51137, Lawrence Livermore Laboratory, Livermore, California, December, 1971.

(11) M. Pilch, Advanced Reactor Safety Research Quarterly Report, NUREG/CR-2238, SAND82-0904 (1 of 4) January-March, 1982.

(12) M. Tomaides and K. T. Whitby, "Generation of Aerosols by Bursting of Single Bubbles", in Fine Particles: Aerosol Generation, Measurement, Sampling, and Analysis, B. Y. H. Liu, Ed., Academic Press, Inc., New York, New York.

(13) J. F. Muir, et al, SAND80-2415; NUREG/CR-2142, Sandia National Laboratories, Albuquerque, NM, July, 1981.

(14) S. R. Brinkley, J. Chem. Phys. 15 107 (1947).

(15) Zion Probabilistic Safety Study, Commonwealth Edison, 1982.

Figure 1

200 Kg of stainless steel at 1970K interacting with limestone concrete.

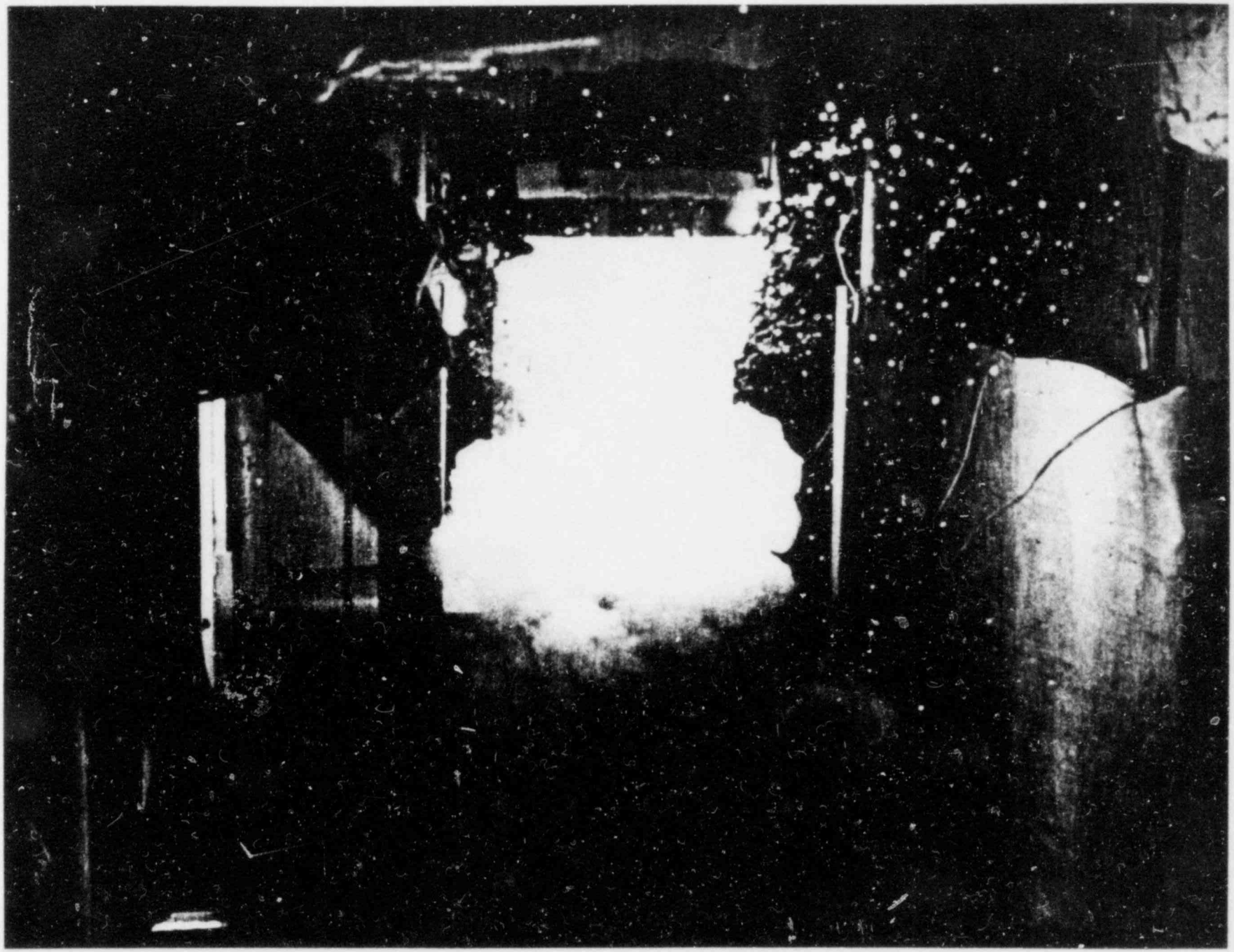

MELT EJECTION AT 600 PSIG

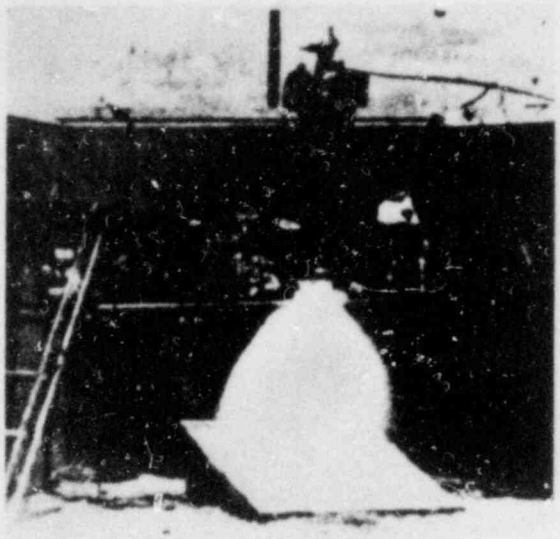

t = 0.05s
MELT EJECTION BEGINS

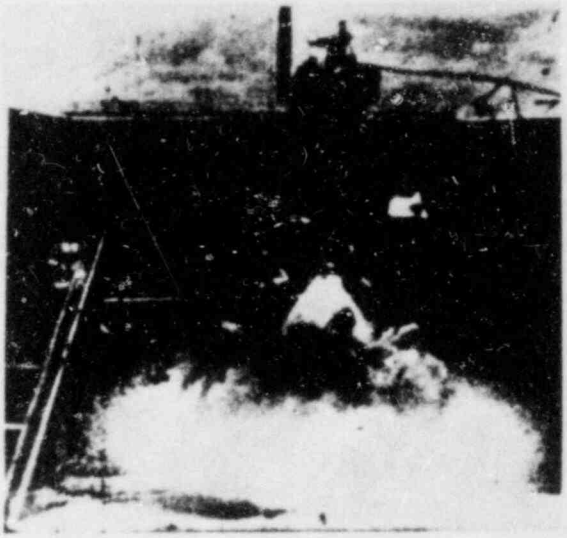

t = 0.1s
VAPOR CONDENSATION

t = 1.15s
MAXIMUM AEROSOL CLOUD

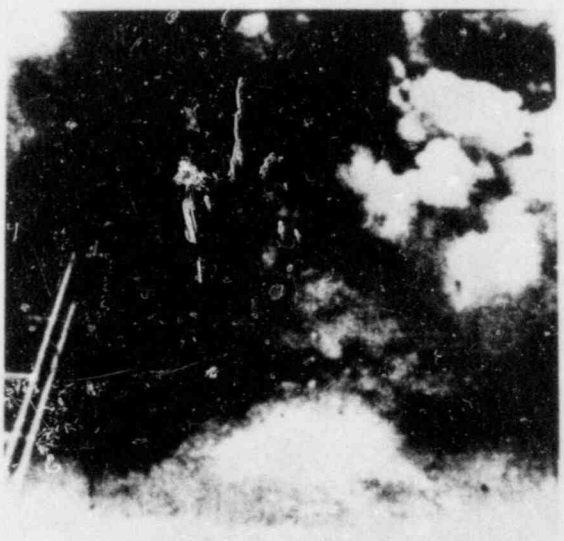

t = 1.95s
EJECTION COMPLETE

TABLE

Input Data on the Core Debris/Concrete Interaction

TIME (HRS)	AVERAGE MELT TEMP(K)	GAS GENERATION RATE (Moles/s)	CONCRETE ADDITION RATE (Kg/s)	TOP POOL SURFACE AREA (cm^2)
0	2550	183.4	5.74	306.8×10^3
1	2316	60.2	4.33	377.4×10^3
2	2419	15.65	2.09	385.6×10^3
3	2681	22.51	1.47	391.5×10^3
4	2859	158.7	3.75	399.8×10^3
5	2350	101.7	7.69	433.0×10^3
6	2042	72.5	7.80	475.3×10^3
7	1962	58.3	5.11	498.9×10^3

Concrete Melt Composition: CaO 16.4 w/o; FeO 6.8 w/o; SiO_2 59.8 w/o;
Na_2O 2.0 w/o; K_2O 5.9 w/o; Al_2O_3 9.1 w/o

Table ___ Initial Melt Compositions Continued

SPECIES	Amounts (Kg) AB	AB-Tellurium	TMLB'	S_2D	V
BaO	54.708	54.708	35.840	51.471	48.344
SrO	50.852	50.852	39.617	48.369	46.950
La_2O_3 (a)	149.062	149.062	149.062	149.062	149.062
CeO_2	219.624	219.624	219.624	219.624	219.624
Nb_2O_5	4.9706	4.9706	4.9706	4.9706	4.9706
CsI	2.252	2.252	0	4.320	0
Zr	0	0	0	0	0
FeO	0	0	0	0	0
Cr_2O_3	0	0	0	0	0

(a) $La_2O_3 + Y_2O_3$ from ORIGEN code

Table ___ Vapor Phase Species Continued

ELEMENT	VAPOR SPECIES
Zirconium	Zr; ZrO; ZrO_2; ZrOH; $Zr(OH)_2$
Cesium	Cs; CsOH; CsO; $Cs_2(OH)_2$; Cs_2O; Cs_2; CsI
Barium	Ba; BaO; BaOH; $Ba(OH)_2$
Strontium	Sr; SrO; SrOH; $Sr(OH)_2$
Lanthanum	La; LaO; LaOH; $La(OH)_2$
Cerium	Ce; CeO; CeOH; $Ce(OH)_2$
Niobium	Nb; NbO; NbO_2; NbOH; $Nb(OH)_2$
Iodine	CsI; HI; I_2; I

TABLE

Vapor Phase Species Recognized by the Model

ELEMENT	VAPOR SPECIES
Hydrogen	H_2; H_2O; H; OH; O; O_2; HI
Iron	Fe; FeO; FeOH; $Fe(OH)_2$
Chromium	Cr; CrO; CrO_2; CrO_3; H_2CrO_4
Nickel	Ni; NiOH; $Ni(OH)_2$
Molybdenum	Mo; MoO; MoO_2; MoO_3; H_2MoO_4 $(MoO_3)_2$; $(MoO_3)_3$
Ruthenium	Ru; RuO; RuO_2; RuO_3; RuO_4
Tin	Sn; SnO; SnOH; $Sn(OH)_2$; SnTe
Antimony	Sb; SbOH; $Sb(OH)_2$; Sb_2; Sb_4; SbTe
Tellurium	Te; TeO; TeO_2; Te_2O_2; $TeO(OH)_2$; Te_2; H_2Te; SnTe; SbTe; AgTe
Silver	Ag; AgOH; $Ag(OH)_2$; AgTe
Manganese	Mn; MnOH; $Mn(OH)_2$
Calcium	Ca; CaO; CaOH; $Ca(OH)_2$
Aluminum	Al; AlO; AlOH; Al_2O; AlO_2; Al_2O_2; $Al(OH)_2$; AlO(OH)
Sodium	Na: NaOH; NaO; $Na_2(OH)_2$; NaH; Na_2
Potassium	K; KOH; KO; $K_2(OH)_2$; KH; K_2
Silicon	Si; SiO; SiO_2; SiOH; $Si(OH)_2$
Uranium	U; UO; UO_2; UO_3; H_2UO_4

TABLE __

Input Initial Melt Composition

SPECIES	Amounts (Kg) AB	AB-Tellurium	TMLB'	S_2D	V
Fe	108748	108748	108563	108738	108714
Cr	16000	16000	16000	16000	16000
Ni	8910	8910	8910	8910	8910
Mo	144.4	144.4	126.4	144.3	140.5
Ru	103.1	103.1	101.3	102.9	102.7
Sn	119.0	119.0	33.9	99.8	68.1
Sb	0.617	0.617	0.391	0.567	0.480
Te	5.900	25.0	0.004	6.83	1.53
Ag	0.700	0.700	0.0004	0.820	0.180
Mn	0.100	0.100	0.100	0.100	0.100
CaO	0	0	0	0	0
Al_2C_3	0	0	0	0	0
Na_2O	0	0	0	0	0
K_2O	0	0	0	0	0
SiO_2	0	0	0	0	0
UO_2	79471	79471	78844	79261	79224
ZrO_2	22475	22475	22468	22475	22474
Cs_2O	14.681	14.681	0	24.798	2.704

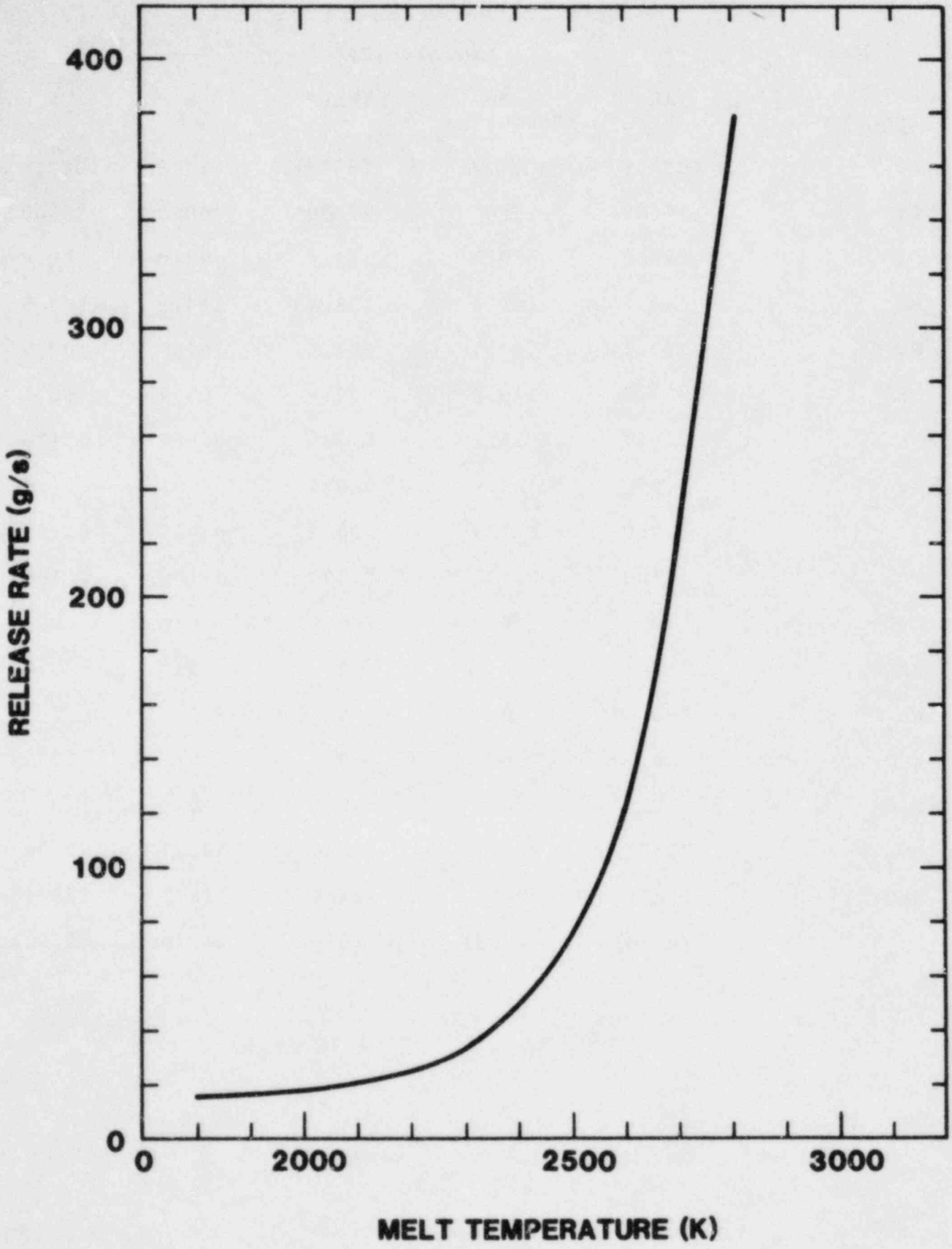
400
300
200
100
0
RELEASE RATE (g/s)
0
2000
2500
3000
MELT TEMPERATURE (K)

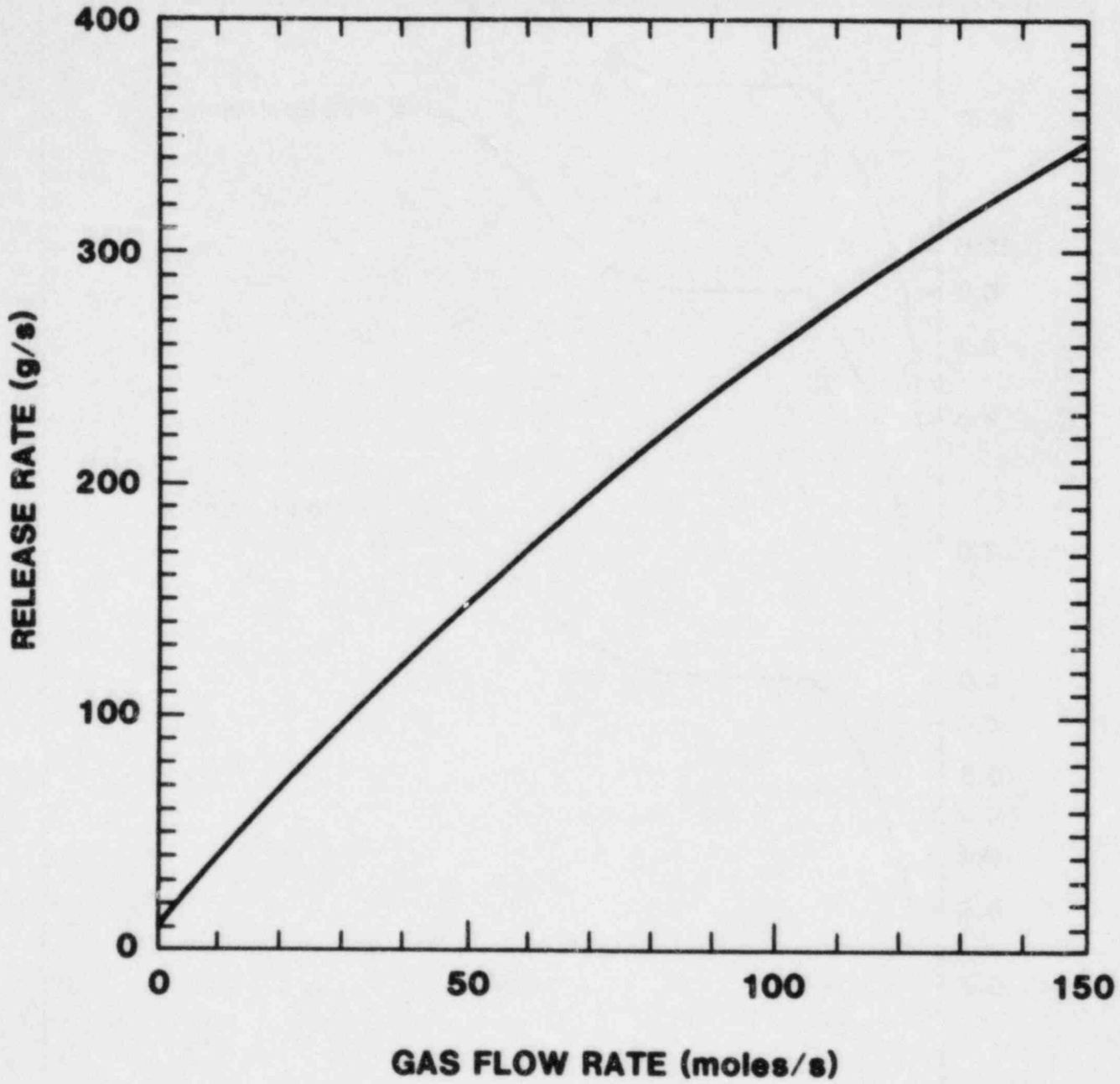
400
300
200
100
0
RELEASE RATE (g/s)
0
50
100
150
GAS FLOW RATE (moles/s)

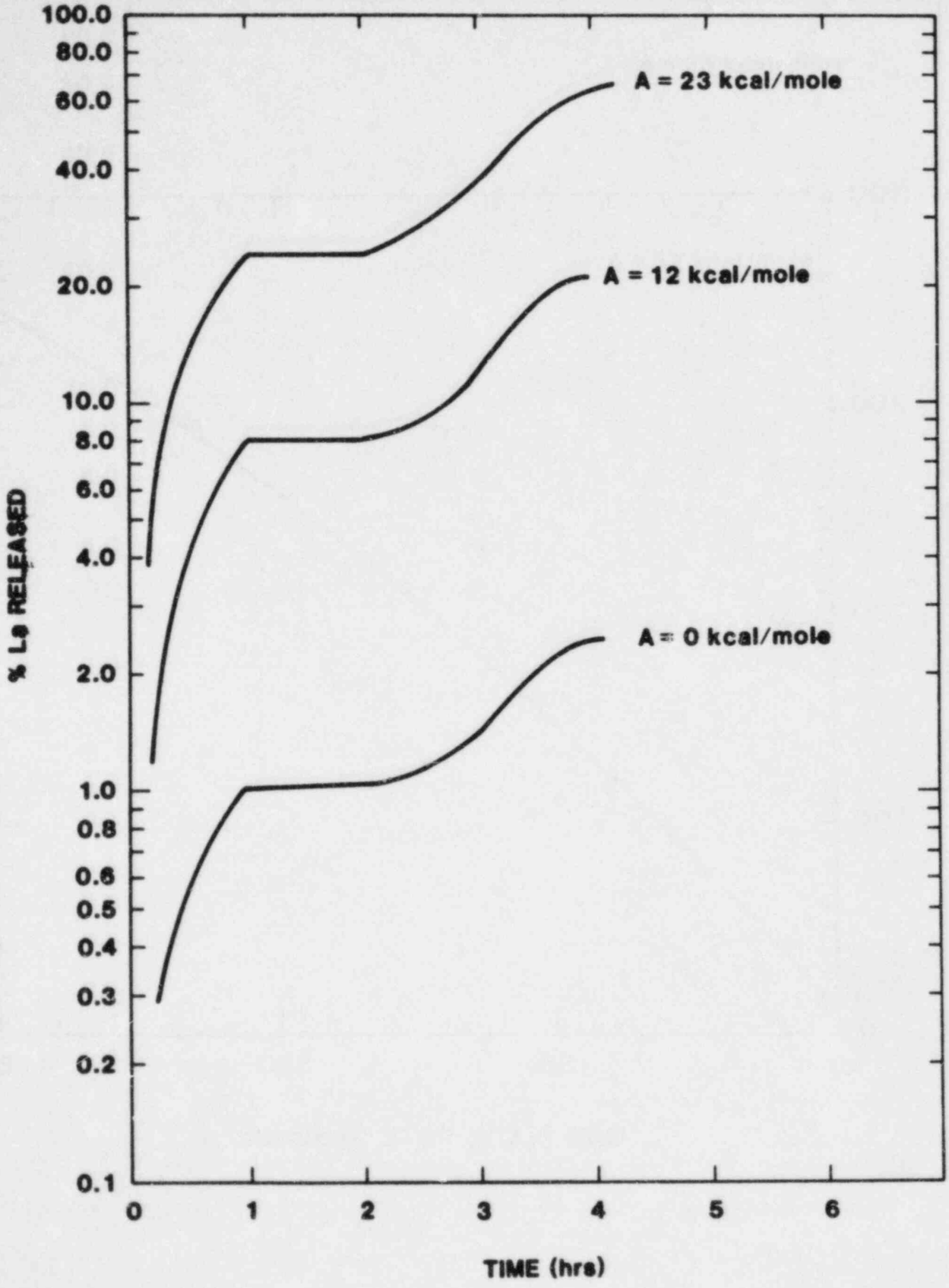
100.0
80.0
60.0
40.0
20.0
10.0
8.0
6.0
4.0
2.0
1.0
0.8
0.6
0.5
0.4
0.3
0.2
0.1
% Lø RELEASED
A = 23 kcal/mole
A = 12 kcal/mole
A = 0 kcal/mole
0
1
2
3
4
5
6
TIME (hrs)

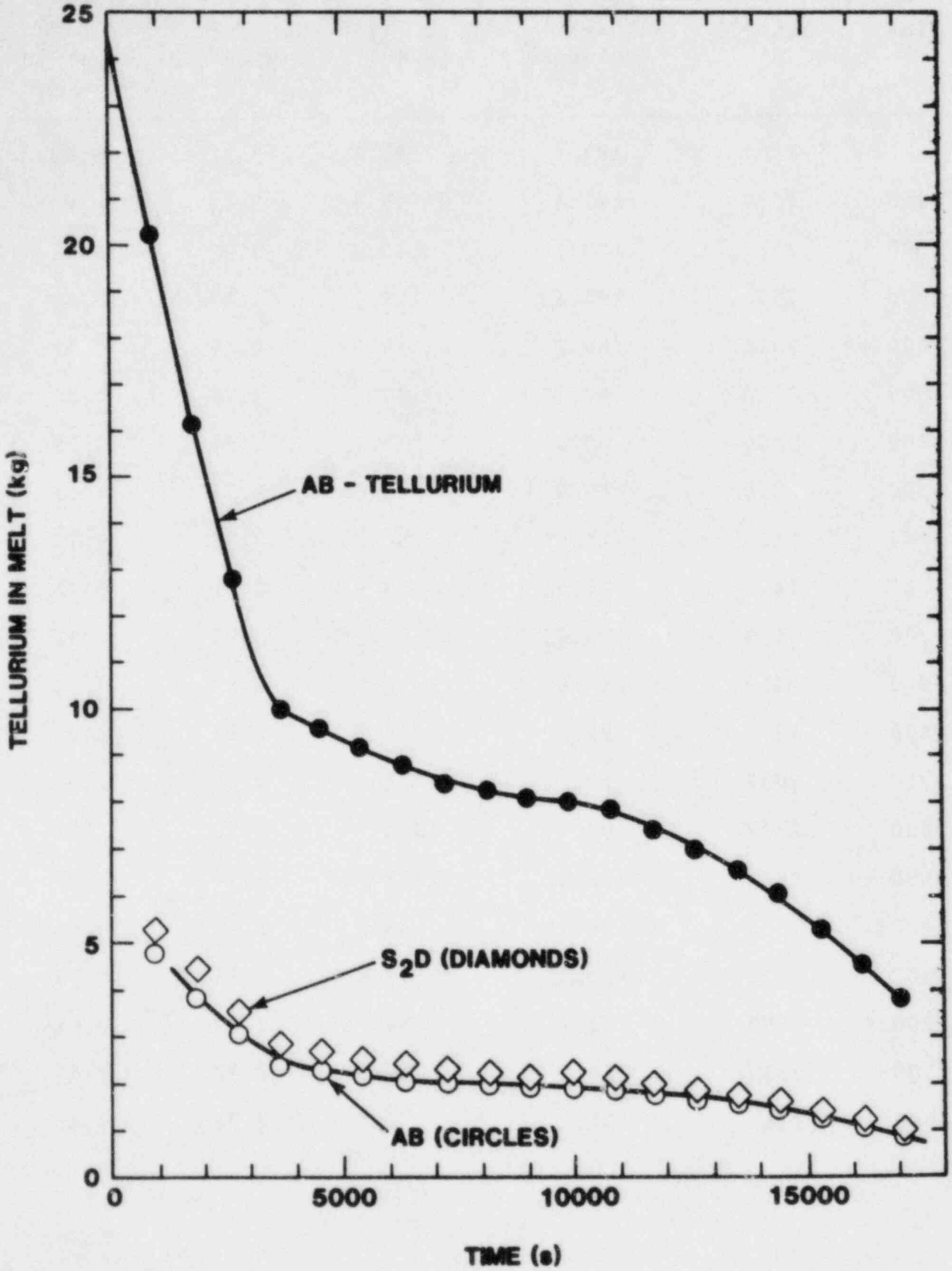
25
20
15
10
5
0
0
5000
10000
15000
TELLURIUM IN MELT (kg)
TIME (s)
AB - TELLURIUM
S_2D (DIAMONDS)
AB (CIRCLES)

RESULTS AB SEQUENCE

Time (s)	Temp[a] (K)	Gas[b] (moles/s)	[A][c] (g/m^3)	ρ[d] (g/cm^3)	μ[e] (μm)
0	2550	183.4	91.1	5.21	0.68
900	2550	183.4	99.3	3.44	0.88
1800	2550	183.4	120.4	3.22	0.88
2700	2550	183.4	128.	3.17	0.90
3600	2316	60.2	19.2	2.78	0.58
4500	2316	60.2	29.5	2.76	0.58
5400	2316	60.2	29.6	2.74	0.58
6300	2316	60.2	29.6	2.74	0.58
7200	2419	15.65	56.0	2.93	0.70
8100	2419	15.65	56.0	2.91	0.71
9000	2419	15.65	56.5	2.90	0.71
9900	2419	15.65	56.9	2.89	0.71
10800	2859	22.51	1325	2.81	2.05
11700	2859	22.51	1345	2.80	2.06
12600	2859	22.51	1364	2.78	2.08
13500	2859	22.51	1382	2.77	2.09
14400	2350	158.7	38.5	2.70	0.64
15300	2350	158.7	37.9	2.71	0.64
16200	2350	158.7	38.1	2.72	0.64
17100	2350	158.7	38.3	2.73	0.64
18000	2042	101.7	9.7	2.22	0.43

RESULTS AB SEQUENCE - Concentration in Aerosol (%)

Species	Time (s) 0	900	3600	7200	10800	14400	18000
FeO	0.012	8.47	13.33	13.06	8.98	11.91	4.94
Cr_2O_3	0.024	5.69	2.23	2.29	4.12	1.43	0.105
Ni	5.08	4.85	2.90	3.86	3.29	3.27	0.800
Mo	0.002	0.002	0.002	0.006	0.007	0.005	0.004
Ru	$1x10^{-5}$	$1x10^{-5}$	$2x10^{-6}$	$5x10^{-6}$	$3x10^{-5}$	$3x10^{-6}$	$1x10^{-7}$
Sn	1.77	1.71	1.68	2.16	0.706	1.78	1.103
Sb	$1x10^{-4}$	$1x10^{-4}$	$1x10^{-4}$	$1x10^{-4}$	$3x10^{-5}$	$1x10^{-4}$	$1.5x10^{-4}$
Te	0.310	0.240	0.257	0.160	0.018	0.147	0.153
Ag	0.022	0.019	0.015	0.014	0.004	0.011	0.006
Mn	0.005	0.004	0.003	0.002	$5x10^{-4}$	0.002	0.001
CaO	0	0.583	1.22	1.57	0.617	1.913	1.26
Al_2O_3	0	0.011	0.021	0.016	0.013	0.027	0.104
Na_2O	0	2.35	5.38	3.98	0.550	5.164	6.29
K_2O	0	13.2	39.64	26.32	2.25	37.82	79.14

RESULTS AB SEQUENCE - Aerosol Composition (%)

Species	Time(s) 0	900	3600	7200	10800	14400	18000
SiO_2	0	35.5	21.23	33.10	71.36	27.14	2.66
UO_2	35.03	26.79	11.59	13.16	7.95	9.12	3.00
ZrO_2	0.169	0.125	0.252	0.108	0.068	0.118	0.303
Cs_2O	4.04	0	0	0	0	0	0
B_2O	0.352	0.248	0.199	0.131	0.026	0.115	0.119
SrO	0.058	0.041	0.027	0.019	0.004	0.016	0.011
La_2O_3	0.133	0.102	0.001	0.022	0.080	0.001	0.002
CeO_2	0.006	0.004	0.003	0.001	0.001	0.001	0.003
Nb_2O_5	0.023	0.019	0.004	0.007	0.017	0.004	$6x10^{-5}$
CsI	52.96	0	0	0	0	0	0

RESULTS FOR AB TELLURIUM

Time (s)	Temp (K)	Gas (moles/s)	[A] (g/m^3)	ρ (g/cm^3)	μ (μm)	[A] (g/s)
0	2550	183.4	92.1	5.213	0.69	413
900	2550	183.4	100	3.455	0.82	449
1800	2550	183.4	121	3.230	0.89	543
2700	2550	183.4	129	3.174	0.91	578
3600	2316	60.2	29.4	2.797	0.58	43.4
4500	2316	60.2	29.8	2.770	0.59	43.8
5400	2316	60.2	29.8	2.75	0.59	43.9
6300	2316	60.2	29.8	2.75	0.59	43.9
7200	2419	15.65	55.9	2.93	0.71	21.4
8100	2419	15.65	56.3	2.92	0.71	21.6
9000	2419	15.65	56.8	2.91	0.72	21.7
9900	2419	15.65	57.2	2.89	0.72	21.9
10800	2859	22.5	1325	2.82	2.07	730
11700	2859	22.5	1346	2.80	2.08	741
12600	2859	22.5	1365	2.78	2.10	751
13500	2859	22.5	1383	2.77	2.11	761
14400	2350	158.7	38.7	2.70	0.64	150
15300	2350	158.7	38.1	2.72	0.64	148
16200	2350	158.7	38.3	2.73	0.64	148
17100	2350	158.7	38.4	2.74	0.64	149
18000	2042	101.7	9.7	2.23	0.43	24.2

AEROSOL COMPOSITION RESULTS FOR AB TELLURIUM

Species	Time (s) 0	900	3600	7200	10800	14400	18000
FeO	0.012		13.22	12.99	8.97	11.86	4.91
Cr_2O_3	0.023		2.21	2.28	4.12	1.43	0.105
Ni	5.03		2.88	3.84	3.29	3.25	0.796
Mo	0.002		0.002	0.006	0.007	0.005	0.004
Ru	$1x10^{-5}$		$2x10^{-6}$	$5x10^{-6}$	$3x10^{-5}$	$3x10^{-6}$	$1x10^{-7}$
Sn	1.801		1.70	2.16	0.704	1.78	1.11
Sb	$1.5x10^{-4}$		$1.7x10^{-4}$	$1.5x10^{-4}$	$3x10^{-5}$	$2x10^{-4}$	$2x10^{-4}$
Te	1.308		1.077	0.673	0.078	0.617	0.637
Ag	0.022		0.015	0.014	0.004	0.011	0.006
Mn	0.005		0.003	0.002	$5x10^{-4}$	0.002	0.001
CaO	0		1.212	1.564	0.617	1.904	1.252
Al_2O_3	0		0.021	0.016	0.013	0.027	0.103
Na_2O	0		5.33	3.96	0.550	5.14	6.26
K_2O	0		39.31	26.18	2.24	37.64	78.8
SiO_2	0		21.05	32.93	71.32	27.01	2.64
UO_2	34.66		11.49	13.09	7.94	9.07	2.98
ZrO_2	0.167		0.250	0.107	0.007	0.118	0.301
Cs_2O	4.02		0	0	0	0	0
BaO	0.348		0.197	0.130	0.026	0.115	0.119
SrO	0.057		0.027	0.019	0.004	0.016	0.011
La_2O_3	0.131		0.002	0.022	0.080	0.001	0.002
CeO_2	0.006		0.003	0.001	0.001	0.001	0.003
Nb_2O_5	0.023		0.004	0.007	0.017	0.004	$5x10^{-5}$
CsI	52.40		0	0	0	0	0

RESULTS FOR TMLB'

Time (s)	Temp (K)	Gas (moles/s)	[A] (g/m^3)	ρ (g/cm^3)	μ (μm)	[A] (g/s)
0	2550	183.4	37.5	9.195	0.42	168
900	2550	183.4	97.9	3.42	0.81	439
1800	2550	183.4	118	3.20	0.87	533
2700	2550	183.4	127	3.14	0.91	569
3600	2316	60.2	28.8	2.76	0.58	42.4
4500	2316	60.2	29.0	2.73	0.58	42.8
5400	2316	60.2	29.1	2.72	0.58	42.8
6300	2316	60.2	29.1	2.71	0.59	42.8
7200	2419	15.65	54.6	2.90	0.71	20.9
8100	2419	15.65	55.1	2.88	0.71	21.1
9000	2419	15.65	55.5	2.87	0.71	21.2
9900	2419	15.65	55.9	2.86	0.72	21.4
10800	2859	22.5	1319	2.80	2.07	726
11700	2859	22.5	1340	2.79	2.08	738
12600	2859	22.5	1359	2.78	2.09	748
13500	2859	22.5	1377	2.76	2.11	758
14400	2350	158.7	38.0	2.67	0.64	147
15300	2350	158.7	37.4	2.69	0.64	145
16200	2350	158.7	37.5	2.70	0.64	146
17100	2350	158.7	37.7	2.71	0.64	146
18000	2041	101.7	9.6	2.21	0.43	23.8

AEROSOL COMPOSITION RESULTS FOR TMLB'

Species	Time (s) 0	900	3600	7200	10800	14400	18000
FeO	0.030	8.63	13.56	13.31	9.03	12.1	4.99
Cr_2O_3	0.058	5.79	2.27	2.34	4.15	1.46	0.106
Ni	12.37	4.92	2.95	3.94	3.31	3.31	0.810
Mo	0.004	0.002	0.002	0.005	0.006	0.005	0.004
Ru	3×10^{-5}	1×10^{-5}	2×10^{-6}	5×10^{-6}	3×10^{-5}	3×10^{-6}	1×10^{-7}
Sn	1.213	0.492	0.485	0.628	0.203	0.515	0.317
Sb	1×10^{-4}	5×10^{-5}	7×10^{-5}	7×10^{-5}	2×10^{-5}	8×10^{-5}	9×10^{-5}
Te	5×10^{-4}	2×10^{-4}	2×10^{-4}	1×10^{-4}	1×10^{-5}	1×10^{-4}	1×10^{-4}
Ag	3×10^{-6}	1×10^{-6}	8×10^{-7}	8×10^{-7}	2×10^{-7}	6×10^{-7}	3×10^{-7}
Mn	0.012	0.004	0.003	0.002	5×10^{-4}	0.002	0.001
CaO	0	0.594	1.24	1.603	0.621	1.94	1.27
Al_2O_3	0	0.011	0.021	0.016	0.013	0.028	0.105
Na_2O	0	2.39	5.46	4.06	0.553	5.24	6.35
K_2O	0	13.45	40.28	26.80	2.26	38.4	79.9
SiO_2	0	36.20	21.60	33.74	71.80	27.57	2.68
UO_2	84.83	27.05	11.70	13.31	7.93	9.19	3.01
ZrO_2	0.413	0.127	0.256	0.110	0.007	0.120	0.306
Cs_2O	0	0	0	0	0	0	0
BaO	0.563	0.166	0.133	0.087	0.017	0.077	0.079
SrO	0.110	0.032	0.021	0.015	0.003	0.013	0.009
La_2O_3	0.323	0.104	0.002	0.023	0.081	8×10^{-4}	0.002
CeO_2	0.014	0.004	0.003	0.001	0.001	0.001	0.003
Nb_2O_5	0.056	0.020	0.004	0.007	0.002	0.004	6×10^{-5}
CsI	0	0	0	0	0	0	0

RESULTS FOR S_2D

Time (s)	Temp (K)	Gas (moles/s)	[A] (g/m^3)	ρ (g/cm^3)	μ (μm)	[A] (g/s)
0	2550	183.4	132	4.74	0.80	593
900	2550	183.4	183	3.44	0.81	444
1800	2550	183.4	120	3.22	0.89	539
2700	2550	183.4	128	3.16	0.91	574
3600	2316	60.2	29.1	2.78	0.58	42.9
4500	2316	60.2	29.4	2.75	0.58	43.3
5400	2316	60.2	29.5	2.74	0.59	43.4
6300	2316	60.2	29.5	2.73	0.59	43.4
7200	2419	15.65	55.4	2.92	0.71	21.2
8100	2419	15.65	55.9	2.90	0.71	21.4
9000	2419	15.65	56.3	2.89	0.71	21.5
9900	2419	15.65	56.7	2.88	0.72	21.7
10800	2859	22.5	1324	2.81	2.07	729
11700	2859	22.5	1344	2.80	2.08	740
12600	2859	22.5	1364	2.78	2.09	751
13500	2859	22.5	1381	2.77	2.11	760
14400	2350	158.7	38.4	2.69	0.64	149
15300	2350	158.7	37.8	2.71	0.64	147
16200	2350	158.7	38.0	2.72	0.64	147
17100	2350	158.7	38.2	2.73	0.64	148
18000	2042	101.7	9.6	2.92	0.43	24

AEROSOL COMPOSITION RESULTS FOR S_2D

Species	Time (s) 0	900	3600	7200	10800	14400	18000
FeO	0.0085	8.50	13.37	13.11	8.99	11.95	4.95
Cr_2O_3	0.016	5.71	2.24	2.30	4.129	1.438	0.105
Ni	3.50	4.86	2.91	3.88	3.294	3.277	0.801
Mo	0.001	0.002	0.002	0.006	0.007	0.005	0.004
Ru	8×10^{-6}	1×10^{-5}	2×10^{-6}	5×10^{-6}	3×10^{-5}	3×10^{-6}	1×10^{-7}
Sn	1.023	1.440	1.417	1.822	0.593	1.498	0.927
Sb	6×10^{-5}	8×10^{-5}	1×10^{-4}	1×10^{-4}	3×10^{-5}	1×10^{-4}	1×10^{-4}
Te	0.247	0.279	0.298	0.186	0.021	0.171	0.177
Ag	0.018	0.022	0.017	0.016	0.004	0.013	0.007
Mn	0.004	0.004	0.003	0.002	5×10^{-4}	0.001	0.001
CaO	0	0.585	1.226	1.578	0.618	1.919	1.26
Al_2O_3	0	0.011	0.021	0.016	0.013	0.027	0.104
Na_2O	0	2.358	5.391	4.00	0.550	5.179	6.299
K_2O	0	13.27	39.74	26.41	2.25	37.93	79.28
SiO_2	0	35.63	21.30	33.22	71.46	27.22	2.66
UO_2	24.12	26.81	11.60	13.17	7.94	9.12	3.00
ZrO_2	0.117	0.125	0.253	0.108	0.007	0.118	0.303
Cs_2O	4.71	0	0	0	0	0	0
BaO	0.228	0.235	0.188	0.123	0.024	0.109	0.113
SrO	0.038	0.039	0.026	0.018	0.004	0.015	0.011
La_2O_3	0.092	0.102	0.002	0.022	0.080	8×10^{-4}	0.002
CeO_2	0.004	0.004	0.003	0.001	0.004	0.001	0.003
Nb_2O_5	0.016	0.019	0.004	0.007	0.017	0.004	6×10^{-5}
CsI	65.85	0	0	0	0	0	0

RESULTS FOR SEQUENCE V

Time (s)	Temp (K)	Gas (moles/s)	[A] (g/m^3)	ρ (g/cm^3)	μ (μm)	[A] (g/s)
0	2550	183.4	33.1	9.04	0.41	150
900	2550	183.4	95.6	3.30	0.816	434
1800	2550	183.4	117.6	3.11	0.89	534
2700	2550	183.4	125.9	3.06	0.92	572
3600	2316	60.2	28.7	2.72	0.58	42.3
4500	2316	60.2	29.04	2.69	0.59	42.8
5400	2316	60.2	29.11	2.67	0.59	42.9
6300	2316	60.2	29.10	2.66	0.59	42.8
7200	2419	15.65	54.77	2.82	0.71	21.0
8100	2419	15.65	55.28	2.81	0.72	21.2
9000	2419	15.65	55.76	2.80	0.72	21.3
9900	2419	15.65	56.22	2.79	0.72	21.5
10800	2859	22.5	1360	2.74	2.10	747
11700	2859	22.5	1382	2.72	2.12	759
12600	2859	22.5	1403	2.71	2.13	771
13500	2859	22.5	1422	2.70	2.15	781
14400	2350	158.7	38.3	2.62	0.65	148.5
15300	2350	158.7	37.8	2.63	0.65	146.6
16200	2350	158.7	38.0	2.64	0.65	147.6
17100	2350	158.7	38.3	2.65	0.65	148.7
18000	2042	101.2	9.7	2.20	0.44	24.2

AEROSOL COMPOSITION RESULTS FOR SEQUENCE V

Species	Time (s) 0	900	3600	7200	10800	14400	18000
FeO	0.036	9.60	14.82	14.76	9.83	13.32	5.34
Cr_2O_3	0.068	6.32	2.41	2.51	4.35	1.56	0.10
Ni	0.236	0.085	0.050	0.068	0.055	0.057	0.014
Mo	0.005	0.002	0.002	0.005	0.006	0.005	0.003
Ru	3×10^{-5}	1×10^{-5}	2×10^{-6}	5×10^{-6}	3×10^{-5}	3×10^{-6}	1×10^{-7}
Sn	2.848	1.041	1.003	1.273	0.393	1.034	0.631
Sb	2×10^{-4}	7×10^{-5}	9×10^{-5}	9×10^{-5}	2×10^{-5}	1×10^{-4}	1×10^{-4}
Te	0.235	0.068	0.067	0.042	0.005	0.037	0.036
Ag	0.017	0.005	0.004	0.004	0.001	0.003	0.002
Mn	0.151	0.004	0.003	0.002	4.8×10^{-4}	0.002	9×10^{-4}
CaO	0	0.606	1.229	1.579	0.604	1.904	1.209
Al_2O_3	0	0.011	0.021	0.016	0.012	0.027	0.103
Na_2O	0	2.496	5.558	4.150	0.553	5.346	6.47
K_2O	0	14.01	40.77	27.23	2.251	38.88	80.11
SiO_2	0	38.67	22.46	35.74	74.68	29.11	2.83
UO_2	92.60	26.55	11.14	12.34	7.12	8.47	2.74
ZrO_2	0.466	0.129	0.255	0.109	0.007	0.118	0.299
Cs_2O	2.026	0	0	0	0	0	0
BaO	0.850	0.225	0.174	0.113	0.022	0.099	0.098
SrO	0.148	0.039	0.025	0.017	0.004	0.014	0.010
La_2O_3	0.374	0.108	0.002	0.023	0.081	0.001	0.002
CeO_2	0.164	0.004	0.003	0.001	0.001	0.001	0.003
Nb_2O_5	0.062	0.019	0.004	0.007	0.016	0.004	5×10^{-5}
CsI	0	0	0	0	0	0	0

APPENDIX D

THE TRAP-MELT CODE

The philosophy and logic structure of the TRAP-MELT code are discussed in the main body of this report. Here we present detailed expressions of the mechanistic treatment for reference purposes. This treatment remains essentially that contained in the published TRAP-MELT manual* and the reader is referred to that document for additional insight.

Master Equation

The master equation set of the TRAP-MELT model is:

$$\frac{d}{dt} M_{im}^k = S_{im}^k + \sum_{n \neq m} {}^m\beta_{in}^k M_{in}^k$$

$$- \sum_{n \neq m} {}^n\beta_{im}^k M_{im}^k \qquad (1)$$

$$+ \sum_{j \neq i} {}^iF_{jm} M_{jm}^k$$

$$- \sum_{j \neq l} {}^jF_{im} M_{im}^k$$

where

M_{im}^k = Mass of radionuclide species k in volume i and state m

S_{im}^k = Source rate of species k in volume i and state m

${}^n\beta_{im}^k$ = Transfer coefficient for transport of species k in volume i from state m to state n

${}^jF_{im}$ = Transfer coefficient for transport of radionuclides in state m from volume i to volume j.

APPENDIX D

THE TRAP-MELT CODE

For a given species k and volume i, therefore, Equation (1) gives, in order of appearance of the terms on the righthand side, the mass source rate to state m, the mass transport rate to state m from other states in volume i, the mass transport rate from state m to other states in volume i and the mass transport rates to and from state m due to flow in and out of volume i.

If m signifies a surface state, ${}^{n}\beta^{k}_{im}$ represents a mass release rate, P. At the present stage of TRAP-MELT, all these terms are set to zero. If m signifies a volume state, ${}^{n}\beta^{k}_{im}$ can be written as

$$ {}^{n}\beta^{k}_{im} = \overline{v_d \frac{A_i}{V_i}} \qquad (2) $$

where v_d is deposition velocity of a given mechanism and A_i is the appropriate deposition surface area. V_i is the volume of the control volume in question. The bar indicates the average over particle mass distribution (if m signifies a particle state) and surface areas.

Each control volume is assumed homogeneously mixed. Mass transport due to flow between volumes can therefore be expressed by

$$ {}^{j}F_{im} = {}^{j}\dot{m}_i / \rho_{si} \; V_i \qquad (3) $$

where

${}^{j}\dot{m}_i$ = Steam mass flow rate from volume i to volume j (input to TRAP-MELT)

ρ_{si} = Density of steam (and hydrogen) in volume i.

Deposition Velocities

(1) Particle settling due to gravity

$$ \tau = \frac{\rho_p d^2 C}{18\mu} = \text{particle response time} \qquad (4) $$

$$ v_d = \tau g $$

where

ρ_p = Particle density
d = Particle diameter
C = Cunningham slip correction factor
μ = Dynamic viscosity of carrier gas
g = gravitational acceleration.

TRAP-MELT distinguishes between settling across and against steam flow. If settling is against the flow, then

$$v_d = v_d - u \qquad u < v_d \tag{5}$$
$$= 0 \qquad u \geq v_d$$

where u = steam flow velocity.

(2) Particle deposition due to diffusion from turbulent flow (Davies*, theoretical expression)

$$v_+ = \frac{Sc^{-2/3}}{14.5\left[\frac{1}{6}\ln\frac{(1+\phi)^2}{1-\phi+\phi^2} + \frac{1}{\sqrt{3}}\tan^{-1}\frac{2\phi-1}{\sqrt{3}} + \frac{\pi}{6\sqrt{3}}\right]} \tag{6}$$

$$\phi = Sc^{1/3}/2.9$$
$$u_+ = \left(\frac{f}{2}\right)^{1/2} u$$
$$f = 0.0014 + 0.125\ Re^{-0.32}$$
$$v_d = v_+ u_+ .$$

Here

Sc = Schmidt number = ν/D
ν = Kinematic viscosity of steam
D = Diffusivity of particle in steam
Re = Steam Reynolds number in the volume of interest
f = Fanning friction factor
u_+ = Steam friction velocity.

*Davies, C. N., Aerosol Science, Academic Press (1966).

(3) Particle deposition due to impaction from turbulent flow (Liu and Agarwal, modified by Lee*).

An empirical correlation of Liu and Agarwal, extended to small particles by Lee, gives:

$$v_+ = 6 \times 10^{-4} \tau_+^2 + 2 \times 10^{-8} \text{ Re} \qquad \tau \leq 0.1 \qquad (7)$$

$$= 0.1 \qquad \tau > 0.1$$

$$\tau_+ = \tau u_*^2/\nu$$

$$v_d = v_+ u_*.$$

(4) Particle deposition due to diffusion from laminar flow (Gormley and Kennedy**).

Laminar flow contradicts the general assumption of homogeneously mixed control volumes that is fundamental to TRAP-MELT. In order to, nevertheless account for deposition under such conditions, a fictitious deposition velocity is introduced that, when used in TRAP-MELT, gives the same rate of deposition as would be calculated by a differential treatment of plug flow. For pipe flow, it can be shown that this deposition velocity is:

$$v_d = \left(1 - \frac{M_o}{M_i}\right) \frac{R}{2L} u \qquad (8)$$

where

R = Pipe radius
L = Pipe length
M_i = Particle mass concentration entering pipe
M_o = Particle mass concentration leaving pipe.

* Gieseke, J. A., et al, NUREG/CR-1264, BMI-2041 (1979).

**Gormley, P. G. and Kennedy, M., Proc. R. Ir. Acad. 52A, 163 (1949).

According to the theoretical analysis (substantiated by numerous experimental investigations) of Gormley and Kennedy:

$$\frac{M_o}{M_i} = 0.8191e^{-7.31h} + 0.0975e^{-44.6h} + 0.0325e^{-114h} \qquad (9)$$

$$h > 0.0156.$$

$$\frac{M_o}{M_i} = 1 - 4.07h^{2/3} + 2.4h + 0.446h^{4/3}$$

$$h < 0.0156$$

$$h = LD/2\,uR^2$$

$$= Pe^{-1}\,L/R$$

where Pe = Peclet number = Sc x Re.

(5) Particle deposition due to thermophoresis (Brock*).

Brock's theoretical treatment of particle deposition in a temperature gradient, ∇T, at a wall surface gives:

$$v_d = -\frac{3}{2}\,\nu\,\psi\,C\,\frac{\nabla T}{T}$$

where

$$\psi = \left(\frac{1}{1 + 3C_m Kn}\right)\left(\frac{k_g/k_p + C_t\,Kn}{1 + 2\,k_g/k_p + 2\,C_t Kn}\right) \qquad (10)$$

C_m = Steam momentum slip coefficient
C_t = Temperature jump coefficient
Kn = Particle Knudsen number
k_g = Thermal conductivity of gas (steam + hydrogen)
k_p = Thermal conductivity of particle.

*Brock, J. R., J. Colloid Sci., 17, 768 (1962).

Note that for large particles, Kn → 0 and

$$\psi \to \frac{k_g/k_p}{1 + 2\,k_g/k_p},$$

yielding an order of magnitude variability in v_d, depending on the choice of k_p. In TRAP-MELT, the necessary temperature gradient in Equation (10) is derived from the simple pipe flow heat transfer correlation:

$$Nu = 0.021\ Re^{0.8}, \tag{11}$$

using the identity

$$h\Delta T = k\nabla T. \tag{12}$$

$\Delta T = T_{wall} - T_{gas}$ is derived from input data. Nu is the Nusselt number.

(6) Vapor sorption on wall surfaces

-- Molecular iodine from steam to stainless steel surfaces (Genco*)

$$v_d = 9.0 \times 10^{-8} e^{8100/k_B T}\ (cm/sec) \tag{13}$$

k_B = Boltzmann's constant.

-- Molecular tellurium on stainless steel 304 (SANDIA**)

$$v_d = 1.0\ (cm/sec) \tag{14}$$

-- Cesium iodide

$$v_d = 0.\ \text{(No data available)} \tag{15}$$

-- Cesium hydroxide (SANDIA**)

$$v_d = 0.01\ (cm/sec). \tag{16}$$

---

* Genco, J. M., et al, BMI-1863 (1969).

** Elrick, R. M. and Sallach, R. A., "High Temperature Fission Product Chemistry and Transport in Steam", Proc. of the Internat'l Meeting on Thermal Nuclear Reactor Safety, August 29-September 2, 1982, Chicago, Illinois.

Species Phase Change

In each control volume, each chemical species is permitted to condense on (or evaporate from) particles and wall surfaces according to the mass transport rate equations:

$$\frac{dC_s}{dt} = -\frac{A_w k_w}{V}(C_s - C_w^s) - \frac{\langle A_p k_p \rangle}{V}(C_s - C_p^s)$$

$$\frac{dM_w}{dt} = A_w k_w (C_s - C_w^s) \qquad (17)$$

$$\frac{dM_p}{dt} = A_p k_p (C_s - C_p^s)$$

where

$C_s = \frac{M_s}{V}$ = concentration of the nuclide vapor in steam

M_s = Total mass of the nuclide vapor in steam

V = Volume of the control volume

M_w = Total mass of nuclide vapor condensed on walls

M_p = Total mass of nuclide vapor condensed on aerosol particles

C_w^s = Equilibrium vapor concentration of the nuclide at the temperature of the wall surfaces (assumed independent of pressure)

C_p^s = Equilibrium vapor concentration of the nuclide at the temperature of the steam (assumed independent of pressure and particle surface curvature)

A_w = Area of wall surfaces

A_p = Surface area of aerosol particle

k_w = Mass transfer coefficient for nuclide transfer between steam and wall surfaces-steam interface

k_p = Mass transfer coefficient for nuclide transfer between steam and particle surface-steam interface

k_w is taken from the Sherwood number (Sh) correlation for turbulent pipe flow (Dittus Boelter):

$$Sh = 0.023\ Re^{0.83} Sc^{0.33} \qquad (18)$$

$$Sc = \text{Schmidt number}$$

$$k_p = D/r$$

with r a particle radius. $\langle A_p k_p \rangle$ is the average value of $A_p k_p$ over the particle size distribution in the control volume of interest.

Equations (17) are solved analytically on the assumption that $\langle A_p k_p \rangle$ changes little over a master time step. This is borne out in practice.

The effect of condensation/evaporation on the particle size distribution is taken into account by noting the total mass (summed over all chemical species considered) transferred to/from the particle state according to Equations (17) over a master time step. This quantity is distributed over the discretized particle size distribution such that each size class is augmented/diminished in proportion to its associated mass transfer rate.

Required vapor pressure data (C_w^s, C_p^s) for I_2, CsI, CsOH, and Te are presently incorporated in the code.

Particle Agglomeration

The aerosol component of the radionuclides tracked by TRAP-MELT is distributed among 20 size classes. Agglomeration among particles in these size classes is treated by a method developed in the QUICK aerosol behavior code* and since validated against numerous experiments. The coupling of this treatment to the flow equations of the TRAP-MELT code is described in the body of this report. Here we exhibit the agglomeration mechanisms considered.

*Jordan, H., et al, "QUICK Users' Manual", NUREG/CR-2105, BMI-2082 (1981).

Brownian Agglomeration

Defining the agglomeration kernel, K_{ij}, by

$$R_{ij} = K_{ij} N_i N_j \tag{19}$$

such that R_{ij} is the rate of agglomeration of the N_i particles per unit volume in size class i with the N_j particles per unit volume in size class j, the kernel for Brownian coagulation can be written:

$$K_{ij} = 4\pi k_B T (B_i + B_j)(r_i + r_j) \tag{20}$$

where

$$B_i = \frac{C}{6\pi\mu r_i}$$

and r_i is a characteristic particle radius for size class i.

Gravitational and Turbulent Coagulation. Following Saffman and Turner*, the combined kernel for gravitational, turbulent shear, and turbulent inertial agglomeration can be written

$$K_{ij} = 2\sqrt{2\pi}\,(r_i + r_j)\left[\varepsilon_{ij}^2(\tau_i - \tau_j)^2 \frac{1.3E}{\nu}^{3/2}\right.$$

$$\left. + \frac{1}{3}\varepsilon_{ij}^2(\tau_i - \tau_j)^2 g^2 + \frac{1}{9}(r_i + r_j)^2 \frac{E}{\nu}\right]^{1/2}$$

where the as yet undefined quantities are:

$$\varepsilon_{ij} = 1.5 \left(\frac{r}{r + r'}\right)^2 \qquad r = \min(r_i, r_j)$$

$$r' = \max(r_i, r_j),$$

*Saffman, P. G. and Turner, J. S., J. Fluid Mechanics, 1, 16 (1956).

the collision efficiency for hydrodynamic interactions and E the turbulent energy density dissipation rate. TRAP-MELT uses Laufer's expression*:

$$E = 0.03146\ u^3/(D\ Re^{3/8}).$$

* U.S. GOVERNMENT PRINTING OFFICE: 1983-381-299:152

*Taken from Delichatsios, M. A. and Probstein, R. F., MIT Fluid Mechanics Lab Publication #74-5 (1974).

UNITED STATES
NUCLEAR REGULATORY COMMISSION
WASHINGTON, D. C. 20555

OCT 17 1984

MEMORANDUM FOR: James C. McKnight
Records Services Branch
Division of Tech. Info. and Doc. Control, ADM

FROM: Christopher P. Ryder
Accident Source Term Program Office
Office of Nuclear Regulatory Research

SUBJECT: PLACEMENT OF BMI-2104 VOLUMES IN PUBLIC DOCUMENTS ROOM

Enclosed are Volumes I through Volume VI of BMI-2104, "Radionuclide Release Under Specific LWR Accident Conditions."

I would like these volumes placed in the Public Documents Room. Should you have any questions, I can be reached at x74337.

Christopher Ryder

Christopher Ryder
Accident Source Term Program Office
Office of Nuclear Regulatory Research

Enclosures: As stated

UNITED STATES
NUCLEAR REGULATORY COMMISSION
WASHINGTON, D.C. 20555